Biocompatible Chemistries for the Construction and Application of Ubiquitin-Derived Activity-Based Probes of Deubiquitinases

A thesis submitted to the School of Chemistry, Trinity College Dublin, The University of Dublin, for the degree of Doctor of Philosophy

Tomasz Pawlak, M.Sc., B.A. (Mod.)

Under the supervision of Prof. Joanna McGouran

Trinity College Dublin, The University of Dublin

February 2026

Declaration

I declare that this thesis has not been submitted as an exercise for this degree at this or any other university and it is entirely my own work, other than where acknowledged.

I agree to deposit this thesis in the University's open access institutional repository or allow the Library to do so on my behalf, subject to Irish Copyright Legislation and Trinity College Library conditions of use and acknowledgement.

I consent to the examiner retaining a copy of the thesis beyond the examining period, should they so wish (EU GDPR May 2018).

Tomasz Pawlak

Abstract

Deubiquitinases (DUBs) are critical regulators of ubiquitin signalling, with direct implications in cancer, neurodegeneration, inflammatory conditions, and autoimmune diseases. This thesis presents the development of novel chemical tools to study DUB function, combining radical-mediated bioconjugation strategies, bioorthogonal chemistry, and lysine-targeted warheads to create novel ubiquitin constructs.

Building on the well-established thiol-yne reaction, a radical-based method for protein coupling was developed, enabling the first examples of linking two proteins *via* this approach. Using this radical thiol-yne strategy, a di-ubiquitin construct containing an internal alkene was generated. Although minor amounts of tri-ubiquitin were also formed *via* a thiol-ene reaction, steric hindrance largely suppressed trimer formation. As a result, access to the alkene was effectively restricted to small molecules, sterically compatible active-site cysteines in DUBs, and potentially other cysteine-containing ubiquitin-binding proteins. The di-ubiquitin probe was partially purified and successfully shown to label the cysteine protease DUB OTUB1 *via* a thiol-ene reaction, demonstrating promising, if modest, labelling that warrants further study. These findings reveal the potential of probes containing internal alkenes to label other cysteine proteases. Complementary approaches, utilising azido-modification of lysine side chains followed by azide–alkyne cycloaddition, enabled the formation of ubiquitin dimers bearing terminal alkenes. Terminal alkenes were shown to undergo a thiol-ene reaction, providing proof of concept for combining these specific biorthogonal methods to achieve controlled protein crosslinking.

To expand the repertoire of DUB-targeting probes, squaramide-functionalized ubiquitin constructs were developed, capable of covalently capturing DUBs *via* lysine residues near their active sites. These probes demonstrated activity against the metalloprotease DUB Rpn11, warranting further investigation to elucidate their binding interactions. Combining the bioorthogonal conjugation methods presented in this thesis shows promise for designing multifunctional, controllable ubiquitin-based probes to dissect DUB specificity and function.

By integrating radical chemistry, bioorthogonal reactions, and lysine-reactive warheads, this work contributes a versatile chemical biology toolkit for probing ubiquitin signalling and advancing our understanding of the roles of DUB in biology.

Acknowledgements

Firstly, I'd like to sincerely thank my supervisor, Professor Joanna McGouran, for her support and guidance, as well as for granting me access to her lab, where I've had the amazing opportunity to work alongside many excellent scientists over the last four years. I'd also like to extend my thanks to the Irish Research Council for funding my project, and the School of Chemistry at Trinity College Dublin for providing me with space, equipment and the guidance and expertise of their staff, befitting a world-class university steeped in history.

I'm especially grateful to Dr. Gary Hessman for his assistance in analysing my MS samples and guiding me through data interpretation on numerous occasions. Additionally, I'd like to thank Dr. John O'Brien and Dr. Manuel Rüther for their assistance with NMR, as well as the other academic, administrative and support staff at TCD and DubChem.

I'm thankful for the support of past and present members of the McGouran group. They have welcomed me with kindness and professionalism. I have learned a lot and improved on my skillset while working with them. By watching the positive outcomes of the excellent organisational skills of Dr. Ellen Fay, I was able to improve on my experimental design approaches and report writing. By witnessing many great talks by Dr. Sean McKenna, I believe my own presentation skills have vastly improved. By experiencing the friendly, open and collaborative style of communication of Dr. André Campaniço, I have learned a lot about efficient and smooth lab management. Seeing how much time and effort Dr. Connor O'Leary put into his work and how much he cared about the lab made me want to put more effort into my own work. On top of that, I have learned many technical skills from every chemist and biologist I've interacted with in the lab. I've especially enjoyed seeing the effort everyone put into presenting their research progress and reviewing the literature. I wish only the best to the current and future members of the lab.

I wanted to express my gratitude to my family. I wanted to say thank you to my wife, Sakiko, who has been my great supporter over the last nine years (I know I'm not the easiest person to live with), as well as our baby, Anzu, whose brilliance, power and sweetness have made me the happiest papa ever.

Lastly, I wanted to thank the reader of this thesis. I appreciate the effort needed to work your way through my writing. I hope you find it useful and informative.

Contents

Abbreviations

°C	degrees Celsius
Å	Angstrom
ABP	Activity-Based Probe
ABPP	Activity-Based Protein Profiling
ADC	Antibody-Drug Conjugate
AfBP	Affinity-Based Probe
AKT	Protein kinase B
Ala	Alanine
Asp	Asparagine
ATXN	Ataxin
BSA	Bovine Serum Albumin
C48	Cysteine 48
C63	Cysteine 63
C91S	Cysteine to Serine mutation at position 91
CBD	Chitin-Binding Domain
CBL-B	Casitas B-lineage Lymphoma proto-oncogene B
CDK	Cyclin-Dependent Kinase
CuAAC	Copper(I)-catalyzed Azide-Alkyne Cycloaddition
CYLD	Cylindromatosis
Cys	Cysteine
DBHDA	2,5-dibromohexanediamide
DEP	Dishevelled, Egl-10 and Pleckstrin domain
DEPTOR	DEP domain-containing mTOR-interacting protein
DIPEA	*N*, *N*-Diisopropylethylamine
DMF	Dimethylformamide
DMSO	Dimethyl sulfoxide
DNA	Deoxyribonucleic acid
DUB	Deubiquitinase
E1	Ubiquitin activating enzyme
E2	Ubiquitin conjugating enzyme
E3	Ubiquitin ligase
EMT	Epithelial-Mesenchymal Transition

et al	Latin for ‘and others’
FDA	Food and Drug Administration
FDR	False Discovery Rate
FGE	Formylglycine-Generating Enzyme
Fmoc	9-Fluorenylmethyloxycarbonyl
G1/S Phase	Gap 1 Phase and Synthesis Phase
GAPDH	Glyceraldehyde-3-Phosphate Dehydrogenase
GCE	Genetic Code Expansion
Glu	Glutamic acid
GRAIL	Gene Related to Anergy in Lymphocytes
H_2O_2	Hydrogen Peroxide
HA	Hemagglutinin
HCl	Hydrochloric acid
HEK293T	Human Embryonic Kidney cells, Experiment No. 293, SV40 T antigen
HER2	Human Epidermal Growth Factor Receptor 2
HIF-1α	Hypoxia-Inducible Factor 1-alpha
His	Histidine
HMTA	Hexamethylenetetramine
HPLC	High-Performance Liquid Chromatography
HPMA	Hydroxypropyl Methacrylate
HRP	Horseradish Peroxidase
IED-DA	Inverse Electron Demand Diels-Alder
IKK	Inhibitor of nuclear factor-κB (IκB) Kinase
Ile	Isoleucine
IPTG	Isopropyl β-D-1-thiogalactopyranoside
IR	Infrared
ITCH	Itchy E3 ubiquitin-protein ligase
JAMM	JAB1/MPN/Mov34 metalloenzyme
K11	Lysine 11
K27	Lysine 27
K29	Lysine 29
K33	Lysine 33
K48	Lysine 48

K48C	Lysine to Cysteine mutation at position 48
K6	Lysine 6
K63	Lysine 63
kDa	kilodalton
LACE	Lysine Acylation using Conjugating Enzymes
LAP	Lithium phenyl-2,4,6-trimethylbenzoylphosphinate
LC	Liquid Chromatography
LCK	Lymphocyte-Specific protein tyrosine Kinase
LC-MS	Liquid chromatography-Mass Spectrometry
LC-MS/MS	Liquid Chromatography-tandem Mass Spectrometry
LUCA	Last Universal Common Ancestor
Lys	Lysine
M1	Methionine 1
MALDI-ToF	Matrix Assisted Laser Desorption Ionization-Time of Flight
MESNa	Sodium 2-mercaptoethanesulfonate
MINDY	MIU-containing novel DUB
MIU	Motif Interacting with Ubiquitin
MJD	Machado-Joseph Disease
MS	Mass Spectrometry
MTGase	Microbial Transglutaminase
mTOR	Mechanistic Target of Rapamycin
MWCO	Molecular-Weight Cut-Off
NAP-5	Nucleic Acid Purification, 0.5 mL
NCL	Native Chemical Ligation
NEDD8 protein 8	Neural precursor cell expressed developmentally downregulated
NF-κB	Nuclear factor kappa-light-chain-enhancer of activated B cells
NHS	N-Hydroxysuccinimide
NIR	Near Infrared
NMR	Nuclear Magnetic Resonance
NSCLC	Non-Small Cell Lung Cancer
OTU	Ovarian Tumour
PBS	Phosphate-Buffered Saline
PBS-T	Phosphate-Buffered Saline-Tween

PDB	Protein Data Bank
PDL	Proximity-Dependent Labelling
PI3K	Phosphoinositide 3-Kinase
PMSF	Phenylmethylsulfonyl Fluoride
PSM	Peptide-Spectrum Match
PTM	Post-Translational Modification
R_f	Retention factor
RNS	Reactive Nitrogen Species
ROS	Reactive Oxygen Species
Rpn11	26S proteasome non-ATPase regulatory subunit 14
RPS27a	Ribosomal Protein S27a
SDS-PAGE	Sodium Dodecyl Sulfate–Polyacrylamide Gel Electrophoresis
SEC	Size-Exclusion Chromatography
Ser	Serine
SET	Single Electron Transfer
SN2	Substitution, Nucleophilic, Bimolecular
SPAAC	Strain-Promoted Azide-Alkyne Cycloaddition,
SUMO	Small Ubiquitin-Like Modifier
SV40 T	Simian virus 40 tumour antigen
TAK1	Mitogen-activated protein kinase kinase kinase 7
TAMRA	5(6)-Carboxytetramethylrhodamine
TE	Tris and EDTA
TEOA	Triethanolamine
TGF-β	Transforming Growth Factor Beta
THPTA	Tris(3-hydroxypropyltriazolylmethyl)amine
TLC	Thin-Layer Chromatography
TNF-α	Tumour Necrosis Factor Alpha
TRAF	TNF Receptor Associated Factors
Tris	Tris(hydroxymethyl)aminomethane
Trp	Tryptophan
Tyr	Tyrosine
UbA52	Ubiquitin A-52 residue ribosomal protein fusion product 1
UbB	Ubiquitin B

UbC	Ubiquitin C
UBL	Ubiquitin-like protein
UBP	Ubiquitin-Specific Protease
UCH	Ubiquitin C-terminal Hydrolase
UFM1	Ubiquitin-Fold Modifier 1
ULK1	Unc-51-like autophagy-activating kinase 1
USP	Ubiquitin-Specific Protease
UV	Ultraviolet
WCX	Weak Cation Exchange
WNT	Wingless/Integrated
WT	Wild Type
ZAP70	Zeta-chain-associated protein kinase 70
ZUFSP	Zinc finger with UFM1-specific peptidase domain protein

Chapter 1: Introduction

1.1. Protein modification and expansion of protein functionalities

The Human Genome Project was completed in 2003,[1] however, sequencing the human genome did not resolve all issues with our understanding of human diseases and their fundamental causes. This is in part due to the impact of dysregulation in protein expression, function or Post-Translational Modifications (PTMs) on disease onset and progression.[2] Proteomics is a discipline that has emerged as a means of untangling the purposes of complex, dynamic, and often transient interactions between proteins.[3]

Challenges associated with selectively labelling, enrichment and detection of proteins, and following their interactions in native systems have prompted the development of biorthogonal reactions that enable selective modification of proteins in their native environments.[4] To be fully biorthogonal, tools using these chemistries should contain functional groups that are not present in living systems, react in a predictable, specified manner under biocompatible conditions and be inert towards other native components.

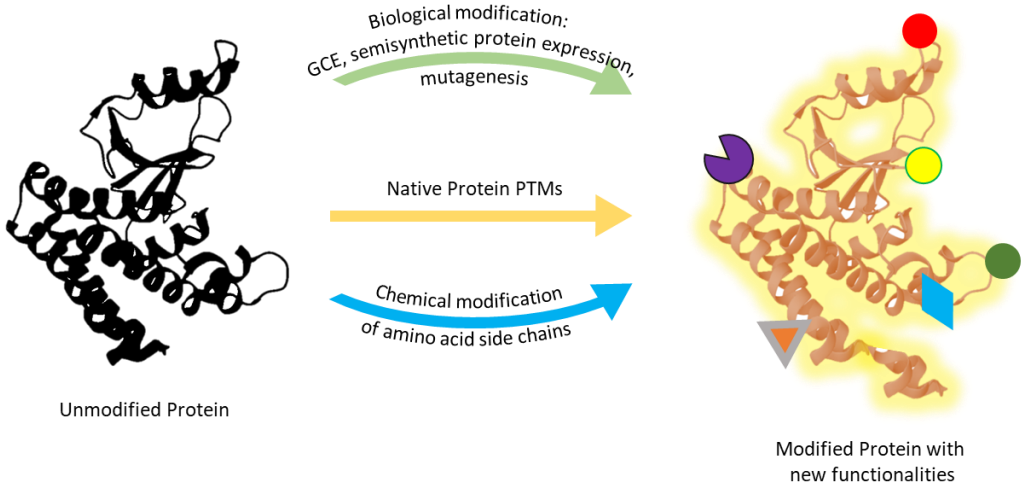

Figure 1: Biological and chemical methods for protein modification.

Chemical and biological modification of proteins affects their physical properties, alters their pharmacokinetics, or grants them novel functionalities. Biological strategies for protein modification depicted in **Figure 1** include native PTMs, Genetic Code Expansion (GCE),[5] semisynthetic protein expression,[6] and mutagenesis,[7] whereas chemical methods include reactions selectively modifying amino acid side chains.[8] Applications of controlled protein modification include: the attachment of polyethylene glycol to therapeutic proteins,[9] to improve solubility and stability;[10]

tagging proteins with fluorophores or affinity tags to facilitate tracking and isolation[11, 12] for academic research[13] and medicine;[14] protein crosslinking;[15] and the tailoring of protein activities for biocatalysis,[16] biosensing,[17] and biomaterials.[18]

1.1.1. Modifying nucleophilic residues in proteins to alter protein functions

Post-translational chemical modification of proteins enables their tracking, and allows control over their localisation, dynamics, and interactions *in vitro* and *in vivo*.[19] Prominent examples of how chemically modified polypeptides have been harnessed include the conjugation of therapeutic molecules to antibodies, to create Antibody-Drug Conjugates (ADCs);[20] the development of new molecular scaffolds such as cyclic peptides for drug discovery;[21] and the modification of enzymatic functionalities.[22] Protein modification efforts have historically been focused on cysteine and lysine residues, due to their chemical reactivity. Cysteine residues are strong nucleophiles[23] with low abundance relative to other amino acids (ranging between 2.26% in mammals and 0.5% in some *Archaea*),[24] yet, due to their involvement in catalysis and disulfide bridge formation, their positions are evolutionarily conserved.[25] Several strategies for the selective modification of cysteine residues have been reported, including maleimide derivatives (**Figure 2 A**),[26] radical thiol-ene chemistry (**Figure 2 B**),[27] and nucleophilic substitution (**Figure 2 C**), amongst others. These approaches have been applied in probing the cysteinome on several occasions.[28-30]

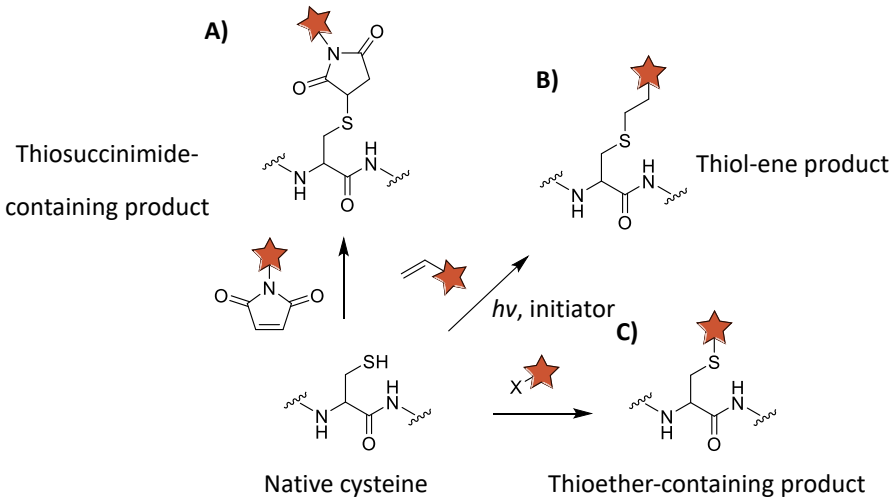

Figure 2: Chemical modification of cysteines using **A**: maleimide derivatives, **B**: thiol-ene reaction, **C**: nucleophilic substitution (X – halide).

Lysine residues on the other hand, are highly abundant[31] and often solvent-exposed, allowing for multiple bioconjugations to be performed in a single reaction,

for lysine-specific yet target-agnostic profiling of the proteome.[32] Lysine side chains contain a primary amine that is positively charged under physiological conditions. Many chemical groups have been used to specifically modify lysine side chains. These include *N*-hydroxysuccinimide (NHS) esters (**Figure 3 C**),[33] sulfonyl halides (**Figure 3 B**),[34] and isothiocyanates (**Figure 3 A**),[35] among others. Reversible lysine-specific probes containing iminoboronates have also been reported.[36] Covalent labelling of targeted lysines in protein systems with small molecule probes, fluorophores, biotin, and other polypeptides have been reported.[37]

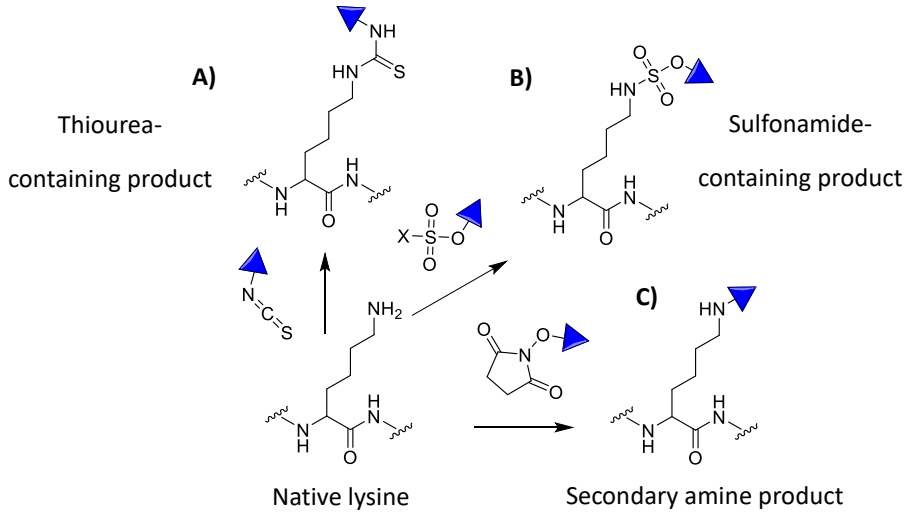

Figure 3: Chemical modification of lysines using **A**: isothiocyanates, **B**: sulfonyl halides (X - halide), **C**: NHS esters.

Although global lysine modification can be useful for probing the proteome, labelling of individual, specific lysine residues in a protein can be highly desirable. Lysines can have significantly different reactivities due to different solvent accessibility and higher-order protein structure. Cravatt and colleagues reported a chemoproteomics platform to quantify which lysine residues were highly reactive in native biological systems.[38] Using the sulfotetetrafluorophenyl (STP) electrophile capable of selectively binding highly reactive lysine residues, they mapped over 9,000 lysine residues and found that 100 had high reactivity. Individual lysine residues could therefore be targeted, based on their reactivity or proximity to lysine-reactive groups. Engineered protein ligands containing lysine-reactive moieties such as 2-hydroxybenzaldehyde have been reported to selectively modify specific lysine residues on the targeted proteins.[39] Selective, proximity-based lysine modification of enzymes has also been reported. Notably, the primary glycolytic intermediate 1,3-bisphosphoglycerate was found to covalently modify lysines in the active site of Glyceraldehyde 3-phosphate dehydrogenase, as well as those in other glycolytic

enzymes, resulting in the capture of these enzymes.[40] In another case, the C-terminal lysine of a protein nanobody has been conjugated to other biomolecules and small molecules, using a chemoenzymatic method termed Lysine Acylation Using Conjugating Enzymes (LACE).[41] This technique employs E2 ubiquitin-conjugating enzymes to attach acyl groups to lysine residues independent of E1 ubiquitin-activating enzymes or E3 ubiquitin ligases. LACE uses a chemically-activated acyl donor and a short, engineered recognition sequence on the target protein to modify a specific, proximate lysine. Collectively, these strategies for cysteine and lysine modification demonstrate the capacity to selectively alter protein properties. The strategies outlined here also underpin the construction of clinically important molecules, such as ADCs.

1.1.2. Linking antibodies to payloads in Antibody-Drug Conjugates (ADCs)

ADCs, seen in **Figure 4**, are a class of biomolecules that combine the high specificity of antibodies for disease-relevant molecular targets with the potent tumoricidal activity of attached payloads for the effective killing of malignant cells.[42] Currently, multiple ADCs have been approved by the FDA as cancer therapies.[43] Several bioconjugation strategies have been used to link antibodies to payloads. New methods for controlled, biocompatible conjugation of antibodies to cytotoxic agents are highly sought after, as approved approaches often yield ADCs with varying drug-to-antibody ratios (DARs) and conjugation sites.[44] Lysine conjugation *via* NHS esters forms amide bonds with lysine residues, while cysteine-based conjugation typically uses maleimide chemistry to link payloads to free thiols after interchain disulfide reduction.

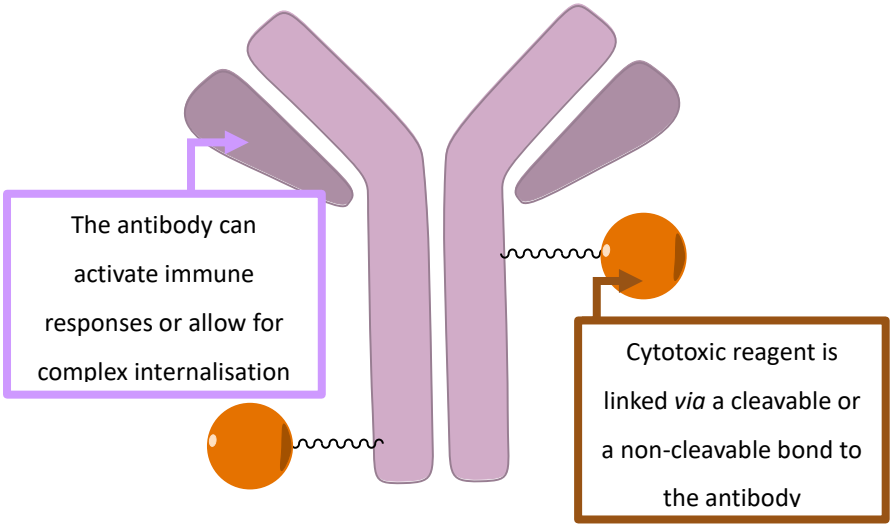

Figure 4: Components of ADCs. Antibodies (in pink) specific to cancer cells allow for complex internalisation, or immune modulation, while cytotoxic agents (in brown) are attached *via* cleavable or non-cleavable linkages.

To improve homogeneity and therapeutic profiles, enzymatic techniques that allow for site-specific incorporation of payloads have been developed. Microbial transglutaminase (MTGase) was used to exchange a glycosylated glutamine for a payload-bearing primary amine in engineered or deglycosylated antibodies, enabling highly controlled attachment of cytotoxic agents.[45] Attachment of branched linkers by MTGase was also achieved, increasing the DARs without compromising the specificity of ADCs.

Sortase A recognises an LPXTG tag engineered into the antibody, mediating precise conjugation with an oligoglycine-functionalized payload.[46] Formylglycine-Generating Enzyme (FGE) introduces an aldehyde tag (CXPXR motif) that can undergo site-specific ligation, enabling uniform and high-precision bioconjugation.[47]

Hsu *et al.* used *N*-acetylglucosaminyltransferase 3 to conjugate azide-containing glycans to several glycoforms of HER2-specific antibodies.[48] Addition of cytotoxic payloads *via* Copper-Catalysed Azide-Alkyne Cycloaddition (CuAAC) was then performed, and cytotoxic effects on cancer cells were shown. This method enabled site-specific conjugation of antibodies, without the need for genetic engineering or glycan synthesis, relying instead of glycan remodelling of antibodies.

1.1.3. Click reactions for bioconjugation

CuAAC reaction allows for efficient, biorthogonal linking of azides with alkynes *via* a 1,2,3-triazole ring formation, facilitated by a copper catalyst. CuAAC originally emerged in 2002 *via* two independent groups: Meldal[49] and Sharpless/Fokin.[50] In this reaction, compounds are linked *via* a stable triazole ring.[51] CuAAC has been used in many biomedical applications,[52] as well as *in vitro* and *in vivo* labelling studies.[53] Recently, CuAAC was used by McKenna *et al.* to create Affinity-Based Probes (AfBPs) capable of interrogating zinc metalloproteases.[54] It is worth mentioning that probing metalloprotease DUBs relies on non-covalent chelating of zinc ions.[55] This is due to metalloproteases not forming covalent intermediates upon activation.

Strain-Promoted Azide-Alkyne Cycloaddition (SPAAC) is a copper-free version of CuAAC reaction introduced by Bertozzi *et al*.[56] It utilizes highly strained cyclooctynes to accelerate azide-alkyne cycloaddition under physiological conditions. Mbua *et al.*[57] used SPAAC for live cell glycan labelling, as well as preparation and derivatisation of different strained cyclooctyne variants.

Biorthogonal click reactions also include Inverse Electron Demand Diels-Alder (IED-DA) reactions, which involve tetrazines and strained alkenes, allowing for 4+2 cycloaddition.[58] They have been used in nucleic acid, protein, antibody, lipid, glycan, and bioactive small molecule conjugation.[59] Collectively, click chemistry conjugations have transformed chemical biology by enabling site-specific, efficient, and tunable bioconjugation.

Radical-based thiol-yne and thiol-ene reactions meet the criteria of click reactions. They are highly efficient, selective when optimised, can proceed in mild conditions, produce minimal side reactions, and are highly versatile. Thiol-yne and thiol-ene reactions have been used in bioconjugation efforts.[60]

1.2. Radical chemistry in synthetic protein modification

Radical reactions have been used for decades for the synthesis of natural products [61] and other small molecules.[62] More recently, they have found use in the pharmaceutical industry.[63] Several examples of protein modification by radicals formed from aromatic and basic[64, 65] side chains have been reported. Beyond radicals these side chains, phenolic radicals derived from the small-molecule tyrosine analogue tyramine have also been used in protein modification. Tyrosyl and tyramide radicals formed under oxidative conditions, or due to single-electron transfer (SET), can dimerise, forming dityrosines and dityramides.[66] Additionally, tyrosyl and tyramide radicals can be formed by metal complexes such as Ni(III) and Ru(III).[67] Tyrosyl radicals can also crosslink to other aromatic and basic residues. This idea was used to crosslink viral capsid proteins under radical conditions *via* their native tyrosines.[68]

Several enzymes can facilitate this radical crosslinking, including peroxidases,[69, 70] tyrosinases,[71] and laccases.[72] In the Proximity-Dependent Labelling (PDL) approach, an enzyme capable of generating tyrosyl radicals is incorporated into a molecular probe. A molecule containing a phenol group and a chemical handle is also incubated with the probe. While the probe interacts with its target, the enzyme produces phenoxyl radicals from nearby phenols, which mediate covalent crosslinking of the chemical handle to the target proteins. The short lifetime of radicals restricts crosslinking of the phenol-bearing chemical handles to the immediate protein microenvironment, which can then be isolated and analysed *via* mass spectrometry-based proteomic approaches.[73, 74] This workflow is illustrated in **Figure 5**. Rhee *et al*.[75] expressed a probe containing horseradish peroxidase (HRP) in mitochondria and incubated it with biotinylated phenol. Phenoxyl radicals enabled covalent attachment of biotin to nearby

tyrosine, tryptophan, histidine, and cysteine residues *via* PDL, facilitating proteomic mapping of mitochondria in living cells.

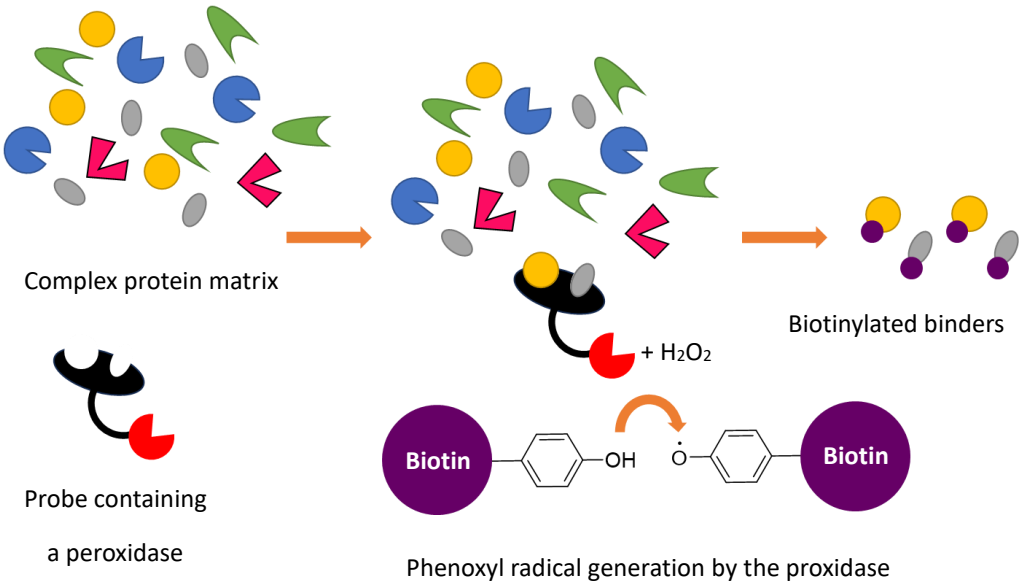

Figure 5: PDL approach for radical labelling of proteins, resulting in biotinylated targets that can be isolated *via* and identified by mass spectrometry.

Radical-based C-C bond-forming methods, such as addition to alkenes or cross-coupling with electron-deficient aryl partners,[76] have been successfully applied to the site-selective modification of peptides, notably through the aryl radical-mediated modification of cysteine residues using eosin Y-catalysed photoredox reactions under visible light.[77] Visible-light[78] and electrochemical[79] radical generation have also facilitated the late-stage functionalization of proteins[80] and in the synthesis of complex molecules.[81]

Building on the success of radical-driven approaches in modifying polypeptides, researchers sought to apply radical reactions to the far more complex environment of protein bioconjugation, due to their localised nature, reaction speed, dependence on proximity, and responsiveness to external stimuli.

Modification of isolated proteins *via* cysteine radicals has been successfully performed on several occasions. Taylor *et al.* leveraged radical thiol-ene chemistry to create Activity-Based Probes (ABPs) for DUBs, which covalently captured purified cysteine DUBs, and native DUBs in HEK293T cell lysates.[82] Unlike traditional nucleophilic probes, radical probes contained a latent alkene warhead that remained inert under ambient conditions. Activation of thiols in cysteine protease DUBs *via*

photoinitiated radical mechanisms, in the presence of alkenes, enabled precise control over the timing of DUB capture. This idea was expanded on, with thiol-ene labelling of DUBs being initiated by exposure to visible light in the presence of Eosin Y.[83, 84]

Mitchell *et al.* reported a method for site-specific peptide and protein labelling, which allowed for the installation of carbon-carbon bonds through radical-mediated desulfurative transformations of cysteines.[85] They used this method for cyclisation of cysteine-containing unprotected peptides in aqueous solution, by visible-light-induced removal of sulphur, resulting in a new hydrocarbon link.[86] This method demonstrated the applicability of blue-light-induced radical reactions for polypeptide modifications across diverse peptide chain lengths, under ambient conditions.

1.2.1. Application of radical chemistry in living systems

Use of radical chemistry in cells has been limited, due to high reactivity of free radicals. Additionally, presence of radical scavengers in cellular milieu dampens the reaction propagation,[87] while the high level of compartmentalization in living cells[88] limits accessibility of targets *in vivo*. Radical reactions are an attractive modality for biorthogonal modification of biomolecules, as they can proceed under mild conditions,[89] unlike traditional reactions which require conditions incompatible with biomolecules.

Despite these hurdles, Geng *et al*.[90] were able to show radical polymerisation *in cellulo*. Their approach for light-mediated free-radical polymerisation utilised a biocompatible radical initiator Irgacure2959, **1** (**Figure 6 A**), and HPMA, **2** (**Figure 6 B**), monomers at non-cytotoxic concentrations. Compound **1** is known to be tolerated by several cell types [91-93,] and the monomers used were not cytotoxic at the tested concentrations. HeLa cells containing monomers were exposed to UV light (365 nm) for 5-15 min, in the presence of compound **1** and once polymers formed, they were isolated. Their identity was confirmed *via* MALDI-ToF. Fluorophore acryloxyethyl thiocarbamoyl rhodamine B (**Figure 6 C**) was then incubated with HPMA, and after introduction to cells and radical initiation, fluorescent polymers were detected.

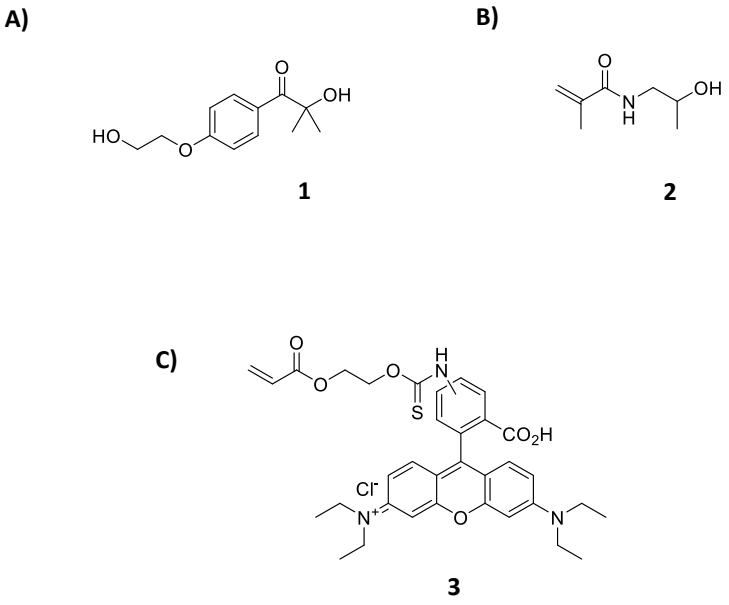

Figure 6 A: 2-Hydroxy-4-(2-hydroxyethoxy)-2-methylpropiophenone (**1**, Irgacure2959), **B:** *N*-(2-hydroxypropyl)methacrylamide (**2**, HPMA), **C**: acryloxyethyl thiocarbamoyl rhodamine B salt (**3**, fluorophore).

Modification of surface-exposed cysteine residues on the surface of living cells, was achieved by Iwasaki and coworkers.[94] Acryloyl-labelled carbohydrates were exposed to visible light, in the presence of Eosin Y, to modify mammalian cell surfaces under mild, biocompatible conditions. The method enabled stable glycan conjugation without compromising cells, demonstrating its utility for surface engineering.

1.2.2. Potential for the use of radical chemistry in biology

Radicals such as Reactive Oxygen Species (ROS) and Reactive Nitrogen Species (RNS) are naturally formed in aerobic cells by various molecular pathways, including cellular metabolism[95] and immune responses.[96] Sources such as heat,[97] ionizing radiation[98] and immune responses[99] can also form radicals in cells.

Unpaired electrons cause oxidative stress in biological environments, which can damage DNA, proteins and lipids, leading to diseases such as cancer, dermatitis, cataracts, stroke, and asthma.[100, 101] Endogenous human antioxidants quench and scavenge radicals. Primary antioxidative enzymes include superoxide dismutase,[102] glutathione peroxidase,[103] catalase,[104] and peroxiredoxins.[107] Secondary antioxidant enzymes which do not neutralise radicals directly, but maintain primary enzymes' activity include: thioredoxin reductases,[105] heme oxygenase-1,[106] thioredoxins,[108] and paraoxonases.[109] Non-enzymatic endogenous antioxidants and radical scavengers

include metal-binding proteins, glutathione, uric acid, melatonin and bilirubin.[110] Exogenous antioxidants, such as flavonoids,[111] vitamins A, E and C, trace minerals, carotenoids and polyphenols,[112] are also well known to combat oxidation.

Exposure to ROS can lead to oxidation of amino acid side chains. Cysteines can be oxidised to form thiyl radicals, which can lead to disulfide formation. Cysteine oxidation to sulfenic, sulfinic and sulfonic acids can also take place.[113] Methionine can be oxidised to form methionine sulfoxide and methionine sulfone,[114] while tryptophan can be oxidised to form a variety of products, including *N*-formylkynurenine, kynurenine, and hydroxytryptophan.[115] All of these modifications can alter protein structures and functions. They can also cause peptide bond cleavage and protein aggregation. Lastly, carbonylation of lysine, arginine, proline, and threonine residues is a known marker of oxidative stress connected to ageing and associated diseases.[116] RNS can modify proteins through nitration of tyrosine residues and S-nitrosation of cysteine residues,[117] or oxidation of tryptophan.[118] Cysteine-derived thiyl radicals are highly reactive in both aqueous and lipidic environments, with polyunsaturated fatty acids in membranes and protein side chains in cytosol being oxidised.[119]

Lipid peroxidation is another result of free radicals in cells, especially in the case of polyunsaturated fatty acids (PUFAs) found in cellular membranes.[120] Following lipid peroxidation, membrane damage, changes in permeability and eventually, cell lysis take place. Toxic aldehydes such as malondialdehyde and 4-hydroxynonenal, which can modify DNA and proteins, are also produced. Oxidised lipids can activate immune responses[121] and contribute to cardiovascular,[122] neurodegenerative,[123] and chronic inflammatory diseases.[124]

Free radicals can abstract hydrogen atoms from the sugar-phosphate backbone of DNA or modify nucleobases, generating a variety of lesions, including base modifications, single- and double-strand breaks, abasic sites, cross-links, and tandem damage clusters.[125] Guanine can be oxidised, which can mispair with adenine, leading to mutations.[126] DNA can also be crosslinked,[127] or DNA-protein adducts can be formed due to the presence of free radicals.[128]

Radical reactions can substantially modify biomolecules due to their reactivity; however, harnessing these reactions with precise control would allow for probing and manipulation of cellular processes in real time, without interfering with native biological functions. This could, in turn, open interesting avenues of research in live-cell imaging, targeted drug activation, and the development of novel tools.

1.3. Activity-Based Probes (ABPs)

ABPs contain three elements:[129] chemical traps (also called 'warheads') that covalently bind active enzymes, reporter tags, and a recognition element (as seen in **Figure 7**). Reporter tags may include chemical handles or peptides that enable the manipulation and isolation of enzymes bound to the probe, as well as fluorophores that allow for tracking of captured enzymes. Importantly, these tags do not interfere with the probe-enzyme interaction.[130]

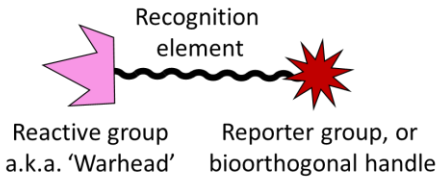

Figure 7: General structure of ABPs.

ABPs have been widely used in medicinal chemistry to support the discovery, design, and synthesis of enzyme inhibitors across several classes, including serine and cysteine proteases.[131, 132] By directly reporting functional target engagement and selectivity in biological systems, ABPs facilitate compound discovery and optimisation, enabling the prioritisation and refinement of active molecules. In drug discovery, small molecule libraries are typically screened using biochemical and phenotypic assays to identify compounds that elicit a desired biological effect,[133] which may subsequently be developed into lead compounds through further pharmacokinetic and pharmacodynamic evaluation.[134] Within this context, ABPs can function either as reversible or irreversible inhibitors, analogous to therapeutic drugs, or as chemical probes for selectively labelling and isolating active enzyme populations.[135] The Activity-Based Protein Profiling (ABPP) approach utilises ABPs to selectively label and interrogate populations of active enzymes in a proteome.[136] This strategy is summarised in **Figure 8**. This facilitates the discovery of novel drug targets and protein binders of small molecules, with the potential to elucidate active sites of targets.[137] ABPs can help gain insight into the metabolic and signalling pathways related to disease, a benefit demonstrated in cancer investigations.[138] Additionally, temporal activation of ABPs is possible through external stimuli. In one example, photoactivatable inhibitors of presenilin 1 and 2 were synthesised. Upon UV irradiation, these probes covalently bound their targets.[139] In another example, a pH-responsive probe was designed, which exhibited near-infrared fluorescence and generated singlet oxygen upon near-infrared light exposure. The probe's activation was pH-dependent: it was protonated and

fluorescent in acidic conditions, while remaining inactive in neutral pH environments.[140]

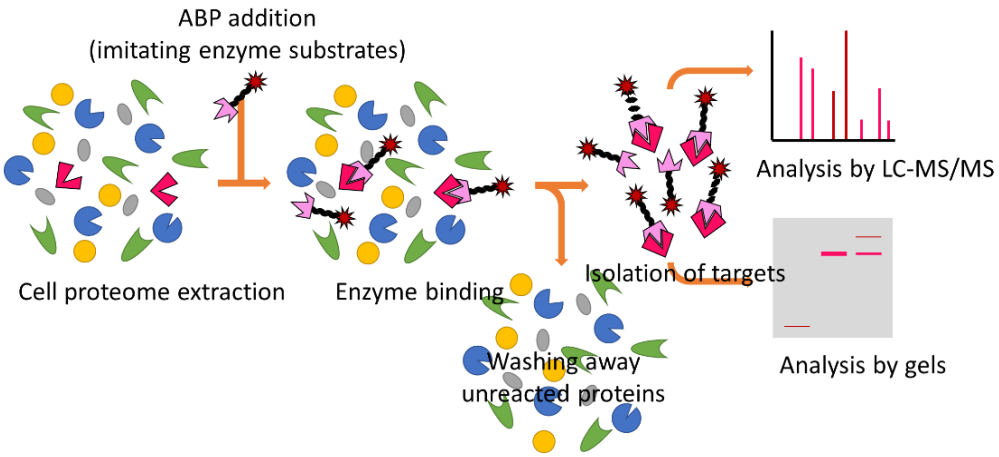

Figure 8: ABPP Strategy for capturing active enzymes using ABPs.

1.4. Ubiquitination

1.4.1. Ubiquitin cascade

One of the early and highly conserved protein systems is ubiquitination,[141] as well as structurally related ubiquitin-like proteins (UBLs),[142] which are thought to have existed in the Last Universal Common Ancestor (LUCA).[143] Ubiquitin itself is a highly conserved, small protein consisting of 76 amino acids, found in all eukaryotic organisms.[144] Ubiquitination is the addition of ubiquitin to other proteins, as a PTM, directing protein substrates to various fates, including involvement in immune cell signalling,[145] regulation of endocytosis,[146] DNA damage response,[147] and proteasomal degradation.[148] In this process, C-terminus of ubiquitin becomes covalently bonded to a lysine residue of a polypeptide substrate, *via* an isopeptide linkage, through the activity of a sophisticated network of Ubiquitin-activating (E1), Ubiquitin-conjugating (E2) and Ubiquitin-ligating (E3) enzymes, as can be seen in **Figure 9**. Ubiquitin itself can be ubiquitinated on one or more of the 7 lysine residues or the amino terminus. Alternatively, or in addition, ubiquitin lysine residues can be modified by ubiquitin-like proteins. Finally, ubiquitin lysines can also be acetylated, while serine and threonine residues can be phosphorylated.

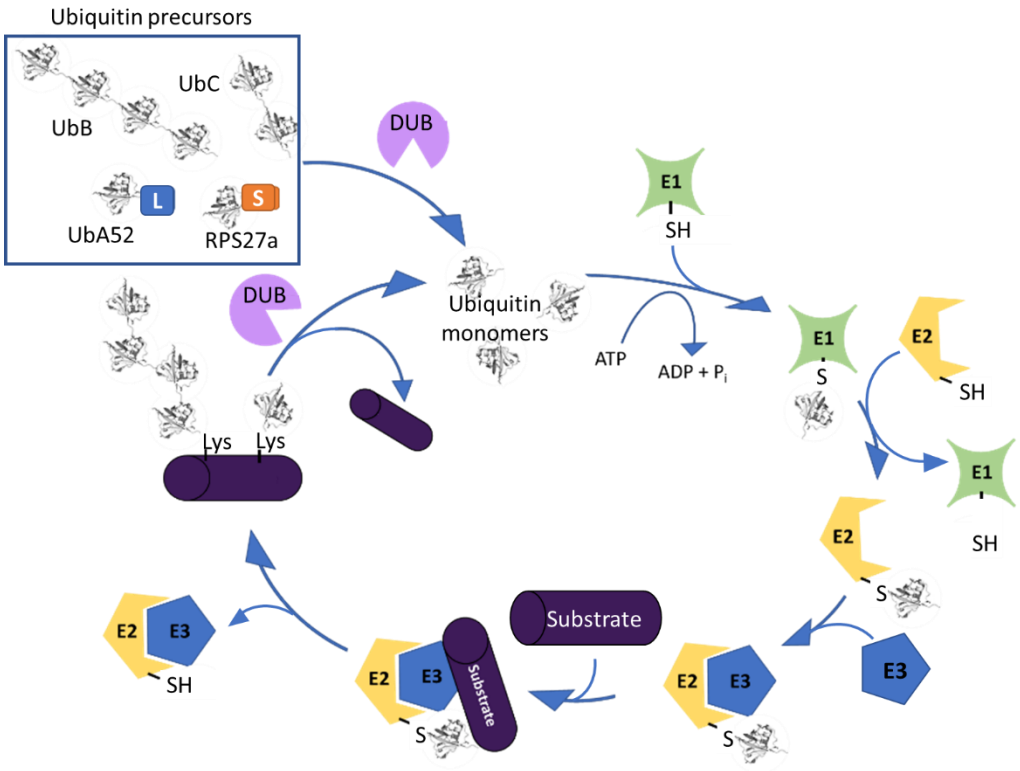

Figure 9: Sequential addition and editing of ubiquitin to other proteins. Ubiquitin, E1, E2, E3, DUBs, and ubiquitin precursors - UbB, UbC, UbA52 are highlighted. *Note.* Image created by the author using Microsoft PowerPoint (Version 2511). Structure of ubiquitin visualised using the PyMOL Molecular Graphics System, Version 3.1.6.1 Schrödinger, LLC. (entry 1UBQ on PDB, in grey).

In the case of polyubiquitination, specific E2/E3 enzyme combinations sequentially add ubiquitin monomers to one or more of the seven lysine residues within the ubiquitin sequence itself, or occasionally to the N-terminal methionine, enabling the formation of ubiquitin polymers with various architectures, including homotypic, heterotypic, mixed, and branched chains.[149, 150] Ubiquitination can be dynamic and transient, therefore regulatory enzymes are needed for precise control over this process. DUBs are a crucial superfamily of isopeptidases specific to ubiquitinated substrates.[151] Specific DUBs cleave isopeptide bonds to edit polyubiquitin chains and remove ubiquitin from substrate proteins.[152] They are also responsible for the initial maturation of ubiquitin from precursor polypeptides, thereby regulating the ubiquitination status and availability of ubiquitin in cells.

The human genome encodes two E1, more than forty E2, six hundred E3 and over a hundred DUB enzymes,[153] highlighting the vast, reversible, and context-specific potential for ubiquitin addition, trimming, and recycling, that remains to be fully characterised. When unbalanced, this vast network of enzymes is implicated in

autoimmune disorders,[154] chronic inflammation,[155] cancer,[156] and neurodegeneration.[157]

1.4.2. Structure of Ubiquitin

It is important to consider the structure of ubiquitin both as a monomer and as a polymer, in order to frame the complexity of ubiquitin's vast and highly regulated interactions with its many binding partners. Polyubiquitin chains can vary in topologies, giving rise to a plethora of unique interactions that take place as a result of processing an unchanging and stable ubiquitin protein.

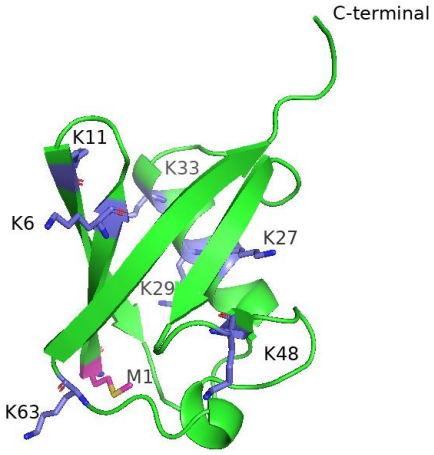

Figure 10: Crystal structure of ubiquitin highlighting potential linkage sites. Visualised using the PyMOL Molecular Graphics System, Version 3.1.6.1 Schrödinger, LLC. (entry 1UBQ on PDB, in green), highlighting seven lysine residues (K6, K11, K27, K29, K33, K48, K63 – in blue), starting methionine (M1 – in magenta), and the C-terminus (the site of isopeptide bond formation).

Ubiquitin (seen with lysine side chains, methionine 1 and C- and N-termini highlighted in **Figure 10**) contains a tight β-grasp fold consisting of a central α-helix, a short 3_{10} helix, and a mixed β-sheet with five strands and seven reverse turns. Three hydrophobic residues found on the α-helix and eleven hydrophobic residues from the β-sheet create a hydrophobic core, reinforced by an extensive hydrogen-bonding network. Due to these structural features, ubiquitin shows high degree of structural stability when faced with changes in pressure,[158] pH,[159] and temperature.[160]

Several ubiquitin-like proteins (UBLs) are also found in eukaryotes which, despite lacking sequence homology with ubiquitin, share its conserved β-grasp fold, highlighting the biological requirement for rigid signalling tags with similar structural features.[161] Small Ubiquitin-Like Modifier (SUMO) is a protein tag impacting substrate degradation, nuclear-cytosolic transport, and the cell's transcriptional regulation.[162]

Neuronal precursor cell-expressed developmentally down-regulated protein 8 (NEDD8) is a protein that tags substrates for roles in cell growth and development.[163] Both deSUMOylases[164] and deNEDDylases[165] reversing these processes exist. Ubiquitin-like analogues and homologues, as well as enzymes for their processing exist in some prokaryotes,[166] and even in extremophilic *Asgard* archaea which are closely related to eukaryotes.[167]

1.4.3. Functional diversity of polyubiquitin chains

Ubiquitin monomers can be covalently linked through isopeptide bonds to form polyubiquitin chains, which mark substrate proteins for distinct cellular pathways. These chains have unique quaternary structures in solution, due to various hydrophobic patches being exposed, or hidden, depending on the linkage and chain length. Notably, structural diversity emerges early on in polymer formation, with distinct three-dimensional confirmations observable in ubiquitin dimers (**Figure 11**).

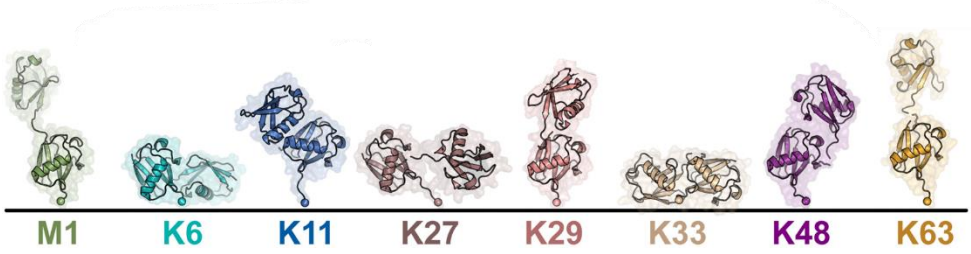

Figure 11: Structural diversity of di-ubiquitin linkage types. The panel displays the distinct three-dimensional conformations adopted by ubiquitin dimers linked *via* the N-terminal methionine (M1) or the seven internal lysine residues (K6-K63). These unique quaternary structures, ranging from compact (e.g., K11, K48) to open (e.g., M1, K63) conformations, dictate the surface exposure of hydrophobic patches. This structural topology serves as a specific code, allowing cellular effectors to distinguish between signals, such as K48-linked chains (proteasomal degradation) and K63-linked chains (signalling and DNA repair). Reproduced with permission from Fanklin, T. G.; Pruneda, J. N., *PLoS Pathogens* **2021**, *17*(3), in Figure 1. Copyright: © 2021 Franklin, Pruneda.

Specific roles of some polyubiquitylated chains in protein processing have been described in the literature. Best-studied are K48-linked polymers.[168] Polyubiquitylated chains of at least four K48-linked monomers target proteins for degradation by the 26S proteosome. The second most studied are the effects of K63-linked polyubiquitination on proteins. Activation of nuclear factor-κB (NF-κB) complex and, therefore, certain immune responses, endocytosis, DNA repair, or

kinases requires K63-linked polyubiquitination.[169] Similar to K48, K11 polyubiquitination is important in protein recycling *via* the proteasome. Linear polyubiquitination through N-terminal Methionine is atypical, although has been shown to participate in immune responses.[170, 171] The purpose of K29-linked linear polyubiquitination is not well understood, however, K29-linked branched polyubiquitination is enriched as a cellular stress response during cell cycle arrest in G1/S phase,[172] and has been implicated in protein degradation during viral infection.[173, 174] The cellular fates of substrates modified with polyubiquitin chains linked *via* K6, K27 and K33 remain poorly understood.

Branched K48/63 chains increase in response to activation of NF-κB signalling,[175] K11 branched ubiquitination is involved in cell cycle control, while K11/48 chains are overrepresented in mitosis,[176] and can be seen as a response to proteotoxic stress.[177] Interestingly, even polyubiquitin chains unanchored to a substrate, so-called 'free chains' have been observed in cellular environments,[178] with functions beyond the standard ubiquitination pathway, such as second messengers in interferon-mediated antiviral responses.[169] Polyubiquitin architecture can be edited by deubiquitinating enzymes (DUBs), which further complicates the tracking of specific polyubiquitination events *in vivo*. Chains linked through different lysine residues adopt distinct structural conformations, exposing specific hydrophobic patches that allow selective binding by downstream partners. This selective recognition directs polyubiquitinated proteins toward different cellular fates. Despite insights into how polyubiquitin chain architecture influences protein fate, considerable gaps remain in our knowledge of the diverse biological roles of polyubiquitin chains.

1.5. Role of DUBs

1.5.1. DUBs and their activities

Over 100 members of the superfamily of DUBs exist in the human genome. They fall into either cysteine protease or zinc metalloprotease classes, based on their mechanism of action. Based on their homology, seven distinct families of DUBs have been described so far. The largest of these is the ubiquitin-specific proteases (USPs). The other families include ubiquitin C-terminal hydrolases (UCHs), ovarian tumour proteases (OTUs), MIU-containing novel DUBs (MINDYs), Machado-Joseph disease protein domain proteases (MJDs), zinc finger with UFM1-specific peptidase domain protein (ZUFSP), and Jab1/Mov34/Mpr1 (JAMM) metalloproteases.[180] Activity of DUBs

in vivo is regulated by their differential expression in tissues, restricted localisation within a cell, and PTMs.[181]

Lack of control over ubiquitin editing contributes to the onset and progression of certain diseases. In some cases, overactive DUBs can inhibit the degradation of misfolded proteins, contributing to their accumulation,[182] or suppress immune signalling pathways, attenuating immune responses.[183] In other cases, inactive or downregulated DUBs fail to stabilise tumour suppressors, leading to their degradation.[184]

1.5.2. Diseases associated with disregulated DUBs

Faulty protein processing is related to several 'Hallmarks of Cancer'.[185-7] As a central mode of marking proteins for degradation, ubiquitination and ubiquitin processing are often dysregulated in cancer. Ubiquitination controls the cell cycle by regulating cyclins and Cyclin-Dependant Kinases (CDKs). Sequential activation, followed by removal of previous cyclin/CDK complexes by ubiquitin-linked proteasomal degradation drives cell cycle progression.[188-190] DUBs also regulate cell proliferation[191] through targeting key signalling pathways in cell proliferation, such as the Wnt/β-catenin pathway.[192, 193] Tumour suppressors are also targets of DUBs.[194] Ubiquitination status of tumour suppressor p53 can be changed by ATXN3,[195] CYLD,[196] OTUB1,[197] OTUD1,[198] amongst others. Changes in ubiquitin status of members of PI3K/AKT/mTOR signalling pathway,[199] Androgen Receptor signalling,[200] and Transforming Growth Factor Beta (TGF-β)[201] are also associated with cancer onset. DUBs target apoptotic machinery, allowing cellular evasion of death.[202-205] Additionally, DNA damage response elements are subject to ubiquitination.[206-210] OTUB1, DUB3, and USP3 stabilise Epithelial–Mesenchymal Transition (EMT) factors in metastatic carcinomas.[211, 212] Rpn11, a component of the 19S regulatory 'lid' of the 26S proteasome, has also been implicated in human cancer.[213] Lastly, high expression of 14-3-3γ has been found in breast cancer and Non-Small Cell Lung Cancer (NSCLC), promoting cell migration,[214] and 14-3-3γ is regulated by USP37 *via* deubiquitination.[215]

Mutations that potentially lead to neurodegenerative diseases, including Alzheimer's, Parkinson's, Huntington's and Amyotrophic Lateral Sclerosis, are often found in genes involved in protein degradation and clearance pathways. Changes in DNA damage response, apoptosis and cell proliferation due to dysregulated DUBs contribute to neurodegeneration. Additionally, autophagy, mitophagy, receptor trafficking and neuroinflammation are affected in the nervous system by issues with

specific DUB activities. DEP-domain containing mTOR interacting protein (DEPTOR), an inhibitor of mTOR is continuously ubiquitinylated and degraded.[216] During starvation, DEPTOR is stabilised by OTUB1 deubiquitination, inactivating mTOR, and leading to the formation of unc-51-like autophagy activating kinase 1 (ULK1) complex, starting autophagosome formation and clearance of toxic proteins. ULK1 is also stabilised by USP20,[217,] which promotes autophagy initiation. DUBs such as USP30,[218] and USP15 oppose the activity of Parkin. Parkin is an E3 ligase that functions as a tumour suppressor by ubiquitinating oncogenic or pro-survival factors such as HIF-1α and mitochondrial GAPDH, promoting their degradation and inhibiting tumour progression. Inhibiting USP30 may have a positive impact on Parkinson's disease prognosis.[219, 220] Uncleared ubiquitylated proteins have been found in intracellular inclusions diagnostic of neurodegenerative diseases, such as: Lewy bodies of Parkinson disease,[221] neurofibrillary tangles and senile plaques of Alzheimer disease,[222] Pick bodies of Pick's disease,[223] Rosenthal fibres in astrocytes of Alexander Disease patients,[224] Lewy body-like hyaline inclusions of Familial Amyotrophic Lateral Sclerosis,[225] and intranuclear inclusions in Huntington's disease.[226] Defects in USP8,[227] USP13,[228] USP14,[229] USP22,[230] USP25,[231] USP46,[232] UCHL1,[233] and ATXN3[234] are also implicated in neurodegeneration *via* disrupted protein degradation.

K63-linked polyubiquitination is vital for the activation of immune responses.[235] Specifically, NF-κB transcription factor regulates innate immunity through transcription of pro-inflammatory cytokines. CYLD is a DUB known to directly impact components of the NF-κB pathway,[236] and its substrates often contain K63-linked polyubiquitin chains. These substrates include Tumour-Necrosis Factor Receptor-Associated Factor (TRAF) family of proteins, TAK1 kinase complex, the IKK regulatory subunit IKKγ, and others.[237] CLYD has also been implicated in susceptibility to bacterial infection. Loss of CYLD allowed for prolonged mouse survival after acute lung injury caused by *Streptococcus pneumoniae*.[238] CYLD additionally diminished NF-κB activation and lowered immune response in the lungs of mice infected with non-typeable *Haemophilus influenzae*.[239] During viral infection, DUBA inhibits self-ubiquitination of E3 ligase TRAF3, and thus suppresses Interferon-I activity.[240, 241] Overexpression of OTUB1 and OTUB2 lowered NF-κB activation and therefore immune response *in vitro*, while their knockdown caused an opposite effect. Deubiquitinating TRAF3 and TRAF6, attenuated innate immunity.[242] CYLD in known to regulate T-cell development from thymocytes[243] as adaptive immunity is activated. CYLD stabilises tyrosine kinase LCK interaction with target kinase ZAP70.[244] ZAP70, in turn, regulates

the maturation of T-cells from double-negative to double-positive cells. Several E3 ligases have been noted to be responsible for targeting self-reactive T-cells for degradation, including CBL-B, TRAF6, GRAIL, ROQUIN and ITCH.[245] USP9X has been found to regulate ITCH,[246] while OTUB1 was seen to allow for T-cell anergy – a process where T-cells are inactive to antigens, but are left alive for extended periods of time in a functionally attenuated state.[247] CYLD is involved in T-cell activation through impacting IKKγ and TAK1.[248] B-cell maturation in adaptive immunity requires signals from the previously described NF-κB pathway, making CYLD a crucial regulator for this process.[249]

Although prokaryotes do not produce ubiquitin, they evolved specific DUBs which cleave polyubiquitin and UBL protein chains.[250] Several examples of DUBs unique to prokaryotes have been described in literature.[251] Viral tegument-like deubiquitinases have been demonstrated to actively diminish cellular ubiquitin-dependent processes, suppressing innate antiviral responses.

1.6. Probing cysteine protease DUBs

DUBs can be probed using a variety of recognition elements, including small molecules that mimic ubiquitin or substrate motifs, inhibitors that selectively engage particular DUBs, and ABPs that covalently label active enzymes. Together, these tools allow the study of DUB activity, specificity, and regulation *in vitro* and in cells, and can also inform the development of therapeutic inhibitors targeting DUBs.

1.6.1. Small-molecule probes of cysteine protease DUBs

Many small-molecule ABPs of DUBs have been reported in the literature.[252, 253] Some of them include fluorescent ABPs such as 8RK59 (**Figure 12 A**, compound **4**), and its rhodamine-tagged derivative 9RK87 (**Figure 12 B**, compound **5**), which covalently label UCHL1 *in vitro*, in cell lysates, live cells and zebrafish embryos.[254] Another UCHL1 probe, GK13S (**Figure 12 C**, compound **6**) has a high specificity for that DUB even in cellular contexts.[255]

A)

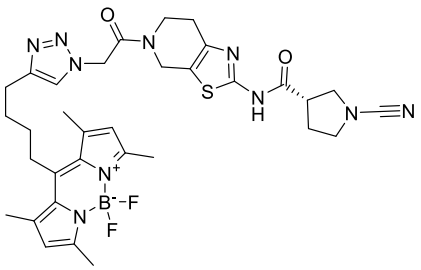

4

B)

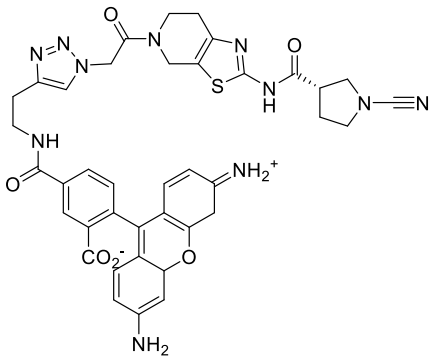

5

C)

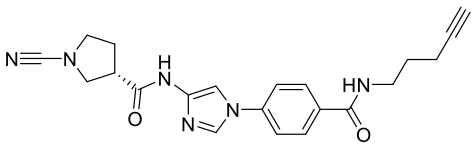

6

Figure 12: UCHL1-specific small-molecule binders. **A:** fluorophore 8RK59 (**4**), **B:** fluorophore 9RK87 (**5**), **C:** cell-permeable ABP of DUBs, GK13S (**6**).

Some small-molecule pan-DUB include IMP-2373 (compound **7**, **Figure 13 A**),[256,] a pan-DUB ABP, and *N*-methylpyrrole derivatives, compounds **8** and **9**, which are USP-specific (**Figure 13 B** and **C**, respectively).[257]

A)

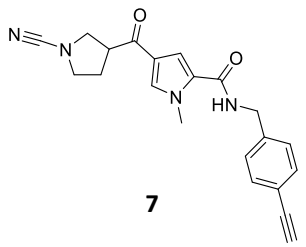

7

B)

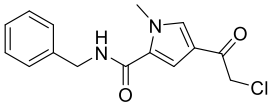

8

C)

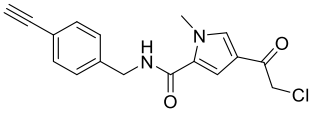

9

Figure 13: Small-molecule binders of DUBs. **A:** IMP-2373 (**7**),
B: *N*-benzyl-4-(2-chloroacetyl)-1-methyl-1H-pyrrole-2-carboxamide (**8**),
C: 4-(2-chloroacetyl)-*N*-(4-ethynylbenzyl)-1-methyl-1H-pyrrole-2-carboxamide (**9**)

1.6.2. Non-covalent protein-based probes of DUBs

DUB activities can be profiled using ABPs with ubiquitin scaffolds, as these contain large recognition elements imitating DUB substrates. First ubiquitin-based covalent probes for DUB activity were reversible, with aldehyde (Ubal, compound **22**, seen in **Figure 15**),[258] and nitrile (Ub-CN, **16**, seen in **Figure 14**)[259] warheads on the C-terminus.[260] Probes **22** and **16** have been used to help crystallization studies, gain mechanistic insights into DUB activities, and reveal protein complex associations.[261, 262] Reversible binding of **22** has helped in structural investigations. For example, OTUB1 study has shown that conformational changes occur upon initial binding to **22**, allosterically increasing the affinity of OTUB1 to the second ubiquitin.[263]

1.6.3. Second-generation covalent probes of DUBs

Irreversible ABPs for DUBs were created as an alternative to reversible binders. The first example of an irreversible ubiquitin-based ABP targeting DUBs contained a vinyl sulfone (Ub-VS, compound **11**, seen in **Figure 14**) trap in place of the C-terminal Gly-76 residue. The Michael acceptor of the vinyl sulfone was situated at ubiquitin's C-terminus, imitating the natural position of DUB attack, and labelled the catalytic cysteine residue *via* conjugate 1,4-Michael addition. Many Ubiquitin and UBL ABPs with thiol-reactive electrophilic warheads that undergo conjugate (1,4) addition have

been reported since, including Ub-VSPh (**12**), and Ub-OEtVS (**14**), thioacrylonitrile (Ub-CN, **16**), vinyl cyanide (Ub-VCN, **13**), methyl ester (Ub-VME, **15**),[264] and dehydroalanine (Ub-Dha-*N*-methylamide, **17**).

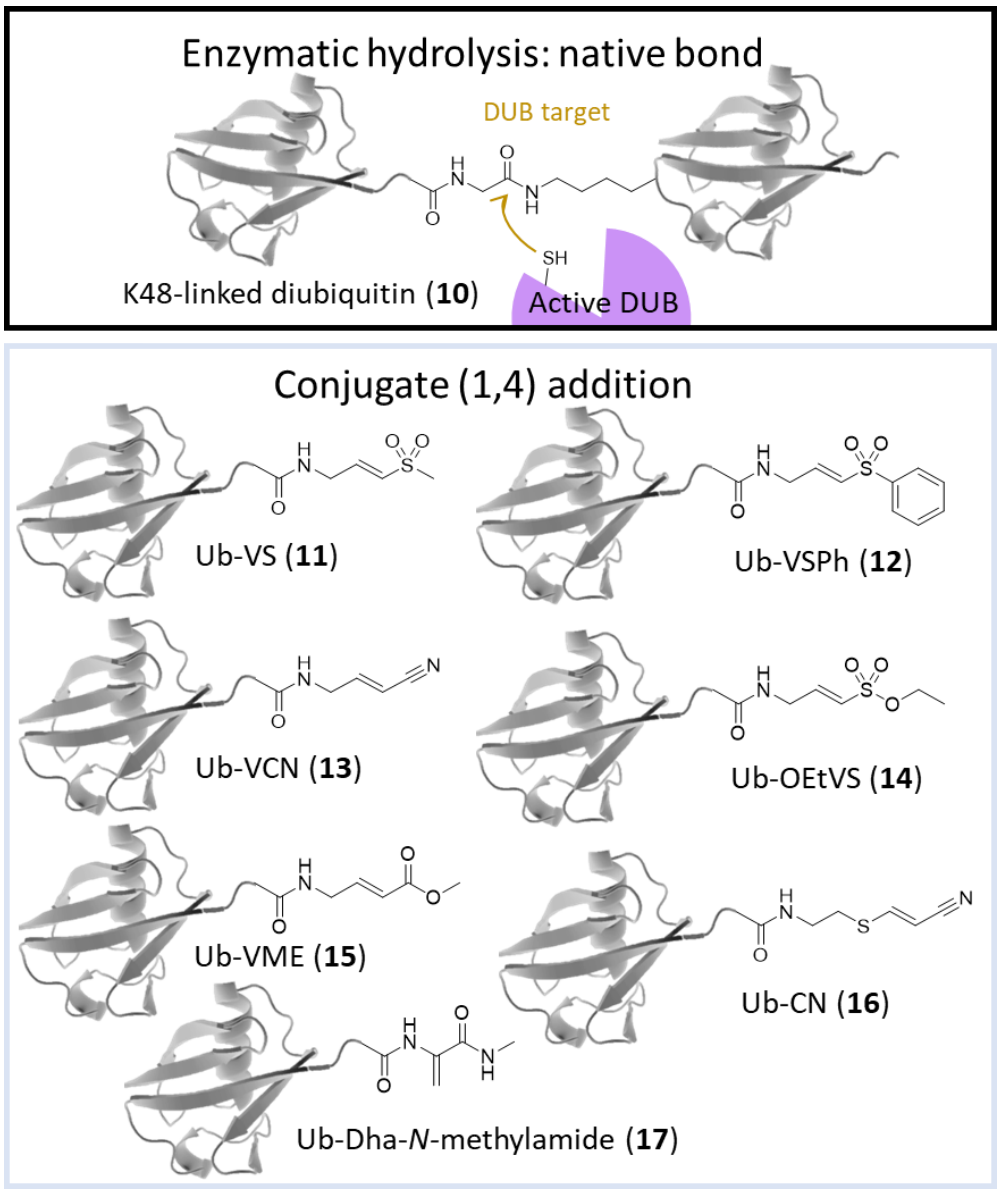

Figure 14: Cysteine-reactive warheads and their mechanisms of action – compared to native isopeptide bond. Ub - Ubiquitin$_{1\text{-}75}$.

Ub-Prg (**23**), which contains an alkyne warhead (seen in **Figure 15**), reacts with cysteine protease DUBs *via* direct (1,2) addition. Catalytic cysteine performs a direct nucleophilic attack on the terminal alkyne.[265] The transition state between an alkyne and a vinyl thioether is stabilised by the oxyanion hole within close proximity to the active site.[266]

Ub-Lac (**21**) is an electrophilic ABP seen in **Figure 15**, which forms an irreversible covalent bond with the catalytic cysteine of DUBs *via* nucleophilic attack and ring opening of the strained β-lactone warhead. Other electrophilic ABPs may incorporate leaving groups, such as halides, enabling nucleophilic substitution by the activated catalytic thiol of a target enzyme. These include Ub-Br2 (**18**), Ub-Br3 (**20**) and Ub-Cl (**19**).[267] Ub-Monomeric probes have been found to broadly target all DUBs, with little preference for any specific family.[267, 268]

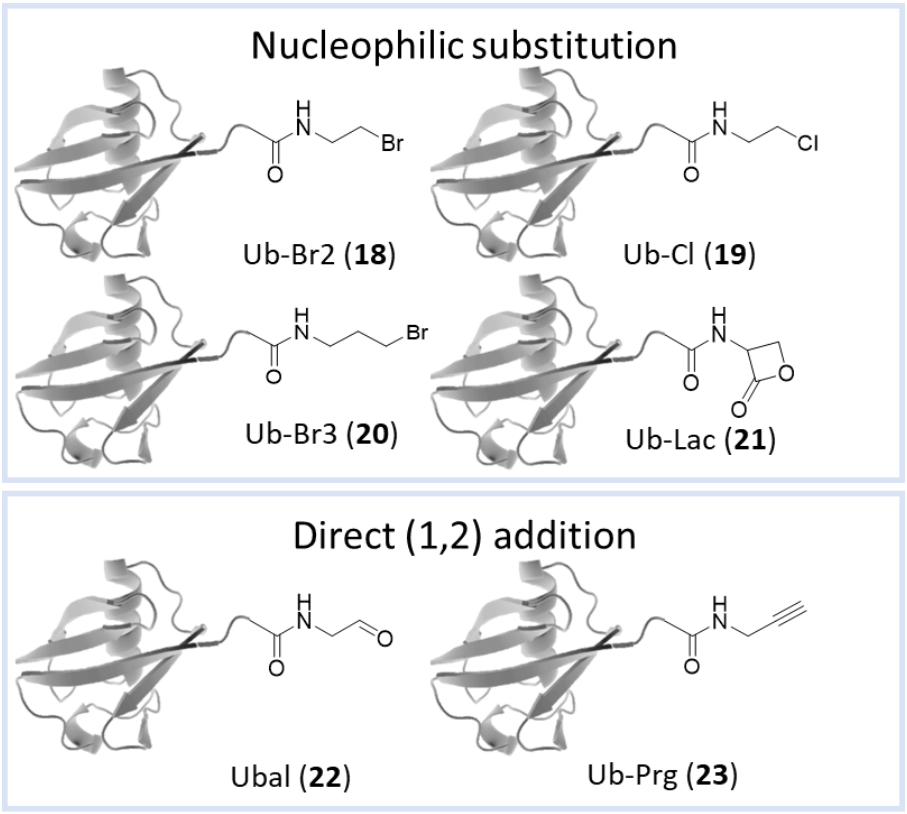

Figure 15: Additional cysteine-reactive monomeric probes of DUBs that act *via* nucleophilic substitution or direct 1,2-addition.

1.6.4. Multimeric ubiquitin probes

Ubiquitin is most commonly found in polymeric forms when functioning in signalling.[269] Di-ubiquitin probes have the advantage of targeting specific DUBs by mimicking the isopeptide linkage and incorporating an extended recognition motif.

Several di-ubiquitin probes have been reported in the literature, featuring chemical traps either between the proximal and distal monomers or within the inter-ubiquitin linker. An azide-containing ubiquitin monomer (**24**) was conjugated to an alkyne-functionalized Ub-VME (**25**) *via* a CuAAC reaction, forming di-ubiquitin

probes with VME-like activity (**Figure 16**).[270] Dimers mimicking all seven isopeptide linkages, as well as a methionine-linked dimer, were synthesised using this approach.

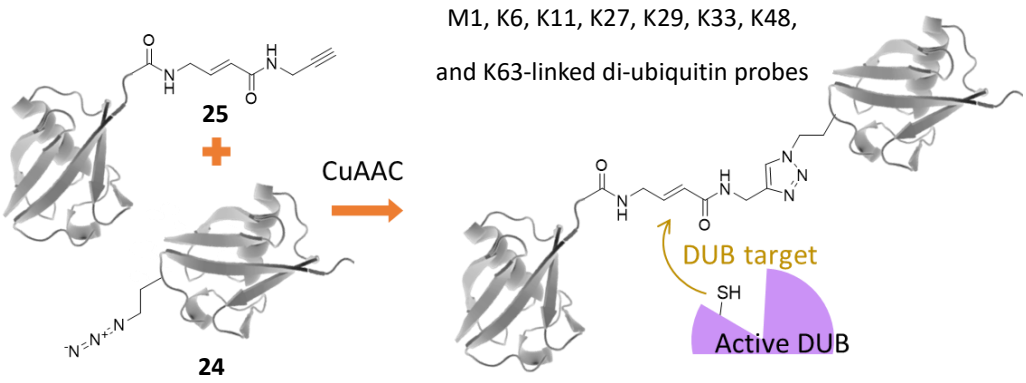

Figure 16: Di-ubiquitin ABPs with VMA-like activity.

Activity-based di-ubiquitin probes designed by McGouran *et al*.[270] exhibit widely varying patterns of enzyme capture and linkage selectivity. For instance, the M1 (linear) di-ubiquitin probe demonstrates unusually broad reactivity, efficiently labelling USP13, USP25, and USP40, despite these DUBs showing little activity toward native linear chains in prior *in vitro* assays.[271] This discrepancy has been attributed to the triazole-based linker used in the probe, which is longer and more rigid than the native isopeptide bond and thus confers reduced specificity and heightened promiscuity. In contrast, many DUB families maintain pronounced linkage preferences. For example, OTUB1 binds strongly to K48-linked di-ubiquitin probes,[272] while OTU7B shows a strong preference for K11-linked probes.[273] The USP16 enzyme displays preferential labelling by K27-linked di-Ub probes, and to a lesser extent, the K29 probe.

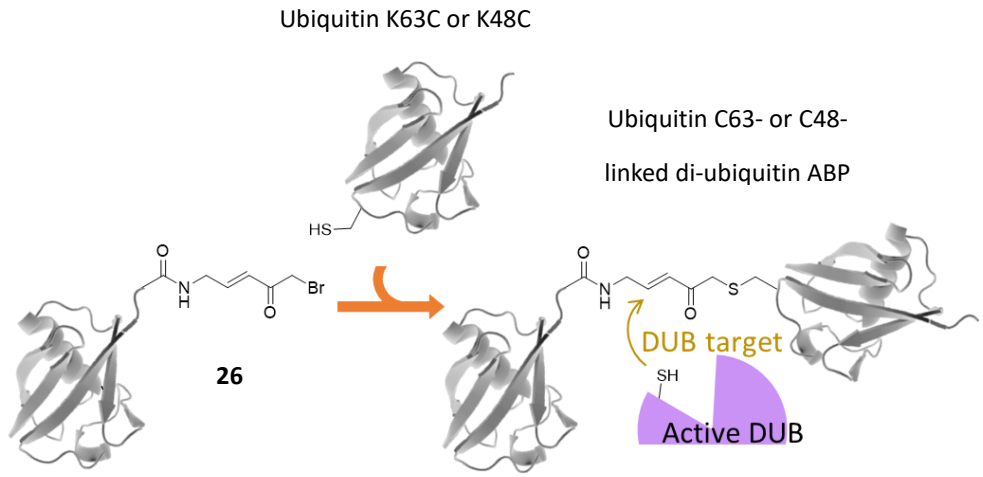

Figure 17: Formation of C63- and C48-linked di-ubiquitin probes.

Formation of another dimeric ubiquitin probe involved conjugation of a ubiquitin containing a reactive α-bromo-vinylketone warhead (**26**) to both a K63C and a K48C ubiquitin mutant, forming two separate probes, each with an α,β-unsaturated ketone linker (**Figure 17**).[274] These probes labelled DUBs *via* a mechanism similar to **15**; however, unlike **15**, C48-linked dimers showed specificity for OTUB1, while C63-linked dimers did not. Both C63 and C48 dimers showed strong binding to USP enzymes, and neither covalently labelled UCH enzymes. The labelling pattern in cell lysates for both C48- and C63-linked dimeric probes was greatly simplified relative to **15**, with each probe giving rise to distinct bands not observed with **15**. This suggested preferential binding of dimeric probes to unique DUBs compared to monomeric ones.

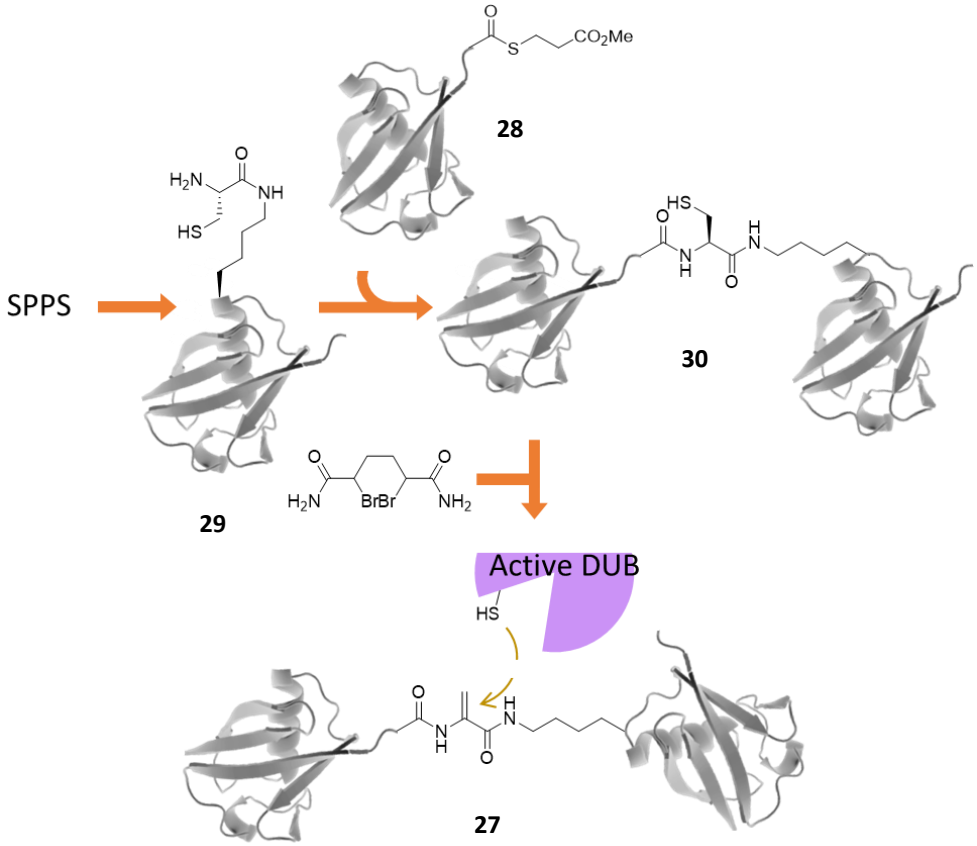

Figure 18: UbGly$_{76}$Dha-Ub formation. SPPS – Solid Phase Peptide Synthesis.

UbGly$_{76}$Dha-Ub (**27**) was also synthesised, as a dimeric ABP (**Figure 18**).[275] Here, two ubiquitin$_{1\text{-}75}$ monomers were first synthesised, one containing methyl 3-mercaptopropionate at the C-terminus (**28**), and the other containing Cysteine at the N-terminus (**29**). Native chemical ligation of the two resulted in thiol-containing **30**, and transformation of linking Cysteine residue into electrophilic Dehydroalanine with 2,5-dibromohexanediamide (DBHDA, **30**) resulted in a di-ubiquitin ABP with Ub-VME-like functionality, **27**. This dimeric ABP had high specificity for OTULIN and

USP5. Polymeric ubiquitin probes have also been reported, further expanding on recognition sequences against DUBs.[276]

Ubiquitin containing an alkyne instead of a lysine can undergo a CuAAC reaction with another ubiquitin containing an azide, enabling the formation of multimeric structures that have been used as probes for ubiquitin-binding proteins, including DUBs.[277]

1.7. Radical probes of DUBs

1.7.1. Probing DUBs *via* radical chemistry

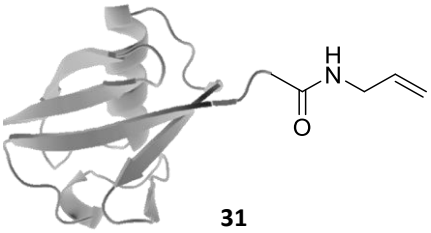

31

Figure 19: Ubiquitin-based ABP containing a terminal alkene (**31**).

A radically-activated ubiquitin ABP for DUBs has been reported, employing a UV-initiated thiol-ene reaction to allow DUB labelling *in vitro*.[82] Specifically, OTUB1, OTUB2, UCHL3 and HEK293T cell lysate containing DUBs were exposed to a terminal-alkene-functionalised ABP (**31**), seen in **Figure 19 A**, under radical conditions. Proteomic analysis revealed that this radical probe labelled DUBs from several classes. The radical thiol-ene reaction used by Taylor *et al*.[82] is summarised in **Scheme 1**. Thiol-ene capturing of DUBs required proton abstraction from a thiol. The resulting thiyl radical reacted with the ubiquitin warhead - a terminal alkene - resulting in a carbon-centred radical. A covalent bond between the C-terminus of the probe and the active site cysteine was formed. Radicals formed propagated this reaction, as long as the sample was exposed to UV light. Alkene-containing probe **31** could have off-target reactions with other proteins containing free thiols; however, preferential labelling of ubiquitin binding proteins was expected. Degassing samples with nitrogen gas was required to improve the rate of DUB labelling, making labelling conditions incompatible with *in vivo* studies. Moreover, UV light has been shown to degrade proteins[278] through mechanisms such as disulfide degradation. Despite these issues, radical chemistry as a novel mode of activating ABPs is attractive, as external stimuli that can be easily controlled (light or heat) initiate radical formation, allowing linking the active site cysteine of DUBs and the alkene probe.

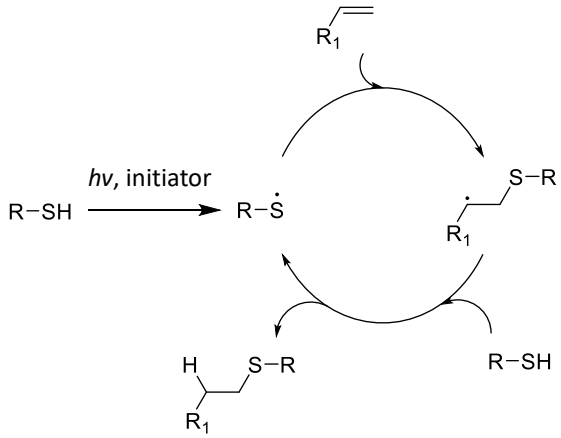

Scheme 1: The radical cycle for a generalised thiol-ene reaction was applied by Neil *et al* to label DUBs with a ubiquitin ABP containing a terminal alkene.

1.8. Thesis objectives

Dysregulation of ubiquitin homeostasis contributes to a variety of diseases, driving the development of inhibitors and probes targeting the ubiquitination machinery. Among these, DUBs play context-specific roles in determining the fate of ubiquitinated proteins, though their functions remain incompletely understood. While small-molecule ABPs and inhibitors have been developed for certain cysteine protease DUBs, and several pan-DUB ABPs have been reported, many DUBs still lack selective tools for interrogation. For example, no covalent small-molecule ABPs have been reported for metalloprotease DUBs.

Monomeric ubiquitin-based ABPs containing electrophilic warheads have shown strong potential in selectively capturing many cysteine protease DUBs. Recent advances include the use of radical thiol-ene reactions to capture DUBs on demand in cell lysates, offering an exciting approach for controlled and temporally precise probing.

To more accurately mimic native DUB substrates, ABPs incorporating larger recognition elements, such as di- and tri-ubiquitin with near-native linkages, have been developed. However, the reviewed literature highlights a lack of multimeric ABPs capable of context-specific and time-resolved probing of polyubiquitin editing by DUBs.

Integrating radical-initiated DUB capture with the linkage-specific recognition of polyubiquitin chains by DUB subsets offers a promising strategy for developing tools that reveal DUB specificities. Such tools could significantly enhance our understanding of DUB function and support the development of targeted DUB inhibitors. This thesis aims to expand the toolbox of protein bioconjugation methods and to form novel probes of DUBs which can be temporarily activated. Methods described in this thesis

could be applied to the construction of novel protein constructs that could target a variety of other cysteine proteases.

Chapter 2 focused on performing light-activated radical thiol-yne and thiol-ene reactions between a ubiquitin construct containing a terminal alkyne and a small molecule containing a thiol. The reaction proceeded *via* sequential thiol-yne and thiol-ene additions, leading to either mono- or bis-adducts, without control over the extent of functionalization. Additionally, biocompatible model systems for thiol-ene labelling of DUBs were explored. One application of the proposed radical thiol-yne bioconjugation method was the controlled formation of dimeric ubiquitin-based ABP with a sterically hindered internal alkene linkage. This construct was designed to mimic native substrates of specific DUB subfamilies and, in principle, could undergo thiol-ene addition at the active site cysteines of DUBs.

In Chapter 3, the controlled formation of di-ubiquitin constructs *via* thiol-yne chemistry was investigated, followed by efforts to purify the resulting products and test their activity in model DUB systems. Due to significant steric hindrance surrounding the internal alkene, the second thiol-ene addition is unlikely to occur efficiently. As a result, the reaction predominantly yielded mono-adducts.

In Chapter 4, the formation of a di-ubiquitin construct containing a terminal alkene was explored. To mimic the native isopeptide linkage found in physiological DUB substrates, lysine residues on the terminal alkene-containing ubiquitin monomer were subjected to azido-exchange, followed by CuAAC reactuion with a second ubiquitin monomer bearing a terminal alkyne. To establish and optimise the azido-modification protocol, initial experiments were performed on Bovine Serum Albumin (BSA), which served as a model protein substrate. This methodology was then applied to a ubiquitin construct containing both an HA tag and a terminal alkene. Subsequent formation of the di-ubiquitin construct *via* click chemistry was reported in a 2024 publication in *Organic & Biomolecular Chemistry*.[279]

To expand probe repertoire to label metalloprotease DUBs, ubiquitin constructs containing lysine-reactive mono-suquaramide warheads were constructed in Chapter 5. Monomeric ubiquitin constructs containing C-terminal mono-squaramides could interact non-covalently with model metalloprotease and cysteine protease DUBs, for long enough to allow covalent binding of non-catalytic lysines near the active site of DUBs.

Chapter 2: Radical bioconjugation of thiol-containing molecules to alkyne-containing ubiquitin ABP

2.1. Objectives

For the construction of di-ubiquitin probes *via* radical thiol-yne reaction, ubiquitin monomers containing an alkyne group and a free thiol were required. The approach selected to achieve this included installation of an alkyne warhead onto the C-terminus of a ubiquitin construct, resulting in ubiquitin with a terminal alkyne **23**, as well as expression and purification of a lysine-to-cysteine ubiquitin mutant, Ubiquitin K48C. The structure of **23** is shown in Scheme 1, which also illustrates its activity as an electrophilic ABP of DUBs. Additionally, ubiquitin-based radical ABP containing a terminal alkene (**31** seen in **Scheme 2**) was prepared, to test biocompatible conditions for thiol-ene labelling of DUBs

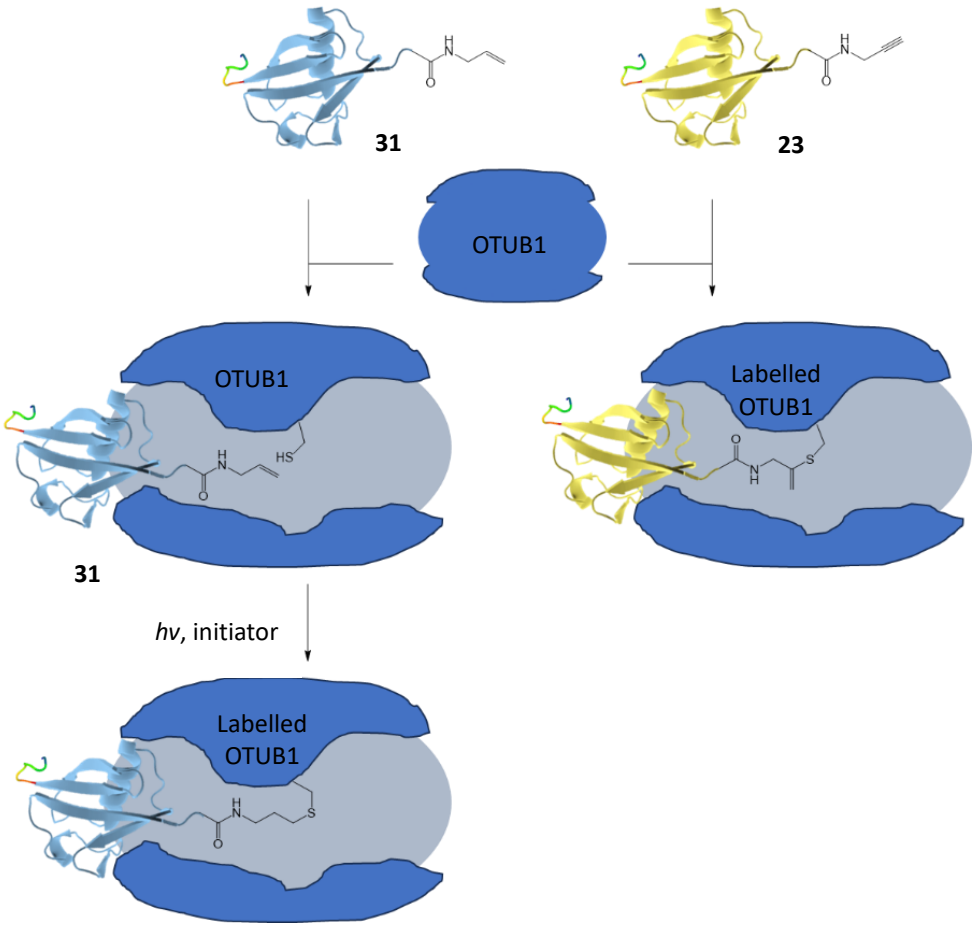

Scheme 2: Comparison of spontaneous versus light-activated DUB labelling mechanisms. (Right) Electrophilic probe **23** undergoes spontaneous nucleophilic attack by the active site cysteine of OTUB1. (Left) Radical-based probe **31** binds non-covalently to the active site, but remains inert in the absence of a trigger.

Biocompatible radical conditions for labelling model DUBs *via* thiol-ene conditions included incubation of radical ABP **31** with OTUB1, in the presence of LAP (**32**), or Riboflavin (**33**) and co-initiators: TEA (**34**) or DIPEA (**35**), followed by visible light or UV irradiation. Radical activator DMPA (**36**), seen in **Figure 20**, and its stabiliser MAP (**37**), previously used by Taylor *et al*. were used for radical initiation, as positive controls. These initiators and co-initiators can be seen in **Figure 20**. The objective was to create a biocompatible protocol for thiol-ene labelling of DUBs that could be used for *in vivo* investigations in the future.

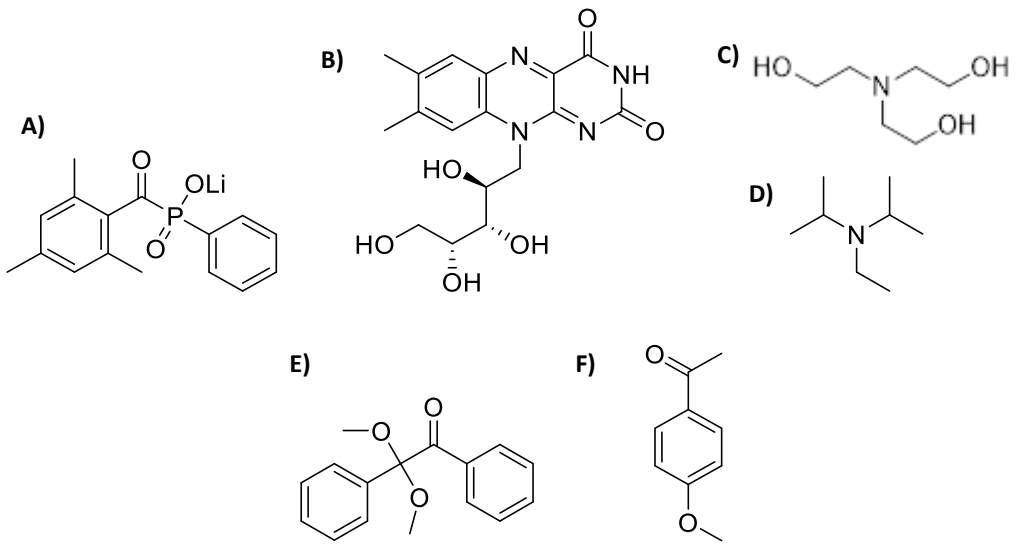

Figure 20 A: Structures of Lithium phenyl-2,4,6-trimethylbenzoylphosphinate (LAP, **32**), **B**: Riboflavin (**33**), triethanolamine (TEA, **34**), **C**: *N*,*N*-Diisopropylethylamine (DIPEA, **35**), **D**: 2,2-dimethoxy-2-phenylacetophenone (DMPA, **36**), 4'-methoxyacetophenone (MAP, **37**).

Final objective of this chapter is the application of radical chemistry for the thiol-yne adduct formation between alkyne-containing ubiquitin monomer and thiol-containing small fluorophores, and large proteins, for the purpose of developing a model system that can be applied later to thiol-containing ubiquitin for di-ubiquitin formation.

2.2. Semi-synthetic construction of ubiquitin ABPs containing alkyne and alkene warheads, their activation, and preparation of Ubiquitin K48C

Following established procedures,[261] monomeric ABPs of DUBs were constructed (**Scheme 3**). Construct **38,** containing an N-terminal human influenza

haemagglutinin (HA) tag, ubiquitin sequence 1-75, and an intein domain linked to a Chitin Binding Domain (CBD) was expressed in BL21 (DE3) *E. coli* cells. After cell lysis, intein-containing **38** was captured on chitin beads, while other cellular components were washed away. An Asp to Ala mutation within the intein sequence resulted in an equilibrium between the amide and thioester bonds at the N-terminus of intein domain. Incubation with excess sodium 2-mercaptoethanesulfonate (MESNa, **39**) allowed for thiolysis, resulting in the elution of **40**, which contained MESNa at the C-terminus. Construct **40** was concentrated using 5 kDa MWCO filters, and *N*-hydroxysuccinimide (**41**) was added to the mixture to activate the thioester, in the presence of a primary amine precursor of the target warhead. The amine could attack the thioester, leading to the insertion of a desired warhead at the C-terminus of the construct. Addition of propargylamine (**45**) and allylamine (**46**) resulted in the formation of **23** and **31**, respectively, both of which have been reported as DUB ABPs.[265]

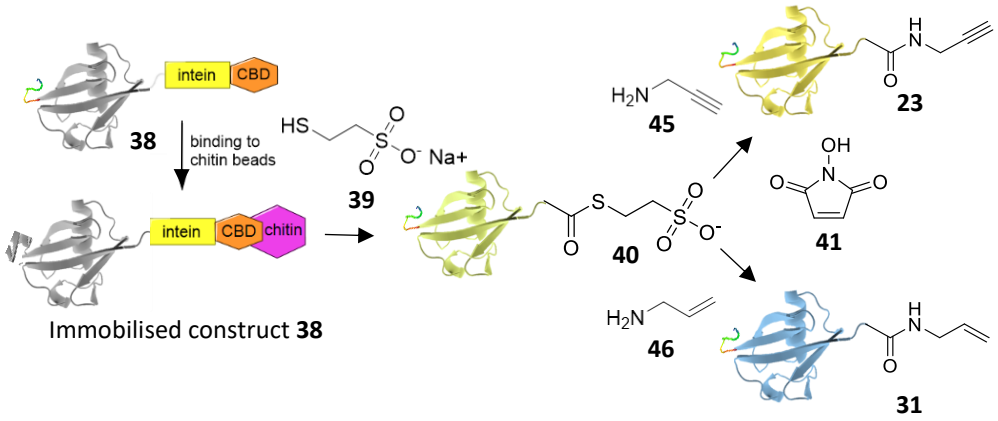

Scheme 3: Construction of monomeric ubiquitin-based probes of DUBs

2.2.1. Identification and activity of established monomeric ABPs

Once constructs **23** and **31** were synthesised, their identities were confirmed by Mass Spectrometric analysis of their tryptic and elastase digests. Trypsin is an endopeptidase, which cuts proteins after arginine and lysine residues, unless proline immediately follows them, while elastase cleaves at the C-terminus of alanine, valine, serine, glycine, leucine or isoleucine. Tryptic digests produced consistent, high-quality peptides. Elastase digests enabled sequencing of protein regions lacking arginine or lysine residues, thereby increasing sequence coverage; however, peptide signals were less consistent and of lower quality. UniProt human protein database was modified to include the HA tag (amino acid sequence: YPYDVPDYA) and variable modifications of glycine were added to account for the warheads when searching LC-MS/MS spectra.

Validated peptide sequences met a 1% Peptide Spectrum Matching False Discovery Rate (PSM FDR). Alkyne-containing ABP **23** was found with 62.88% validated protein coverage after trypsin digestion, and 89.08% non-validated protein coverage after elastase digestion, as seen in **Appendix A**. Alkene-containing ABP **31** trypsin digestion resulted in 79.91% validated protein coverage, and elastase digestion with 70.74% validated protein coverage and the entirety of the HA tag was detected, as seen in **Appendix B**. BSA, as well as a water sample, were treated with trypsin and elastase and run in a sequence on LC-MS alongside both probes, in a random order, to provide a control for the digestion process and account for instrument calibration. BSA was detected by LC-MS/MS as a potential contaminant in the UniProt database, with 26.36% protein coverage after trypsin digestion, and 15.49% protein coverage after elastase digestion, as seen in **Appendix C**. Samples containing water on their own showed the presence of both trypsin and elastase, identified as common contaminants, with 24.28% and 15.49% protein coverage, respectively, as seen in **Appendix D**. Trypsin digestions were performed from this point onwards, unless otherwise stated.

To confirm activity of the resulting constructs as ABPs of DUBs, probes were incubated separately with 1 µg OTUB1 (a model purified DUB), and with 50 µg HEK293T cell lysate, and samples containing alkene probe **31** were incubated with radical initiator **36** and co-initiator **37,** followed by degassing under a nitrogen stream and irradiation with UV light. On the anti-HA Western blot, bands from both constructs **23** and **31** were seen at ~10 kDa (**Figure 21 A**, lanes 1 and 2), while OTUB1 and HEK293T lysate can be seen on the silver stain (in **Figure 21 B**, lanes 3 and 4, respectively). OTUB1 is seen on silver stain to be around 34 kDa in size, and after labelling with alkyne probe **23**, a second band appears in both Western blot and silver stain at 43 kDa in lane 7. Alkene probe **31** labels OTUB1 in lane 5 only under radical conditions, while several bands corresponding to the presence of the HA tag can be seen in **Figure 21 A**, lane 6, suggesting multiple proteins in the cell lysate are labelled under radical conditions by **31**. Thiol-ene labelling of DUBs using alkene probe **31** was shown to require radical intiators previously,[82] therefore negative controls were not included on this gel. OTUB1 labelling intensity with alkene-containing **31** is lower than the alkyne-containing **23**, as seen on the Western blot and silver stain in **Figure 21**. Distinct labelling patterns in the Western blot are seen when cell lysates are incubated with **31** or **23** (lanes 6 and 8).

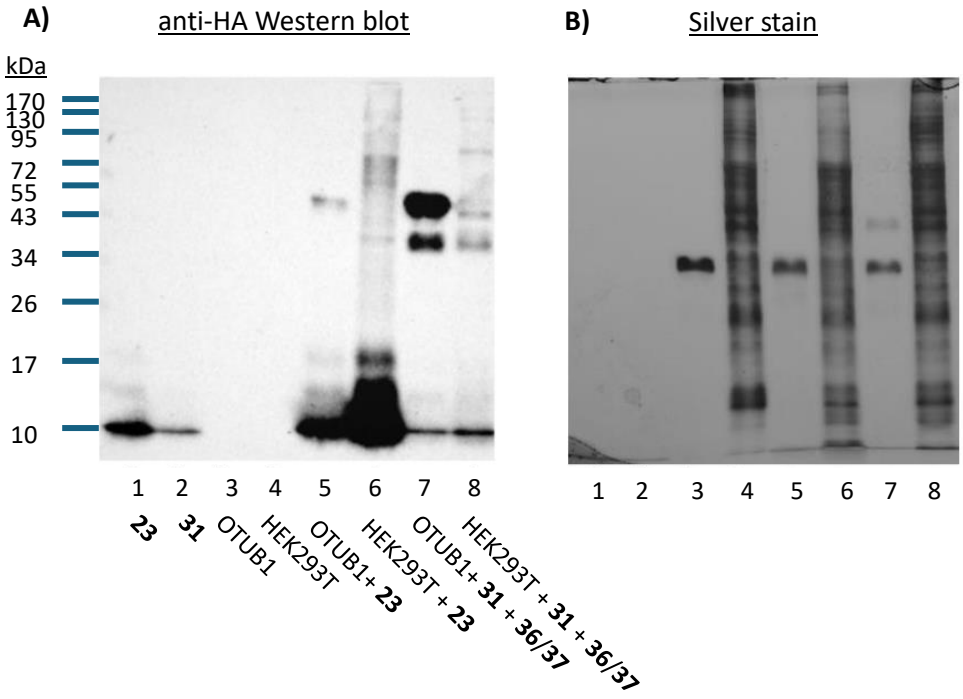

Figure 21 A: Anti-HA Western blot and **B:** silver stain analysis of probes **23** and **31** binding DUBs in model systems, OTUB1 and HEK293T cell lysate. Radical initiation required the addition of **36** and **37**, degassing under a nitrogen stream, and irradiation by UV light for 2.5 min.

2.2.2. Investigating biocompatible radical initiators for thiol-ene chemistry

Monomeric ubiquitin-based ABPs of DUBs with thiol-ene labelling functionalities could be introduced to living systems, if not for several issues, such as cytotoxicity of radical initiators. Additionally, prolonged UV light exposure can cause cell damage.[280, 281] Alternative thiol-ene reaction conditions for labelling recombinant OTUB1 and HEK293T lysates were investigated, beyond DMSO-soluble photoinitiator **36** with co-initiator **37**. Initiator pair **36**/**37** required the removal of oxygen for efficient thiol-ene labelling, and can be activated only using UV. More biocompatible photoinitiator systems are needed. Although precedence in literature exists showcasing thiol-ene ABP initiation using visible light,[84] when biocompatible radical initiators such as Eosin Y are used and the light source is weaker than UV, a low level of DUB labelling in cell lysates is seen. Recently, progress in biocompatible thiol-ene labelling of proteins in cell lysates has been reported.[83] Addition of initiator **1** followed by UV irradiation showed enhanced protein labelling compared to **36**/**37**. Alternative activation of radicals *via* redox mechanism showed most promise, in the case of manganese (III) acetate, as it did not require a light source for radical initiation. Taken

together, several options now exist for minimally cytotoxic thiol-ene radical labelling of DUBs, which can be used to activate the planned di-ubiquitin construct containing an internal alkene linker.

Riboflavin (**33**) was used as an alternative radical initiation system with TEA (**34**) or DIPEA (**35**), and UV or visible light irradiation. Initiator **33** with either co-initiators **34** or **35** did not require the degassing step, and could initiate radicals under visible light, and the results of thiol-ene reaction initiation with this system can be seen in **Figure 22**. Adding aqueous **34** or **35** solutions with initiator **33** showed labelling of OTUB1 similar to **36**/**37**. Lane 1 shows 2 µg alkene probe **31**, and lane 2 contains 1 µg OTUB1. Lanes 3-11 contain 250 µM radical initiators (either **36** in lane 3, or **33** in lanes 4-11) and varying concentrations of co-initiators. 500 µM co-initiators **34** and **35,** seen in lanes 5 and 8, allowed the best labelling of OTUB1. Using **33** instead of **36** as a radical initiator had the advantage of using visible light, instead of UV, alkene probe **31** to label OTUB1 (lanes 10 and 11) *via* radical thiol-ene reaction, although to a lesser extent than with initiator **36** and UV light. The effect of prolonged exposure to visible light (30 min) on OTUB1 labelling by probe **31** was investigated in lanes 10 and 11. Although some labelling of OTUB1 by the alkene-containing **31** was seen, 2 min of UV exposure in the presence of **36**/**37** resulted in a more intense band at 45 kDa in lane 3 than using **35** with co-initiators. Using 0.5 mM **35** as a co-initiator of **33** was seen to provide the best OTUB1 labelling, compared to other concentrations of riboflavin co-initiators, when exposed to UV and visible light.

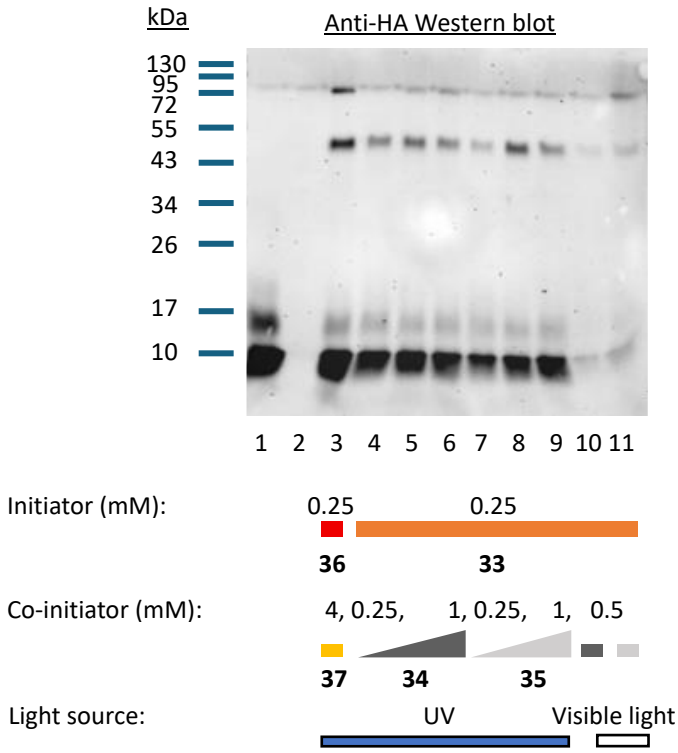

Figure 22: Riboflavin (**37**) as a radical initiator of probe **31**, with increasing concentrations of **34** or **35** as co-initiators, compared to established radical initiators **36**/**37**.

The reaction was further optimised in **Figure 23** by diluting initiator **33** to 125 µM, and using 1 mM of co-initiator **35**. This concentration showed the highest intensity in OTUB1 labelling, seemingly better than the established **36**/**37** system. UV was used as a source of energy, as visible light did not seem to provide better labelling. Silver stain was used to show similar protein content in all wells.

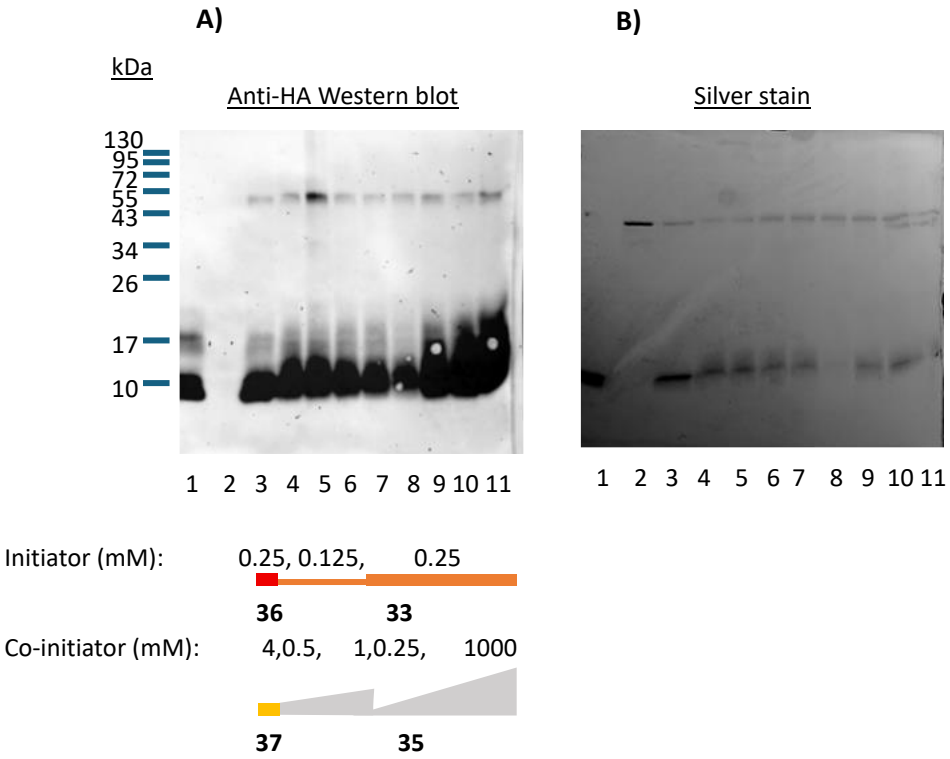

Figure 23 A: Western blot, and **B:** silver stain showing optimisation of **33** and **35** concentrations for radical labelling of OTUB1 by probe **31** under UV light.

Once OTUB1 labelling was optimised, alkene-containing **31** was incubated with HEK293T lysate, followed by radical initiation, as seen in **Figure 23 A**. Lane 1 contained 2 µg of probe **31**, while lane 2 contained 1 µg OTUB1. Lane 3 contained probe **31** incubated with the cell lysate, followed by **36**/**37** addition and UV irradiation for 2.5 min. Lanes 4 and 5 contained increasing amounts of initiator **35**, while lane 6 contained 250 µM of initiator **33** and no co-initiators, and was seen to label the cell lysate faintly. Lane 7 contained both 250 µM **33** and 500 µM **35**, and did not show an increase in band intensity. Lane 8 was a negative control and contained the cell lysate, with **36**/**37**, without probe **31**. Initiators **36**/**37** showed better labelling intensities in HEK293T lysates. **Figure 22 B** shows even loading of lysate samples in all lanes.

It is known that riboflavin **33** at 0.01–100 µM is not cytotoxic in mouse fibroblasts when kept in the dark, while showing marginal cytotoxicity at 1 µM under UV light (340-400 nm).[282] 500 µM of **33** was seen to be slightly cytotoxic for corneal cells when exposed to UV light for 30 min (at 370 nm).[283] Melanoma cells exposed to visible light for over 10 min at 10–25 µM of **33**, and bladder cancer cells exposed for 24 h at 10 µM of **33** showed signs of cell death.[284] In the case of **36**/**37** radical initiation

system, 2 mM of **36** and brief UV exposure (1–2 min) resulted in 5–30% drop in cell viability.[285]

Although the exact dose of radical initiators required to cause cell death depends on the cells investigated, as well as the length of UV exposure, **36**/**37** is more cytotoxic at higher concentrations (≥2 mM) under 365 nm UV due to radical generation, while riboflavin **33** is more cytotoxic at lower concentrations due to ROS production. **33**'s cytotoxic effect plateaus at 0.1–0.5 mM, while **36**/**37** becomes increasingly destructive beyond 2–4 mM under UV. The results in **Figure 24** show that radical labelling of purified DUBs such as OTUB1 with probe **31** can be achieved with alternative, potentially less cytotoxic radical initiators. Riboflavin **33** requires both light and oxygen to generate radicals, while the presence of radical quenchers, such as superoxide dismutase, catalase, glutathione peroxidase and vitamins C, E, glutathione and melatonin, as well as other antioxidants[286] in cell lysates, could significantly hamper radical labelling. Previously optimised conditions with **36**/**37** were found to be more suitable for lysate labelling.

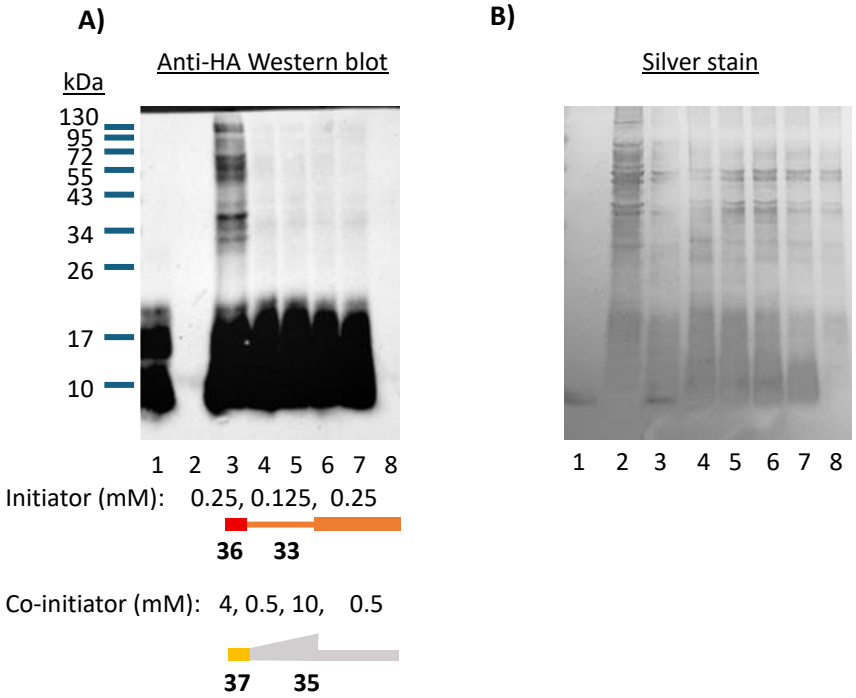

Figure 24: **33**-initiated radical labelling of HEK293T lysate by **31**.

Lithium phenyl-2,4,6-trimethylbenzoylphosphinate (LAP, **32**) has several distinct advantages over riboflavin **33** for radical initiation. LAP **32** is more soluble in water compared to **33**,[287] and doesn't require co-initiators. Radical initiation under visible light with the addition of **32** provided encouraging results, as labelling of HEK293T lysates and OTUB1 was seen without the need for degassing of samples, nor

the presence of co-initiators. Lane 1 in **Figure 25** contained 1 µg OTUB1, lane 2 contained both probe **31** and OTUB1, without radical initiation, and lane 3 contained 2 µg **31**. Lanes 4, 5, and 6 contained probe **31** incubated with OTUB1 after irradiation with UV for 3 minutes, at 2.5, 1, and 0.5 mM LAP **32**, respectively. Labelling under visible light was performed on ice, in lanes 7, 8, 9 and 10 to make sure heat did not cause the reaction. Labelling signal was seen at 55 kDa in samples irradiated with UV and visible light. That could be due to bis-labelling of OTUB1 *via* catalytic Cysteine 91 and non-catalytic Cysteine 23, or the probe oligomerized before reacting under the tested conditions. Alternatively, labelled OTUB1 dimer (68 kDa), or a cross-linked species are the cause for the observed band. Interestingly, excess LAP **32** presence was detrimental to OTUB1 labelling, and 5 mM of **32** in lane 8 did not show any sign of OTUB1 labelling.

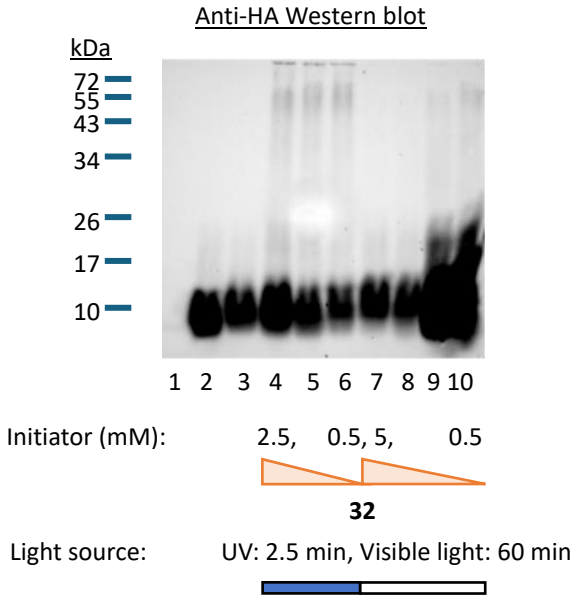

Figure 25: Anti-HA blot showing LAP **32** as a radical initiator of probe **31** for OTUB1 labelling.

LAP **32** was used as a radical initiator of thiol-ene reaction between alkene-containing probe **31** and HEK293T lysate, as seen in **Figure 26**. Lane 1 contained HEK293T lysate, while lane 2 contained probe **31** with lysate, and lane 3 contained probe **31**. Here again, lower concentrations of LAP seem to improve labelling of proteins when exposed to both UV and visible light. At 5 mM LAP **32** (lane 7), no labelling of lysate can be seen when visible light is used as the source of energy, while the best signal is obtained at 0.5 mM **32** (lane 6) when exposed to UV light, and around 10 mM **32** (lane 9) when exposed to visible light.

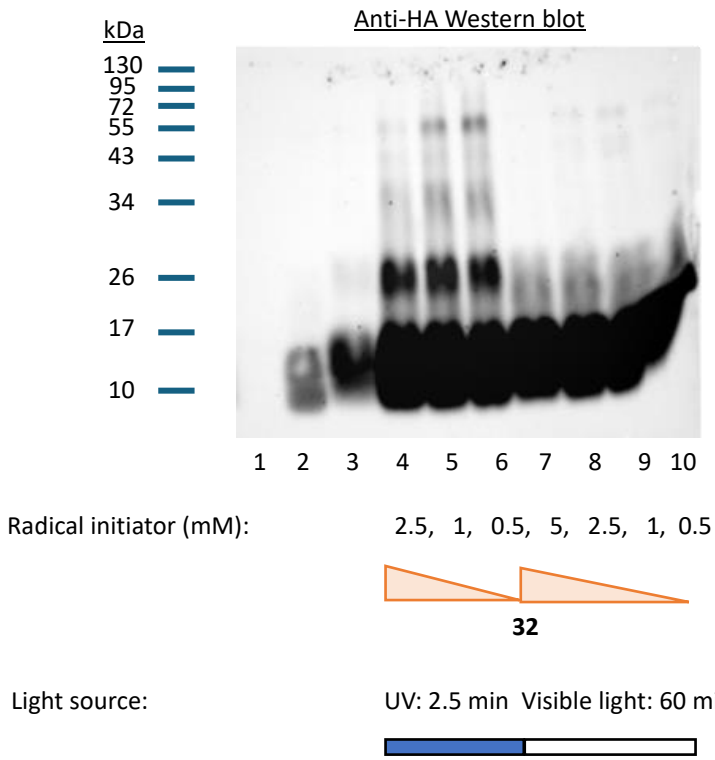

Figure 26: Compound **32** used to initiate radical labelling of HEK293T lysate by probe **31.**

Out of the tested radical initiation systems, LAP **32** seems to present a good compromise in terms of showing some labelling of OTUB1, as well as potentially allowing *in vivo* labelling, due to good water solubility, use of visible light for thiol-ene activation, and lack of degassing required for **36**/**37** radical activation. It was envisioned that the construction of di-ubiquitin probes *via* thiol-yne reaction could be performed using established methods such as **36**/**37** radical initiators and degassing. Thiol-ene activation of the dimeric construct in vitro could then be performed using biocompatible radical chemistry, with **32** as a radical initiator under visible light, or Irgacure2959 **1** under UV light.

2.3. Small molecule adduct formation *via* thiol-yne reaction

2.3.1. Thiol-yne reaction between 23 and fluorophore 42

Previous studies by the McGouran group have revealed conditions needed for free-radical-initiated thiol-ene reaction between thiol-containing DUBs and ubiquitin probes containing alkene warheads.[82] In this section, alkyne probe **23** was shown to undergo a similar thiol-yne conjugation reaction with thiol-containing small fluorophores and proteins under radical conditions. Thiol-yne reaction should result in

an internal alkenyl sulfide moiety connecting **23** and its binding partner. The goal of this work is for the newly formed alkene linkage to undergo further functionalisation *via* thiol-ene chemistry, creating a time-resolved trapping mechanism for other thiol-containing molecules.

To study this idea, a small fluorophore containing a free thiol group was first used as a model for the proposed thiol-yne reaction, as seen in **Scheme 4 A**. Thiol-containing fluorophore **42**, generously provided by Dr. Laura Ramirez Lázaro, has an excitation maximum in the near UV range (~300 nm), while having emission in the yellow/green range (~500 nm), features that can be used in gel visualisation.

A thiol-yne reaction was performed between **42** and **23**, resulting in the protein being modified with either one or two molecules of the fluorophore **42**, resulting in **72.** This was visualised *via* SDS-PAGE. Fluorescence of the adducts at 600 nm was confirmed, as seen in **Scheme 4 B**. **23** incubated with **42** without radical initiation formed no adducts, which was visualised by a slight fluorescent band containing unreacted molecules (lane 1). Under radical conditions, **23** reacted with **42**, forming a fluorescent band slightly above the unreacted molecule (lane 2). Increase in fluorescence was due to adduct formation with the fluorophore, *via* thiol-yne and potentially thiol-ene reactions. Alkyne-containing **23** alone was present in lane 3, and emitted faint background fluorescence when visualised. To confirm the reproducibility of the observed reaction, technical replicates of samples in lanes 1 and 2 were resolved on the same gel, in lanes 4 and 5, respectively (annotated as rep.2).

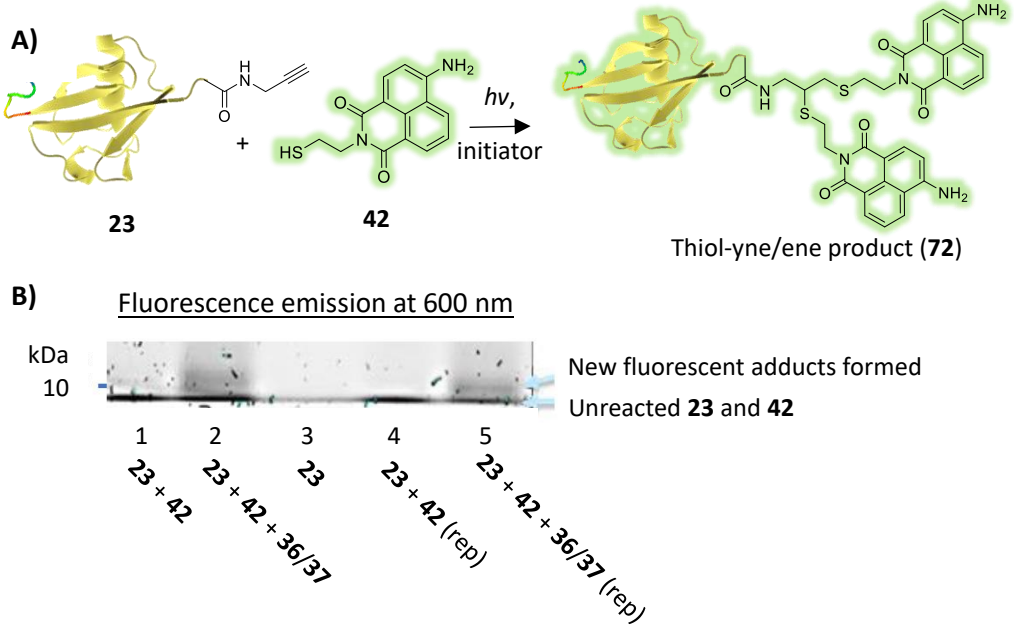

Scheme 4 A: Construction of thiol-yne and thiol-ene adducts between **23** and **42**, **B**: Fluorescence detection of adducts resolved *via* 18% SDS-PAGE.

To remove signal interference from unreacted fluorophore **42**, NAP-5 gel filtration columns, followed by concentration using a 5 kDa molecular weight cut-off filter were employed after radical initiation, prior to resolving samples on SDS-PAGE. Effects of purifying thiol-yne products can be seen in **Figure 26**, in both Ethidium Bromide fluorescence visualisation method and the silver stain.

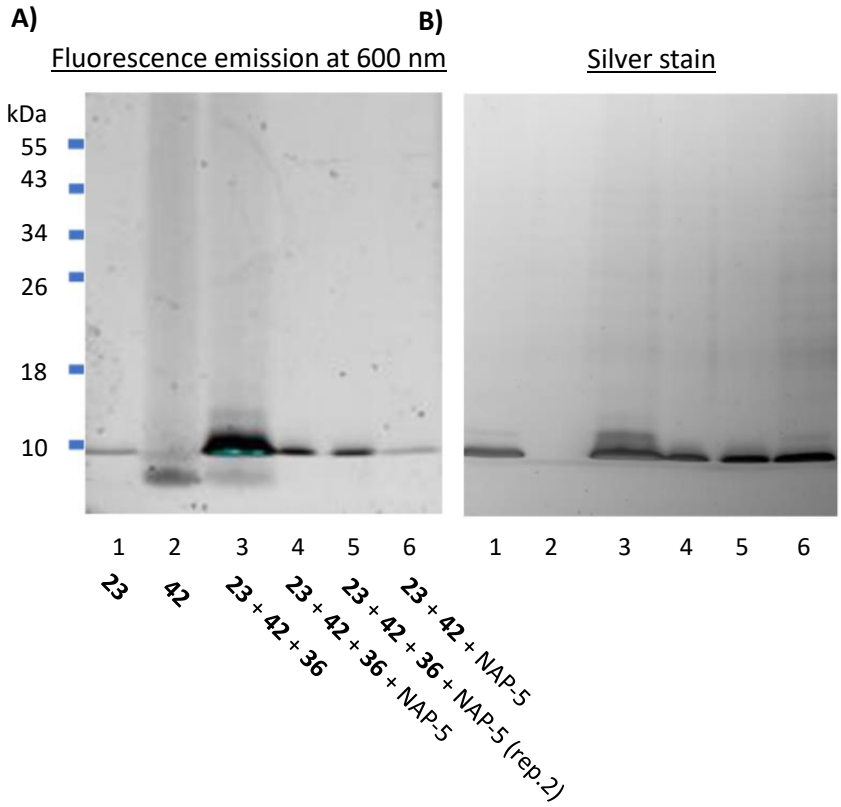

Figure 27 A: NAP-5 purification of thiol-yne product and its visualization *via* 12% SDS/PAGE, visualized by fluorescence at 600 nm, and **B**: silver stain.

Alkyne probe **23** alone displayed slight autofluorescence (lane 1). Fluorescence signal from compound **42** was observed in lane 2, where the fluorophore migrated with the dye front, forming a band near the bottom of the gel. A smearing effect throughout the entire length of the lane was observed in samples that contained the fluorophore, which were not purified *via* NAP-5 columns, due to the low solubility of fluorophore **42** in water. Lane 3 contains the product of a thiol-yne reaction between **23** and **42**, without removal of unreacted fluorophore **42** from the sample prior to injecting onto a gel. Smearing of compound **42** seen in lane 3, **Figure 27 A** interfered with the visualisation of **23** and **42** adducts, by artificially enhancing the fluorescence background throughout the lane. Silver stain shows that similar protein amounts have been injected in lane 3 as in lane 1. Lanes 4 and 5 in **Figure 27** contain technical

replicates of the thiol-yne reaction between **23** and **42**, after NAP-5 purification, annotated as 'rep.2'. NAP-5 columns were used to separate unbound small molecules from proteins by trapping small molecules and allowing proteins and protein adducts to pass through. Fluorescence signal after NAP-5 purification diminished when compared to lane 3, confirming that unbound **42** interfered with the fluorescence of thiol-yne reaction products, which still retained some fluorescence when compared to alkyne probe **23** alone, as seen in lane 1. Lane 6 contained probe **23** and the fluorophore **42** without radical initiation, after NAP-5 purification. The fluorescence signal seen in this lane is almost equivalent to the autofluorescence of probe **23** alone (lane 1), suggesting that the majority of unreacted fluorophore **42** was removed.

To determine if non-specific binding between fluorophore **42** and ubiquitin could account for fluorescence changes observed under radical conditions, two ubiquitin variants: Ubiquitin K48C and wild type Ubiquitin (Ubiquitin WT) were incubated with **42**, in the presence or absence of radical initiators, as seen in **Figure 28**. Importantly, these proteins did not contain alkyne moieties. They also did not contain the HA tag, which provides an additional 9 amino acids to alkyne-containing **23**, however, it was not expected that compound **42** would interact with this tag. Lane 1 contained **23** alone, and lane 2 contained **42**. Lane 3 contained **23** incubated with **42**, without radical initiation. Out of the three proteins tested, only probe **23** incubated with compound **42** showed an increase in fluorescence after radical initiation, seen in lane 4, compared to the same protein incubated with compound **42**, without radical initiation. No background fluorescence was seen in Ubiquitin WT (lane 5). No difference in fluorescence intensity was observed when Ubiquitin WT was incubated with fluorophore **42** without radical initiation (lane 6) or under radical conditions (lane 7) - both samples showed similar fluorescence intensity to **42** alone (lane 2). Ubiquitin K48C showed no background fluorescence on its own; however, faint fluorescent signal did appear in samples containing Ubiquitin K48C and **42** (lanes 9 and 10). Fluorescence intensity, however, did not change between UbK48C incubated with **42** in the absence (lane 9) or presence (lane 10) of radical conditions. Some non-specific reactivity between the fluorophore and the cysteine mutant could account for this signal.

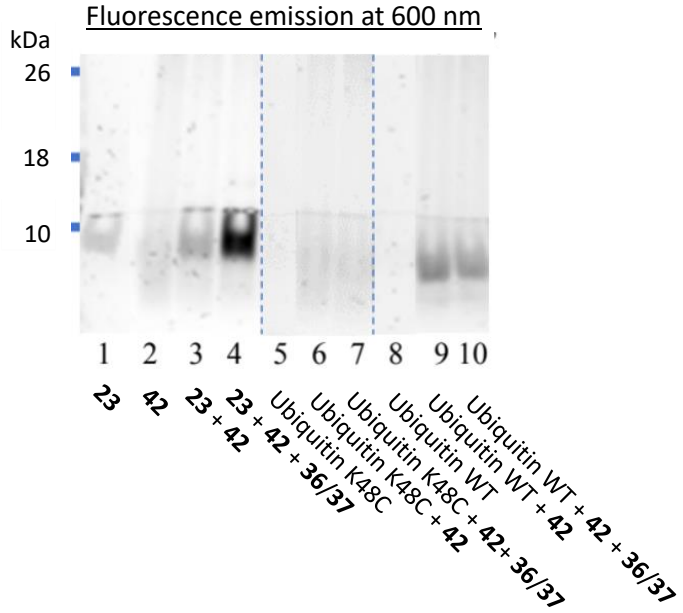

Figure 28: Testing the interaction between **42** and different ubiquitin variants under radical conditions.

UV light exposure required for the radical-mediated thiol-yne reaction between **23** and **42** was investigated to optimise the reaction. As seen in **Figure 29**, probe **23** alone displayed background fluorescence (lane 1) and compound **42** on its own showed streaking effect (lane 2), both of which have been discussed in **Figure 27**. Alkyne-containing probe **23** incubated with compound **42** without radical initiation, and without NAP-5 purification (lane 3) showed a combined background signal from the protein and unreacted **42**. A clear fluorescent band forming at around 10 kDa mark was observed when **23** and **42** were incubated with radical initiators, after just 30 seconds under UV light (lane 4), which suggested fluorescent adduct formation. A noticeable increase in fluorescence intensity took place when the concentration of radical initiators was kept constant, but UV light exposure was prolonged (lanes 4-7). Optimal signal intensity was seen after 15 minutes of UV exposure (lane 7). UV exposure was not prolonged past 2 h, as protein degradation was seen at that time point.

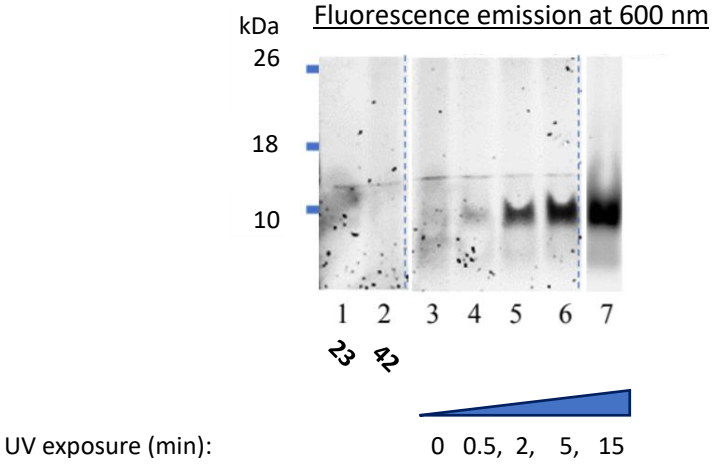

Figure 29: UV exposure time course for the thiol-yne/ene reaction between alkyne-containing **23** and thiol-containing **42**.

2.3.2. Thiol-yne reaction between 23 and TAMRA-thiol 43

Successful conjugation of **23** to thiol-containing fluorophore **42** under radical conditions *via* thiol-yne reaction warranted further investigation into other thiol-containing fluorophores. Investigating other fluorophores would confirm the robustness of the assay, optimise thiol-yne reaction yields, and test the general principle of the reaction for other molecules and its versatility in biomolecular conjugation. Additionally, several features of **42** were found to affect the visualisation of thiol-yne reaction on a gel, such as significant background interference from probe **23** autofluorescence due to broad excitation and emission maxima, as well as 'smearing' of **42** on SDS-PAGE due to its high hydrophobicity. A second fluorophore, TAMRA-thiol **43** was selected for further studies. The structure of **43** and the reaction can be seen in **Scheme 5**, resulting in construct **73**.

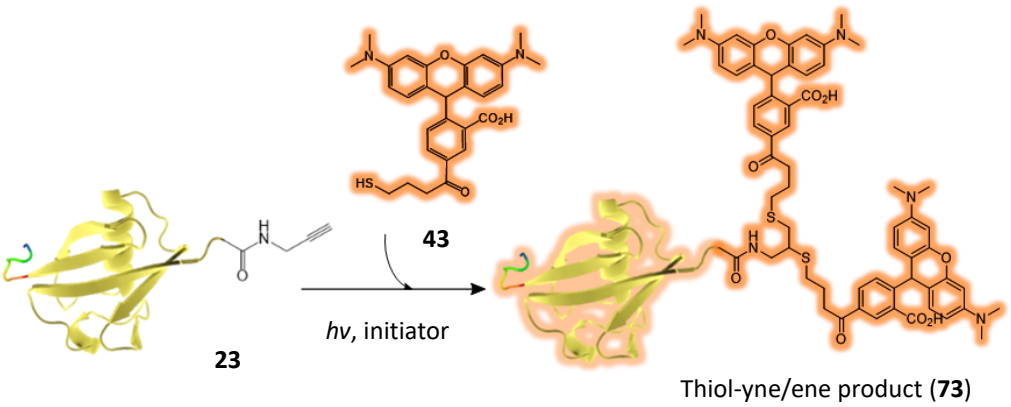

Scheme 5: **23** and **43** interaction under radical conditions.

Fluorophore **43** has a moderate to high solubility in DMSO (>10 mg/mL), high quantum yield, high extinction coefficient (≥ 70,000 cm-1M-1), and a more specific excitation/emission maxima (551/573 nm),[288] which can be used for SDS-PAGE visualisation. High fluorescence intensity allows for direct visualisation of thiol-yne product formation on a gel, and the specificity of excitation and emission wavelengths helps differentiate between the **43**-conjugated proteins and interference from the background.

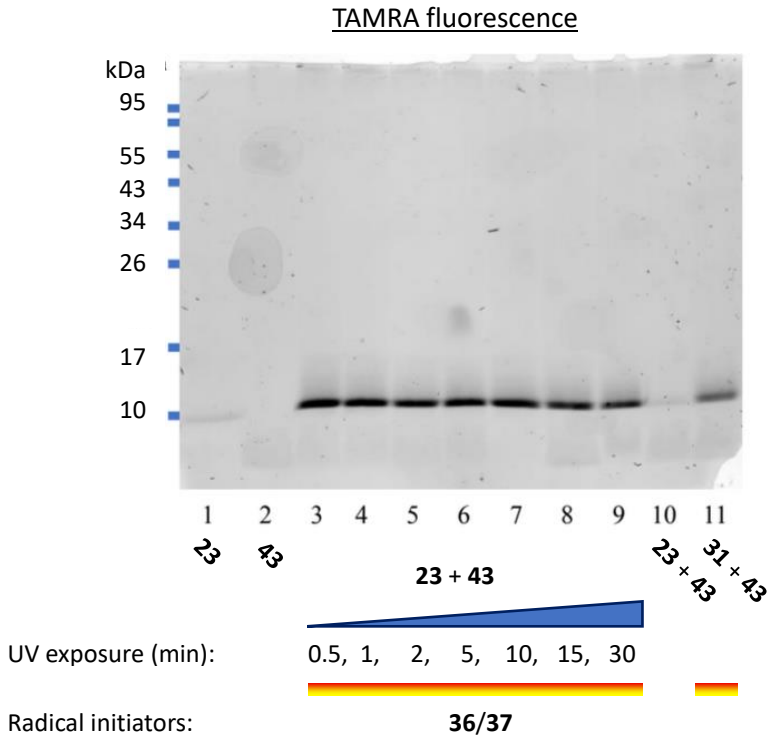

Figure 30: UV exposure time course for the thiol-yne/ene reaction between the alkyne probe **23** or the alkene probe **31**, and thiol-containing **43**.

Results of a time course for the thiol-yne reaction between alkyne probe **23** and thiol-containing compound **43** can be seen in **Figure 30**. Alkyne probe **23** alone (lane 1) displayed very faint background fluorescence at 10 kDa mark. Similarly, unreacted **43** formed a slightly fluorescent band (lane 2). High fluorescent intensity can be seen in a sample containing **23** incubated with **43**, under radical conditions, after 30 sec of UV exposure (lane 3). Fluorescence intensity remains the same after between 30 sec and 15 min of UV exposure under radical conditions (lanes 3-8), suggesting the reaction was completed. Fluorescence slightly diminishes after 30 min (lane 9). As a control, alkyne-containing **23** was incubated with thiol-containing **43** without radical

initiation (lane 10), which resulted in a very faint background fluorescence. Terminal alkene-containing **31** was incubated with thiol-containing **43** and radical initiators **36**/**37**, followed by UV irradiation for 15 minutes (lane 11). This resulted in a fluorescent band of roughly half the intensity of **23** reacting with **43**, providing evidence for the thiol-yne reaction between **23** and **43** proceeding to thiol-ene reaction, resulting in the addition of a second **43** fluorophore.

2.3.3. Addition of thiol-containing small molecules to labelled DUBs *via* thiol-ene chemistry

Alkyne probe **23** labels cysteine protease DUBs *via* direct electrophilic addition. This reaction is stabilised by an oxyanion hole near the catalytic centre of DUBs, and results in a vinyl sulfide,[289,] which should be able to undergo thiol-ene reaction with molecules containing a free thiol group, under radical conditions (summarised in **Scheme 6**).

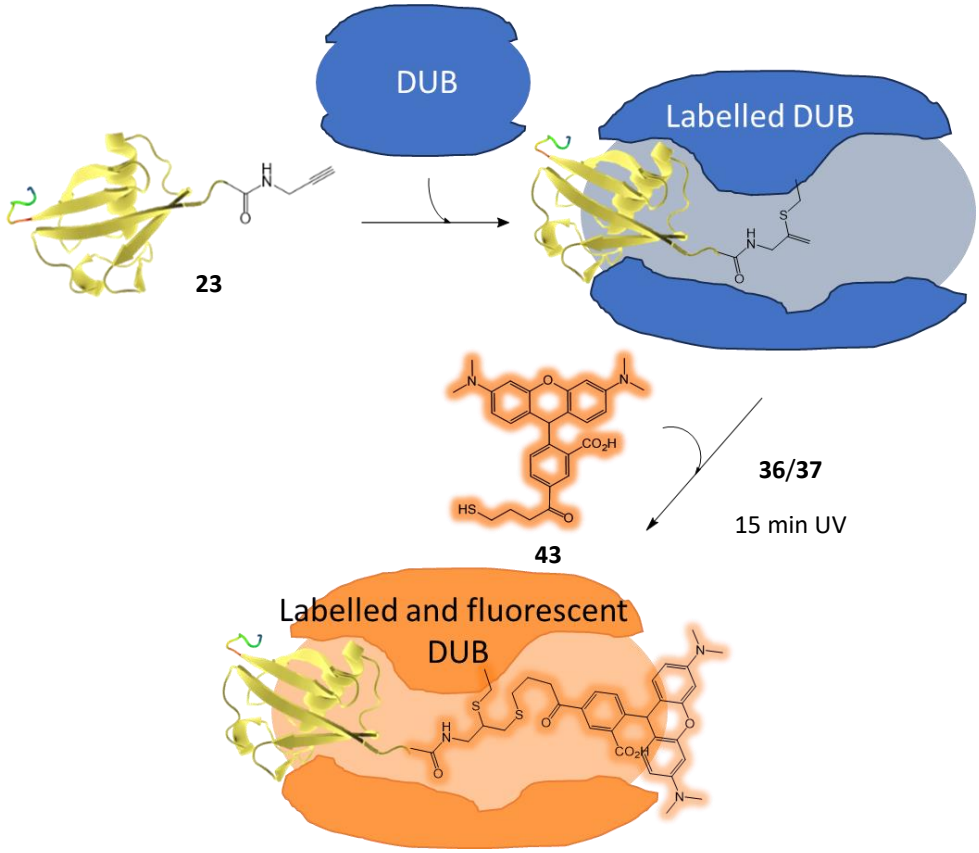

Scheme 6: Electrophilic addition of probe **23** to OTUB1, followed by radical thiol-ene reaction of the complex with thiol-containing **43**.

Reaction between thiol-containing molecules (**43** and OTUB1) and the alkyne-containing **23** under radical conditions was investigated in **Figure 31**. Probe **23** is seen in lane 1, fluorophore **43** in lane 2, and OTUB1 in lane 3. Lane 4 contains **23**

interacting with OTUB1 *via* electrophilic addition, resulting in labelling seen in the anti-HA Western blot, and on the silver stain, at 43 kDa. Lane 5 contains probe **23** incubated with compound **43**, without further purification. A band in this lane at 10 kDa can be seen on the Western blot, which was also faintly seen *via* TAMRA fluorescence, showing slight conjugationof probe **23** by **43** without radical initiation. Lane 6 contains alkyne probe **23** incubated under radical conditions with **43**, without further purification, followed by the addition of OTUB1 and further incubation. Anti-HA Western blot only shows a band at 10 kDa due to the presence of probe **23**, and no labelling of OTUB1 can be seen at 43 kDa. Alkyne-containing **23** did not label OTUB1, as the probe **23** was modified by TAMRA-thiol. The presence of OTUB1 is seen *via* TAMRA fluorescence at 34 kDa. OTUB1 fluorescence suggests that a non-specific interaction between **43** and OTUB1 could be taking place. Lane 7 contains OTUB1 incubated with **23**, followed by the addition of **43** and radical initiation. This resulted in a complex seen at 43 kDa on the anti-HA Western blot, which was also fluorescent. Lane 8 contains **23** incubated with **43** and OTUB1. It shows OTUB1 labelling at 43 kDa. Lane 9 contains OTUB1 incubated with **43**, and here, OTUB1 shows binding to the fluorophore *via* non-specific interaction. Lane 10 contains OTUB1 incubated with **43**, with radical initiation. OTUB1 was seen to fluoresce more intensely than without radical initiation, suggesting non-specific radical interaction between the two molecules. Lane 11 contains alkyne probe **23** incubated with the fluorophore **43** under radical conditions. An increase in fluorescence can be seen at 10 kDa on the Western blot, alongside fluoresces due to TAMRA-thiol covalently binding the probe **23**.

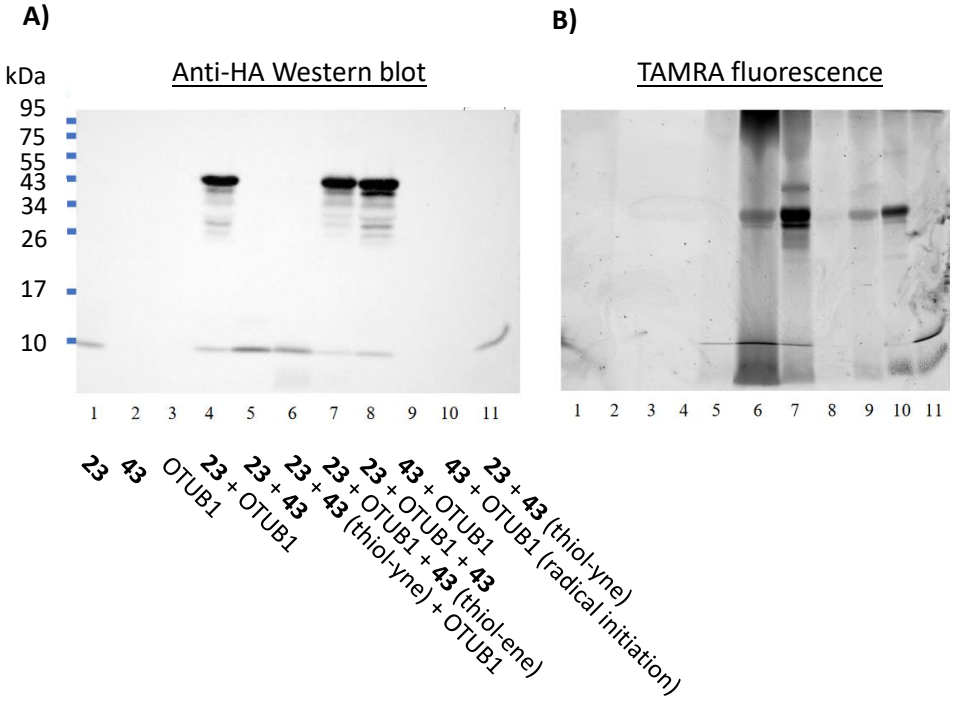

Figure 31 A: Anti-HA Western blot showing fluorophore **43** complex formation with probe **23** and OTUB1, under radical and non-radical conditions. **B**: TAMRA fluorescence of each sample injected on SDS-PAGE.

These results suggest that TAMRA-thiol **43** can interact non-specifically with proteins such as OTUB1, which do not contain alkyne moieties. Although radical initiation increases fluorescence intensity of the resulting complex, it is unlikely that thiol-ene reaction on its own results in this fluorescent signal. To test the idea of non-specific binding of compound **43**, a titration of the fluorophore with labelled OTUB1 was performed next.

Alkyne probe **23** was incubated with OTUB1, followed by the addition of various concentrations of fluorophore **43** (from 10 to 0.1 mM). Samples were then incubated in radical conditions, under UV light for 2.5 min. **Figure 32 A** shows TAMRA fluorescence of both OTUB1 and OTUB1 labelled with probe **23** diminishes as the concentration of compound **43** lowers, at a similar rate for both. Lane 1 contains probe **23**, lane 2 contains OTUB1, and lane 3 contains OTUB1 incubated with **23**. Background fluorescence due to protein presence in all three lanes was noted. Lanes 4-11 contain OTUB1 incubated with alkyne probe **23**, followed by fluorophore **43** addition at various concentrations, and radical initiation. Fluorescence intensity in lanes 4-11 diminished with lowered fluorophore concentration, however signal intensity in each lane at both 34 and 43 kDa stayed at a similar level. This result suggests that under radical

conditions both labelled and unlabelled OTUB1 were non-specifically modified by the fluorophore **43** . Silver stain in **Figure 31 B** shows equal loading of proteins in each well.

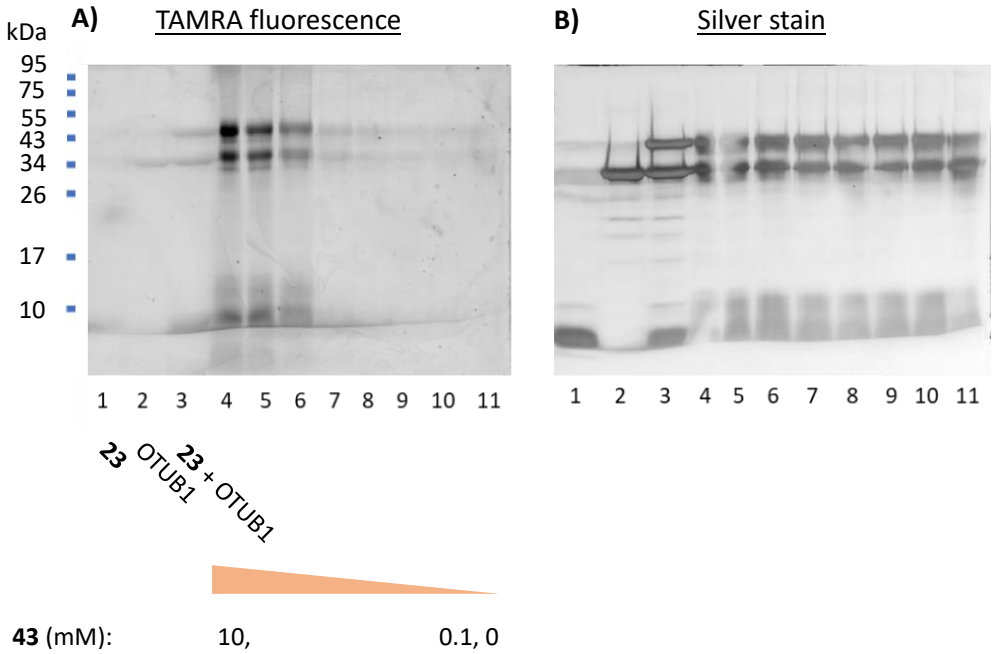

Figure 32 A: Titration of TAMRA-thiol **43** under radical conditions, checking non-specific binding to OTUB1/**23** complex, **B**: silver stain of the same gel.

In conclusion, TAMRA-thiol **43** was seen to interact non-specifically with proteins under radical conditions. The clear interaction between the first thiol-containing fluorophore, **42** and the alkyne probe **23** under radical conditions was enough to encourage protein thiol-yne coupling studies.

2.4. Protein model thiol-yne reaction optimisation with BSA

Following successful demonstration of thiol-yne reaction between a small molecule containing a thiol and alkyne-bearing ubiquitin, protein conjugation using thiol-yne reaction was attempted. BSA was chosen as a protein model for optimising thiol-yne bioconjugation reaction as it contains one free thiol group, and seventeen interchain disulfide bonds. Additionally, BSA should interact with ubiquitin through hydrophobic forces and those, following denaturation, are not expected to be visualised in a gel. Serum albumin usually binds a variety of molecules in blood, such as bilirubin, fatty acids, hormones, metal ions, drugs and toxins, in a non-covalent manner, and is responsible for maintaining fluid balance and regulating blood pH.[290] Any covalent interaction between probe **23** and BSA is therefore only expected to

happen due to radical thiol-yne/ene reaction. A schematic showing radical labelling of BSA is shown in **Scheme 7**.

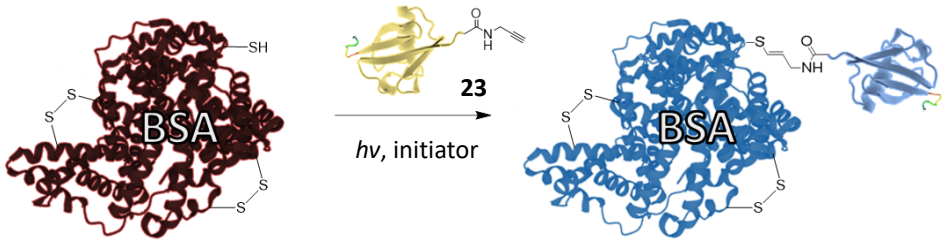

BSA labelled with **23**

Scheme 7: Proposed thiol-yne reaction for coupling of probe **23** to BSA.

Using conditions optimised in the previous section, the thiol-yne reaction was successfully performed between alkyne-containing **23** and BSA, as seen in **Figure 33**. Lane 1 in **Figure 33 B** contained probe **23**, and lane 2 contained 1 µg BSA, which was visible on the silver stain, at 72 kDa. Lanes 3-9 in **Figure 33 A** showed how an increase in BSA quantity allowed for an increase in labelling with the alkyne probe **23** (band formed above 72 kDa on the anti-HA Western blot). Bands above 130 kDa suggest that UV irradiation in radical conditions breaks down disulfide bridges, allowing for multiple probes **23** to bind through thiol-yne and thiol-ene couplings. Truncated and hydrolysed variants of BSA and other proteins related to BSA manufacturing can be seen in lanes 6-11 on the silver stain, beneath 66 kDa.

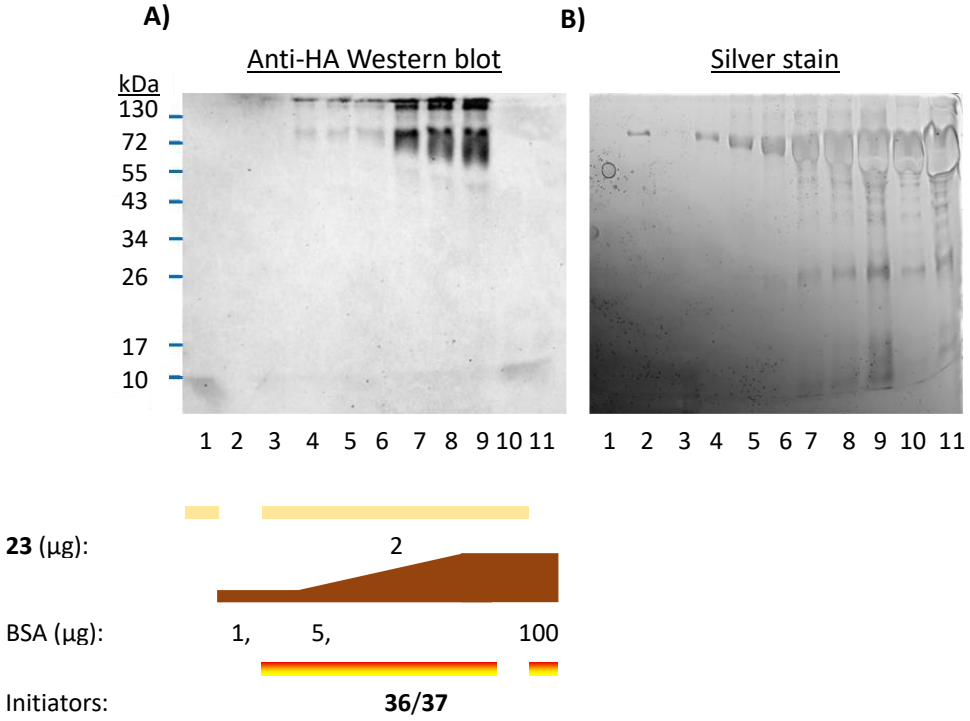

Figure 33 A: Radical thiol-yne reaction between probe **23** and BSA. **B**: Silver stain showing change in concentration of BSA in each lane.

It was noted that without UV radiation, 1 µg of BSA can be visualised *via* silver stain (lane 2), however, once irradiated in the presence of alkyne probe **23**, (lane 3), 1 µg of BSA shows diminished signal, suggesting exposure of the protein to **36**/**37** and UV leads to some degree of degradation. This experiment highlighted the correlation between a change in concentration of thiols and radical-initiated thiol-yne reaction yield, as the same amount of probe **23** was used in each lane, yet an increase in signal intensity on the anti-HA Western blot was seen when the concentration of BSA increased. To investigate the effect of UV exposure on the thiol-yne protein conjugation, BSA amount was increased to 200 µg, and UV irradiation was performed under radical conditions for up to 2 hours, seen in **Figure 34**. Lane 1 on the anti-HA Western blot contained 2 µg of probe **23**, lane 2 contained 200 µg BSA, and lane 3 contained probe **23** incubated with 200 µg BSA. Samples in lanes 4-9 contained 2 µg of probe **23** and 200 µg BSA as in lane 3, exposed to UV light for an increasing amount of time. **Figure 34 A** showed the strongest signal intensity after 10-20 minutes of UV irradiation (lanes 5-7), and almost no signal after 2 hours under UV. For protein bioconjugation *via* thiol-yne reaction using **36**/**37** as radical initiators, UV exposure time was set to be 15 min from this point onward, unless otherwise specified. **Figure 34 B** shows a large concentration of BSA was used for labelling *via* the thiol-yne reaction.

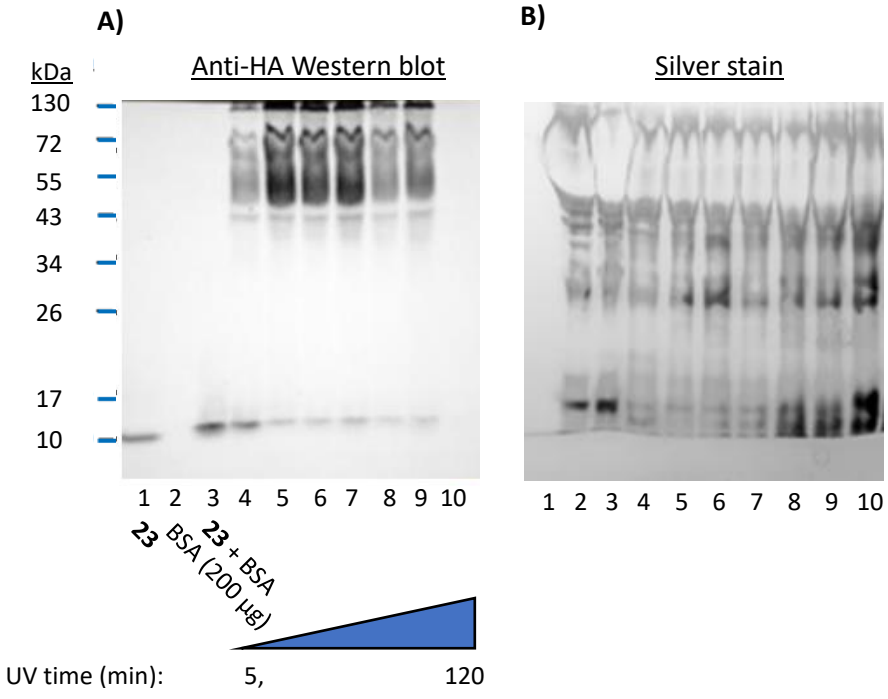

Figure 34: UV exposure time course for the thiol-yne/ene reaction between **23** and BSA.

2.5. Conclusions and future outlook

These results confirmed the hypothesis that proteins containing alkyne moieties, proteins containing thiols, can undergo thiol-yne reaction, under radical conditions, in aqueous environments, possibly following on to thiol-ene conjugation to other thiol-containing molecules. Protocol for thiol-yne/ene reactions between small fluorophores and a ubiquitin construct containing a terminal alkyne was optimised. The first example of time-resolved protein-protein conjugation *via* radical thiol-yne/ene reactions was presented. The exact number of alkyne-containing monomers binding to BSA is unknown, because even though **Figure 32** shows a band in the anti-HA Western blot at 72 kDa, which would correspond to one monomer addition, there is a second band seen at above 130 kDa, which could be due to multimeric BSA impurities, or due to several probes **23** reacting with BSA monomers. It is assumed that thiol-yne/ene reactions could occur between truncated BSA molecules containing free thiols and alkyne-containing **23**, resulting in products seen at 43 and 55 kDa. It is envisioned that structural studies could help visualise the exact nature of bioconjugation using thiol-yne/ene reactions, as well as determine if any damage to protein sequence or structure occurred. Presented thiol-yne/ene reaction for conjugation of proteins could be used for time-resolved site-specific cross-linking of proteins, which could be applied in ABP design for a variety of protein targets, including enzymes such as DUBs.

Adduct formation between a fluorophore containing a thiol and the alkyne probe **23** was successfully performed, which was followed by the first example of protein-protein thiol-yne reaction. Encouraged by these results, the construction of a biocompatible radical di-ubiquitin ABP of DUBs was envisioned.

Chapter 3: Radical di-ubiquitin formation, purification and application

3.1. Objectives

The main objective of this chapter is the formation of a di-ubiquitin construct containing an internal alkene, as seen in **Scheme 8**. Thiol-yne reaction between one monomer containing a C-terminal alkyne and another containing a single lysine-to-cysteine substitution would result in the desired product. Steric hindrance would prevent a second thiol addition *via* thiol-ene reaction.

A di-ubiquitin construct linked at position 48 was chosen as a target construct, due to several known DUBs targeting K48-linked polyubiquitination, and an established link between their dysregulation and disease states. Ubiquitin K48C mutant was selected as the target thiol-containing protein, alongside alkyne-containing **23**. The specific aims of this chapter are: expression and purification of the Ubiquitin K48C mutant, synthesis of the di-ubiquitin construct (**44**) *via* thiol-yne coupling, exploring two distinct radical initiation systems, and the optimization of an in-solution purification strategy to isolate the final probe.

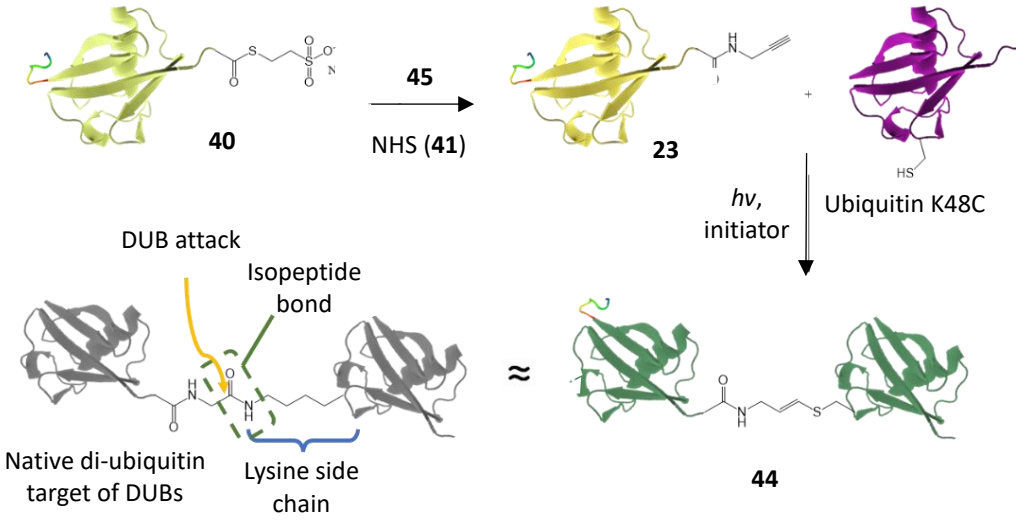

Scheme 8: Comparing native di-ubiquitin target of DUBs with the proposed semi-synthetic di-ubiquitin **44**.

The secondary objective is the biorthogonal, time-resolved labelling of model cysteine protease DUB, OTUB1, *via* radical thiol-ene reaction, as seen in **Scheme 9**. In order to label DUBs with alkene-containing constructs, biocompatible radical initiation systems will be explored. Two aqueous, visible-light-induced, radical initiators were

explored for thiol-ene labelling of DUBs, alongside a previously published radical thiol-ene system for labelling DUBs.

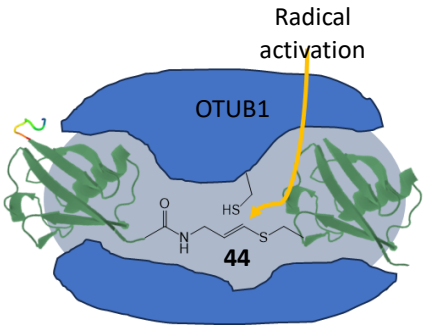

Scheme 9: Thiol-ene reaction between di-ubiquitin construct **44** and model DUB, OTUB1.

3.2. Thiol-yne reaction for controlled di-ubiquitin ABP formation

3.2.1. Preparation of thiol-containing ubiquitin mutant

Performing the thiol-yne reaction between two ubiquitin proteins required alkyne-containing **23** and a thiol-containing ubiquitin monomer. Ubiquitin contains no thiols; therefore, a lysine-to-cysteine mutant was needed. Ubiquitin K48C mutant was selected as a model for di-ubiquitin construct formation to allow validation against DUBs known to target this linkage, such as OTUB1.

Plasmid pET3a-Ub-K48C containing Ubiquitin K48C was obtained from Addgene in DH5α *E. coli* cell stab. Cells were streaked, single colonies isolated, glycerol stocks made, and the plasmid was extracted and purified following a standard protocol.[291] Competent BL21 (DE3) cells were transformed with the purified plasmid and overexpressed with 0.4 mM IPTG.[292] Cells were pelleted and frozen, followed by their lysis and optimisation of the protein purification process, as seen in **Figure 34**. The purification process started with cell growth (lanes 1-3), cell lysis (lane 4), followed by protein precipitation with 0.5 % Perchloric acid (lane 6), and the removal of the precipitate by centrifugation, as seen in the literature.[293] Soluble proteins were then dialysed to remove the acid (lane 7). Knowing that the melting temperature for the wild type ubiquitin was calculated to be 90.6 °C,[294] a heating step was added (lane 8). Dialysed, soluble proteins were incubated at 85 °C for 5 min, and the insoluble precipitate was again removed by centrifugation. The soluble fraction was filtered using 10 kDa Vivaspin500 (lane 9) and concentrated using 5 kDa MWCO filters (lane

11). Digestion with trypsin showed 62.88% validated sequence coverage of ubiquitin, although peptides containing K48C mutation were not detected. Mass Spectrometric results are visualised in the **Appendix E**. The process required for the purification of the mutant was assessed *via* silver stain (**Figure 35**).

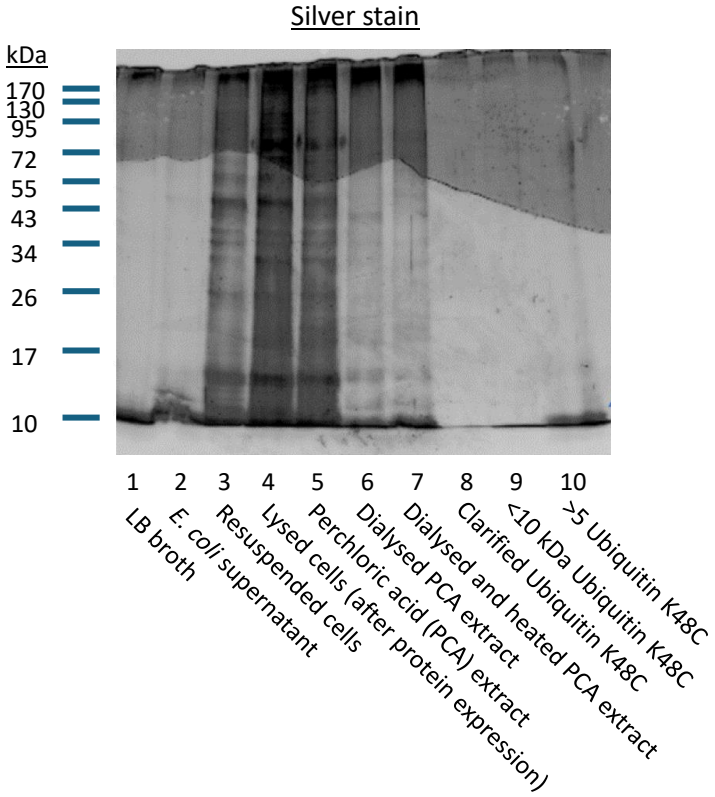

Figure 35: Silver stain analysis of Ubiquitin K48C purification process.

3.2.2. Controlled di-ubiquitin formation

Radical thiol-yne reaction between purified Ubiquitin K48C and probe **23** was successfully performed, as seen in **Figure 36 A**. Excess ubiquitin K48C was used for the first trial of di-ubiquitin formation, as thiol concentration is considered rate-limiting for the reaction.[295] 200, 400 and 800 µg of Ubiquitin K48C showed full conversion with 2 µg of alkyne probe **23** to dimers (**44**) in lanes 4, 5, and 10, **Figure 36 B** (at 17 kDa), while evidence of trimers was also seen (26 kDa). Silver stain showed excess Ubiquitin K48C used (**Figure 45 C**).

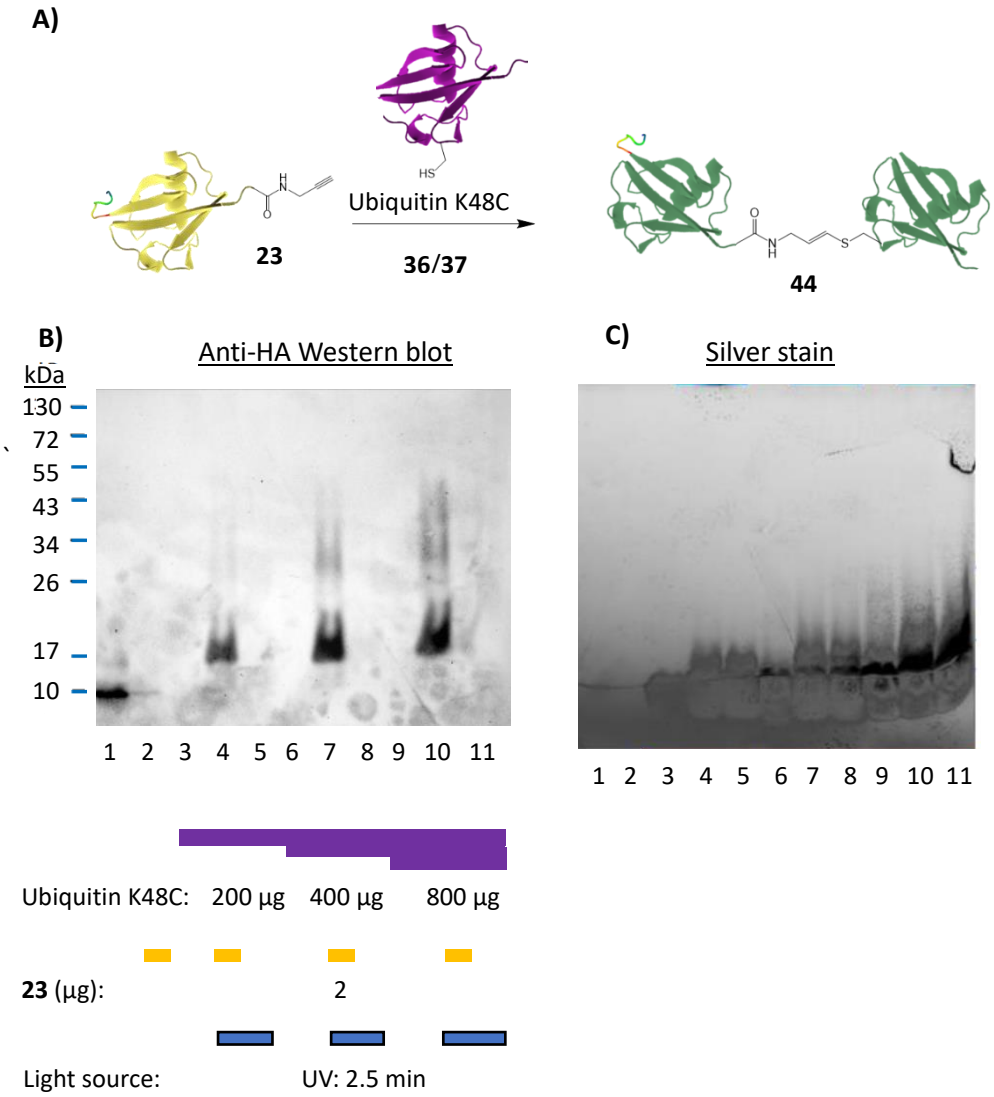

Figure 36 A: Schematic showcasing di-ubiquitin formation *via* thiol-yne reaction. **B**: Anti-HA Western blot for the thiol-yne reaction between probe **23** and Ubiquitin K48C. **C**: Silver stain of the same reactions.

It was noted that, unlike with thiol-yne reaction between probe **23** and BSA, full conversion of monomers **23** and Ubiquitin K48C to dimers **44** seemed to take place at high Ubiquitin K48C concentrations. Two additional batches of Ubiquitin K48C were prepared to test purification and thiol-yne reaction reproducibility, and the minimal amount of Ubiquitin K48C required to initiate dimer formation was investigated.

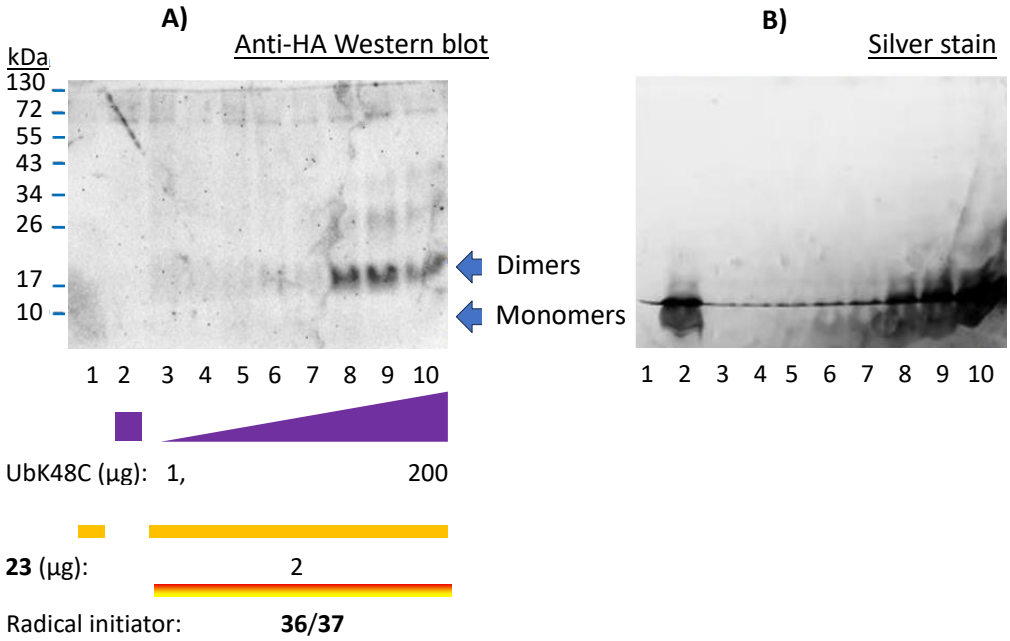

Figure 37 A: Dimer **44** formation at increased thiol concentrations. **B**: silver stain.

Figure 37 shows alkyne probe **23** undergoing radical thiol-yne reaction with increasing concentrations of Ubiquitin K48C. Interestingly, at a ratio of 50:1 (100 µg thiol to 2 µg alkyne), formation of dimers can be clearly seen at 17 kDa. When lower amounts of Ubiquitin K48C were used, some conversion to **44** was seen; however, dimers seem to produce broadened bands of lower intensities, due to diffusion of proteins on the gel. Low protein content might mean that thiols are less likely to be in proximity to alkynes to allow coupling.

3.2.3. Further Investigating thiol-yne reaction between two ubiquitin monomers

It has been noted that for coupling between Ubiquitin K48C and probe **23** was very inefficient, and reaction optimisation was attempted. Thiol-yne reaction should ideally proceed in a 1:1 ratio of thiol to alkyne; therefore methods of optimising dimer formation were investigated next.

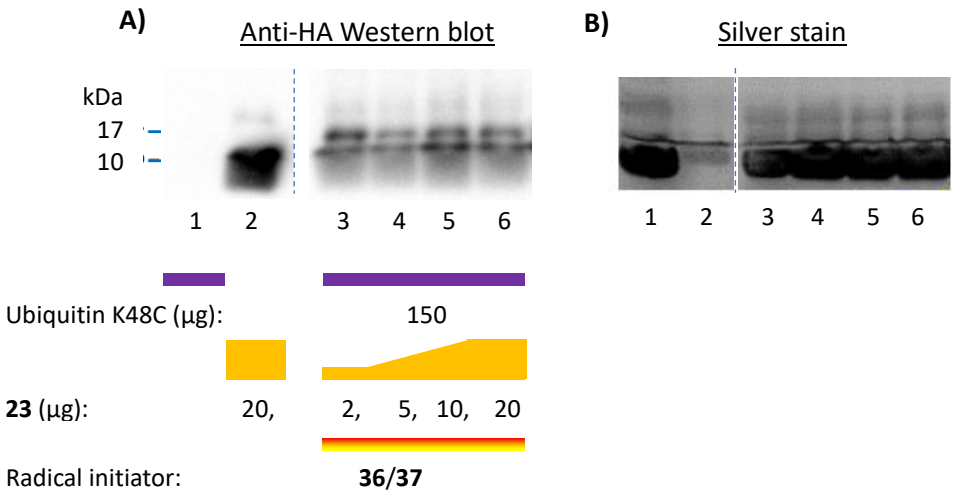

Figure 38 A: Di-ubiquitin formation at increased alkyne concentrations. **B**: silver stain showing even sample loading in lane 1, and in lanes 3-6.

Increasing the amount of alkyne-containing **23** to improve di-ubiquitin **44** yield was attempted, as seen in **Figure 38 A**. Lane 1 contained 150 µg Ubiquitin K48C, and lane 2 contained 20 µg **23**. Lanes 3-6 contained between 2 and 20 µg of probe **23**, incubated with 150 µg Ubiquitin K48C. No improvement was observed between samples with 1:75, 1:30, 1:15, and 1:7.5 ratios of alkyne to thiol. **Figure 38 B** shows even loading of samples in lanes 1, and 3-6. Additionally, the effect of heating the reaction on dimer formation was investigated. Unfortunately, heating the samples up to 70 °C while shaking, followed by UV irradiation in radical conditions, did not improve the dimer drastically (**Figure 39 A**, lanes 3-7, anti-HA Western blot and silver stain). Lanes 5 and 7 seem to show slightly improved dimer formation, after incubation at 50 °C and 70 °C for 90 min.

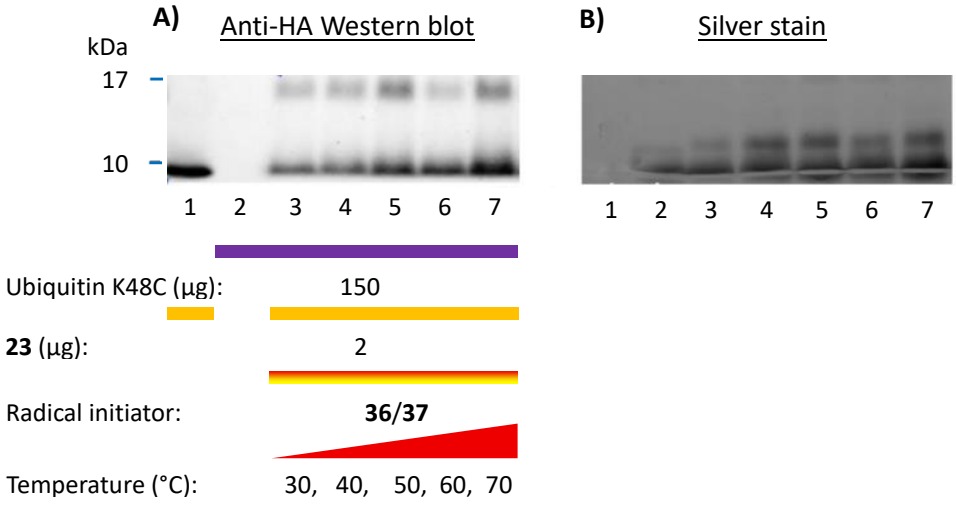

Figure 39 A: Di-ubiquitin formation at increased temperature. **B**: Silver stain showing even sample loading in lanes 2-7.

Changing the radical initiator to compound **1**, a UV-activated, commercially available radical initiator, significantly improved the reaction yields compared to radical initiation with **36**/**37**, as shown in **Figure 40**. Lane 1 contains **23**, lane 2 contains Ubiquitin K48C (100 µg), and lane 3 contains **23** with Ubiquitin K48C. Lanes 4-6 contain 2 µg of **23** each, and an increasing amount of Ubiquitin K48C, with high concentrations of **1** (10 mM), followed by UV exposure for 2.5 min. This contrasted significantly with µM concentrations of raical initiators **36**/**37**, and 15-min UV irradiation used in lanes 7-9. Lower UV exposure time and high concentration of compound **1** resulted in better dimer formation and lower protein degradation compared to **36**/**37**.

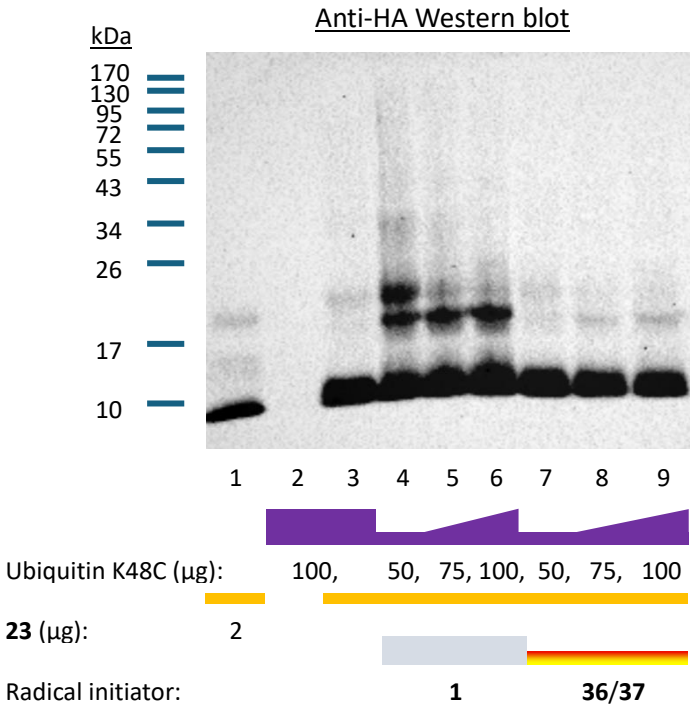

Figure 40: Compounds **1** and **36**/**37**, as radical thiol-yne initiators.

3.2.4. Reaction Templating

It has been noted in **Figure 37 A** that for dimer formation between a thiol of Ubiquitin K48C and an alkyne probe, a ratio of 10:1 is required. As thiol-yne reaction would ideally proceed in a 1:1 ratio of thiol to alkyne, a method of optimising dimer formation was investigated. One hypothesis was that the introduction of a catalytically inactive OTUB1 (C91S) mutant, which can accommodate both proximal and distal ubiquitin monomers, would allow monomers to align in the binding pocket, facilitating thiol-yne reaction. This idea is summarised in **Scheme 10**.

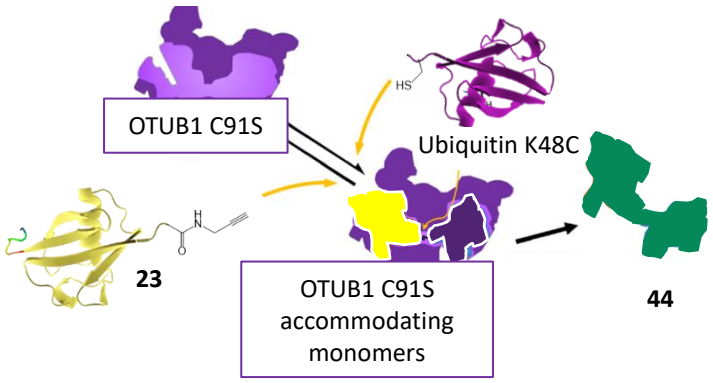

Scheme 10: Catalytically inactive OTUB1 C91S to be used for templating of di-ubiquitin formation *via* thiol-yne reaction.

Templating of the reaction due to the presence of OTUB1 C91S was not observed to a significant degree, despite several attempts, at various ratios of OTUB1 C91S, probe **23** and Ubiquitin K48C. Almost a complete loss of signal at 10 kDa can be seen in **Figure 41 A**, when OTUB1 C91S is added to the thiol-yne reaction (lane 11), compared to the same reaction without OTUB1 C91S (lane 7), however, it is unclear from the anti-HA Western blot alone whether the quantity of dimers has increased. Only an increase in the thiol-containing monomer had a significant effect on the formation of the dimeric **44**, as seen in **Figure 41**, and the idea of templated thiol-yne reaction was not pursued further.

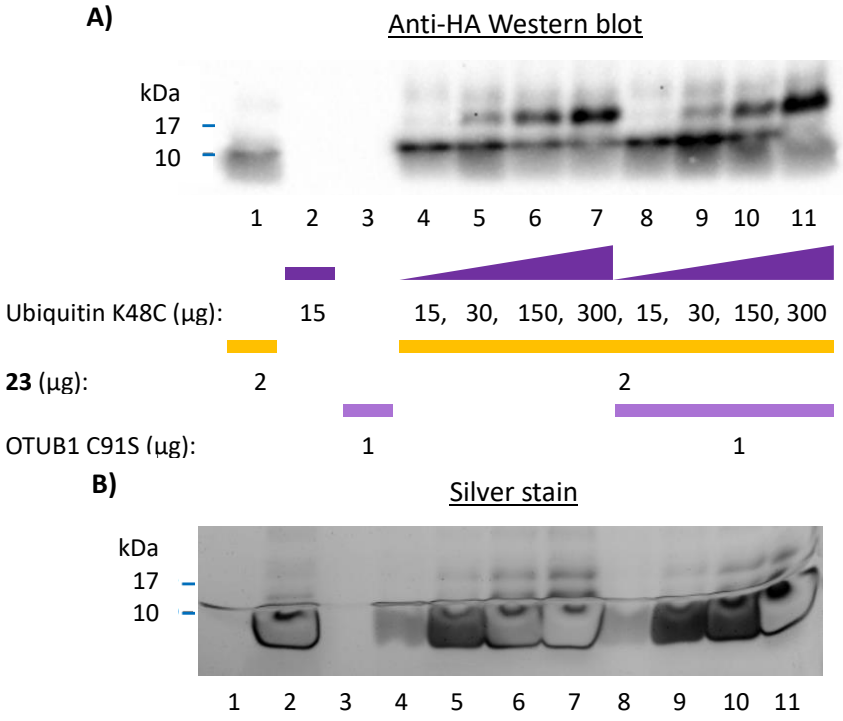

Figure 41 A: Catalytically inactive OTUB1 C91S trial for templated thiol-yne dimer formation. **B**: Silver stain.

3.3. Labelling of model DUBs *via* thiol-ene reaction

So far, it was demonstrated that thiol-yne reaction between proteins results in covalently bound constructs, which should contain internal alkenes. For di-ubiquitin constructs to label OTUB1, non-covalent interactions between the construct and a DUB must occur first, followed by radical thiol-ene reaction of the alkene to the catalytic cysteine. Presence of unreacted probe **23** after dimer formation would have priority reacting with DUBs, as no activation is required for the alkyne warhead of probe **23**. To test this, dimeric **44** was prepared, and without further purification, incubated with OTUB1 and HEK293T lysate, followed by radical activation with **36**/**37** under UV light. **Figure 42** illustrates **23** reacting with Ubiquitin K48C, forming **44** (lane 1). Lane 2 contains OTUB1. No additional band can be seen at 52 kDa in lane 3, which contained dimeric construct **44** alongside a mixture of unreacted monomers. Instead, probe **23** seems to label OTUB1, resulting in a band at 43 kDa. Lane 4 contains HEK293T lysate, and lane 5 contains the lysate incubated with a mixture of monomers and dimers, followed by radical activation. Although many proteins seem to be labelled in HEK293T lysate treated with the crude mixture containing dimers, these bands are due to DUBs being labelled by **23** *via* direct nucleophilic attack by the catalytic cysteines of DUBs. Silver stain visualisation was performed to ensure equal loading of proteins. This experiment has not been able to show dimers labelling OTUB1. Low dimer yield, and the presence of unreacted monomers prevent visualisation of dimers labelling OTUB1,

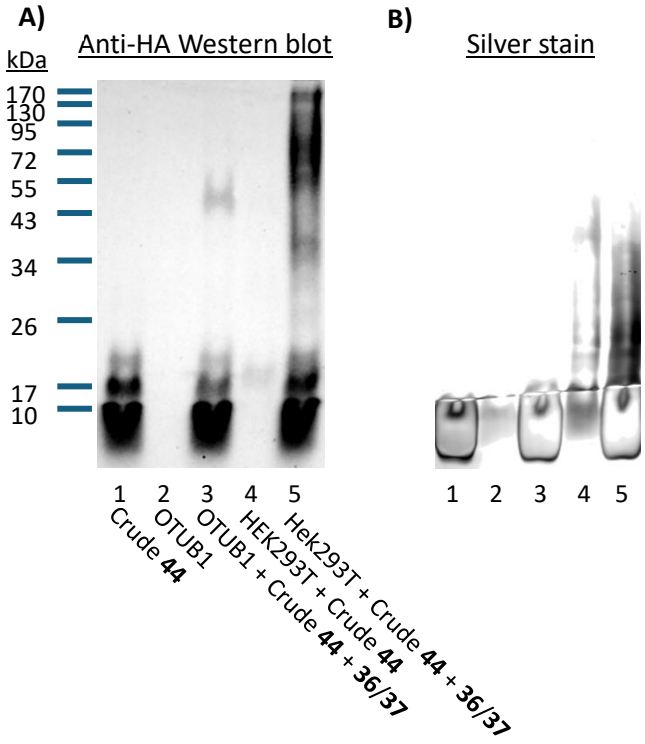

Figure 42: Crude **44** reacting with OTUB1 and HEK293T under radical conditions.

3.3.1. CuAAC for reacting with alkyne-containing 23 in crude 44

In mixtures containing mono- and di-ubiquitin, the unreacted alkyne-containing probe **23** interacted with OTUB1 by covalently binding catalytic cysteines. This interaction prevented construct **44** from labelling of the OTUB1 under radical conditions *via* a thiol-ene reaction. CuAAC reaction was therefore performed on the crude **44** to covalently bind any unreacted probe **23**, as seen in **Scheme 11**.

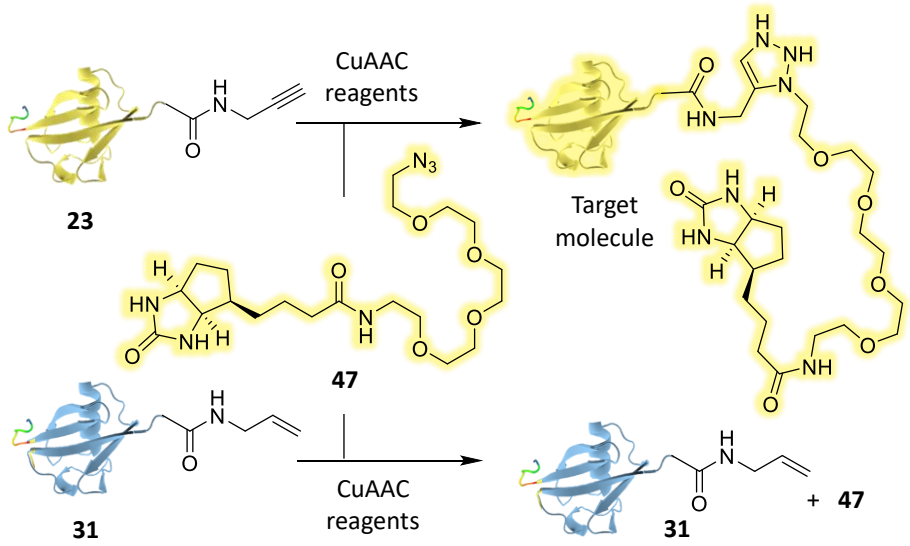

Scheme 11: CuAAC reaction between constructs **23** and **31**, and compound **47**.

CuAAC reaction can help differentiate between probes with alkyne and alkene warheads, **31** and **23** were separately treated with biotin-PEG4-azide (**47**), which was generously provided by Dr. Sean McKenna. CuAAC cocktail containing Copper(II) sulfate, sodium ascorbate and Tris(3-hydroxypropyltriazolylmethyl)amine (THPTA) was then added to both samples. Next, activity of the molecules as ABPs was checked, as seen in **Figure 43 A**. Probe **23** can be seen in lane 1 and probe **31** in lane 2 of the anti-HA Western blot. OTUB1 can be seen in lane 3 of the silver stain. OTUB1 was incubated with **23**, showcasing labelling of OTUB1 in lane 4. Probe **23** was reacted with biotinylated azide **47**, and then incubated with OTUB1. Labelling of the OTUB1 diminished almost completely, as seen in lane 5. In lane 6, **31** was incubated with OTUB1, followed by radical activation, and lane 7 contained **31** reacted with **47**, incubated with OTUB1, followed by radical activation (lane 7). Although small drop in signal efficiency was seen in lane 7, OTUB1 was labelled by both probe **31** and probe **31** treated with **47** under radical conditions. Lanes 8-11 contain the same samples as lanes 4-7, with the addition of NAP-5 purification after CuAAC reaction, to check if the CuAAC reagents or unreacted **47** interfere with the activity of the constructs. Anti-biotin Western blot (**Figure 43 B**) shows successful removal of most unreacted **47** by

NAP-5 purification, when lane 5 is compared to lane 9. Unreacted **47** covalently interacts with OTUB1 in lane 5, while after NAP-5 purification, only probe **23** (seen at 10 kDa) is biotinylated (lane 9).

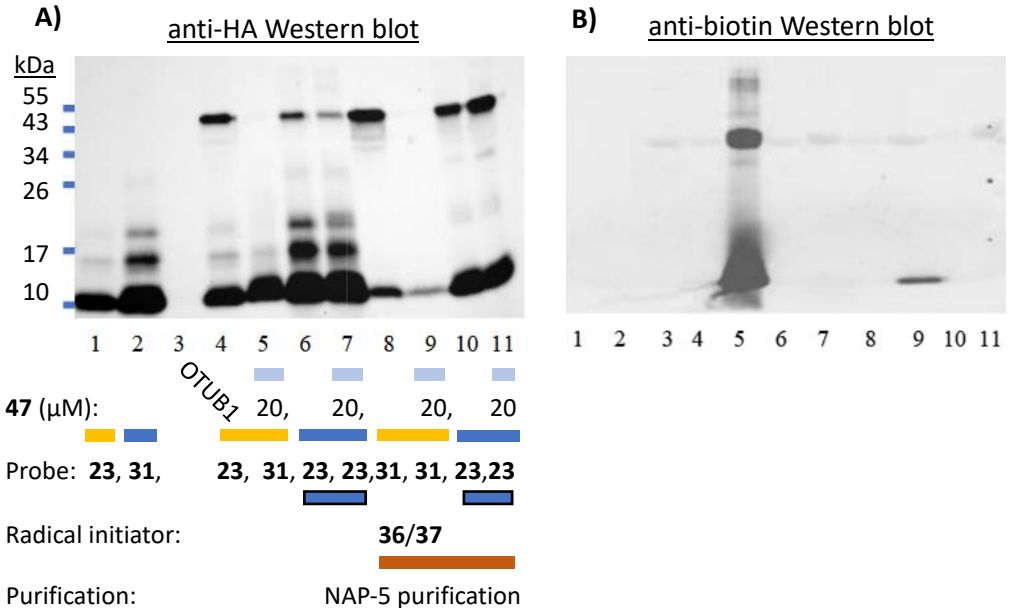

Figure 43: CuAAC reaction inhibits activity of **23** as ABP of OTUB1, while not affecting activity of **31**.

Thiol-yne reaction between alkyne-containing **23** and thiol-containing Ubiquitin K48C was then performed once more, resulting in crude **44**. Crude **44** was reacted with azide **47** using established protocols,[313] with results seen in **Figure 44**. OTUB1 was then incubated with crude **44** reacted with **47**, followed by radical initiation. CuAAC reaction requires an azide and a terminal alkyne, and alkenes do not participate in this reaction.[296] CuAAC reaction should not interfere with a thiol-ene reaction between dimeric **44** and OTUB1, and should instead interfere with unreacted probe **23**, preventing it from labelling OTUB1.

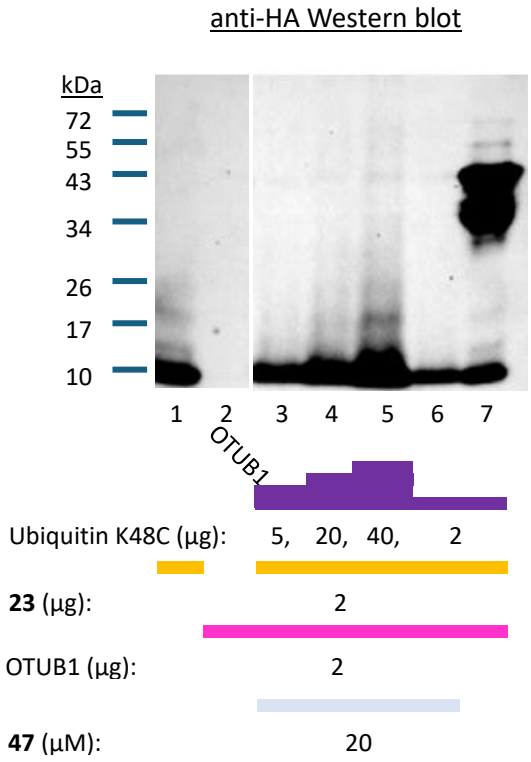

Figure 44: Thiol-yne reaction between probe **23** and Ubiquitin K48C, followed by CuAAC reaction with azide **47**, and thiol-ene labelling of OTUB1.

Due to successful CuAAC reaction with unreacted probe **23**, labelling of OTUB1 is very faint. No clear band at 52 kDa can be seen in lanes 3, 4, or 5, showing no clear thiol-ene labelling of OTUB1 by dimers. Lane 1 contains probe **23**, and lane 2 OTUB1. Lanes 3-6 contain 5, 20, 40 and 2 µg of Ubiquitin K48C, respectively, which were reacted with probe **23** under radical conditions, followed by NAP-5 purification and CuAAC reaction with azide **47**. Reacted constructs were incubated with OTUB1 (seen in **Figure 44**, lanes 3, 4, 5 and 6), followed by second radical initiation. Dimers **44** can be seen forming at 17 kDa, at increasing amounts of thiol-containing ubiquitin mutant. Labelling of OTUB1 with unreacted probe **23** can be seen at 43 kDa in those lanes. The crude **44** needs to be purified and concentrated for the thiol-ene labelling of OTUB1 to be clearly visible on the Western blot.

3.3.2. Dimer Purification *via* Size-Exclusion Chromatography (SEC)

A Size-Exclusion Chromatography (SEC) method using Shim-pack Bio Diol-120, 3um, 4.6x300 column was developed for the purification of di-ubiquitin constructs. Di-ubiquitin constructs were formed through thiol-yne reaction, as previously described. Briefly, 2 µg of probe **23** was mixed with 50 µg Ubiquitin K48C, in the presence of **36** (250 mM) and **37** (250 mM). Samples were irradiated with UV light for

15 min and then diluted 2x in deionised water to stop the reaction. Samples were injected at 40 µL on a SEC column *via* direct injection, under isocratic flow, without the removal of radical initiators. Mobile phase initially consisted of distilled water, pH 7. This approach resulted in **SEC Chromatogram 1**. Protein monomers (**23** and Ubiquitin K48C), dimers (**44**), as well as larger aggregates appear to be eluting at the same time, between 9-15.5 min, compared to the standards available in the column's certificate of analysis. Anti-HA Western blot of fractionated run showed HA-tagged dimers and monomers co-eluted (**Figure 45**, lane 3). Monomers containing the HA tag were found in most of the fractions, from 10 min (lane 2) until the end of the run (lane 9), although the highest concentration of monomers can be seen in fractions eluting between 10-13 min.

SEC Chromatogram 1

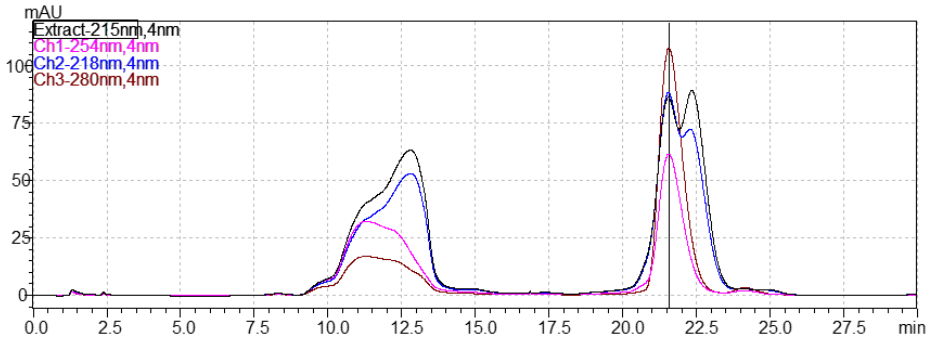

Anti-HA Western blot

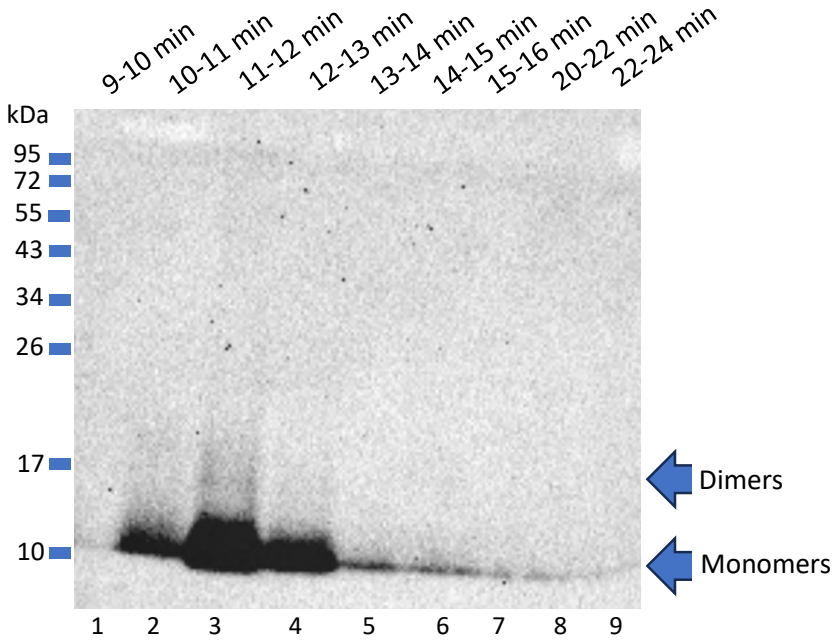

Figure 45: First attempt at purification of dimer **44** using SEC. **Chromatogram 1** shows proteins eluting between 9-15 min, with overlapping peaks. Lanes 2-9 in the Western blot show monomers containing HA tag at 10 kDa, while dimers can be seen in lane 3 only, at 17 kDa. Majority of both monomers and dimers coelute in lane 3.

To improve the separation of dimers, the ionic strength of the mobile phase was increased. 25 mM ammonium bicarbonate was selected as the additive, as its volatility ensures compatibility with downstream mass spectrometric analysis and biological assays. As shown in **SEC Chromatogram 2**, the addition of salt caused the dimer **44** to elute earlier compared to the water-only mobile phase, likely by reducing non-specific interactions with the stationary phase. Western blot in **Figure 46** shows dimers eluting at the same time as monomers containing the HA tag (lane 1), although the addition of ammonium bicarbonate allowed for slightly earlier elution of dimers. Monomers containing the HA tag are continuously eluted from 10-15 min.

SEC Chromatogram 2

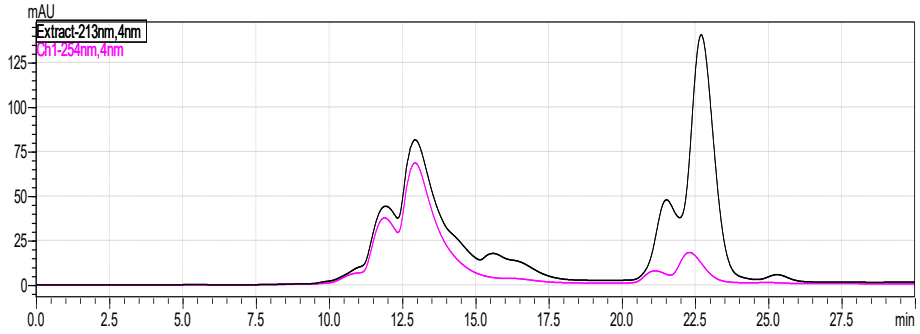

Anti-HA Western blot

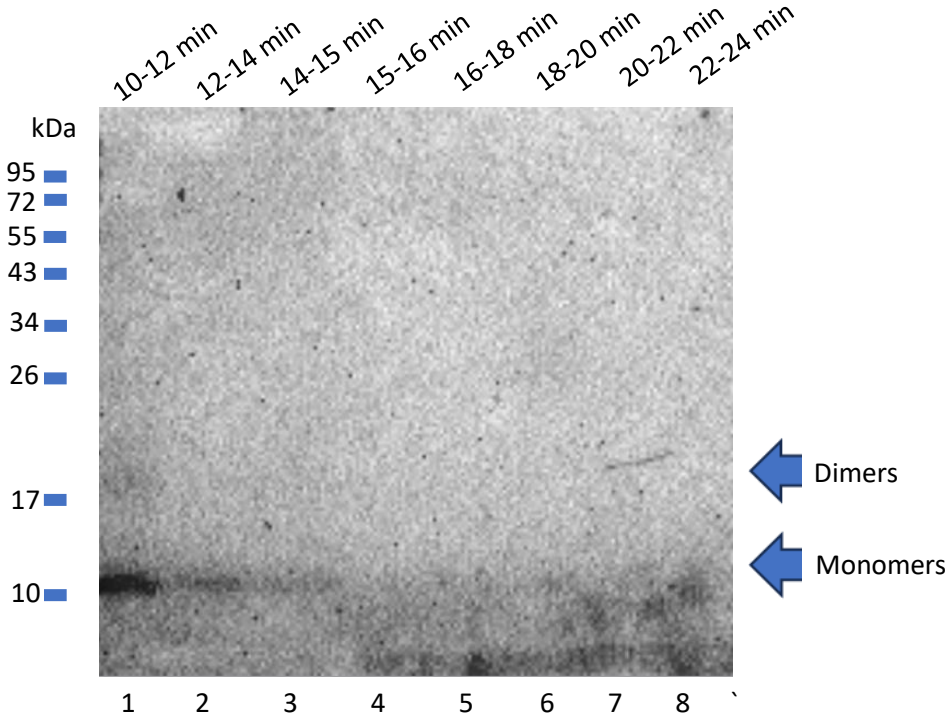

Figure 46: Addition of 25 mM ammonium bicarbonate to the mobile phase resulted in a slight improvement in peak sharpness, seen in **Chromatogram 2**. This did not help noticeably with protein species separation, as seen in the Western blot - lanes 1-8 the show monomers containing HA tag at 10 kDa, while dimers can be seen at 17 kDa. Majority of both monomers and dimers coelute in lane 1.

Mobile phase composition was then adjusted to 0.2 M Na_2HPO_4, 0.2 M NaCl (pH 7.0), and a flowrate of 0.4 mL/min was used. Radical initiators were also removed from samples using 5 kDa Vivaspin500 concentrators. Under these conditions, improvement in peak separation was noted, as seen in **SEC Chromatogram 3**, however anti-HA Western blot still determined incomplete separation of proteins (**Figure 47**). HA-tag containing ubiquitin monomers **23** started to elute at 5 min (**lane 1**), and

continued until 12 min (**lane 4**), with most HA-Ubiquitin present in 9-12 min fraction (**lane 4**). Although HA-tagged dimers **44** showed the highest signal intensity in a fraction eluted between 7-9 min (**lane 3**), they could also be seen in between 6-7 min and 9-12 min.

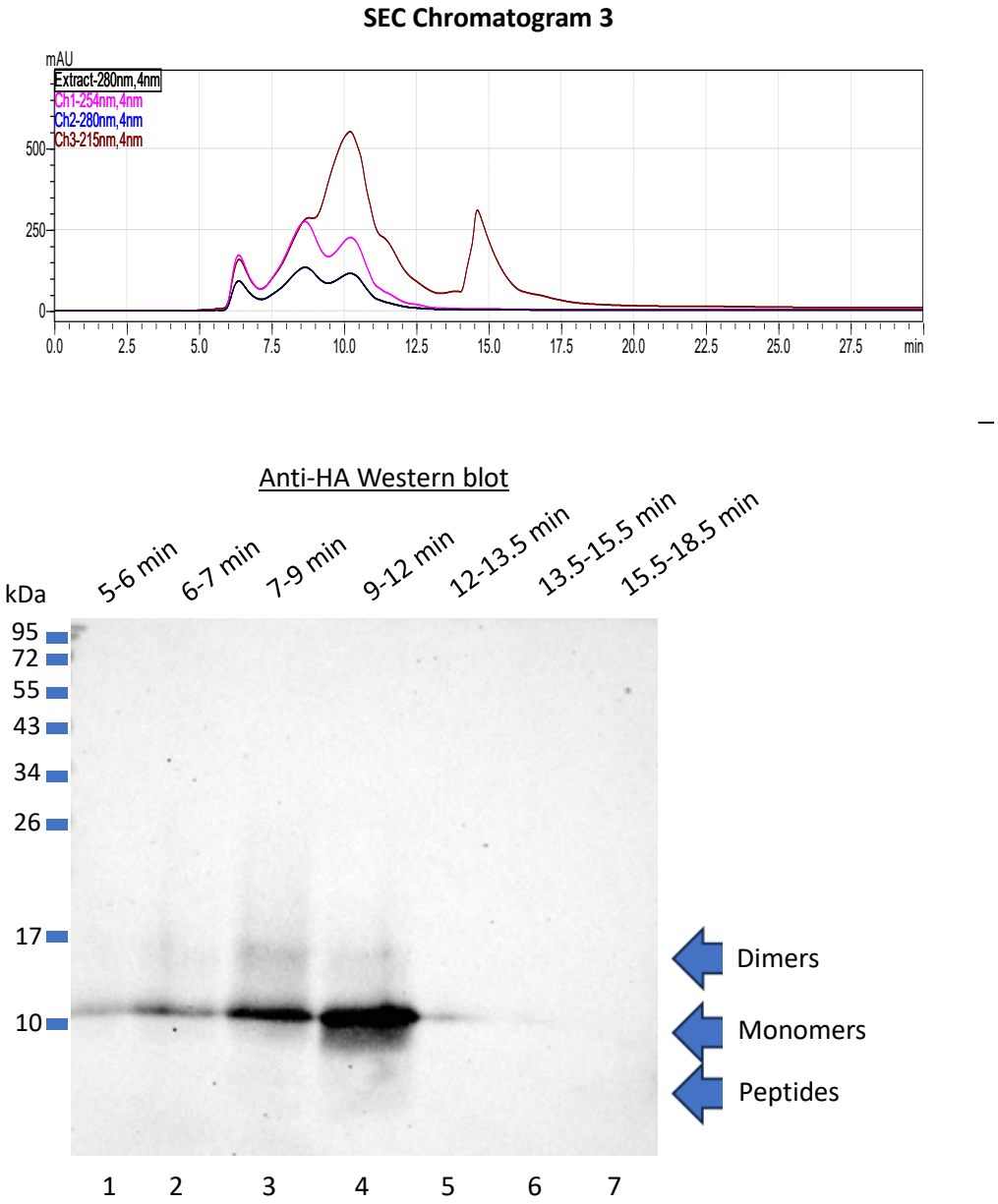

Figure 47: Increasing NaCl concentration in the mobile phase to 0.2 M resulted in an improved, although not complete dimer separation, as seen in **Chromatogram 3**. This resulted in an improvement in the separation of dimers and monomers, as seen in the Western blot, with majority of dimers seen in lane 3, while the majority of monomers are in lane 4. Monomers are coeluting with dimers (lane 3).

It was hypothesised that increasing the amount of NaCl would further improve protein resolution on the column by interfering with the electrostatic interactions

between the proteins, as well as between the proteins and the column. The concentration of NaCl was increased to 0.4 M; however, once the samples were injected on the column, absorbance dropped significantly, indicating proteins were crashing out of solution (as seen in **Chromatogram 4**). Additionally, Western blot (**Figure 48**) showed a decrease in peak separation and in signal intensity. Only two fractions eluting between 7-9 min and later between 13-15 min showed a significant presence of HA-tagged monoubiquitin **23** (lane 1 and lane 4).

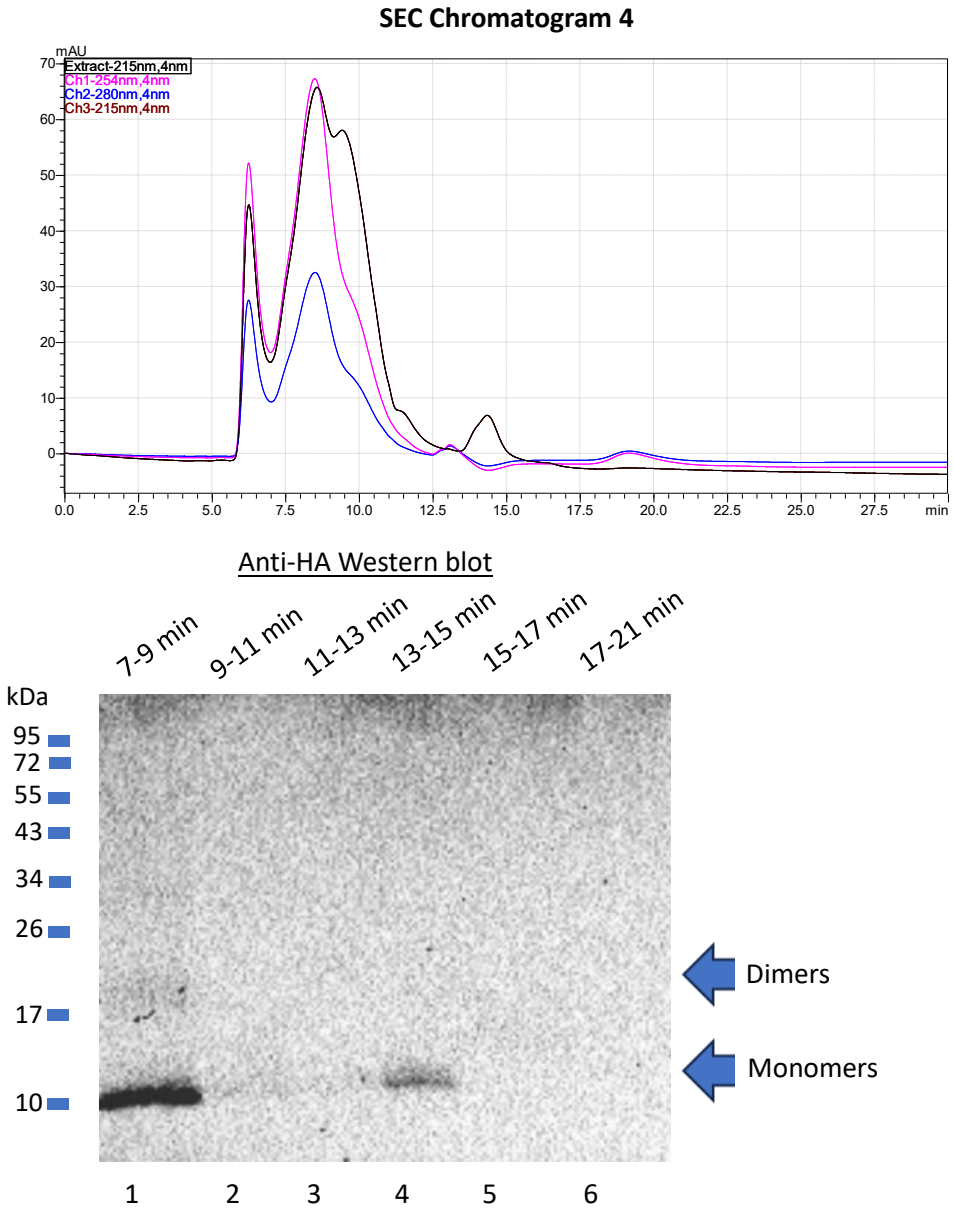

Figure 48: Increasing NaCl concentration to 0.4 M NaCl resulted in protein precipitation, as seed by the drop in peak intensity seen in **Chromatogram 4**. This did not result in a noticeable improvement in the separation of dimers and monomers, as seen in the Western blot. Monomers are mostly coeluting with dimers (lane 1).

At 1M NaCl in the mobile phase, the vast majority of proteins precipitated out of solution, resulting in **SEC Chromatogram 5, Figure 49**. Fractions collected during that run did not contain enough HA-tagged proteins to allow for Western blot visualisation.

SEC Chromatogram 5

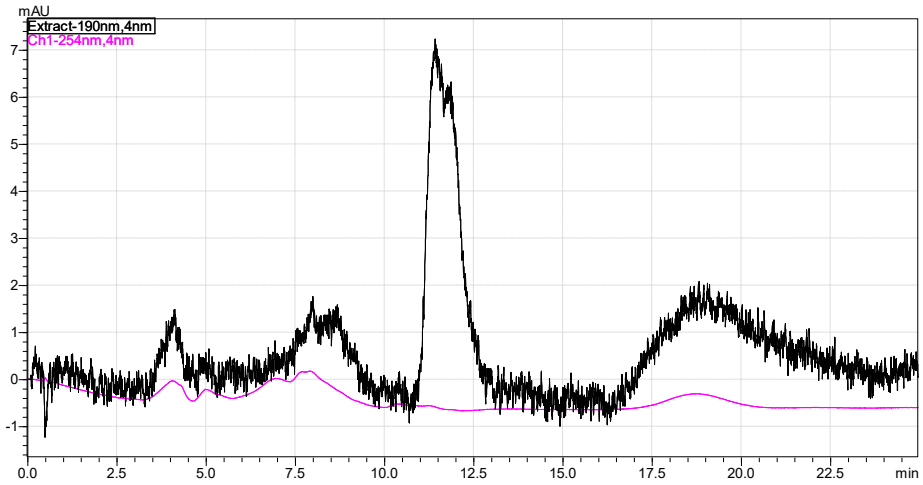

Figure 49: Majority of proteins precipitated at 1 M NaCl, as seen by the drastic drop in a signal intensity in **Chromatogram 5**. Western blot could not be visualized due to the lack of signal from the HA tag, and low protein content in each lane.

Salt content in the mobile phase was adjusted back to 0.2 M Na_2HPO_4, 0.2 M NaCl (pH 7.0). Increase in flow rate should allow for sharper peaks; however, as seen in **SEC Chromatogram 6**, **Figure 50**, although doubling the flow rate to 0.8 mL/min decreased retention times, it did not improve peak separation. Two large peaks can be seen starting at 6.5 min and ending at 10 min, which are due to peptides present in the starting materials used, or due to protein degradation under radical conditions, which were not efficiently removed by filtering through 5 kDa concentrators.

SEC Chromatogram 6

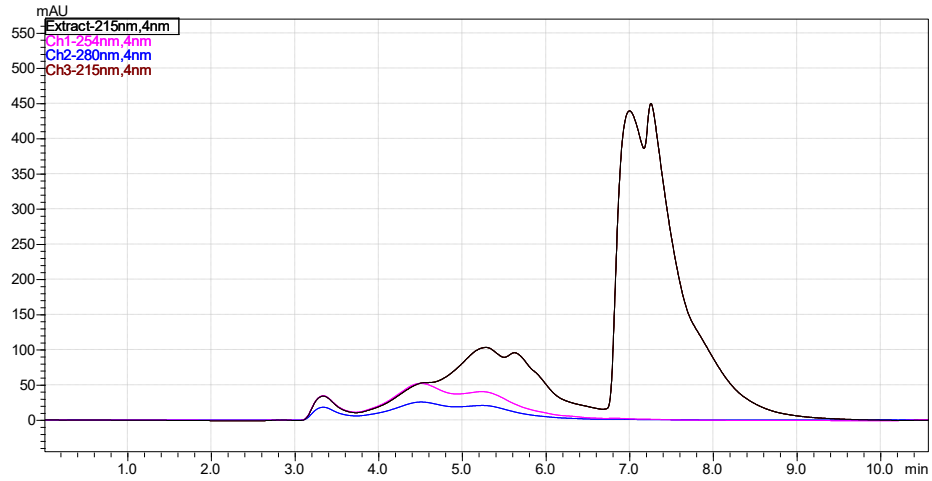

Figure 50: NaCl concentration of 0.2 M in the mobile phase was chosen for further method optimization. **Chromatogram 3** shows that a 2-fold increase in flowrate did not result in better peak resolution for peaks eluting between 3 and 6.5 min.

30% acetonitrile was then added to the mobile phase that contained 0.2 M Na_2HPO_4, 0.2 M NaCl (pH7) with the hope of improving protein separation by minimising any potential interactions between hydrophobic residues of proteins and the stationary phase. Flow rate was adjusted back to 0.4 mL/min. No improvement in protein separation was achieved, however, as seen in **SEC Chromatogram 7**, **Figure 51**, and fractions had to be dried out to remove organic solvent. Once dry, samples would have to be reconstituted in homogenate buffer before downstream analysis by Western blot or their use as ABPs. No Western blot analysis was carried out for these samples, due to a lack of improvement in dimer **44** separation.

SEC Chromatogram 7

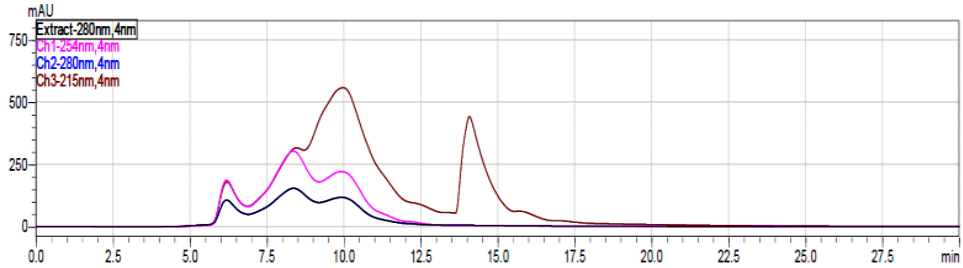

Figure 51: Addition of 30% acetonitrile to the mobile phase that contained 0.2 M Na_2HPO_4, 0.2 M NaCl, however it did not improve peak resolution.

Increasing NaCl content to 0.25 M and decreasing Na_2HPO_4 to 0.1 M allowed for a slight improvement of peak resolution, without affecting protein solubility (**SEC Chromatogram 8**). Western blot in **Figure 52** shows each of the eluted fractions incubated with OTUB1, a model deubiquitinase, followed by radical initiation. Fraction

eluting at 7-9 min contained HA-tagged mono and di-ubiquitin. OTUB1 was labelled by construct **23** present in this fraction (lane 3). Unfortunately, due to small quantities of di-ubiquitin formation, due to low efficiency of thiol-yne reaction, no clear signal from OTUB1 labelled with HA-tagged di-ubiquitin can be seen. OTUB1 labelled with HA-tagged monoubiquitin **23** is most clearly visible in the fraction eluting at 9-11 min, highlighting the improvement in removal of monomers from earlier fractions.

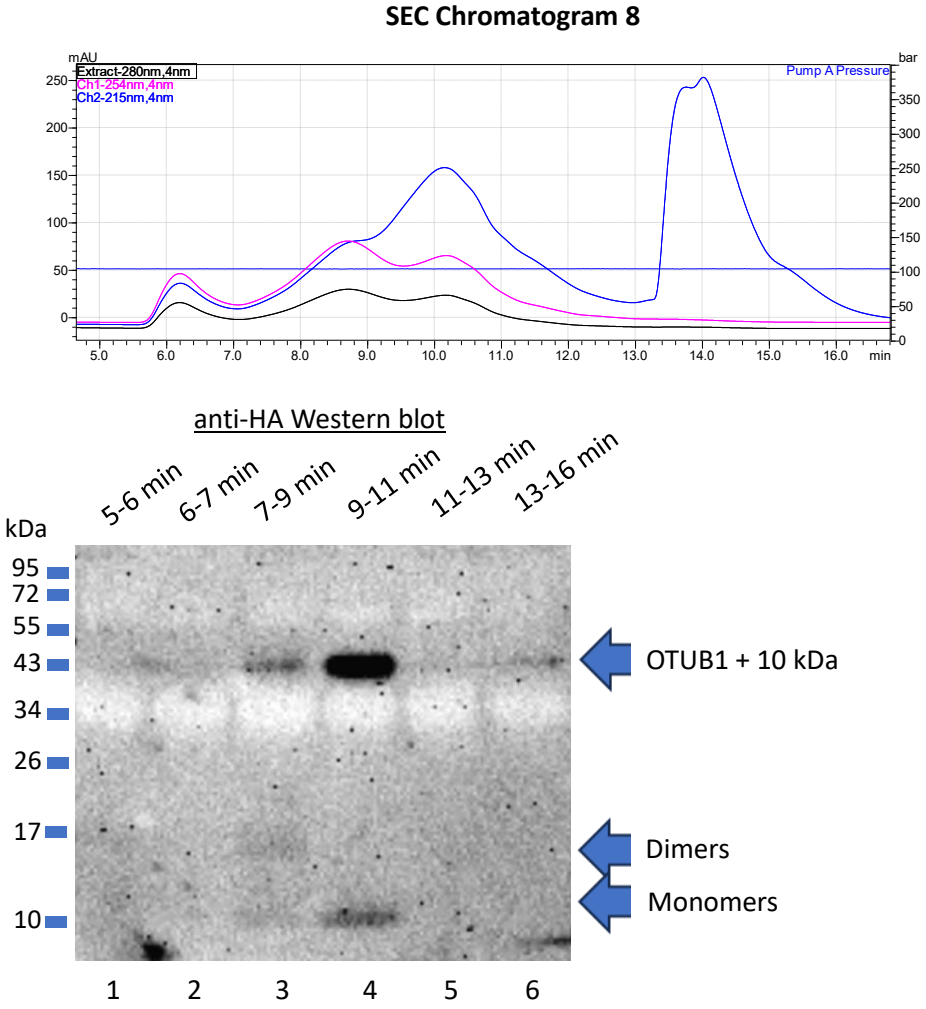

Figure 52: SEC method was changed, with NaCl at 0.25 M, Na_2HPO_4 at 0.1 M, pH 7, flowrate of 0.2 mL/min. This resulted in an improved peaks resolution, as seen in **Chromatogram 8**. This method did not affect protein solubility substantially. The anti-HA Western blot shows each fraction collected being concentrated and desalted using 5 kDa Vivaspin filters being incubated with OTUB1 under radical conditions. No clear labelling of OTUB1 with dimers was seen.

NaCl concentration was increased to 0.3 M, in an attempt to further improve separation of dimers. Three separate samples containing dimer **44** were run on SEC and fractionated at 5-6 min, 6-8 min, 8-10.5 min, and 10.5-13 min (as seen in **Chromatogram 9**). Respective fractions from each of the three runs were pooled and

concentrated using 5 kDa filter, followed by their incubation in the presence of OTUB1, and radical initiation.

Western blot in **Figure 53** shows that HA-tagged **23** elutes from the SEC column between 6-13 min (lanes 2, 3, and 4), with the most intense signal coming from the fraction eluting at 8-10.5 min (lane 3). HA-tagged dimeric **44** is eluted from the column between 6-10.5 min (lanes 2, and 3). Alkyne probe **23** eluting between 10.5-13 min (lane 4), has similar signal intensity to monomers eluted between 6-8 min (lane 2), however, without the presence of dimeric **44**, highlighting improved separation of dimers from monomers. OTUB1 was labelled by probe **23** in lanes 2, 3, and 4, however, only lanes 2 and 3 show signs of labelling OTUB1 with HA-tagged di-ubiquitin constructs under radical conditions. This is the first evidence of a thiol-ene reaction between an alkene-linked di-ubiquitin and a model DUB. Band intensity due to HA-tagged monoubiquitin-labelled OTUB1 in lanes 2 and 4 show that the amount of HA-tagged monoubiquitin is very similar in both samples. The only major difference between the two fractions is the presence of HA-labelled di-ubiquitin, and OTUB1 being labelled by it. Lane 3 also seems to show a band corresponding to OTUB1 being labelled with HA-tagged di-ubiquitin, providing further evidence for the activity of the HA-tagged di-ubiquitin construct as a radical ABP. The fraction containing eluant from 6-7 min (lane 1) contained a negligible amount of HA-tagged ubiquitin and did not label OTUB1 significantly.

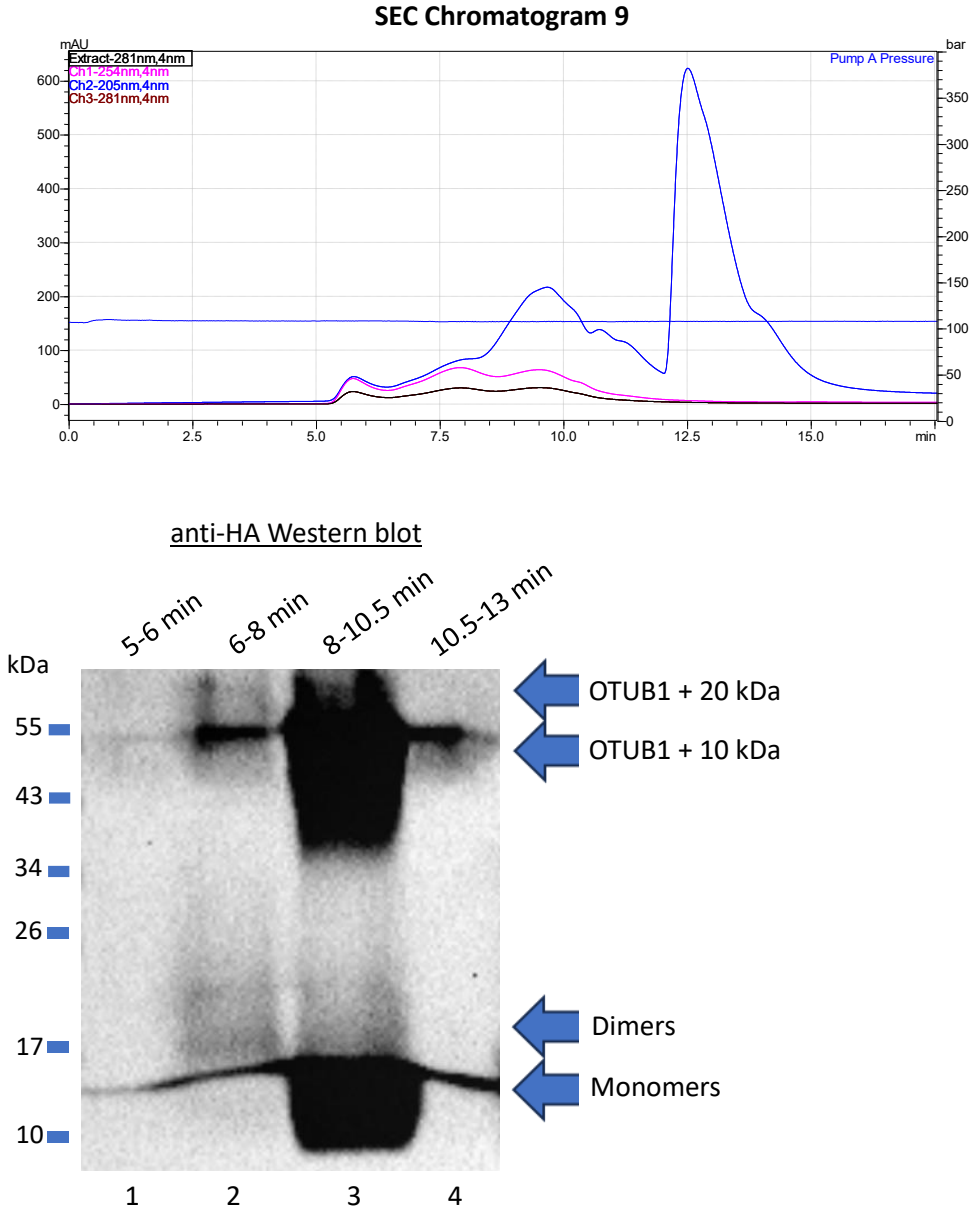

Figure 53: NaCl concentration was increased to 0.3 M, in an attempt to further improve separation of dimers. Three separate samples containing dimer **44** were run on SEC and fractionated at 5-6 min, 6-8 min, 8-10.5 min, and 10.5-13 min. **Chromatogram 9** shows a representative chromatogram. Respective fractions from each of the three runs were pooled and concentrated using 5 kDa filter, followed by their incubation in the presence of OTUB1, and radical initiation. Anti-HA Western blot shows the first example of alkene-containing di-ubiquitin construct labelling OTUB1 *via* thiol-ene reaction.

In an attempt to determine the exact moment at which HA-tagged di-ubiquitin is eluted, without the presence of HA-tagged monoubiquitin **23**, seven independent thiol-yne reactions were injected on the SEC column, and fractionated every 30 s

starting at 5 min and ending at 11 min, as seen in **SEC Chromatogram 10**. Respective fractions from all seven runs were pooled, concentrated using 5 kDa concentrators and incubated with OTUB1, followed by radical activation. Western blot in **Figure 54** shows that HA-tagged di-ubiquitin is eluted between 7.5-10 min, while HA-tagged monoubiquitin is eluted between 8-11 min. OTUB1 labelling under radical conditions in the corresponding lanes supports this observation. It seems that only 30 s between 7.5-8 min (lane 5) contain mostly HA-tagged di-ubiquitin, although in minuscule quantities, with the majority of the dimers being eluted alongside monomers between 8-11 min (lanes 6, 7, 8, 9, 10, and 11). Resolution provided by this approach is not sufficient for robust purification of HA-tagged di-ubiquitin **44**, and another method of dimer purification needs to be utilised.

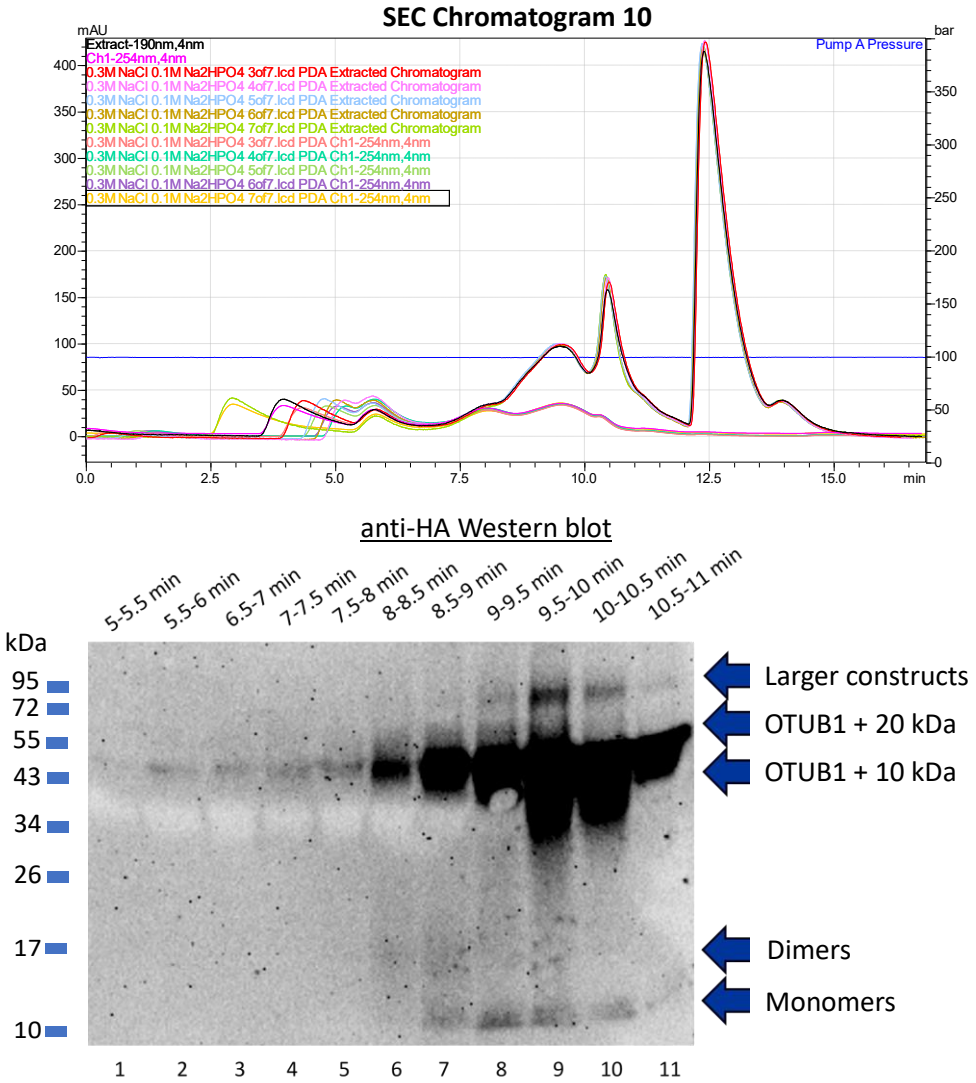

Figure 54: Seven samples containing dimer **44** were separated *via* SEC, as seen in **Chromatogram 10**. Each run was separated into 30 sec fractions, pooled, concentrated and desalted, incubated with OTUB1 under radical conditions. Dimers elute between 8 – 10 min, while monomers between 8.5 – 11 min. This leaves 30 sec between 8-8.5 min where only dimers are eluted.

One approach that was attempted was the simplification of matrix in SEC samples, by re-injecting fractions containing mixtures of mono and di-ubiquitin constructs, to further isolate them while in solution, based on their size. Timepoints between 7-10 min seen in **SEC Chromatogram 11, Figure 55** were chosen for that purpose. Between 7-8 min, HA-tagged di-ubiquitin constructs with little presence of mono-ubiquitin are expected. Between 8-9 min, a mixture of monomers and dimers is expected, while between 10-11 min, mostly monomers should be present.

SEC Chromatogram 11

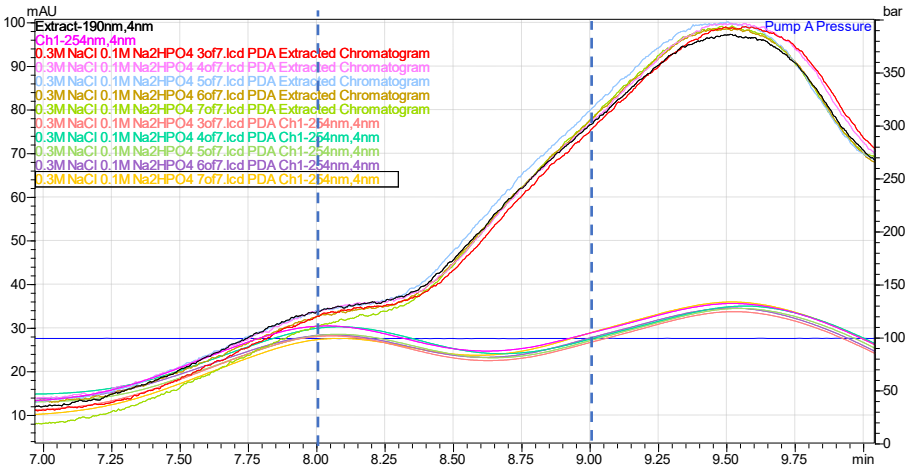

Figure 55: Seven samples containing dimer **44** were injected on SEC, fractionated at times between 7-8, 8-9 and 9-10 min, desalted and concentrated into three samples.

When a fraction collected between 7-8 min seen in **SEC Chromatogram 11** was concentrated from 400 µL to 60 µL using 5 kDa filters, and reinjected 20 µL at a time *via* direct injection on the SEC column, **SEC Chromatogram 12, Figure 56** was the result. Although absorbance diminished drastically after re-injection of the selected fraction, separation of di-ubiquitin constructs (seen as a peak eluting between 6-8.5 min) was improved significantly. Some monomers still can be seen eluting from the column from 8.5-12 min, which was expected.

SEC Chromatogram 12

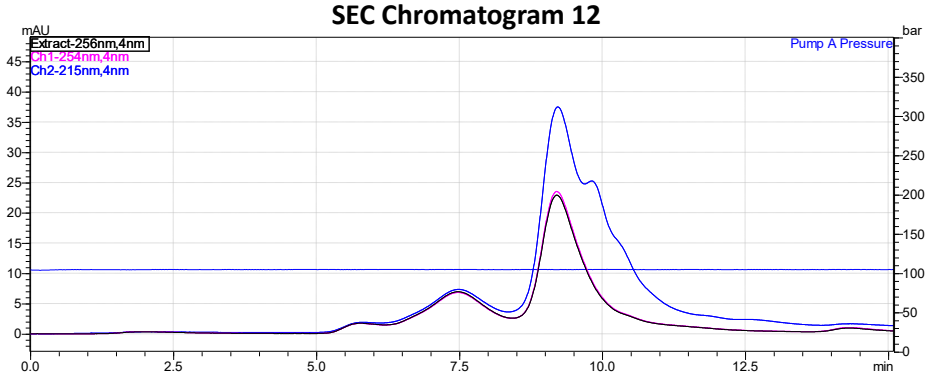

Figure 56: Pooled fraction containing eluent between 7-8 min seen in **Chromatogram 11** was run on SEC, as seen in **Chromatogram 12**. Peak separation has improved, but a clear drop in signal intensity was observed, and the presence of both monomers and dimers is still clear. Although promising, this approach requires further fractionation to completely separate dimers from monomers.

When a concentrated fraction containing a mixture of monomers and dimers was injected on the SEC column (fraction eluting at 8-9 min seen in **SEC Chromatogram 11**), peaks presumably belonging to monomers and dimers were seen to overlap to a significant degree. As seen in **Chromatogram 13, Figure 57** these peaks elute between 7-10.5 min.

SEC Chromatogram 13

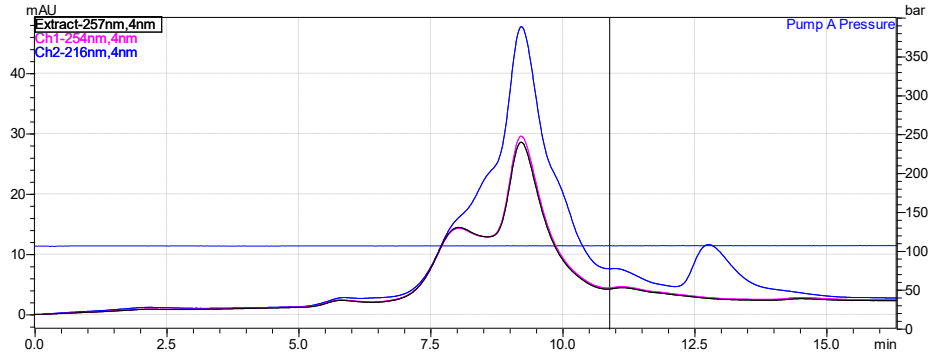

Figure 57: Pooled fraction containing eluent between 8-9 min seen in **Chromatogram 11** was run on SEC, as seen in **Chromatogram 13**. A clear drop in signal intensity was observed, both monomers and dimers are present.

Lastly, when the concentrated fraction containing eluant between 9-10 min from **Chromatogram 11** was re-injected, mostly monomers were found (eluting between 8-10.5 min) as seen in **SEC Chromatogram 14, Figure 58**.

SEC Chromatogram 14

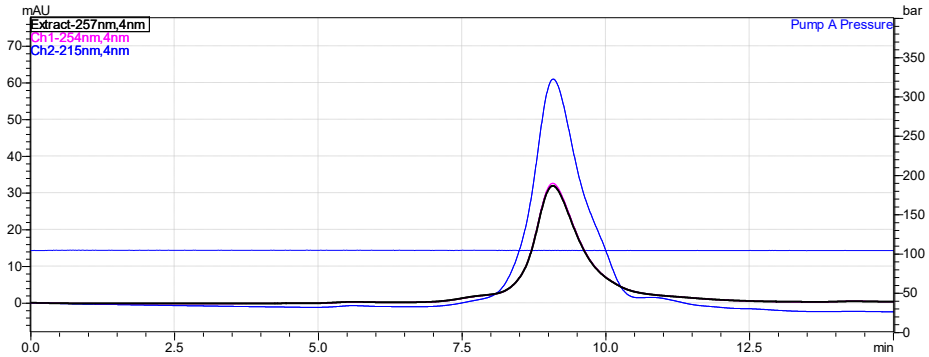

Figure 58: Pooled fraction containing eluent between 9-10 min seen in **Chromatogram 11** was run on SEC, as seen in **Chromatogram 14**. A clear drop in signal intensity was observed, mostly monomers are present.

Western blot containing re-injected and concentrated fractions from **SEC Chromatograms 12, 13 and 14** did not contain enough HA-tagged proteins to be visualised. Next, 20 samples containing di-ubiquitin **44** were fractionated, and their fractions were pooled, followed by their concentration. Unfortunately, re-injecting and fractionating the pooled sample resulted in significant losses, and the double-purified **44** was not detectable on the anti-HA Western blot. Due to persistent issues in isolating dimers using SEC, further attempts were not carried out, and alternative methods for di-ubiquitin construction were explored. In the future, alternative modes of separation, such as ion exchange chromatography could be attempted in order to separate monomers from dimers.

3.4. Alternative approach for di-ubiquitin construction

Alternative strategies for constructing di-ubiquitin ABPs containing an internal alkene linker connecting monomers were explored. In formulating this new approach, the absence of alkyne-containing ubiquitin monomer, higher conversion of dimers from monomers, and maintaining an internal alkene were required. The strategy chosen involved attachment of a linear hydrocarbon chain containing an internal double bond and a terminal primary amine to HA-ubiquitin$_{1\text{-}75}$-MESNa. The second terminus needed to be substituted by the side chain of distal ubiquitin at position 48, linking monomers. Resulting dimers would retain the internal alkene, resembling putative sites of DUB attack. 4-Bromobut-2-en-1-amine **51** was seen as a perfect candidate to be installed *via* NCL onto the proximal ubiquitin construct, followed by substitution of alkyl halide with thiolate of Ubiquitin K48C, resulting in the target thioether bond. The resulting dimer **48** would contain an additional CH_2 between the

alkene and the sulfur atom, in contrast to dimer **44**, which would bring the double bond closer to the catalytic thiol of DUBs. Retrosynthetic analysis shown in **Scheme 12** highlights the route needed for obtaining the desired di-ubiquitin construct. Optimising coupling conditions between monomers, ideally converting all starting monomers to dimers, was seen as the greatest challenge. That's because previous work on the thiol-yne product **44** showed unreacted monomers containing alkynes bind cysteine protease DUBs. Additionally, it was established that one-step purification of dimers by the selected HPLC modality was not achievable for the thiol-yne product; thus, improving coupling yield could greatly help in dimer isolation.

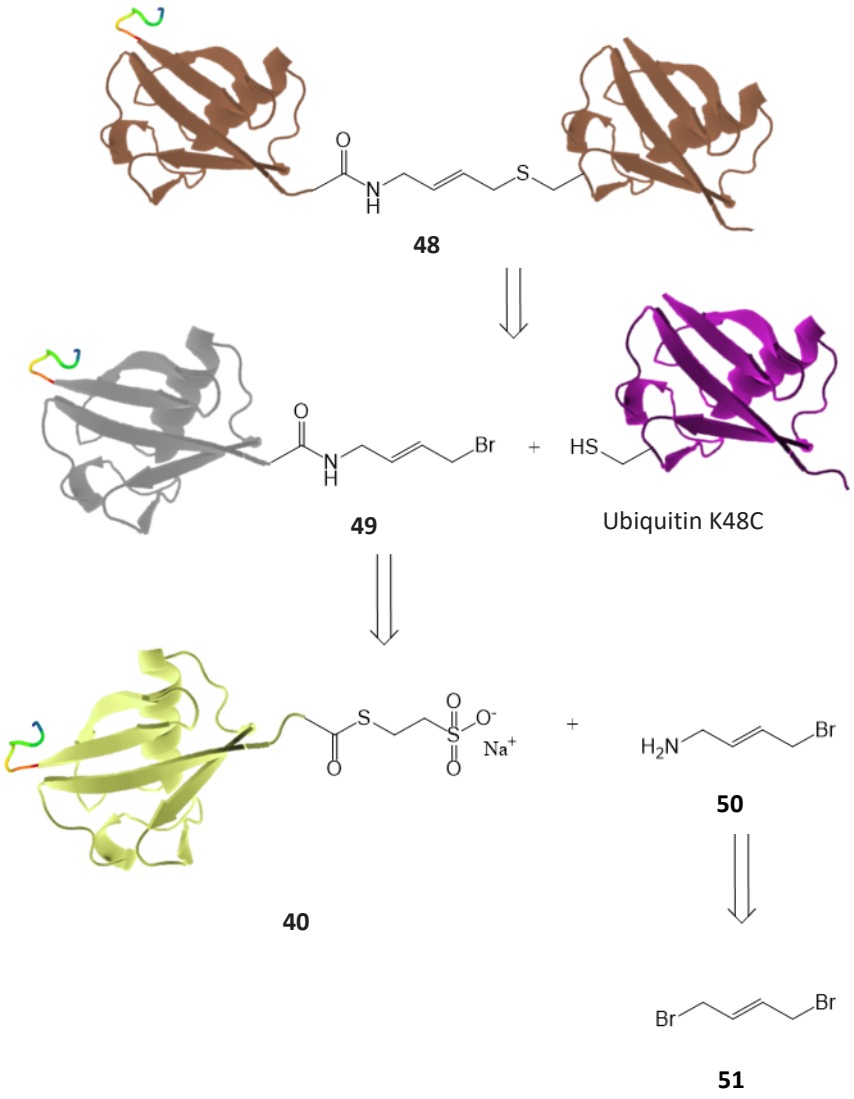

Scheme 12: Retrosynthesis of construct **48**.

(2*E*)-4-Bromobut-2-en-1-amine **50** was selected as a target linking molecule; however, it was not available commercially. A di-brominated analogue was seen as a potential starting point for target molecule synthesis. 1,4-dibromo but-2-ene **51**

specifically contains the correct number of carbons required to resemble the native substrate when connecting ubiquitin monomers. Modification of one terminal bromine with a primary amine was required. Exchanging bromide for phthalimide or hexamethylenetetramine (HMTA), used in Gabriel Amine Synthesis[297] and Delepine Amine Synthesis[298,] respectively, was seen as a potential synthesis. Several other methods for primary amine formation have been considered, including the reduction of Nitro compounds and Nitriles, the Leuckart Reaction, Hofmann Bromamide Degradation, and the Curtius Rearrangement; however, most of them have significant drawbacks. Reduction of Nitriles and Nitro compounds was not attempted due to the inaccessibility of starting materials, and the use of metal catalysts, which in trace amounts could interfere with the reaction. Reducing conditions were seen as likely to convert the internal alkene to an alkane. Overalkylation was likely to be a problem in Leuckart Reaction,[299] and this reaction was not explored.

Strong basic conditions required for Hofmann Bromamide Degradation could result in the loss of both terminal bromides, with the final product containing both an internal and a terminal alkene.[300] It is therefore unlikely target molecule would be synthesised using this approach.

Unstable and potentially explosive intermediates are produced in the Curtius Rearrangement,[301] and less hazardous synthetic routes were required.[302] Lastly, cross metathesis between linear hydrocarbons containing: terminal alkenes and bromides, as well as symmetric terminal diamines and dibromides, was also considered; however, due lack of selectivity,[303] and a high cost of transition metal catalysts,[304] this idea was not further explored. Using a protection/deprotection strategy for primary amine formation was seen as the most straightforward solution to form the target molecule.

3.4.1. Gabriel synthesis

Gabriel synthesis is a method of obtaining primary amines, without the risk of secondary or tertiary amines' formation.[305] In this reaction, an alkyl halide reacts with potassium phthalimide, resulting in *N*-alkyl phthalimide. The phthalimide protecting group is then removed in basic or acidic environments by reacting the protected product with hydrazine to form the primary amine. When hydrazine is used for phthalimide deprotection, 2,3-dihydro-1,4-phthalazinedione is formed as a side product. Protected 2-(4-Bromobut-2-en-1-yl)isoindoline-1,3-dione (**52**) was synthesised *via* Gabriel synthesis, as described in the literature,[306] in good yield (87%). **51** was reacted at room temperature with potassium phthalimide in DMF, while stirring, for 21 h.

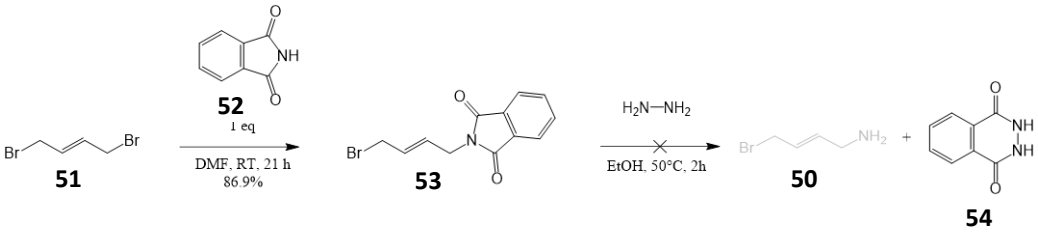

Scheme 13: Unsuccessful linker formation *via* Gabriel synthesis.

Resulting (*E*)-2-(4-Bromobut-2-en-1-yl)isoindoline-1,3-dione (**5**) was then reacted with hydrazine, in EtOH, as seen in **Scheme 13**. Unfortunately, the final product was not obtained and it was hypothesised that product degradation occurred during the basic workup. Presence of 2,3-dihydro-1,4-phthalazinedione (**54**) was, confirmed, which suggests that product **50** might have formed in the reaction. The reaction was repeated at room temperature; however, no product formation was observed. Hydrazine concentration was reduced 5-fold, in case hydrazine participated in SN2 reaction, which removed one terminal bromide. Reaction was repeated in reflux conditions; however, TLC showed several spots, suggesting degradation of the product. Alternative methods of phthalimide deprotection were sought after to assess the potential negative impact of hydrazinolysis on the target molecule.

3.4.2. Deprotection with sodium borohydrate

An exceptionally mild method for deprotection of phthalimides has been reported in 1984,[307] as seen in **Scheme 14**. Using the published procedure, the phthalimide moiety was expected to be reduced to O-hydroxymethyl benzamide, which would have lactonized to release the primary amine **50** and side product phthalide (**55**). After an 21 h reaction, degradation of the starting material was

observed, although the presence of side product **55** was noted. $NaBH_4$ solution is strongly basic (pH 12), suggesting again that the terminal bromide is unstable in basic environments.

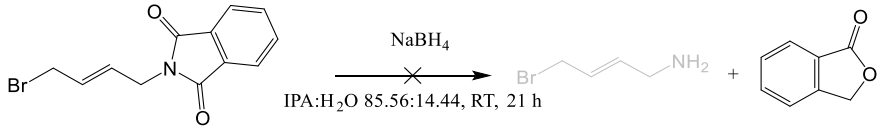

53 **50** **55**

Scheme 14: Mild deprotection of phthalimide without hydrazine.

3.4.3. Delepine synthesis

Following a published procedure,[308] (*E*)-4-Bromobut-2-en-1-amine **50** was synthesised using Delepine amine synthesis. In this reaction, alkyl halide reacts with hexamethylenetetramine (HMTA) in DMF, under inert, slightly basic conditions. Nitrogen atom in HMTA first attacks the primary carbon in the alkyl halide, *via* SN2 reaction, forming a quaternary ammonium salt (**56**). Hydrolysis of HMTA is performed in concentrated HCl, resulting in a deprotected molecule with a primary amine, as well as formaldehyde and ammonium chloride.

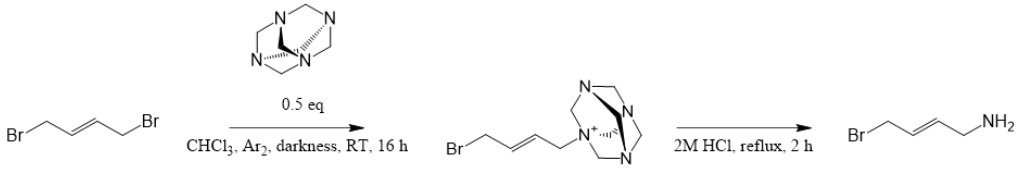

51 **56** **50**

Scheme 15: Successful formation of the linker containing an internal alkene.

Protection with HMTA was successfully achieved, as seen in **Scheme 15**. 1 eq of (T)-1,4-dibromobut-2-ene was reacted with 0.5 eq HMTA, affording (E)-1-(4-bromobut-2-en-1-yl)-1,3,5,7-tetraazaadamantan-1-ium, presence of which was confirmed *via* IR and mass spectrometric analysis. This intermediate was not further characterised.

Salt **56** was hydrolysed in 2M HCl, under reflux conditions, for 2 h. The release of the protecting group was confirmed by the formation of a new spot on TLC that reacted with ninhydrin stain at the end of the reaction. Identity of the crude product **50** was confirmed by NMR and mass spectrometry. After basifying the solution to pH 8, the solution was extracted with DCM twice, dried with sodium sulphate and filtered, and both the organic extract and the aqueous solution were dried under vacuum. Neither NMR, mass spectrometry nor TLC analysis were able to conclusively determine presence of the target molecule in the organic extract, nor in the aqueous phase. It is presumed that the product degraded in a basic environment.

The reaction was repeated until hydrolysis of the product in acid, and the crude product was dried under vacuum. Purification attempts on Weak-Cation Exchange (WCX) and Normal Phase flash chromatography did not result in product purification, and TLC showed product degradation when WCX resin was treated with increasingly basic mobile phase (linear gradient 0 – 0.3 M NaOH).

Crude product **50** was therefore incubated with MESNa-containing **40**, to create construct **49**, followed immediately by incubation with ubiquitin K48C. Western blot seen in **Figure 59** shows no di-ubiquitin (**48**) formation, due to construct **49** failing to form in acidic conditions. This approach was abandoned, and the intermediate products were not analysed further.

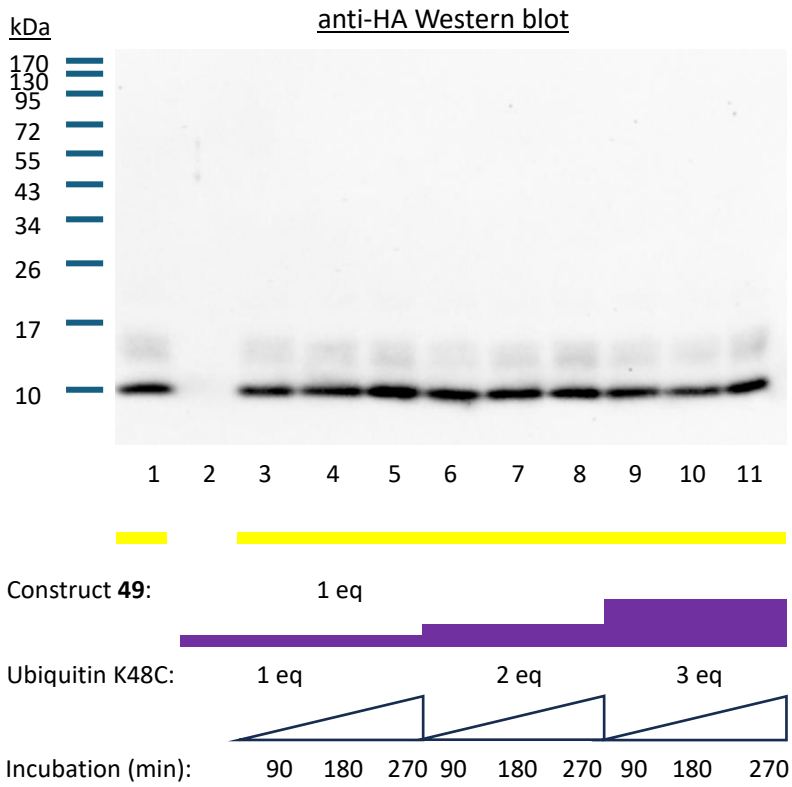

Figure 59: Unsuccessful formation of di-ubiquitin construct **6**, likely due to the linker molecule degrading in basic environments.

3.5. Conclusions and future outlook

Di-ubiquitin construct containing an internal alkene linking ubiquitin monomers has been formed, and the validity of thiol-yne reaction for protein bioconjugation has been shown through a series of reactions between alkyne-containing ubiquitin monomers, a small thiol-containing fluorophore, as well as two proteins containing cysteine residues (BSA and Ubiquitin K48C).

Thiol-ene activation of crude di-ubiquitin constructs, and labelling of a model DUB, OTUB1, were shown. Progress has been made in di-ubiquitin construct purification; however, due to low reaction yields, a pure di-ubiquitin construct was not isolated. In the future, using different radical initiators could improve thiol-yne yields; however, improved yields would have to be combined with improved purification methods. Different separation modalities could be employed, such as ion-exchange chromatography or tangential flow filtration. Combining improvements in product formation and purification would lead to the isolation of pure dimers. Pure dimers could be identified *via* MALDI-ToF mass spectrometry and tested against a panel of purified DUBs to confirm construct affinities and DUB specificities. Affinity pull-down experiments against HA-tagged targets, followed by tryptic digestion of the resulting proteins and their proteomics identification, could allow for the discovery of new, K48-specific DUBs. A panel of di-ubiquitin probes linked by an internal alkene at the remaining six lysines could be formed. These constructs would help determine the specificities of DUBs. Biocompatible thiol-ene probe activation would need to be further investigated, with the potential use of radical initiators activated by near-infrared light.

The addition of cell-permeable cyclic peptides, or other methods allowing biomolecules to cross membranes, such as nanoparticles and micelles, would allow for translation of the radical di-ubiquitin probes to cells. Biological activity assays could then be performed, with the intent of capturing or blocking DUBs related to disease, for a deeper understanding of biochemical mechanisms behind pathologies, as well as interrogation of DUB inhibitors and their targets.

Chapter 4: Alternative approaches for lysine-specific protein conjugation

4.1. Objectives

The primary objective of this chapter was the controlled formation of a di-ubiquitin **58** containing a terminal alkene, seen in **Scheme 16**. To achieve this, imidazole-1-sulfonyl azide **59** was successfully used for azido-substitution of lysines in model protein systems, including terminal alkene-containing **31**. Copper-catalyzed Azide-Alkyne Cycloaddition (CuAAC) reaction was then performed between azido-modified **57** and terminal alkyne-containing **23**, resulting in a di-ubiquitin construct with a terminal alkene **58**.

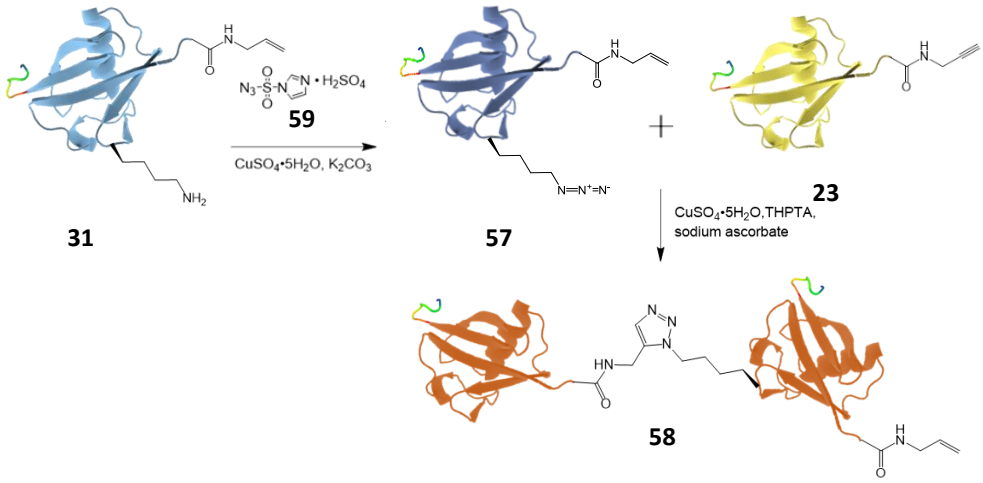

Scheme 16: Di-ubiquitin construct formation by azido-substitution of lysines on one monomer, followed by CuAAC reaction to an alkyne-containing monomer.

A secondary objective of the chapter was the application of dimer **58** for the thiol-ene chemistry for covalent labelling of thiol-containing proteins. Thiol-ene reaction between alkene-containing **58** and cysteine-containing model proteins: OTUB1, and Ubiquitin K48C mutant was attempted; however, no clear labelling of the DUB model with dimers, nor controlled tri-ubiquitin formation was initially observed.

4.2. Formation of di-ubiquitin construct with a terminal alkene

Polyubiquitin chains are primarily connected *via* isopeptide bonds connecting lysine side chains of a distal ubiquitin to the C-terminus of a proximal ubiquitin. Therefore, Di- and multi-ubiquitin ABPs of DUBs containing covalent warheads at sites where isopeptide linkages in native polyubiquitin chains are found, imitate sites of DUB attack. A strategy for the controlled formation of di-ubiquitin ABPs containing an internal alkene *via* thiol-yne reaction was described in Chapter 3. Purification of product dimer **44** using Size Exclusion Chromatography (SEC) was attempted; however, only partial purification of dimers was achieved.

Due to the technical challenges in purifying dimers, purification efforts were abandoned. Alternative warheads yielding di-ubiquitin constructs with internal alkenes were explored. Attempted Delepine amine synthesis resulted in a hexamethylenetetramine-protected target molecule. When exposed to strongly acidic conditions, the protecting group was removed, and the target molecule was formed. Installing the resulting molecule onto the C-terminus of MESNa-containing **40** and coupling that construct to a thiol-containing Ubiquitin K48C was attempted; however, due to the warhead's instability in basic conditions, the construct did not form **dimers**.

Forming a di-ubiquitin construct with a terminal alkene (**31**) instead of an internal alkene linkage (**44**) was attempted, as probe **31** has the potential to label protein populations distinct from **44**, under radical conditions. Previously reported di-ubiquitin ABPs of DUBs exploited the fact that several ubiquitin binding sites can exist near catalytic domains of DUBs, allowing for polyubiquitin chains or other protein substrates to bind. Flierman *et al*.[309] created a panel of di-ubiquitin ABPs, linked at all 7 lysine residues, with propargylamine warheads at the C-termini. K11-linked di-ubiquitin probe with a terminal alkyne showed high specificity for OTUD2, while OTUD3 was shown to bind K11 and K6-linked di-ubiquitin probes with terminal alkynes. McGouran *et al*.[270] showed ubiquitin monomers containing a C-terminal Michael acceptor warhead followed by a terminal alkyne, covalently bound to 8 ubiquitin variants, using CuAAC reaction, where each of the 7 lysines, and one methionine (M1) were mutated to azidohomoalanine. This resulted in a series of di-ubiquitin probes, containing warheads in between monomers. Probes containing warheads at the linkage site between ubiquitin monomers were found to be broadly reactive, but some showed unexpected linkage preferences, especially for noncanonical chains (OTUB1 for K48, OTU7B for K11, USP15/16/24 for K27/29/11, respectively). The positioning of the warhead either between or at the terminus of di-ubiquitin probes affected which DUBs

were labelled, due to specific binding pockets being occupied by ubiquitin monomers, and the proximity of warheads to the DUBs' catalytic cysteines. In both papers, USP14 was captured by several ABPs, and the position of the warhead at the terminus or the linker did not affect the reactivity to USP14 much. Construct **44,** containing an internal alkene linker, could undergo thiol-ene reaction at the active site of K48-specific cysteine protease DUBs, while dimer **58,** containing a terminal alkene, could undergo thiol-ene reaction with other DUBs. Novel radical di-ubiquitin **58** described in this chapter has the advantage of time-resolved capture of specific DUB populations, *via* radical thiol-ene reaction.

4.2.1. Azido-substitution of lysines in amino acids and short peptides

Diazotransfer reagent, imidazole-1-sulfonyl azide **59** was synthesised as described in the literature,[310] characterised and generously donated by Dr. Susannah Calvert. Dr. Calvert used azide **59** to successfully modify primary amines with an azide group in an amino acid model system, Fmoc-Lys-OH, as well as in a model heptapeptide, H_2N-Trp-His-Ile-Ser-Lys-Glu-Tyr-$CONH_2$, which contained two NH_2 groups. The procedure for compound **59** formation can be seen in **Scheme 17** below:

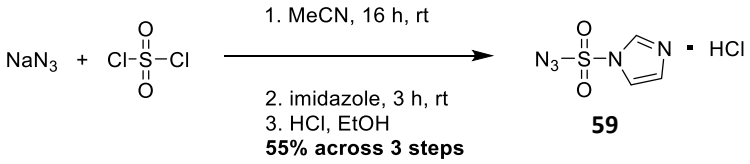

Scheme 17: Imidazole-1-sulfonyl azide **59** formation.

4.2.2. Novel approach in protein bioconjugation through lysine modification

BSA was selected as a model protein to optimise reaction conditions, as it contains 59 lysines and a terminal primary amine, all of which could be modified by the azido-transfer reaction. The concentration of imidazole-1-sulfonyl azide **59** was varied from 0.1 mg/mL to 10 mg/mL to determine the equivalents necessary for the modification of a single primary amine.

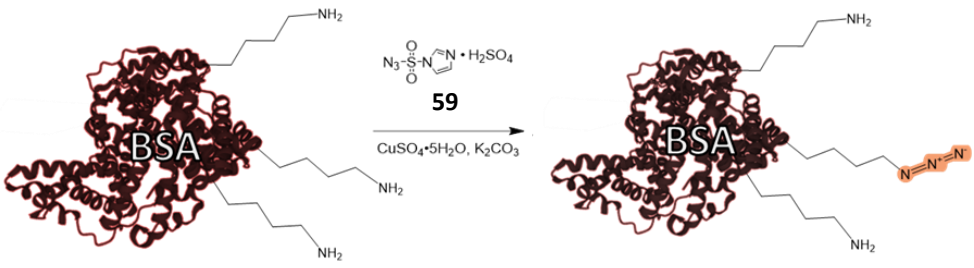

BSA Azido-modified BSA

Scheme 18: BSA lysine modification with compound **59**.

Scheme 18 shows the reaction schematic for a single modified lysine in BSA. A bar chart summarising Mass Spectrometric results, with protein coverage in blue, and number of modified lysines in orange, averaged over two analytical replicates, is presented in **Figure 60** below. A clear correlation between increasing diazotransfer reagent concentration and an increase in the number of azido-modified lysines can be seen. 10 mg/mL of imidazole-1-sulfonyl azide **59** contains 89 eq azide per 1 eq amine in BSA, resulting in azido-modification of 10 out of 15 observed lysines. 5 mg/mL compound **59** contains 44 eq azide per 1 eq amine in BSA, resulting in azido-modification of 8 out of 12 observed lysines. 2.5 mg/mL compound **59** contains 22 eq azide per 1 eq amine in BSA, resulting in azido-modification of 6 out of 10 observed lysines. 1 mg/mL compound **59** contains 8 eq azide per 1 eq amine in BSA, resulting in azido-modification of 5 out of 11 observed lysines. 0.5 mg/mL compound **59** contains 4 eq azide per 1 eq amine in BSA, resulting in azido-modification of 3 out of 11 observed lysines. 0.1 mg/mL compound **59** contains 0.8 eq azide per 1 eq amine in BSA, resulting in azido-modification of 1 out of 10 observed lysines. Neat BSA contained no azido-modified lysines, and 7 lysines overall were observed. Mass Spectrometric results can be found in **Appendix F**.

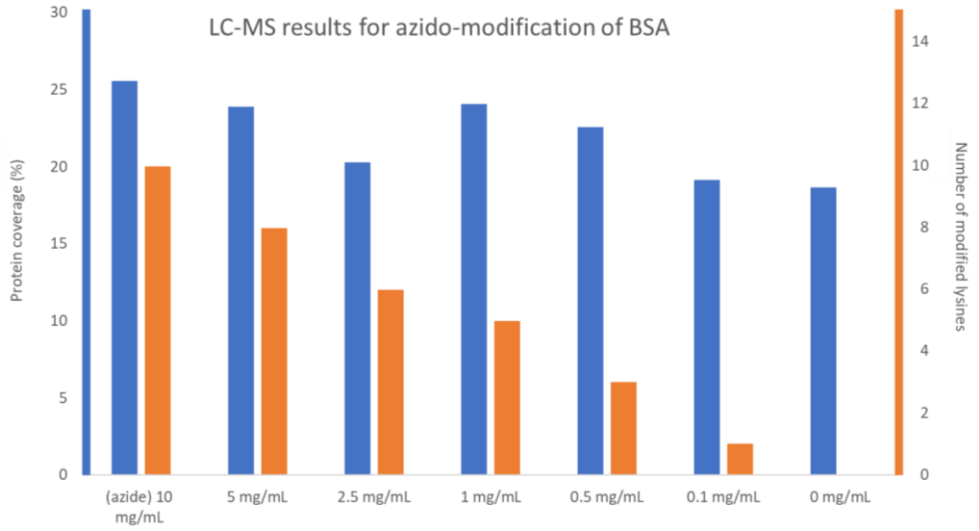

Figure 60: Summary of LC-MS/MS results showing number of modified lysines at varying concentrations of imidazole-1-sulfonyl azide **59**.

Table 1 below summarises results from LC-MS/MS runs, which were performed and analysed in duplicate. Specific positions of modified lysines in BSA, alongside numerical values showing protein coverage, and ratios of protein and primary amine to imidazole-1-sulfonyl azide **59** in each reaction are outlined.

Azdio-modification was added as a variable modification for lysine residues (+ 25.99 Da), and files were searched against the PDB human proteome database.

Table 1: Summary of LC-MS/MS results showing specific lysines modified on BSA by treatment with imidazole-1-sulfonyl azide **59**.

Eq azide **59** per amine	Protein coverage (%)	Unmodified lysines observed	Modified lysines observed
89	25.54	K12, K20, K51, K388, K533	K204, K211, K221, K224, K232, K239, K377, K413, K431, K524
44	23.89	K51, K204, K388, K533	K211, K221, K224, K232, K239, K413, K431, K524
22	20.26	K51, K204, K239, K431	K211, K221, K224, K232, K413, K524
8	24.05	K51, K204, K239, K375, K431, K533	K211, K221, K224, K232, K413
4	22.57	K51, K204, K224, K232, K239, K524, K533	K211, K221, K413
0.8	19.11	K51, K204, K221, K224, K232, K239, K388, K524, K533	K413
0	18.62	K51, K204, K232, K273, K388, K413, K533	-

The number of azido-modified lysines changed depending on the equivalents of diazotransfer reagent used. Different lysines show different reactivity to azido modification. Factors such as proximity to other amino acids, solvent exposure, and pKa/acidity have been identified as potentially contributing to this sequential reactivity of lysines, in the case of another non-enzymatic modification of lysines, acylation.[311]

Having optimised the diazotransfer reaction on BSA, and observed surprising levels of site selectivity, the reaction was attempted on alkene ABP **31**. Probe **31** consists of Ubiquitin$_{1\text{-}75}$ (containing 7 lysines), a terminal alkene on the C-terminus, and a terminal primary amine on the HA tag. The HA tag consists of 9 amino acids: YPYDVPDYA. Inspired by work done by McGouran *et al*.[270] a di-ubiquitin probe with a terminal alkene **58** instead of an internal alkene seen in dimeric construct **44** was proposed. First, selective azido-modification of a single lysine was carried out on alkene-containing **31** to afford azido-substituted derivative **57**. Di-ubiquitin probe **58** was synthesised by reacting alkyne-containing **23** with one azido-substituted lysine of **57**, using the CuAAC reaction, allowing for bioconjugation at physiological conditions in high yields.

Probe **31** was treated with several concentrations of azide **59** (10, 5, 2.5, 1, 0.5, 0.1 and 0 mg/mL), however, only at 10 mg/mL of the azide, a single lysine modification at position K48 was detected, out of 4 lysines observed.

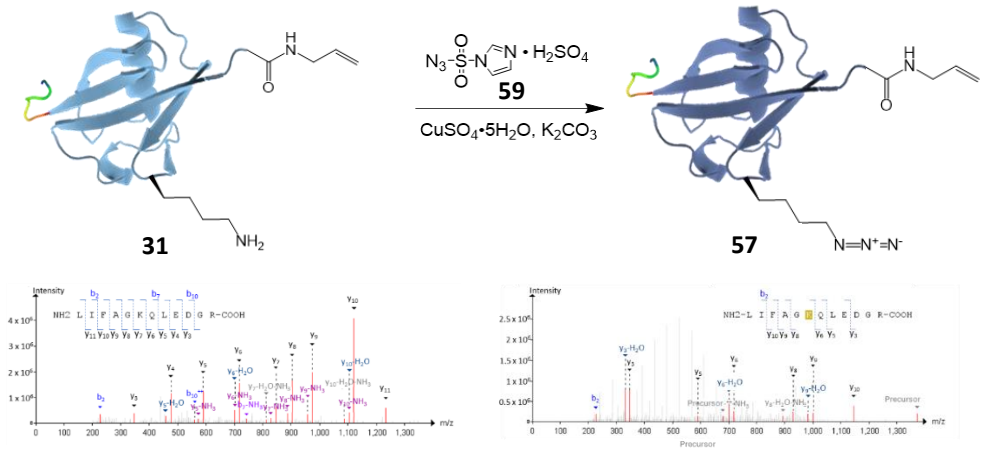

Figure 61: Azido-modification of lysines on probe **31**, alongside LC-MS/MS spectra of the peptide containing K48 before and after modification.

Identity of the substituted lysine, K48, was determined by LC-MS/MS analysis of tryptic digests, as seen in **Figure 61**. The sequence of the alkene ABP **31** was confirmed by 69.43% of validated peptide sequences, while azido-modified **57** by 39.3% of validated peptide sequences. Mass Spectrometric results can be found in **Appendix F**.

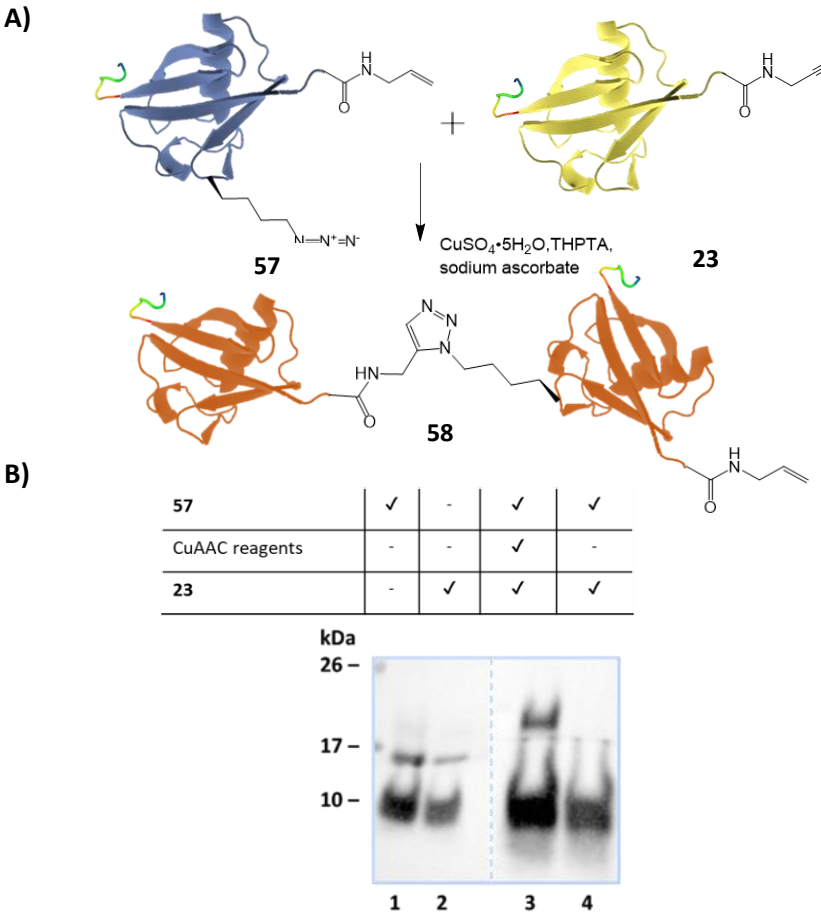

Figure 62: Anti-HA Western blot showing di-ubiquitin formation *via* CuACC.

Azido-modified **57** was reacted with the alkyne probe **23** using CuACC (**Figure 62 A**). The reaction product was visualised by Anti-HA WB (Fig. 3B). Treatment of probe **31** with 10 mg/mL compound **59** (a ratio of 1:125 of primary amines in probe **31** to azide **59**), followed by CuAAC reaction with an additional 2 µg of probe **23** resulted in di-ubiquitin formation. Lanes 1 and 2 in **Figure 62 B** contain 2 µg of probe **31** and 2 µg of probe **23,** respectively. 2 µg of probe **23** and 2 µg of azido-substituted **57** were incubated in the presence (lane 3) and absence (lane 4) of CuAAC coupling reagents. When both constructs were incubated in the presence of CuAAC reagents, in lane 3, a new band formed at 20 kDa, showcasing di-ubiquitin formation. When no CuAAC reagents were present, in lane 4, no additional band was observed, as no dimers formed.

Tryptic digests of alkyne probe **23** incubated alongside 5, 10 and 20 mg/mL of azide **59** were analysed by LC-MS, and only one azido-modification of lysine K48 was found when probe **23** was incubated with 10 mg/mL of azide **59**.

4.2.3. Trials of azido-substituted 31 as ABP of OTUB1

Scheme 19 showcases an attempted radical-initiated thiol-ene reaction between dimer **58** and cysteine protease OTUB1. It was postulated that dimer **58** would have its' terminal alkene in the proximity of OTUB1's catalytic cysteine, and following radical activation, thiol-ene reaction would covalently link OTUB1 to dimer **58**.

First, the azido-substitution reaction between probe **31** and compound **59** (at 5 mg/mL) was performed, but no significant difference in anti-HA Western blot signal intensity at 20 kDa was observed. This observation, combined with LC-MS data, suggests that only negligible amounts of di-ubiquitin formed, primarily because the azido-transfer reaction does not result in azido-modified lysines.

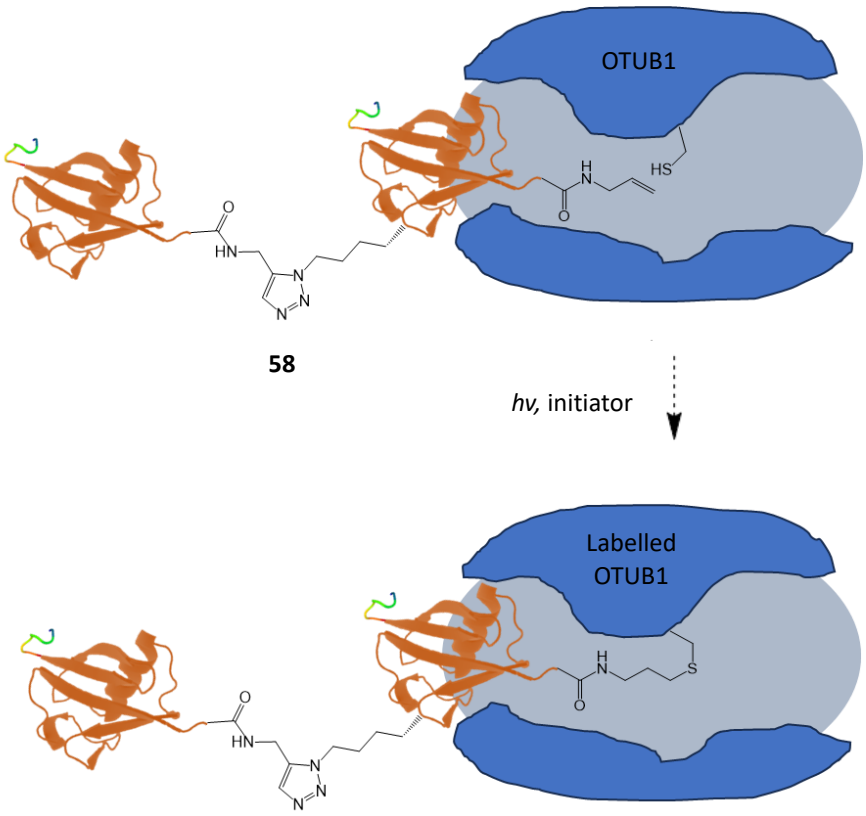

Scheme 19: Radical labelling of OTUB1 by dimer **58**.

Figure 63, shows the second attempt at forming di-ubiquitin constructs with terminal alkenes, as well as continuation of OTUB1 labelling trials with these constructs, under radical conditions. Azido-substitution reaction was performed at 10 mg/mL of compound **59**, and a significant increase in signal intensity can be seen at 20 kDa. Alongside LC-MS data, this provides evidence for di-ubiquitin formation *via* subsequent CuAAC reaction. Probe **31** was incubated alongside OTUB1 for 90 min at 37 °C, then mixed with radical initiator, degassed and exposed to UV for 3 min. OTUB1 was incubated alongside probe **23**, and separately, with probe **31,** under radical conditions were used as a positive control, resulting in covalent labelling of OTUB1.

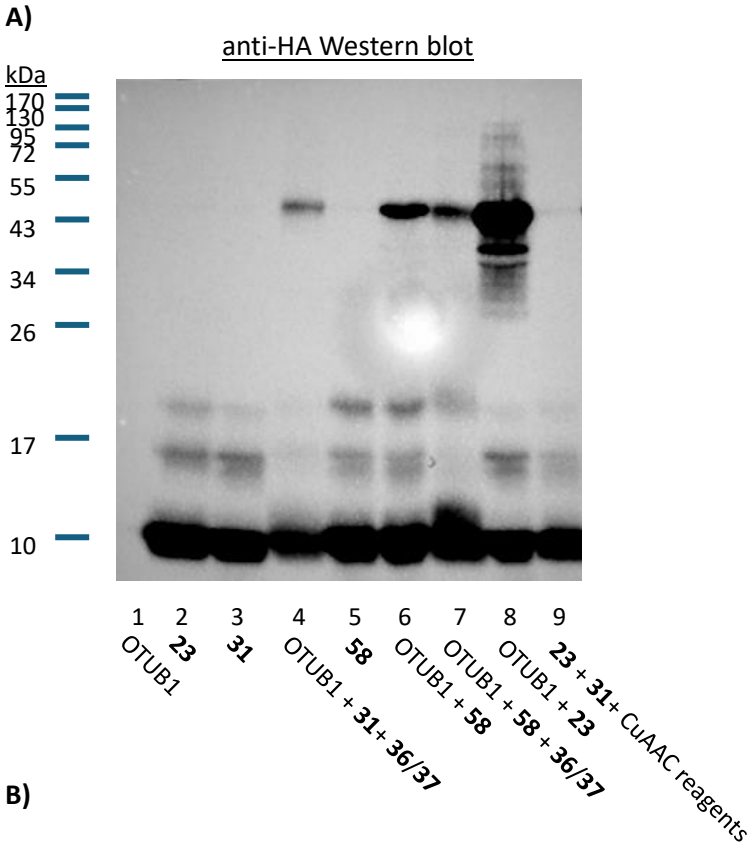

Figure 63 A: Anti-HA Western blot and silver stain showing attempted OTUB1 labeling with di-ubiquitin **58**, **B**: silver stain of the same reactions.

Lane 1 in **Figure 63** contains 2 μg of OTUB1, which can be seen on the silver stain. Lane 2 contains 2 μg of the alkyne ABP **23**, and lane 3 contains 2 μg of the alkene ABP **31**, both of which form a band on the anti-HA Western blot at the 10 kDa mark. Lane 4 contains 2 μg OTUB1 incubated alongside 2 μg of probe **31**, followed by **36**/**37** addition and radical initiation under UV light. This is a positive control of monomeric radical ABP labelling OTUB1, where a band can be seen at 45 kDa on an anti-HA Western blot. Lane 5 contains 2 μg of probe **31**, azido-substituted with 10 mg/mL compound **59**, purified with a NAP-5 column and concentrated using 5 kDa MWCO filter, resulting in azido-modified **57**, followed by CuAAC reaction with an additional 2 μg of probe **23**. A substantial increase in band intensity at around 20 kDa can be seen in the anti-HA Western blot, representing formation of di-ubiquitin construct **58** *via* CuAAC reaction. Lane 6 contains the same constructs as lane 5, with the final addition of 2 μg OTUB1, without radical initiation, while lane 7 contains di-ubiquitin construct **58** as in lane 5, with the addition of 2 μg OTUB1 and radical initiation with **36**/**37** under UV light. No significant change in band intensities, nor formation of a new band at 55 kDa can be seen in the anti-HA Western blot, showing that no significant labelling of OTUB1 with di-ubiquitin **58** took place in the presence, or absence of radical initiators. There was a drop in signal intensity of a band at 13 kDa in the anti-HA Western blot, in lane 7, which is due to radical initiators degrading one of the side-products. Lane 8 contains a positive control, 2 μg of probe **23** incubated alongside 2 μg OTUB1. This results in a very strong band at 45 kDa in the anti-HA Western blot, due to electrophilic addition of probe **23** to OTUB1. Lane 9 contains 2 μg of probe **31**, purified by NAP-5 and concentrated with a 5 kDa MWCO filter, followed by the addition of CuAAC reagents alongside an additional 2 μg of probe **23**. No change in band intensity at 20 kDa mark can be seen in the anti-HA Western blot, as no CuAAC reaction took place.

It is unclear from stained gels and Western blots alone whether OTUB1 was labelled with 20 kDa di-ubiquitin adducts in samples where radical initiators were added, compared to samples where no radical initiation took place. The presence of probe **23** in both cases labels OTUB1 preferentially, obscuring any di-ubiquitin binding under radical conditions. At 20 mg/mL of compound **59**, no bands at 10 kDa were observed on the anti-HA Western blot, and a significant drop in signal intensity was seen on the silver stain, suggesting that elevated concentrations of imidazole-1-sulfonyl azide degrade ubiquitin or interfere with the HA tag itself.

4.2.4. Combining bioorthogonal chemistries for multi-ubiquitin formation

Combining bioorthogonal chemistries for sequential modification of protein electrophilic residues has been used in the past for the modification of antibody ADCs with two distinct payloads.[312]

Figure 64 A shows the schematic for sequential bioorthogonal reactions between ubiquitin constructs. First, azido-substitution of lysines on probe **23** (formation of **57**) was performed, followed by CuAAC reaction with probe **31** (formation of dimer **58**), and lastly a, thiol-yne reaction with construct **59**, resulting in tri-ubiquitin formation (**60**). **Figure 64 B** presents the anti-HA Western blot analysis of the initial attempt to synthesize a tri-ubiquitin construct by combining CuAAC, azido-exchange, and thiol-ene chemistries. However, no distinct band was observed at the expected molecular weight of ~27 kDa, indicating that the formation of the trimeric species was unsuccessful. It was noted that since the radical reaction requires a large excess of thiol to an alkene or alkyne, the final step in trimer formation may yield low amounts of the product.

A)

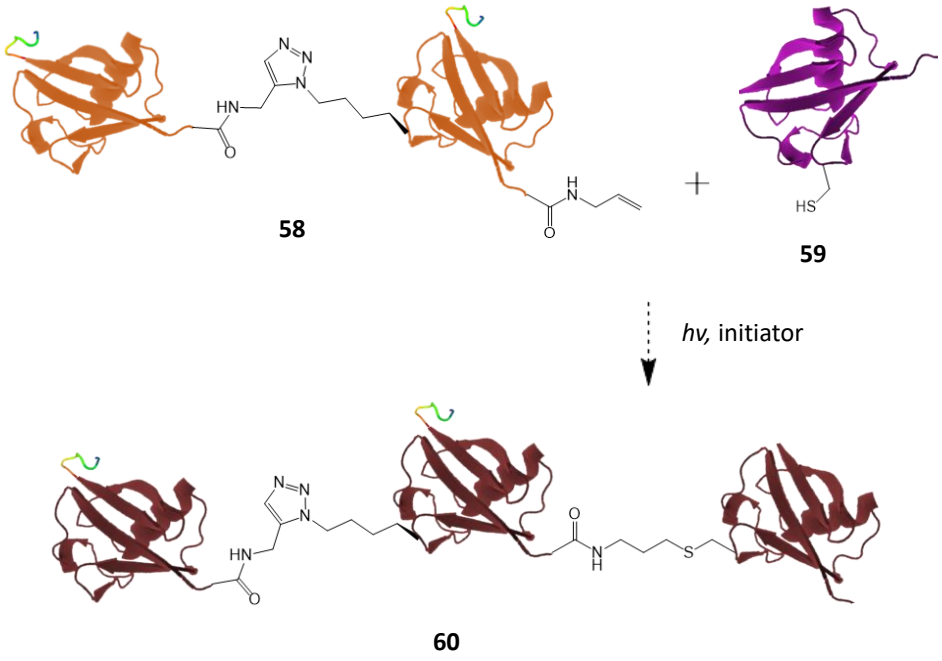

B)

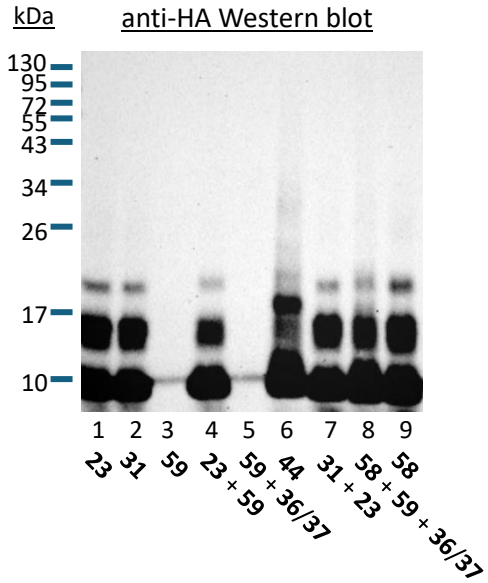

Figure 64 A: Schematic for tri-ubiquitin formation combining bioorthogonal reactions. **B**: Gels showing the first attempt at tri-ubiquitin formation *via* thiol-yne reaction, followed by azido-substitution and CuAAC reactions.

Alkyne-containing **23** incubated alongside ubiquitin K48C resulted in no dimer formation (lane 4), compared to dimers being formed in the presence of radical initiators (construct **44** in lane 6). Probes **23** and **31** were incubated together without CuAAC reagents, as seen in lane 7, as a negative control for dimeric **58**, which contained a terminal alkene, seen in lane 9. Lane 8 contained dimer **58** incubated alongside

ubiquitin K48C, followed by radical initiation. Unfortunately, no clear evidence of trimer **60** was seen, and no additional bands at 28 kDa in the anti-HA Western blot were revealed. Some loss of signal intensity at 20 kDa suggests that radical initiation either started forming trimers (**60**) or that probe **31** starts to degrade under radical conditions.

Following this experiment, the order of reactions was changed, with thiol-yne/ene reaction occurring first, followed by azido-substitution of lysine residues, and then by a CuAAC reaction. When optimised, bioconjugation *via* CuAAC reaction can have nearly quantitative product yields,[313] while bioconjugation using radical, thiol-yne reaction can result in several products, and often results in moderate to low yields.[314] Yields of azido-modification of lysines in protein and peptide models were reported to be moderately high.[315] For those reasons, the order of reactions was altered, with the lower-yielding thiol-yne reaction proceeding first, resulting in dimeric **44**, followed by azido-modification of lysines, and finally, high-yielding CuAAC reaction with probe **23**. As a result, a tri-ubiquitin **62** was formed, structure of which can be seen in **Figure 65 A**.

A band at 17 kDa can be seen in lane 3 on the anti-HA Western blot (**Figure 65 B**), showing di-ubiquitin **44** prepared *via* thiol-yne reaction. A faint band at 27 kDa can be seen, suggesting that under radical conditions, thiol-ene reaction took place between dimer **44** and ubiquitin K48C. Mixture containing dimer **44** detected in lane 3 was desalted using a NAP-5 column, followed by 5 kDa MWCO filter concentration. The purification step resulted in a significant loss in signal intensity at 10 and 17 kDa on the anti-HA Western blot, and the silver stain shows loss of protein content, as seen in lane 4. The resulting construct in lane 4 was treated with imidazole-1-sulfonyl azide **59**, and the azido-exchanged dimer was again purified *via* NAP-5 column, and concentrated using 5 kDa MWCO filter. An additional 2 µg of probe **23** was incubated with azido-exchanged **61** in lane 5. In lane 6, CuAAC reaction was performed between azido-exchanged **61** and dimer **44**, resulting in faint trimers observed at 27 kDa (containing two 10 kDa monomers and one 7 kDa monomer), as well as unintended tetramers at 37 kDa (three 10 kDa monomers and one 7 kDa monomer) and larger multimers. These results suggest that full control over radical reaction was not achieved, and multimeric side products that do not contain an internal alkene could form. Lane 7 contains the same sample as in lane 6, which was purified using a NAP-5 column, and concentrated using a 5 kDa MWCO filter.

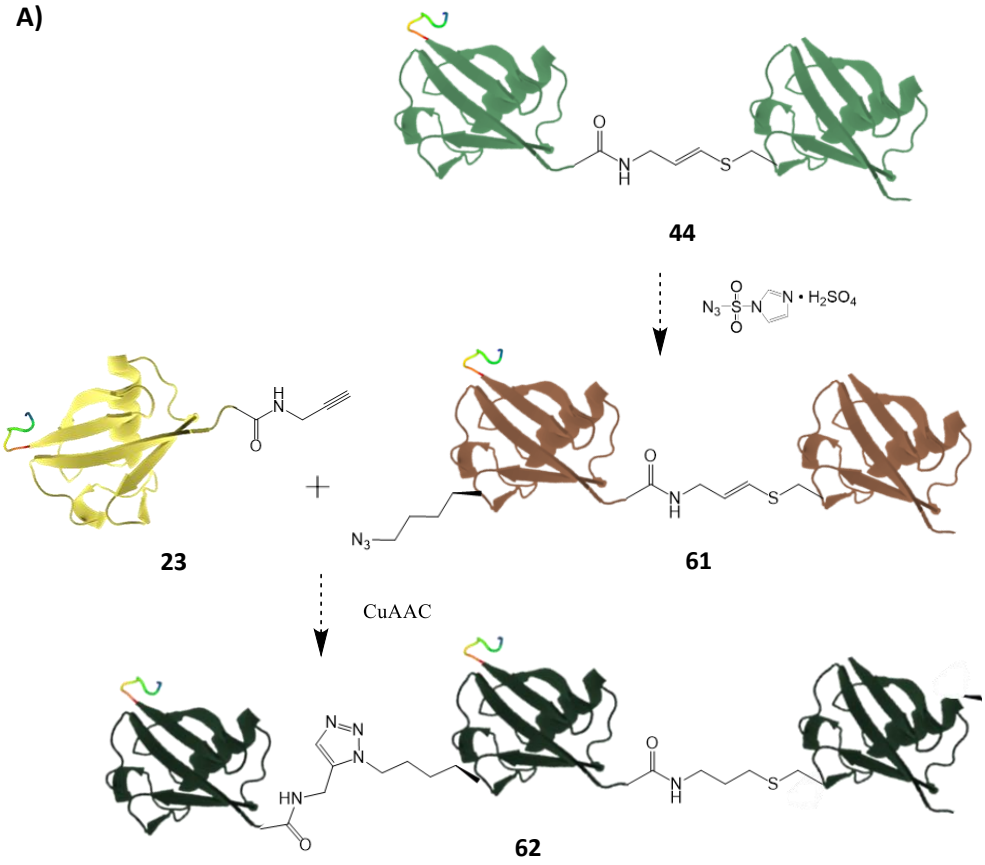

Figure 65 A: Tri-ubiquitin formation schematic. **B:** Anti-HA Western blot and silver stain showing successful tri- and multi-ubiquitin construct formation.

To test whether larger multimers could be constructed *via* azido-substitution of lysines in alkyne probe **23**, followed by CuAAC reaction, as seen in **Figure 66 A**. Anti-HA Western blot in **Figure 66 B** shows the uncontrolled formation of multiubiquitin constructs, after **23** was azido-modified, and a CuAAC reaction was

performed. In lane 1, 2 µg of alkye probe **23** alone can be seen. Lane 2 contains 2 µg of azido-modified **63**. Lane 3 contains NAP-5 purified, azido-modified **63** that was concentrated using 5 kDa MWCO filters. Significant losses of the construct were noted due to loss of signal at 10 kDa on the Western blot, and a decrease in band thickness on silver stain. In lane 4, an additional 2 µg of probe **23** were added to the purified, concentrated and azido-modified **63**. Lane 5 contains 2 µg of **23**, incubated alongside CuAAC reagents, which did not result in dimers or multimers. Lane 6 contains the same constructs as lane 4, incubated with CuAAC reagents, NAP-5 column purified and concentrated *via* 5 kDa MWCO filter. Several new bands, including trimers (**64**), can be seen in lane 7. Although trimers **64** are the intended product of this reaction, larger multimers are also clearly visible. This is likely due to the presence of a terminal alkyne within trimer **64**, which can continue on coupling to azido-substituted construct **63**, as well as probe **23** *via* CuAAC reaction. CuAAC reagent concentrations would need to be optimised, to selectively form trimers, and stop further uncontrolled CuAAC reaction between azido-substituted **63** and the alkyne-containing **23**.

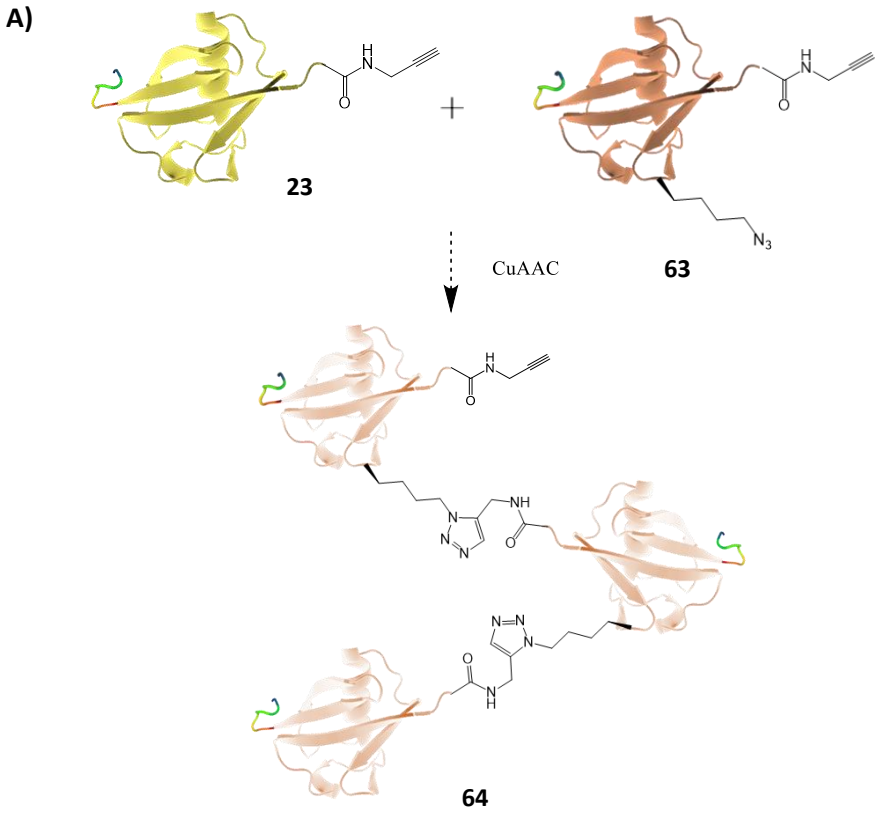

Figure 66 A: Schematic showing uncontrolled multi-ubiquitin formation *via* thiol-yne and CuAAC reactions. **B:** Gels showing multi-ubiquitin formation.

4.3. Conclusions and future outlook

This chapter focused on chemical azido-modification of primary amines in lysine residues of protein model systems. In the case of BSA, azido-modification of lysines followed a sequential order, that depended on diazo transfer reagent concentration, which was determined by LC-MS/MS analysis of tryptic digests of protein samples. K413 was modified first, followed by K211 and K221. Other lysines, including K224 and K232 followed. In all samples combined, on average, 22.36% of BSA was sequenced. A slight improvement in protein coverage and peptide identification in samples that contained higher amounts of diazo-transfer reagent was noted. Out of the lysines that were found in each sample, a clear positive trend was found between the number and sequence of lysines being modified, and the concentration of imidazole-1-sulfonyl azide **59** used in each reaction.

Proton acidity and specific environments of each lysine contributed to residue reactivity. This phenomenon has been seen in literature,[316] for other proteins, suggesting order of azido-modification of lysines will vary between proteins, yet within the protein, it will remain consistent.

Radical ubiquitin ABP (**31**) was also azido-modified; however, here, despite a large excess of imidazole-1-sulfonyl azide **59** to primary amine (125:1), only one lysine was confirmed to have been modified. LC-MS/MS analysis of tryptic digests has confirmed that out of 4 lysines detected, only K48 was azido-substituted. CuAAC reaction between azide-containing **57** and alkyne-containing ABP **23** resulted in dimer formation. When lower concentrations of diazotransfer reagent were used, no modification was seen on Western blots or *via* mass spectrometry, while higher concentrations completely removed anti-HA Western blot signal, and produced no modified lysine LC-MS/MS spectra, suggesting degradation of the model protein at elevated imidazole-1-sulfonyl azide **59** concentrations.

Azido-modification of protein models, as well as CuAAC reaction between constructs **57** and **23** presented in this chapter, were published in 2024, in *Organic and Biomolecular Chemistry*.[279]

Bioorthogonal thiol-yne, azido-substitution and CuAAC reactions were combined, allowing conjugation of ubiquitin monomers, resulting in polymeric constructs. These constructs can be further purified, and their use as multimeric ABPs of DUBs explored. Purification of multimeric ubiquitin-based constructs and evaluation of their activities as ABPs of DUBs could also be performed. Due to the technical

difficulties in purification of dimeric and multimeric constructs using SEC, attempts at their purification were not pursued in this work.

Additionally, site-selective modification of lysines with an azide group was observed in BSA model, which could be leveraged in various proteins, including antibodies, for the installation of drugs, fluorophores, and other chemical tags in a controlled manner. It is assumed that the presented strategy would need to be optimised for each protein of interest. Chemical reasons for sequential azido-modification of specific lysines could be modelled, taking into consideration the 3D structure of each protein, the acidity of specific protons and solvent accessibility of each lysine. Future work could also include quantification of the degree of azido-exchange of lysines in large proteins, such as BSA, using 2,4,6-Trinitrobenzene Sulfonic Acid (TNBS) assay.[317]

Chapter 5: Squaramide-containing ubiquitin constructs for labelling of lysines in DUBs

5.1. Chapter objectives

In this chapter, formation and application ubiquitin constructs containing lysine-binding moieties is explored. These constructs utilize mono-squaramide reactivity with primary amines, and due to affinity of DUBs to ubiquitin, could bind lysines near catalytic residues of DUBs.

The first objective was the formation of a mono-squaramide warhead 3-ethoxy-4-hydrazineylcyclobut-3-ene-1,2-dione (**65** in **Figure 67**). This mono-squaramide was to be attached to the C-terminus of HA-ubiquitin$_{1-75}$, forming a ubiquitin construct which could react with primary amines. Labelling of OTUB1, a cysteine protease DUB, as well as its catalytically inactive variant: OTUB1 C91S, and Rpn11, a model metalloprotease would then be attempted. Determination of the specific residues being modified would then be explored by using *N*-ethylmaleimide (NEM) and Phenylmethylsulfonyl fluoride (PSMF), which are established cysteine and serine protease inhibitors, respectively.

Currently, there are no covalent ABPs of metalloprotease DUBs. The second objective was the covalent capture of Rpn11, a model metalloprotease DUB. Covalent Rpn11 ABPs are needed, because Rpn11 activity is transient and strictly dependent on proteasome engagement, complicating detection and analysis of its biologically relevant active state. Once faint labelling of DUBs by the squaramide-containing ubiquitin construct was observed, efforts to improve their binding were undertaken. Specifically, the linker between the squaramide warhead and the ubiquitin recognition element was extended by two carbons, resulting in 3-((2-aminoethyl)amino)-4-ethoxycyclobut-3-ene-1,2-dione (**66** in **Figure 66**). Compound **66** was then installed on the C-terminus of HA-ubiquitin$_{1-75}$, and tested against purified model DUBs.

A)

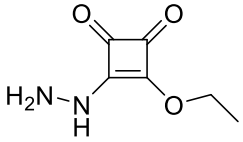

65

B)

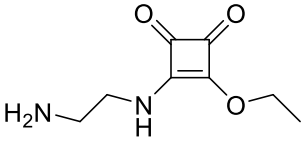

66

Figure 67 A: 3-ethoxy-4-hydrazineylcyclobut-3-ene-1,2-dione (**65**), **B** 3-((2-aminoethyl)amino)-4-ethoxycyclobut-3-ene-1,2-dione (**66**).

5.2. Targeting non-catalytic lysines near active sites of DUBs

Bioconjugation *via* the squaramide moiety allows for sequential joining of two NH2-containing biomolecules. Squaric acid esters have been used in literature for bioconjugation, with proteins being linked to glycans,[318] polymers to antibodies,[319] and peptides to RNA.[320] First amine addition to a squaric acid diester results in mono-squaramide, and can be performed at room temperature and neutral pH. The remaining ester becomes less electrophilic, due to resonance stabilisation between newly formed C-N bond, and electron donation from the first substituent delocalizing into the ring. Another primary amine can displace the leftover ester under basic pH, or in the presence of a strong nucleophile. Proteins with a strong affinity for ubiquitin, such as DUBs, could bind squaramide-containing HA-ubiquitin$_{1\text{-}75}$ construct, while the C-terminal mono-squaramide could covalently bind nearby lysines. Choosing squaramide derivatives as warheads targeting lysines instead of more broadly-targeting electrophilic warheads has the advantage of avoiding off-target labelling of other nucleophilic residues, which has the potential to simplify the sample matrix when the construct is applied to cell lysates.

To conjugate ubiquitin to a lysine found near the catalytic residues of DUBs, a squaramide warhead targeting non-catalytic lysines was designed. OTUB1 and OTUB1 C91S were chosen as DUB models to be labelled by mono-squaramide ubiquitin constructs. The distance from wild type ubiquitin's C-terminal carboxylate to the catalytic cysteine 91 in OTUB1 is around 12.5 Å.[321] Crystal structure of OTUB1 (entry 2ZFY on PDB) seen in **Figure 68**, shows lysine 84 (orange) within 8.6 Å from cysteine 91 (green). It is reasonable to assume that a monosubstituted squaramide warhead found on the C-terminus of HA-ubiquitin$_{1\text{-}75}$ would have access to lysine residues near OTUB1's active site, such as lysine 84. OTUB1 C91S cannot be labelled by probe **23**, due to a lack of cysteine at position 91, however lysine 84 is still available for targeting with mono-squaramide ubiquitin construct.

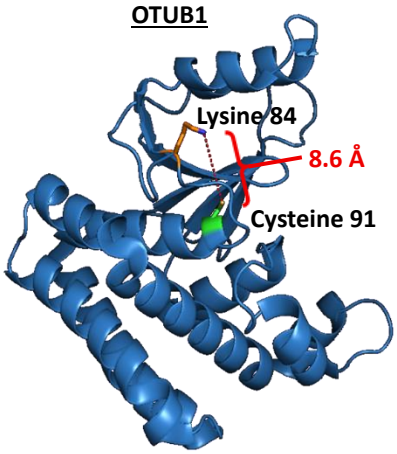

Figure 68: Structure of OTUB1 (entry 2ZFY on PDB, in blue), visualised using the PyMOL Molecular Graphics System, Version 3.1.6.1 Schrödinger, LLC. with lysine 84 (highlighted in orange) and cysteine 91 (highlighted in green). Distance between the two is 8.6 Å (highlighted in red).

All known deubiquitinating metalloproteases contain zinc ions, which are coordinated by histidine, aspartate and serine residues. These residues activate water molecules, which attack isopeptide bonds. Metalloprotease DUBs do not form covalent intermediates with their substrates,[322] and although several ABPs chelating zinc ions have been reported for DUBs,[323] no covalent ABPs have been reported to date. The strategy proposed in this chapter could allow covalent capturing of metalloprotease DUBs, such as Rpn11, by allowing mono-squaramide ubiquitin constructs to bind lysines near the active site. Rpn11 is a component of the 26S protease, involved in ATP-dependent degradation of ubiquitinated proteins. Interestingly, Rpn11 itself specifically recognises K63-linked polyubiquitin chains, and its role in the 26S proteosome remains unclear.

5.2.1. Squaramide warhead synthesis

Diethyl squarate (**67**) was mixed with hydrazine, as seen in **Scheme 20**, and the product (**65**) was dried and stored at -20 °C. Once solubilised in DMSO, compound **65** was stable for 1 week at 4 °C, after which NH_2 protons began coalescing with NH protons, as observed by NMR, suggesting loss of the primary amine.

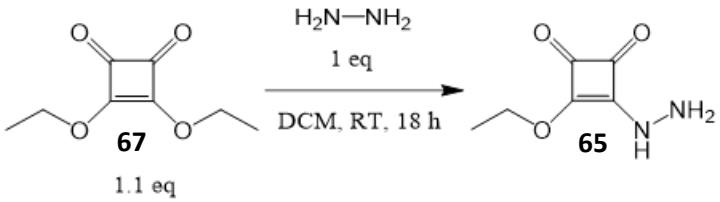

Scheme 20: Formation of mono-squaramide (3-ethoxy-4-hydrazineylcyclobut-3-ene-1,2-dione) **65**.

5.2.2. Squaramide-containing ubiquitin construct formation

It was expected that under slightly basic conditions (pH 7.5) installation of mono-squaramide amine **65** onto the C-terminus of HA-Ubiquitin$_{1-75}$-MESNa (**40**) would be possible.[324] No modification of ubiquitin lysines or the N-terminus by compound **65** should take place, as compound **65** was diluted substantially in this reaction.

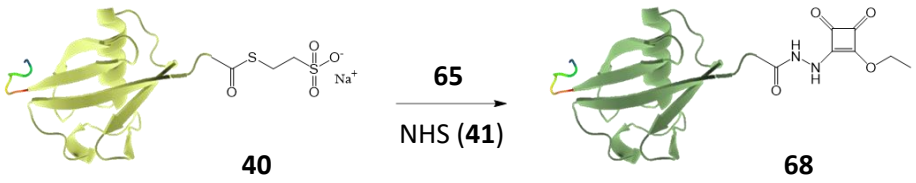

Scheme 21: Formation of construct **68**, by reacting compound **65** with construct **40**.

Scheme 21 shows the formation of construct **68**. Once **68** was ready, its activity as a lysine-specific DUB probe was investigated.

5.2.3. Testing squaramide-containing ubiquitin constructs against OTUB1 and OTUB1 C91S

Non-covalent interactions between construct **68** and OTUB1 should allow for the squaramide moiety to interact with any nearby lysines. Lysine 84 of OTUB1 may be subject to modification by the squaramide probe. This idea is summarised in **Figure 69 A**.

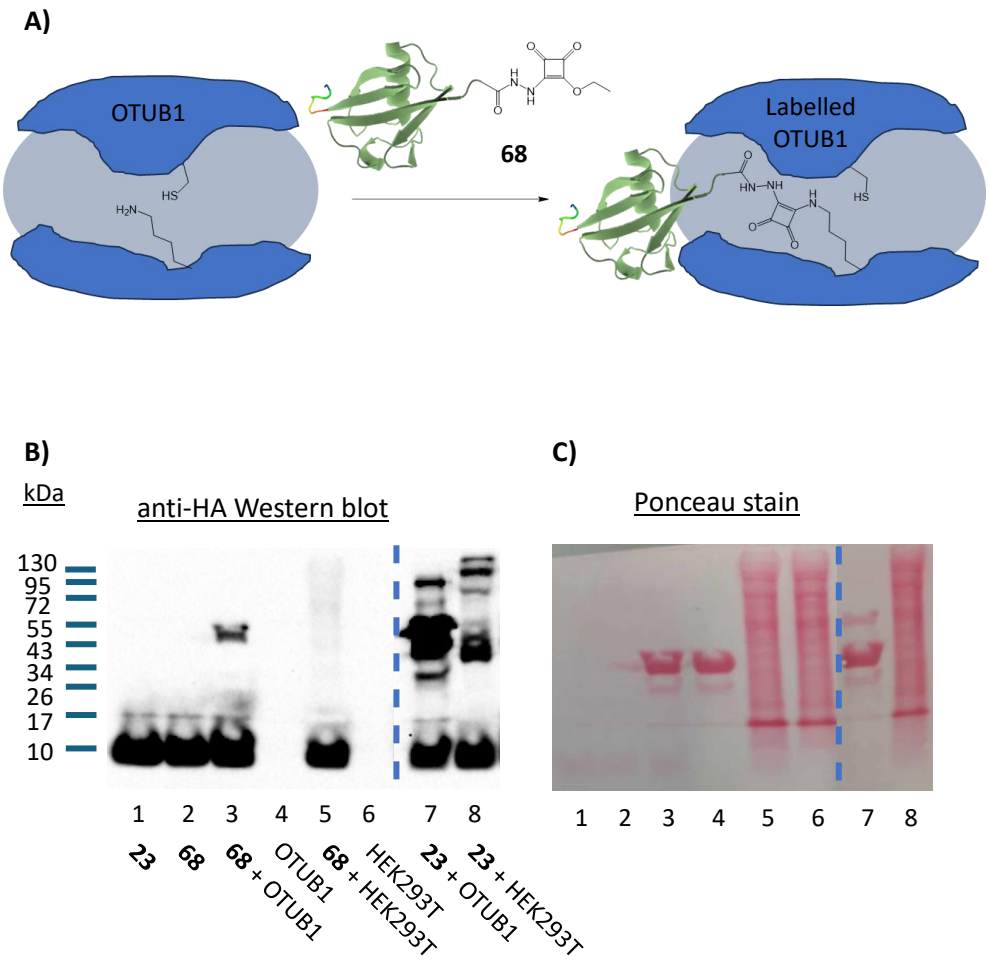

Figure 69 A: Covalent labelling of DUBs using a squaramide warhead in construct **68**, **B**: anti-HA Western blot comparing reactivities of constructs **3** and **4** towards OTUB1 and HEK293T lysate, **C**: Ponceau stain of the same Western blot.

Squaramide-containing **68** covalently interacted with OTUB1, and proteins found in HEK293T lysate, as seen in **Figure 69 B** and **C**. **Figure 69 B** shows that construct **68** labels OTUB1 to a small degree (lane 3), compared to **23** (lane 7). Construct **68** appears to also label a large number of proteins found in the HEK293T lysate, as seen in **Figure 69 B**, lane 5. Alkyne-containing **23** labels fewer targets in HEK293T lysate, compared to construct **68**; however, signal intensity from the proteins labelled with probe **23** is significantly stronger than with construct **68**. Ponceau stain in **Figure 69 C** was used to verify even loading of all samples. Although some reactivity towards OTUB1 was seen, further experiments determining which specific residues were being covalently modified were required.

Figure 70 shows an anti-HA Western blot comparing the reactivities of constructs **23**, and **68** towards OTUB1, and catalytically-inactive OTUB1 C91S. Probe **23** is seen to bind OTUB1, producing a strong signal at 55 kDa and above, as seen in lane 5, **Figure 70**. Probe **23** does not bind OTUB1 C91S, as seen in lane 6, as expected. Probe **68** binds both OTUB1 and OTUB1 C91S to a similar extent, as seen in lanes 8 and 9, respectively, suggesting residues other than cysteine are being covalently modified by the squaramide-containing **68**. When the concentration of OTUB1 variants is halved (in lane 7), signal intensity at 55 kDa is also halved. Halving the enzyme concentration and observing a halved signal intensity from ABP labelling suggests that the signal is directly proportional to the amount of enzyme present, indicating a quantitative and specific binding interaction. The binding of probe **68** to OTUB1 is weaker compared to probe **23**.

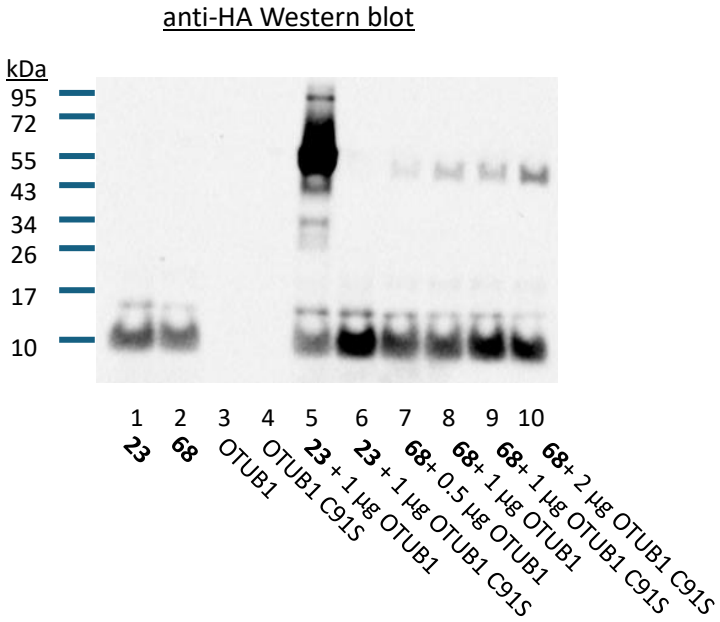

Figure 70: Reactivity of probe **68** against OTUB1 and against catalytically-inactive OTUB C91S, compared to reactivity of probe **23**.

Building on the observation that probe **68** binds the cysteine protease DUB, OTUB1, even in its catalytically inactive variant, it is possible that targeting lysine residues specifically could provide an effective means for probing all DUBs, including metalloproteases. The use of a lysine-specific ABP is advantageous because it avoids the broad reactivity seen with electrophilic warheads, such as sulfonyl fluorides, which can bind both lysines and cysteines.[325] These types of warheads could lead to non-selective binding across different proteases, thereby reducing the specificity of the probe. By focusing on lysine residues, the ABP enhances the selectivity for all DUBs

Chapter 5: Squaramide-containing ubiquitin construct for labelling lysines in DUBs which contain lysines near their active sites. Further studies on the specificity of the squaramide-containing **68** were conducted by inhibiting lysine and cysteine residues.

5.2.4. Inhibition of cysteines and lysines

Figure 71 shows probe **68** labelling both OTUB1 and OTUB1 C91S to a very similar extent, providing some evidence that residues other than cysteine or serine are being covalently modified by the squaramide warhead. Squaramides are known to only target primary amines, such as those found in lysine side chains.[326-329] No evidence of binding to other nucleophilic side chains, including histidines, tyrosines or serines in proteins was found. To provide further evidence that the squaramide moiety is not binding the catalytic cysteine in OTUB1, or the serine mutant in OTUB1 C91S, selective protease inhibitors were employed. NEM is a cysteine protease inhibitor, which alkylates free sulfhydryl groups,[330] while PMSF is a serine protease inhibitor,[331] which sulfonylates serines. **Figure 71 A** shows the structures of NEM and PMSF. **Figure 71 D** and **E** show the first trial of selectively inhibiting the catalytic cysteine of OTUB1, and serine in OTUB1 C91S.

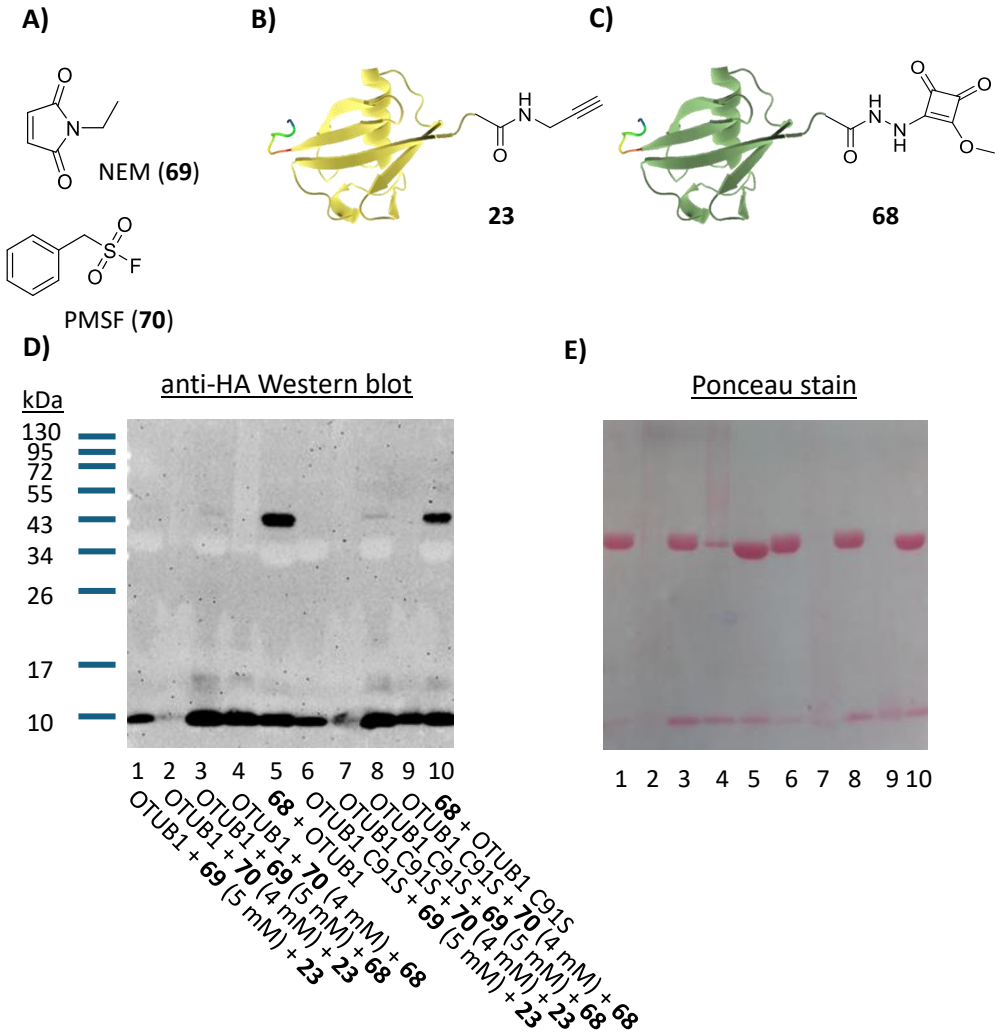

Figure 71 A: Structures of NEM (**69**) and PMSF (**70**). **B**: Structure of probe **23**. **C**: Structure of **68**. **D**: anti-HA Western blot showing labelling of OTUB1 and OTUB1 C91S after treatment with cysteine and serine protease inhibitors, using constructs **23** and **68**. **E**: Ponceau stain of the same blot.

Lane 1 in **Figure 71 D** contains OTUB1 treated with 5 mM NEM, for 5 min, followed by incubation with probe**23**. **Figure 71 D**, lane 1 shows a complete lack of labelling of OTUB1, signified by the lack of a band at 45 kDa. Lane 1 in **Figure 71 E**, shows no OTUB1 degradation by the treatment with the cysteine protease inhibitor. **23**, an alkyne-containing ubiquitin monomer seen in **Figure 71 B**, was not expected to react with OTUB1, as the catalytic cysteine was alkylated by NEM. Lane 2 on the Ponceau stain shows degradation of OTUB1, after treatment with 4 mM PMSF for 5 min, in the presence of **23**. Lane 3 in **Figure 71 D** shows an almost complete disappearance of 45 kDa band, resulting from the treatment of OTUB1 with 5 mM NEM, followed by incubation with **68**, a squaramide-containing ubiquitin monomer seen in **Figure 71 C**. It was not expected that the binding of probe **68** could be disrupted by NEM at 5 mM.

Increasing the concentration of NEM to 10 mM was necessary to bind the amino groups of lysine residues;[332] therefore, at 5 mM, NEM may begin binding lysines, potentially interfering with the activity of the squaramide warhead. Lane 4 in both **B** and **C** shows that PMSF at 4 mM incubated for 5 min with OTUB1, degrades the enzyme. Lane 6 in both **B** and **C** did not show labelling of OTUB1, due to OTUB1 C91S not being captured by **23**. Lane 7 showed that treatment of OTUB1 C91S with 4 mM PMSF caused protein degradation, as seen in **Figure 71 E**. Lane 8 showed a drop in signal intensity at 45 kDa in **Figure 71 D**, after OTUB1 C91S was treated with NEM, followed by treatment with probe **68**, compared to lane 10, which showed uninhibited labelling of the catalytically inactive DUB with probe **68**. Lane 9 in **Figure 71 E** shows degradation of the catalytically inactive DUB after treatment with 4 mM PMSF. Inhibition of cysteine and serine proteases with NEM and PMSF was attempted once more. This time, PMSF concentration was lowered from 4 mM to 2 mM, not to denature the tested DUBs, and NEM was increased to demonstrate inhibition of both cysteines and lysines in both OTUB1 variants.

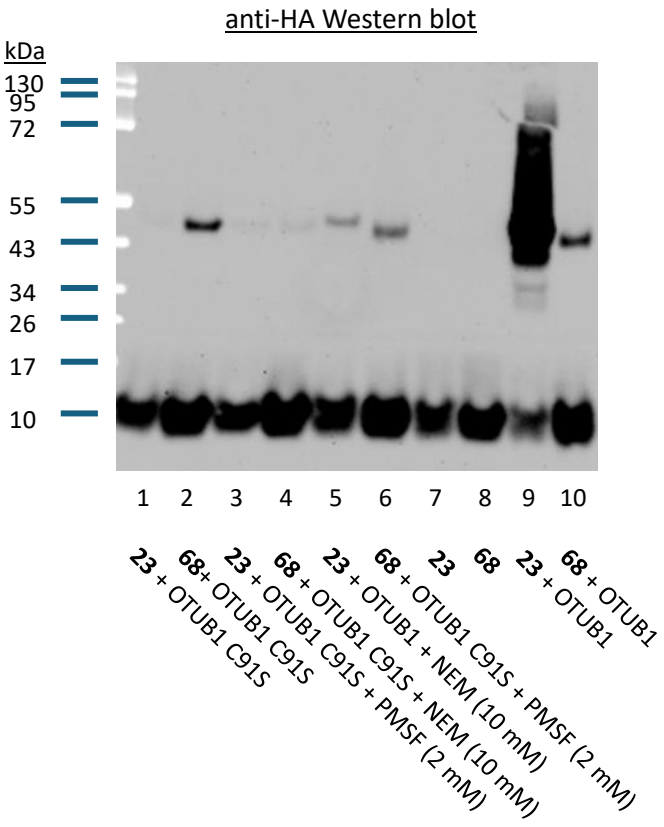

Figure 72: Inhibition of OTUB1 and OTUB1 C91S with 10 mM NEM or 2 mM PMSF, followed by incubation with constructs **23** or **68**.

Figure 72 provides a detailed analysis of the binding behaviour of constructs **23** and **68** with OTUB1 C91S and wild-type OTUB1, under various treatment conditions.

In lane 1, alkyne probe **23** does not bind to OTUB1 C91S, which lacks the catalytic cysteine at position 91. In contrast, lane 9 shows robust binding of probe **23** to wild-type OTUB1, indicating that the wild-type protein can engage with probe **23** effectively. Lane 2 presents the squaramide-containing **68** binding to OTUB1 C91S, with a signal intensity almost identical to that seen in lane 10 for probe **68** binding to wild-type OTUB1. This similar binding pattern suggests that probe **68** may interact with a site other than the active-site cysteine, or it binds to a non-catalytic serine in C91S mutant. In lane 3, after treatment with 2 mM NEM, there is a faint labelling of OTUB1 C91S with probe **23**, a result similar to lane 1. This suggests that NEM may not be fully inhibiting the binding of probe **23** under these conditions. Lane 4 shows that when OTUB1 C91S is treated with 10 mM NEM, probe **68** fails to bind, indicating that the higher concentration of NEM inhibits nucleophilic residues involved in binding.

Further, lane 5 demonstrates the effect of 10 mM NEM on probe **23** binding to OTUB1 C91S. At this concentration, NEM effectively inhibits binding by modifying cysteines,[333] leading to an almost complete loss of signal when compared to lane 9, where probe **23** binds wild-type OTUB1 without inhibition. Lane 6 reveals that OTUB1 C91S, after treatment with 2 mM PMSF, still shows binding to squaramide-containing **68**, although with diminished intensity. This reduced binding strength may be due to the protein degradation caused by PMSF treatment, as PMSF is known to inhibit serine proteases and possibly degrade proteins.

Finally, lanes 7 and 8 show the binding of constructs **23** and **68**, respectively. Notably, probe **68** was still able to bind OTUB1 C91S after a 5 min treatment with 2 mM PMSF (as shown in lane 6). This observation is significant because it suggests that the squaramide-containing **68** does not interact with serine residues, further supporting the hypothesis that its binding site is independent of the active-site cysteine or any serine residue in position 91.

Together, these results give insights into the binding of constructs **23** and **68** with OTUB1 and OTUB1 C91S, revealing differences in their binding mechanisms and susceptibility to inhibition by nucleophilic reagents.

PMSF concentration was then further lowered, as 0.1 to 1 mM PMSF already inhibits serine proteases.[334] NEM concentration was also lowered to 1 mM, with little inhibition of cysteines, to compare the effects of both inhibitors at the same

concentrations. **Figure 73 A** and **B**, lane 1 shows that treatment of OTUB1 with 1 mM NEM has no substantial effect on the ability of probe **23** to bind covalently. OTUB1 treated with 1 mM PMSF or 1 mM NEM has very little effect on the binding of probe **23**, as seen in lanes 1 and 2, in both **Figure 73 A** and **B**. In lane 3, OTUB1 was treated with 1 mM NEM, resulting in significant inhibition of probe **68** activity. Lane 4 shows a slight activity decrease of probe **68** after OTUB1 is treated with 1 mM PMSF, compared to lane 5, which shows uninhibited binding of probe **68** to OTUB1. It is possible that even slight alterations of the active site, including modification of serine by PMSF, lead to a lowering in the labelling efficiency of probe **68**. Lanes 6 and 7 in the anti-HA Western blot show that alkyne-containing **23** doesn't interact with OTUB1 C91S almost at all. Lanes 8 and 9 show how treatment of OTUB1 C91S with 1 mM NEM and PMSF, respectively, lowers the efficiency of probe **68**, compared to full labelling seen in lane 10. Lane 11 contains probe **68** on its own.

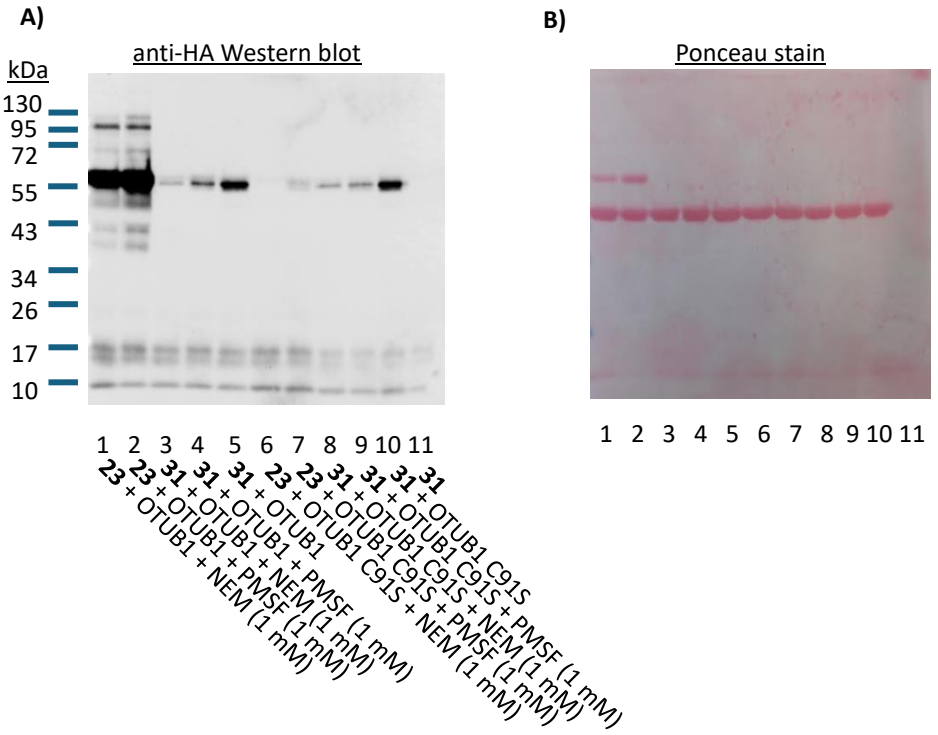

Figure 73 A: anti-HA Western blot showing inhibition of OTUB1 and OTUB1 C91S with 1 mM NEM or 1 mM PMSF, followed by incubation with constructs **23** or **68**. **B**: Ponceau stain of the same blot.

Taken together, these results indicate that the binding of probe **23** to cysteine 91 in OTUB1 is minimally inhibited by 1 mM NEM, while 5 mM and 10 mM NEM led to inhibition of both OTUB1 and construct **68** binding to lysines in the OTUB1 C91S variant. Freshly prepared 4 mM PMSF incubated with OTUB1 and OTUB1 C91S degrades both

Chapter 5: Squaramide-containing ubiquitin construct for labelling lysines in DUBs

enzymes. At 2 mM PMSF, probe **68** covalently interacted with OTUB1 C91S, and neither OTUB1 nor OTUB1 C91S were degraded. There was a slight drop in signal intensity of OTUB1 C91S labelling with probe **68**, after treatment with 2 mM PMSF. At 1 mM PMSF, the binding of neither constructs **23** nor **68** to the tested DUBs was affected substantially.

5.2.5. Optimising squaramide construct binding

The effect of incubation time on the binding of probe **68** to OTUB1 was investigated next. OTUB1 and OTUB1 C91S were incubated with probe **68** for between 30 min and 2 h, as seen in **Figure 74**. Marginal improvement in labelling of both DUBs was seen after 2 h of incubation at 37 °C in **Figure 74 A**. Ponceau stain **(Figure 74 B)** was performed to verify even sample loading in each well.

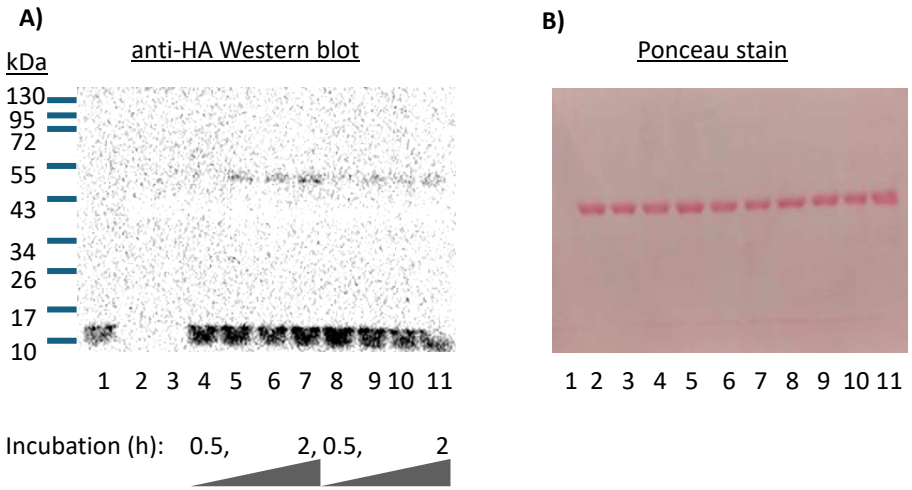

Figure 74 A: Effect of change of incubation time on OTUB1 and OTUB1 C91S labelling with probe **68**. **B:** Ponceau stain of the same blot.

It was hypothesised that, to label lysines near the active site of DUBs more effectively, a longer, more flexible linker between the ubiquitin recognition element and the squaramide warhead would be required. Extending the linker too much could result in unintended reactivity with lysines in ubiquitin itself, potentially interfering with the targeted binding.

5.3. Using squaramide-containing ubiquitin construct to bind Rpn11

Labelling of catalytically inactive OTUB1 C91S was encouraging enough to attempt binding Rpn11 (a model metalloprotease DUB involved in the proteosomal degradation of ubiquitinated proteins), to probe **68**. Rpn8/11 heterodimer was expressed, purified and generously provided by Dr. Sean McKenna. **Figure 75 A** shows

the scheme for labelling lysines near the active site of DUBs, with metalloproteases such as Rpn11 being captured alongside cysteine protease DUBs.

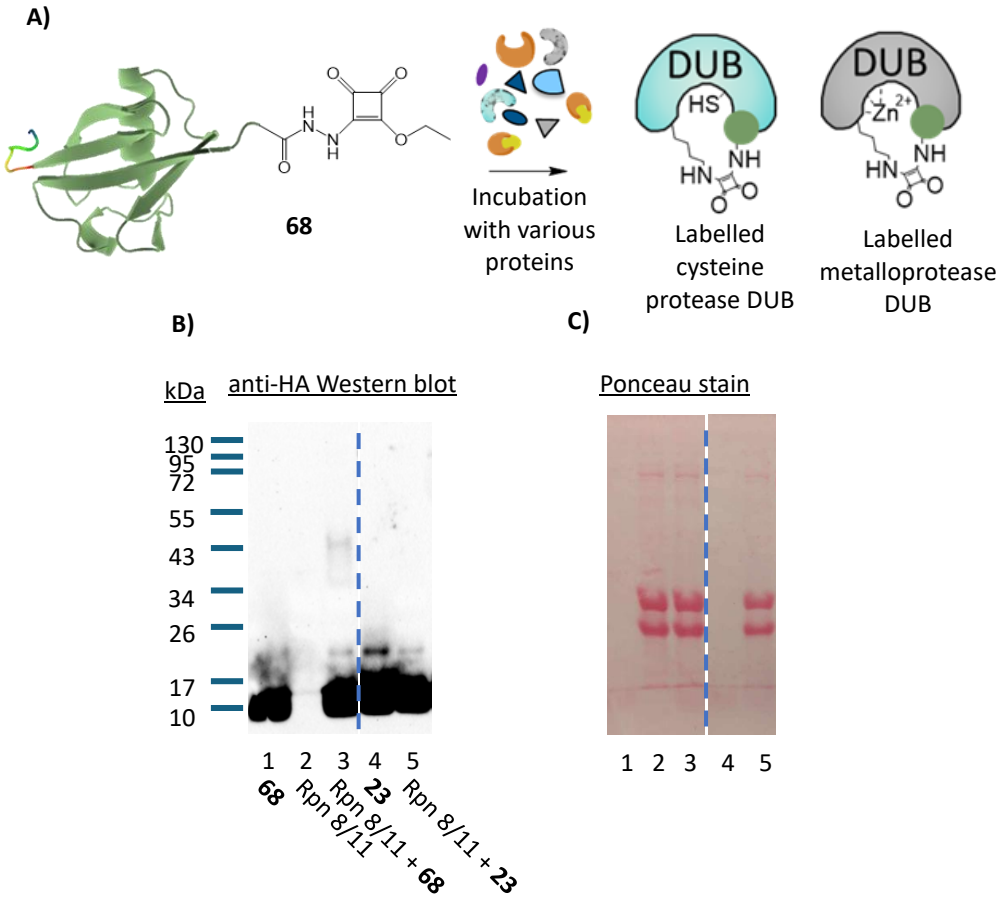

Figure 75 A: Scheme showing selective labelling of DUBs, in the presence of other proteins. **B**: anti-HE Western blot showing Incubation of 1 µg of constructs **23** and **68** with 4 µg Rpn 8/11 heterodimer (2 µg of Rpn 8 and Rpn 11 each). **C**: Ponceau stain of the same blot.

Figure 75 B shows that, after incubation of probe **68** with Rpn8/11 heterodimer, some labelling of the Rpn11 (34 kDa band seen in **Figure 75 C**) is seen (43 kDa band seen in **Figure 75 B**), in lane 3. To a lesser extent, Rpn8 (26 kDa band seen in **Figure 75 C**) is also labelled (35 kDa band seen in **Figure 75 B**). Lane 5 shows that probe **23** incubated with Rpn8/11 heterodimer does not label either of the proteins.

Heterodimer of Rpn8/Rpn11 (entry 4OCL on PDB, seen in **Figure 76**) doesn't contain lysines within 12 Å of the catalytic Zn^{2+} ion (grey ball), however when the distance is extended to 20 Å (seen in **Figure 76**, protein backbone in purple), lysines 36,

39, 127, 148, and 150 (side chains in yellow), which, if in proximity to the squaramide-containing **68**, could be labelled.

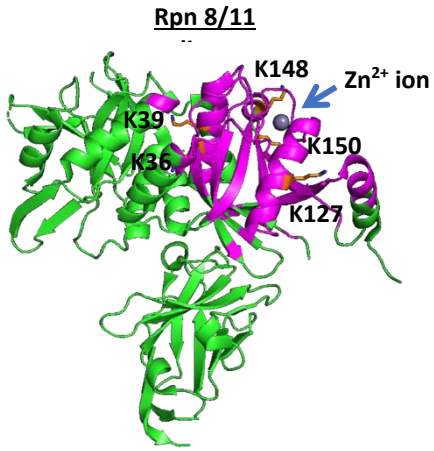

Figure 76: Structure of Rpn8/Rpn11 heterodimer visualised using the PyMOL Molecular Graphics System, Version 3.1.6.1 Schrödinger, LLC. (entry 4OCL on PDB) in green, with Zn^{2+} ion in grey (highlighted by a blue arrow) backbone of residues within 20 Å of Zn^{2+} in purple, with lysine sidechains highlighted in orange.

Extending the time of incubation of the Rpn8/11 heterodimer with probe **68** was then attempted, as seen in **Figure 77**. Rpn8/11 heterodimer was incubated at 37 °C with the squaramide-containing **68** as well as the alkyne-containing **23**, for over 2 h. Lane 1 contained probe **23**, while lane 2 contained probe **68**. Faint labelling of Rpn11 by probe **68** was seen after 2 h incubation (**Figure 77 A**, lane 8). This was an improvement over 1 and 1.5 h incubation seen in lanes 6 and 7, respectively. No significant interaction between probe **23** and Rpn8/11 heterodimer could be seen in **Figure 77 A**, lanes 3-5.

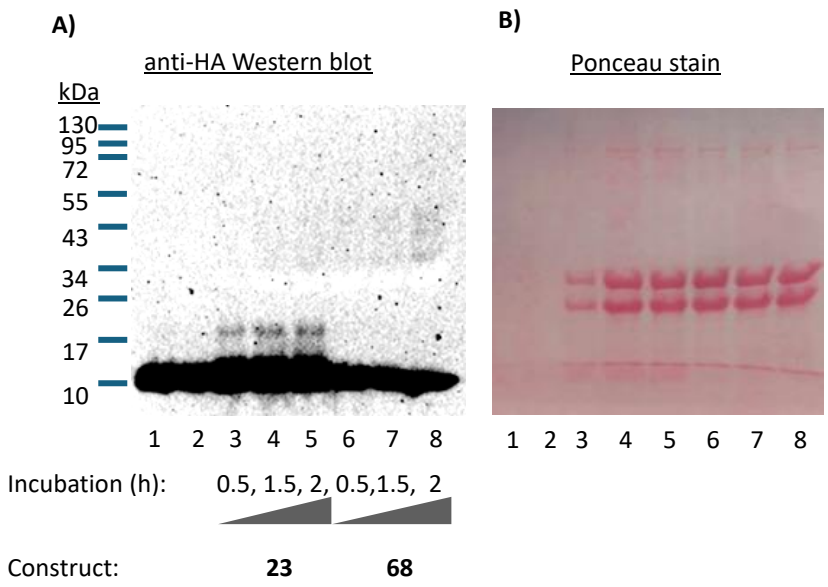

Figure 77 A: anti-HA Western blot showing time course for incubation of Rpn 8/11 with constructs **23** and **68**. **B**: Ponceau stain of the same blot.

5.3.1. Extending the linker between ubiquitin and the squaramide warhead

Extending the linker between ubiquitin and the squaramide warhead by two carbons could enhance binding to lysines near the active sites of DUBs. To form the squaramide warhead, diethyl squarate (**67**) was first mixed with ethylenediamine. **Scheme 22** shows this reaction. Upon reaction completion, product (**66**) was dried and stored at -20 °C until reacting it with HA-Ubiquitin$_{1\text{-}75}$-MESNa.

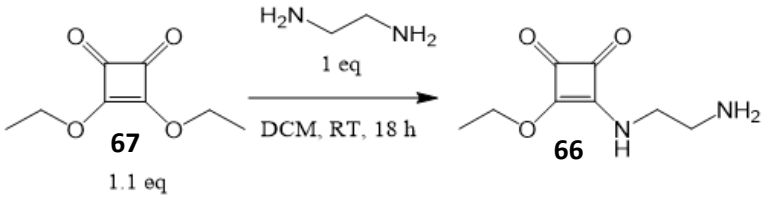

Scheme 22: Formation of mono-squaramide warhead **66**, by reacting 1.1 eq diethyl squarate (**67**) with 1 eq ethylenediamine.

Construct **71** was then formed, as seen in **Scheme 23**. Activity of construct **71** as a lysine-specific DUB probe was investigated next.

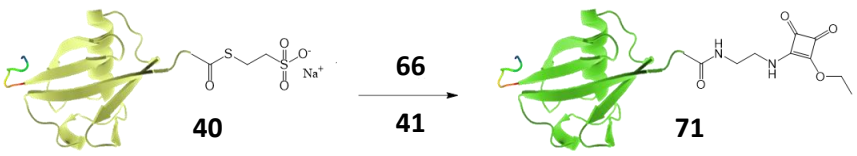

Scheme 23: Forming construct **71**, by reacting compound **66** with construct **40**.

Labelling of OTUB1 and catalytically inactive OTUB1 C91S by construct **71** was attempted next, and compared with probe **68**, as seen in **Figure 78**.

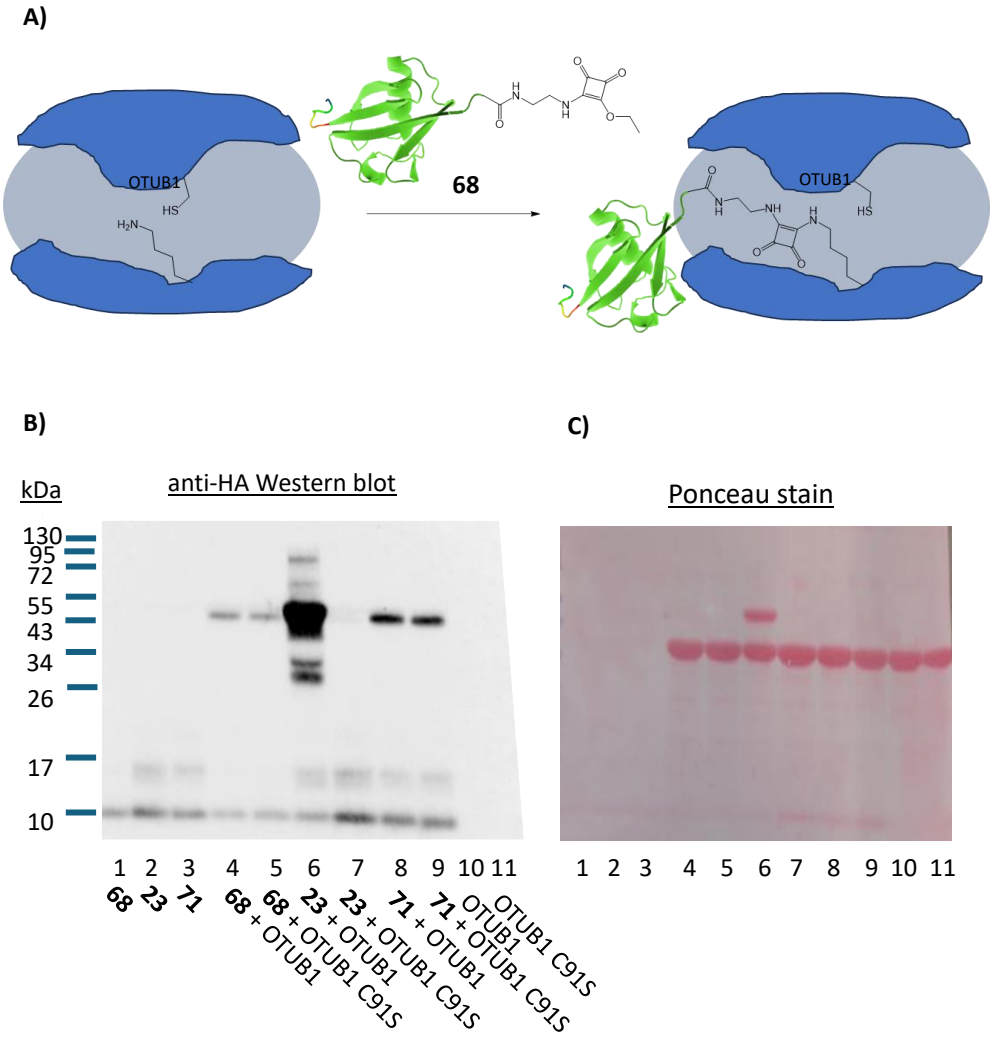

Figure 78 A: Scheme showing construct **71** binding DUBs, **B**: anti-HA Western blot showing construct **71** binding OTUB1 and OTUB1 C91S, compared to constructs **23** and **68**, **C:** ponceau stain of the same blot.

Figure 78 A shows a schematic of the squaramide-containing construct **71** binding to OTUB1. Extending the linker has the potential to provide greater flexibility of the warhead, as well as bridging the distance to lysine 84 in OTUB1, resulting in a stronger signal on the anti-HA Western blot at 43 kDa. Construct**71** was also incubated with BSA, to check for any off-target reactivity to lysines found in proteins that should not interact with ubiquitin to a substantial degree.

Lanes 1, 2 and 3 in **Figure 78 B** contain constructs **68**, **23** and **71,** respectively. Lanes 4 and 5 show **68** binding OTUB1 and OTUB1 C91S, respectively. Lane 6 shows **23** labelling OTUB1, which is also visible on the Ponceau stain (**Figure 78 C**), while lane 7

in **Figure 78 B** shows that probe **23** does not covalently bind OTUB1 C91S. Lanes 8 and 9 show probe **71** binding both OTUB1 and OTUB1 C91S to a similar extent. It is worth noting that the intensity of the bands at 43 kDa in lanes 8 and 9 is significantly more intense than that in lanes 4 and 5. Lastly, probe **71** was incubated with BSA, as well as with OTUB1 C91S, as seen in **Figure 79**. Alkyne probe **23** was also incubated with BSA and OTUB1 C91S. No labelling of BSA was seen by either of the two probes, suggesting no off-target reactivity from either of the two probes.

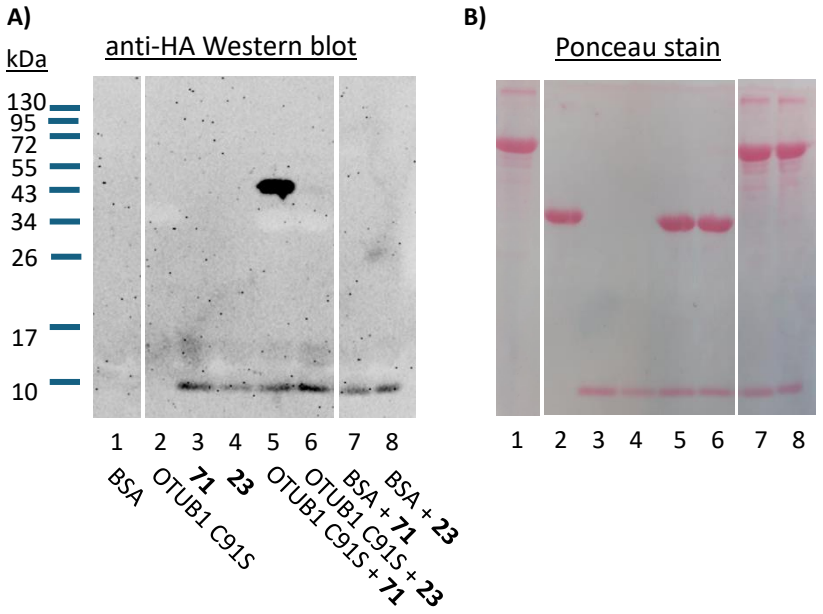

Figure 79 A: anti-HA Western blot showing 1 µg probe **71** binding 2 µg OTUB1 C91S and not 2 µg BSA, as well as 1 µg probe **23** incubated with OTUB1 C91S and BSA. **B:** ponceau stain of the same blot.

Figure 79 A shows that only OTUB1 C91S is significantly labelled by probe **71**, and probe **23** does not label either BSA or OTUB1 C91S. Lanes 1, 2, 3 and 4, show BSA, OTUB1 C91S, **71** and **23** on their own. Lane 5 in the anti-HA Western blot shows construct **71** binding OTUB1 C91S, while, in this experiment, probe **23** in lane 6 didn't bind OTUB1 C91S. Lanes 7 and 8 contain probes **23** and **71,** respectively, incubated with BSA. Neither of the constructs was seen to label BSA. These results further support the hypothesis that squaramide-containing ubiquitin constructs can selectively label ubiquitin-binding proteins with minimal off-target reactivity.

5.4. Conclusions and future outlook

In conclusion, the mono-squaramide warhead (**65**) was successfully synthesised and subsequently attached to construct **40**, resulting in a ubiquitin-based construct, **68**, with a C-terminal mono-squaramide. Probe **68** effectively labelled both

OTUB1 and the catalytically inactive OTUB1 C91S, and showed signs of protein labelling in HEK293T cell lysates, due to lysine modification of ubiquitin-binding proteins. When OTUB1 C91S was incubated with 1 mM and 2 mM PMSF, followed by incubation with probe **68**, there was no significant loss of labelling signal, indicating that probe **68** did not bind to serine residues. However, at a lower NEM concentration (1 mM), some reduction in probe **68** activity was observed with both OTUB1 C91S and OTUB1. At higher NEM concentrations (10 mM), binding to OTUB1 C91S was inhibited, suggesting that lysine residues near the DUB's active site, as well as cysteines, were modified under these conditions. Notably, a 5 mM NEM concentration only slightly diminished the binding of probe **68** to both OTUB1 and OTUB1 C91S, indicating a weaker effect at this intermediate concentration. Probe **68** showed some labelling activity towards Rpn8/11 heterodimer, with a slight preference for Rpn11. Extending the linker connecting the squaramide warhead and ubiquitin by two carbons was performed, resulting in mono-squaramide (**71**). The squaramide-containing construct **71** was then formed by reacting warhead **66** with construct **40**, and construct **71** showed more intense labelling of both OTUB1 and OTUB1 C91S than probe **68**. Construct **71** did not bind BSA, which suggested that direct binding to ubiquitin is required for covalent binding of construct **71**. It remains to be tested whether construct **71** binds Rpn8 in the Rpn8/11 heterodimer. A panel of ubiquitin binding partners, including cysteine and metalloprotease DUBs, E2 conjugases and E3 ligases, could be tested against probe **71**, along with proteins unrelated to the ubiquitination system, to determine the specificities of probe **71**. Additionally, affinity enrichment of construct **71** binders in cell lysates, followed by their identification by proteomics methods, could be performed in the future. Selective modification of lysine residues in target proteins offers a powerful approach for protein bioconjugation, enabling the attachment of various functional groups, tags, or probes to specific sites. This strategy can also be used to capture targeted enzymes by exploiting their non-catalytic residues, which are often critical for protein-protein interactions, stability, or substrate recognition.

Chapter 6: Conclusions and future work

This thesis presents the design of dimeric ubiquitin constructs featuring internal and terminal alkenes, assembled using biocompatible chemical strategies. These constructs provide a platform for probing the dynamics of ubiquitin editing in a selective and time-resolved manner, using radical thiol-ene chemistry to capture active DUBs. Beyond ubiquitin, the methods developed here offer versatile tools for the controlled linking and functionalisation of other proteins.

Chapter 2 showcases the development of a bioconjugation method between an alkyne-containing ubiquitin construct and small molecular fluorophores *via* a controlled radical-initiated thiol-yne reaction. This reaction proceeded through to a thiol-ene addition of a second thiol-containing molecule. Additionally, Chapter 2 introduces the first example of radical thiol-yne protein–protein conjugation, achieved between an alkyne-containing ubiquitin construct and BSA. This study highlights the impact of thiol concentration on modulating the reaction yield. Lastly, an investigation into biocompatible systems for radical thiol-ene initiation expands the range of available conditions for *in vitro* activation of radical probes of DUBs.

Chapter 3 demonstrates that the thiol-yne reaction can be used to form di-ubiquitin constructs and, to a lesser extent, tri-ubiquitin constructs through sequential thiol-ene coupling of a second thiol-containing monomer. This finding is noteworthy, as it confirms that internal alkenes between protein units can undergo radical thiol-ene reactions; however, the efficiency of these reactions is constrained by steric hindrance from the participating macromolecules. Importantly, this steric hindrance may help restrict reactivity to proteins that naturally engage with ubiquitin, such as DUBs, thereby reducing non-specific interactions. Certain DUBs can recognise di- and multi-ubiquitin constructs in their active sites, and this can be exploited to interrogate members of the DUB families that selectively bind di-ubiquitin and preferentially cleave isopeptide bonds linked *via* different lysine residues.

Di-ubiquitin yields were enhanced by increasing thiol concentrations and optimisation of radical initiators. Complete consumption of the alkyne-containing monomers was not seen. Partial purification of dimers *via* HPLC was achieved; however, complete isolation of the dimers was unsuccessful due to the large amounts of thiol-containing monomers required for the reaction.

Testing different radical initiators could improve thiol-yne product yields, which, combined with different modes of separating di-ubiquitin probes, such as ion exchange chromatography or large-scale tangential flow filtration, could result in the isolation of pure dimers. Removal of unreacted alkyne-containing monomers *via* CuAAC reaction could also be employed to help in di-ubiquitin purification.

An alternative, non-radical method for introducing an internal alkene between ubiquitin monomers was devised, although it ultimately did not result in the required dimers. Other non-radical means of ubiquitin dimerisation that would result in internal alkenes could be investigated in the future.

Chapter 4 shows the formation of di-ubiquitin constructs containing a terminal alkene. The approach used for the dimer construction combined biorthogonal azido-modification of lysines of one monomer, followed by CuAAC reaction with an alkyne-containing monomer. The terminal alkene of that construct was shown to have thiol-ene functionality. This approach can be used for site-specific labelling of other proteins, as well as for constructing molecular probes for measuring activities of enzymes other than DUBs. It can also be employed as a strategy for ADC construction, where selective azido-modification of antibody lysines can be followed by CuAAC reaction with alkyne-containing cytotoxic payloads or the introduction of orthogonal chemical handles.

Once di-ubiquitin constructs containing internal and terminal alkene warheads are purified, they can be tested against a panel of purified DUBs to check their specificities. A panel of di-ubiquitin constructs with internal and terminal alkenes mimicking isopeptide bonds targeted by various DUBs can then be constructed. These, in turn, can be used to help unravel DUB specificities *in vitro*. A strategy for the use of di-ubiquitin constructs *in vivo* can be designed, such as the incorporation of membrane-crossing peptides into the construct, and radical activation using blue or infrared light, alongside appropriate radical initiators. Resulting constructs can be tested against different diseased and healthy cells, to help unravel DUB specificities and their contribution to disease states.

Chapter 5 highlights squaramides as potential lysine-specific warheads of ubiquitin-based probes. Ubiquitin constructs containing squaramides were able to capture OTUB1 as well as catalytically inactive OTUB1 C91S, *via* non-catalytic lysines near the active sites of DUBs. The exact binding mode to DUBs and specific residues targeted by squaramide-containing constructs can be confirmed in the future by

structural studies of the complexes, *via* cryo-EM, X-ray crystallography, and multidimensional NMR.

One of the synthesised ubiquitin constructs containing a squaramide warhead was explored as a molecular probe of Rpn11, a metalloprotease DUB. In the future, testing of ubiquitin constructs linked to squaramide warheads *via* extended linkers against Rpn11 and other DUBs could be performed. Monomeric squaramide-containing constructs can be used in the future for proteomics investigations into their specificities as selective probes of DUBs.

Chapter 7: Materials and methods

7.1. General biochemical methods

7.1.1. Buffers

- **2X Reducing sample buffer**: 0.2 M Tris-Cl pH 6.8, 30% glycerol, 0.4% β-mercaptoethanol, 9% SDS, 0.1 % bromophenol blue.
- **Blotting transfer buffer**: 25 mM Tri, 190 mM Glycine, 20% MeOH).
- **BSA blocking buffer**: 5% BSA in PBS-T.
- **Cell resuspension buffer** for plasmid extraction: 25 mM Tris-HCl pH 8, 50 mM glucose, 10 mM EDTA, in deionised water.
- **Cell denaturation buffer**: 0.2 N NaCl, 1% SDS, in deionised water.
- **Column buffer**: 50 mM HEPES pH 6.8, 100 mM NaOAc, in deionised water.
- **Dialysis buffer**: NH_4OAc 50 mM, 1 mM EDTA, 1 mM DTT; pH 4.5.
- **Homogenate buffer**: 50 mM Tris-Cl pH 7.4, 5 mM $MgCl_2$, 250 mM sucrose, 1 mM dithiothreitol (DTT), in deionised water.
- **MESNa solution**: 50 mM Sodium 2-mercaptoethanesulfonate, in deionised water.
- **Ni elution buffer A**: 50 mM sodium phosphate pH 8.0, 300 mM NaCl, 150 mM imidazole.
- **Ni elution buffer B**: 50 mM sodium phosphate pH 8.0, 300 mM NaCl, 300 mM imidazole.
- **Ni wash buffer**: 50 mM sodium phosphate pH 8.0, 300 mM NaCl, 10 mM imidazole.
- **MS buffer A**: 98% desionised water, 2% MeCN, 0.1 % TFA.
- **MS buffer B**: 80% MeCN, 20% deionised water, 0.1% TFA.
- **OTUB1/OTUB1$_{C91S}$ storage buffer**: 20 mM Tris-Cl pH 8.0, 1mM DTT, 10% glycerol, 50 mM NaCl.
- **PBS**: 8 mM Na_2HPO_4, 150 mM NaCl, 2 mM KH_2PO_4, 3 mM KCl, in deionised water.

- **PBS-T**: 8 mM Na_2HPO_4, 150 mM NaCl, 2 mM KH_2PO_4, 3 mM KCl, 0.1% Tween 20, in deionised water.
- **Phenol/Chloroform/Isoamyl alcohol solution**: 25/24/1 ratio.
- **Ponceau stain**: 1 mg of Ponceau S powder (Sigma Aldrich) in 5 mL of glacial acetic acid, and 90 mL deionised water.
- **Renaturation buffer**: 3 M sodium acetate, 11.5% glacial acetic acid, in deionised water.
- **Silver stain developer solution**: 3% K_2CO_3, 0.05% formaldehyde.
- **Silver stain fixative solution:** 40% EtOH, 10% AcOH.
- **Skimmed milk blocking buffer**: 5% skimmed milk powder in PBS-T.
- **TE buffer**: 10 mM Tris-HCl pH 8, 1 mM EDTA, in deionised water.
- **Urea buffer**: 6 M urea, 33 mM Tris-Cl, pH 7.8.

7.1.2. Chitin column preparation and use

Chitin bead slurry (New England Biolabs) stored at 4 °C in 20% EtOH was resuspended by mixing, and 5 mL of the slurry was poured into a capped plastic purification column. A filter paper was placed inside the column, the storage solution was drained, and the beads were primed with 50 mL of ice-cold column buffer, taking care not to allow them to dry out. Clarified cell lysate containing expressed proteins was then poured through the chitin-binding beads at 4 °C. The column was then washed with 50 mL of ice-cold column buffer. The column was then washed with 10 mL of ice-cold MESNa solution, and then capped. An additional 5 mL of MESNa solution was added. The top of the column was sealed, and the column was incubated 20 h at 37 °C, 120 rpm. Construct **40** was eluted from the beads. The column was then washed with 10 mL of column buffer, and both solutions were combined for further concentration. 50 mL of deionised water was poured through the column, followed by 25 mL of 0.3 M sodium hydroxide. The column was capped and incubated for 30 min at room temperature, with 5 mL of 0.3 M sodium hydroxide. 100 mL of deionised water was poured through the column, followed and 10 mL 20% EtOH solution. The column was capped, and an additional 5 mL of 20% EtOH solution was poured onto the chitin beads. The column was stored at 4 °C until further use. The column was reused up to 5 times.

7.1.3. NAP-5 column preparation and use

NAP-5 desalting column (GE Healthcare, Illinois USA) was fixed above a waste beaker. The column cap was removed, and the storage solution was fully drained. 500 µL of the sample to be purified was applied through the column. When the liquid was fully drained from the column, 1 mL of column buffer was applied, and the eluant containing the desalted sample was captured into a fresh Eppendorf tube. To clean the NAP-5 column, 10 mL of column buffer was poured through the column, allowing it to fully drip through, followed by 10 mL of 20% ethanol solution. The capped NAP-5 column was stored in 5 mL of 20% ethanol solution at room temperature. NAP-5 columns were reused up to 10 times.

7.1.4. HEK293T lysate preparation

HEK293T immortalised cells were gifted by the Bowie group (TBSI, School of Biochemistry and Immunology), and stored as cell pellets at -80 °C. Cells were resuspended in between 100 µL and 250 µL of ice-cold homogenate buffer (depending on the size of the cell pellet), transferred to a 1.5 mL Eppendorf tube, and approximately the same volume of glass beads was added to the cell suspension. An additional volume of between 100 µL and 250 µL of homogenate buffer was added, and the solution was vortexed using a benchtop vortex for 20 seconds. Immediately afterwards, Eppendorf with the cell lysate was placed on ice for 90 seconds. Cell lysis by vortex followed by resting on ice was repeated an additional 20 times. The Eppendorf tube was then centrifuged at 13200 rpm for 5 minutes, and the supernatant was mixed by pipetting and aliquoted 10 µL at a time. Aliquots were stored at -80 °C.

7.1.5. Protein and DNA quantification

Absorbances at 215 nm and 280 nm were used to measure the protein content in each full protein or protein digest sample. For DNA quantification, absorbance at 260 nm was measured. The 260/280 nm ratio was also recorded, with values between 1.8 and 2.0 indicating pure plasmid DNA. The NanoDrop application was opened, and the appropriate measurement setting was selected. The stage was washed with deionised water and blotted dry using a lint-free tissue. Once the stage was dry, a droplet of deionised water was placed onto it, and the instrument was closed to initialise. After initialisation, the water was wiped off with a lint-free tissue, and a droplet of the experimental buffer was placed on the stage. A 'blank' measurement was taken, after which the buffer was wiped off using a lint-free tissue. The sample was then applied, measured, and the results were recorded with a screenshot. Finally, the stage was

wiped with a lint-free tissue, rinsed with deionised water, and the instrument was cleaned by washing the stage once more with deionised water and blotting it dry.

7.1.6. SDS-PAGE (12% Acrylamide)

Sodium Dodecyl Sulphate Polyacrylamide Gel Electrophoresis (SDS-PAGE) is used to separate proteins based on their molecular weight. Samples were prepared for separation by adding an equal volume of reducing sample buffer, followed by heating at 95 °C for 5 minutes. Samples were loaded onto the gel alongside Fisher's EZ-Run TM Pre-Stained Rec Protein Ladder. Proteins were separated on a 12% acrylamide gel (resolving gel: 1.3 mL 1.5 M Tris-Cl pH 6.8, 1.5 mL 40% acrylamide/bis-acrylamide 29:1, 2 mL dH_2O, 50 µL 10% SDS, 50 µL 10% ammonium persulfate APS, 5 µL Tetramethylethylenediamine TEMED; stacking gel: 630 µL 0.5 M Tris-Cl pH 6.8, 300 µL acrylamide/bis-acrylamide 29:1, 1.3 mL dH_2O, 25 µL 10% SDS, 25 µL 10% APS, 2.5 µL TEMED). Separation was achieved by passing a current of 150 V through the gel submerged in SDS-PAGE running buffer for 1–2 hours (25 mM Tris, 190 mM Glycine, 1% SDS) and visualised either by Western blotting, silver staining or Ponceau staining.

7.1.7. Anti-HA Western blot

A nitrocellulose membrane (GE Healthcare, Illinois USA) was soaked in a blotting transfer buffer along with the filter papers and sponges. The transfer stack was assembled with a plastic cover on the outside, followed by two wetted layers of sponges, followed by one wetted filter on top of the sponges. The gel was placed on the wetted filter, followed by a wetted nitrocellulose paper. Another wetted filter was placed on top of the membrane, followed by two additional wetted sponges and another plastic cover. The assembled stack was clamped. Once the transfer stack was assembled, it was submerged in blotting transfer buffer, and proteins were transferred onto the nitrocellulose membrane 18 h by passing a current of 15 V through the gel. The membrane was incubated in a skimmed milk blocking buffer (5% skimmed milk powder in PBS-T) for 1 h at room temperature, 120 rpm, before immunoblotting. The primary mouse monoclonal anti-HA antibody (Biolegend, California USA) was diluted 1:2,000 in blocking buffer and incubated with the membrane for 1 h at room temperature, 120 rpm. The membrane was washed with PBS-T (3 times for 4 min each time) and PBS (2 times for 4 min each time). The secondary antibody, Peroxidase conjugated AffiniPure Goat Anti-Mouse IgG (H+L) (Jackson ImmunoResearch, Cambridgeshire UK), was diluted in blocking buffer 1:4,000, added to the membrane and incubated for an additional 1 h at room temperature with gentle shaking. The membrane was washed with PBS-T (3 times for 4 min each time), PBS (3 times for 4

min each time) and kept in deionised water briefly before being imaged. Pierce ECL western blotting substrate (Thermo Fisher, Massachusetts USA) was used to visualise the chemiluminescence. BioRad and ImageJ software were used to process images obtained through Western blotting.

7.1.8. Anti-Biotin Western blot

A nitrocellulose membrane (GE Healthcare, Illinois, USA) was soaked in a blotting transfer buffer (25 mM Tris, 190 mM Glycine, 20% MeOH) along with the filter papers and sponges. The transfer stack was assembled as described in section 1.7. The blot was submerged in blotting transfer buffer, followed by two ice packs on either side of the transfer stack and proteins were transferred onto the nitrocellulose membrane 18 h by passing 15 V current through the gel. The membrane was incubated in BSA blocking buffer for 1 h at room temperature before immunoblotting. The blocking buffer was removed and replaced with an antibody solution (12 mL 2.5% BSA in PBS-T with 2.4 µL of IRDye 800CW- Streptavidin). The membrane was incubated at room temperature for 1 h, 120 rpm. The membrane was rinsed for 4 min in PBS-T, room temperature, 120 rpm, and the used PBS-T was discarded. The washing step was repeated 3 more times. Biotin-containing molecules were visualised using the Odyssea IR membrane reader, as streptavidin bound to biotin was attached to IR-active dye. Images were processed using ImageJ software.

7.1.9. Silver stain

Gels were treated with siler stain fixative solution at room temperature for 1 h, 120 rpm. Gels were washed in 20% EtOH (2 times for 10 min each time), then in dH_2O (2 times for 10 min each time). Gels were sensitised in aq. $Na_2S_2O_3$ (0.02%) for 45 s and then immediately washed with dH_2O (2 times for 1 min each time). Gels were incubated in a silver staining solution at 4 °C for a minimum of 20 min and up to 2 h, at 120 rpm. Following this, gels were washed in dH_2O (2 times for 30 s each time) and transferred to silver stain developer solution. Development was stopped using 5% AcOH. Images were made using Typhoon FLA9500 (GE Healthcare, Illinois USA). Once images were digitised, ImageJ software was used to process these images.

7.1.10. Ponceau stain

Ponceau stain was poured over the Western blot membrane, after overnight transfer, and left for 5 min at rt, 120 rpm. Excess ponceau stain was poured off and reused for up to 5 times. The nitrocellulose membrane was washed twice with 5% acetic acid in

water, 2 min at a time. A picture of the membrane was taken and the aqueous acetic acid was poured off, followed by Western blot.

7.2. Synthesis of HA-tagged ubiquitin constructs

7.2.1. HA-Ubqiuitin$_{1\text{-}75}$-MESNa **40**

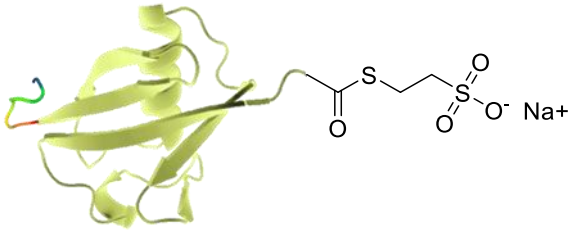

40

Expression and purification of HA-Ubqiuitin$_{1\text{-}75}$-MESNa **40** was carried out as per published procedures.[268, 336] Briefly, BL21 (DE3) competent cells transfected with a pTYB2 encoding haemagglutinin (HA) tagged on the N-terminus Ubiquitin$_{(1\text{-}75)}$ protein, and chitin-binding domain (CBD) fused to a linker on the carboxy terminus were transferred from a glycerol stock to 8 mL of autoclaved room temperature Lysogeny Broth (LB) medium with 100 µg/mL ampicillin. The inoculated broth was incubated at 37 °C, 180 rpm 20 h. Inoculated broth was poured into a conical flask containing 300 mL autoclaved 1x LB broth, with 1x ampicillin. Cells were incubated at 37 °C, 180 rpm for 3 h 45 min, or until the UV absorbance measured at 600 nm (Optical Density, OD_{600}) reached between 0.6-0.9. Bacteria were then treated with 0.2 M Isopropylthio-β-galactoside (IPTG), and incubated at room temperature, 180 rpm, 18 h, to express the target protein. Cells were pelleted at 6000 rpm for 15 min at room temperature, and dry pellets were kept at -20 °C. All spent consumables and media were left overnight in 1x Vircon solution and disposed of in the sink. Frozen cell pellets containing HA-Ubiquitin$_{(1\text{-}75)}$-intein-CBD were reconstituted in 25 mL of cold column buffer and lysed *via* sonication on ice. Lysate was centrifuged at 12000 rpm for 45 min at 4 °C, and supernatant was poured directly onto a primed Chitin column. After incubating for 18 h at 37 °C, 180 rpm, HA-Ubiquitin$_{(1\text{-}75)}$-MESNa **40** was eluted, and concentrated to 500 µL using 5 kDa Vivaspin500 concentrators (Sartorious, Göttingen Germany). The purified construct was applied to the NAP-5 desalting column. After desalting, the construct was concentrated once again with a fresh 5 kDa Vivaspin500 concentrator to 500 µL, and the protein content was checked *via* NanoDrop (2 mg/mL, 500 µL). Construct **40** was either used immediately or frozen at -20 °C overnight.

7.2.2. HA-Ubiquitin$_{1-75}$-CH_2-C-CH 23

23

45 µL of 2 M aqueous *N*-hydroxysuccinimide **41** solution was mixed with 10 µL of 100 mM Tris buffer (pH 7.5), creating 'NHS solution'. 'NHS solution' was added to an Eppendorf tube containing 500 µL of construct **40** and incubated at 37 °C for 10 min, at 60 rpm. In a separate tube, 15 µL of propargylamine **45** was added to 56 µL of 1:1 H_2O:DMSO solution. After incubation of construct **40** with 'NHS solution' for 10 min, propargylamine **45** in H_2O:DMSO was added, and the solution was incubated for a further 3 h at 37 °C, 60 rpm. A new NAP-5 column was used to purify probe **23**, and after desalting, probe **23** was concentrated *via* 5 kDa Vivaspin500 concentrators. Protein content was measured by absorbance at 280 nm, *via* NanoDrop (1.71 mg/mL, 200 µL), and aliquots were frozen at -80 °C.

7.2.3. HA-Ubiquitin$_{1-75}$-CH_2-CH-CH_2 31

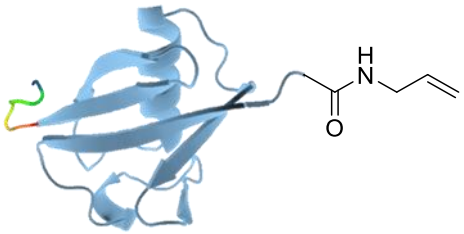

31

45 µL of 2 M aqueous *N*-hydroxysuccinimide **41** solution was mixed with 10 µL of 100 mM Tris buffer (pH 7.5), creating 'NHS solution'. 'NHS solution' was added to an Eppendorf tube containing 500 µL of construct **40** and incubated at 37 °C for 10 min, at 60 rpm. In a separate tube, 15 µL of allylamine **45** was added to 56 µL of 1:1 H_2O:DMSO solution. After incubation of construct **40** with 'NHS solution' for 10 min, allylamine **45** in H_2O:DMSO was added, and the solution was incubated for a further 3 h at 37 °C, 60 rpm. A new NAP-5 column was used to purify probe **31**, and after desalting, probe **31** was concentrated *via* 5 kDa Vivaspin500 concentrators. Protein content was measured by absorbance at 280 nm, *via* NanoDrop (0.92 mg/mL, 200 µL), and aliquots were frozen at -80 °C.

7.2.4. HA-Ubiquitin$_{1-75}$-NH-$C_6H_5NO_3$ 68

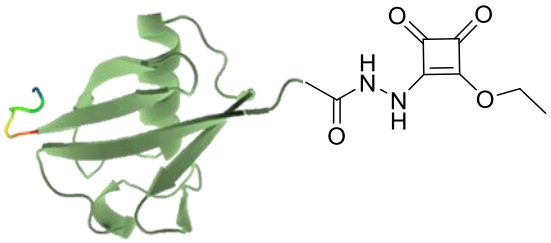

68

45 µL of 2 M aqueous *N*-hydroxysuccinimide **41** solution was mixed with 10 µL of 100 mM Tris buffer (pH 7.5), creating 'NHS solution'. 'NHS solution' was added to an Eppendorf tube containing 500 µL of **40** and incubated at 37 °C for 10 min, at 60 rpm. In a separate tube, 15 µL of compound **65** dissolved in DMSO was added to 56 µL of 1:1 H_2O:DMSO solution. After incubation of construct **40** with 'NHS solution' for 10 min, compound **65** in H_2O:DMSO was added, and the solution was incubated for a further 3 h at 37 °C, 60 rpm. A new NAP-5 column was used to purify probe **68**, and after desalting, probe **68** was concentrated *via* 5 kDa Vivaspin500 concentrators. Protein content was measured by absorbance at 280 nm, *via* NanoDrop (7.34 mg/mL, 150 µL), and aliquots were frozen at -80 °C.

7.2.5. HA-Ubiquitin$_{1-75}$-CH_2-CH_2-NH-$C_6H_5NO_3$ 71

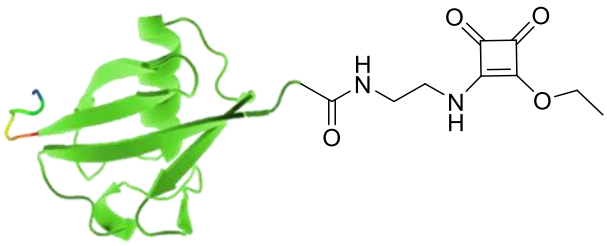

71

45 µL of 2 M aqueous *N*-hydroxysuccinimide **41** solution was mixed with 10 µL of 100 mM Tris buffer (pH 7.5), creating 'NHS solution'. 'NHS solution' was added to a new tube containing 500 µL of construct **40** and incubated at 37 °C for 10 min, at 60 rpm. In a separate tube, 15 µL of warhead **66** dissolved in DMSO was added to 56 µL of 1:1 H_2O:DMSO solution. After incubation of construct **40** with 'NHS solution' for 10 min, **66** in H_2O:DMSO was added, and the solution was incubated for a further 3 h at 37 °C, 60 rpm. A new NAP-5 column was used to purify construct **71**, and after desalting, construct **71** was concentrated *via* 5 kDa Vivaspin500 concentrators. Protein content was measured by absorbance at 280 nm, *via* NanoDrop (14.6 mg/mL, 100 µL), and aliquots were frozen at -80 °C.

7.2.6. Ubiquitin K48C expression and purification

Plasmid pET3a-Ub-K48C containing Ubiquitin K48C was obtained as a DH5α *E. coli* cell stab from Addgene. Cells were streaked on LB agar plates (100 µg/mL ampicillin), single colonies were isolated, and glycerol stocks were made, as per Addgene protocols.[291] Plasmid was extracted and purified as per kit-free alkaline plasmid extraction protocol as per Addgene protocols.[291] For plasmid purification, Phenol/Cloroform/Isoamyl alcohol solution was used, where phases were saturated by mixing vigorously for 30 seconds and leaving to separate 16 h at 4 °C. The phenol phase containing the plasmid was used. Plasmid purity was determined by checking $OD_{260/280}$. A value between 1.7–1.9 was accepted as sufficiently pure for transfection. Competent BL21 (DE3) cells obtained from Thermo Fisher Scientific were transfected with the purified plasmid and overexpressed with 0.4 mM IPTG, as per the manufacturer's protocol.[292] Cells were grown in fresh LB media containing 100 µg/mL ampicillin (first in 8 mL 18 h at 37 °C, 180 rpm, then in 300 mL for 4 h, 180 rpm), induced with 120 µL of 1 M IPTG and incubated at 37 °C at 180 rpm, pelleted by centrifugation (6000 rpm, 5 min, rt), resuspended in 25 mL column buffer and lysed *via* sonication. Lysate was centrifuged at 12000 rpm for 45 min at room temperature. The clarified supernatant was acidified to 0.5% perchloric acid in a dropwise fashion and centrifuged once more for an additional 45 min at room temperature. Supernatant was poured into a 5 kDa Servacell dialysis sleeve (Serva, Heidelberg, Germany) and dialysed for 4 h at 4 °C, and then 18 h at 4 °C in a fresh dialysis buffer. The dialysed extract was concentrated *via* VivaSpin500 5 kDa concentrator and aliquoted. Protein concentration was measured by NanoDrop (9.05 mg/mL, 200 µL) and aliquots were frozen at -80 °C.

7.2.7. WT Ubiquitin expression and purification

WT Ubiquitin was expressed as per the literature procedures.[270] Competent BL21 (DE3) cells containing a plasmid encoding WT Ubiquitin were grown in LB media containing 100 µg/mL ampicillin, first in 8 mL 17 h at 37 °C, 180 rpm, then in 300 mL for 4 h, 180 rpm. Protein expression was induced with 120 µL of 1 M IPTG, and cells were incubated at 37 °C at 180 rpm. Cells were pelleted by centrifugation and lysed *via* sonication. The lysate was centrifuged at 12000 rpm for 45 min at room temperature. Clarified supernatant was slowly acidified with perchloric acid to a final concentration of 0.5% acid. The lysate was centrifuged at 12000 rpm for an additional 45 min at room temperature. The supernatant was poured into 5 kDa Servacell dialysis sleeve and dialysed for 4 h at 4 °C, and then 18 h at 4 °C in a fresh dialysis buffer. Dialysed extract was concentrated *via* VivaSpin500 5 kDa concentrator and aliquoted. The protein

concentration was measured by NanoDrop (5.4 mg/mL, 150 µL), and aliquots were frozen at -80 °C.

7.2.8. OTUB1 C91S and OTUB1 expression and His-tag purification

The expression and purification of His tagged OTUB1 and OTUB1 with Cys-to-Ser mutant at position 91 (inactive OTUB1 variant) were carried out according to literature procedures.[268, 336] N-terminal His6 tagged OTUB1 or $OTUB1_{C91S}$ were transferred from a glycerol stock into 8 mL LB medium containing 100 µg/mL kanamycin and grown for 18 h at 37 °C, 180 rpm. Cells were transferred into fresh 300 mL LB medium containing 100 µg/mL kanamycin and grown at 37 °C at 180 rpm, and OD_{600} measurements were taken using NanoDrop, until a value of between 0.6 and 0.9 was reached. 120 µL of 1M IPTG was added, giving a final concentration of 0.4 mM and the bacteria were incubated at room temperature 18 h with vigorous shaking. The cells were pelleted *via* centrifugation at 6000 rpm for 15 min. Cells were reconstituted in 25 mL ice-cold homogenate buffer containing 20 mM PMSF and lysed *via* sonication. Cell lysate was centrifuged at 12000 rpm for 45 min, at room temperature. Ni NTA agarose resin (Sigma-Aldrich, Missouri, USA) (1.5 mL, 1:1 suspension in 20 % EtOH) was centrifuged at 2200 rpm for 5 min at room temperature, and the supernatant was discarded. 700 µL of deionised water was added to the beads, which were gently inverted until the resin was fully resuspended. The resulting solution was centrifuged at 2,200 rpm at room temperature for 5 min, and the supernatant was discarded. Washing the beads in distilled water was repeated once more. 1.4 mL Ni wash buffer was added to the resin, which was transferred to the clarified lysate in a 50 mL Falcon tube and incubated 17 h at 4 °C with rolling. The resin was centrifuged at 2200 rpm for 5 min at room temperature, and the supernatant was discarded. Ni wash buffer (1 mL) was added to the resin, which was fully resuspended by gentle inversion and centrifuged at 2200 rpm for 5 min at room temperature. This wash step was repeated four times, and the supernatant was discarded after each washing step. 0.7 mL Ni elution buffer A was added to the resin, which was resuspended by gentle pipetting. The solution was centrifuged at 2200 rpm for 5 min at room temperature, and the supernatants from these washes were pooled in clean microcentrifuge tubes. This elution step was repeated 3 more times, and eluents were combined. A final wash step was carried out with 1 mL Ni elution buffer B at 2200 rpm for 5 min at room temperature, and the supernatant was discarded. Pooled eluates were concentrated in a VivaSpin500 10 kDa centrifugal concentrators in at 9000 rpm, 500 µL at a time, at room temperature, to a final concentration of 50 µL. Ni wash buffer (450 µL) was added to the tubes and

concentrated to 50 µL in a centrifuge at 9000 rpm, room temperature. This wash step was repeated, the solution was resuspended in 150 µL of OTUB1/OTUB1$_{C91S}$ storage buffer, and pure OTUB1 or OTUB1$_{C91S}$ were aliquoted 10 µL at a time. Protein concentration was measured by NanoDrop (6.05 mg/mL, 100 µL for OTUB1; 5.7 mg/mL, 100 µL for OTUB1$_{C91S}$), and aliquots were frozen at -80 °C.

7.3. HPLC protein purification

7.3.1. HPLC hardware and software

LabSolutions Lite chromatography software was used to run the Shimadzu LC-10 analytical system with a PDA detector, and to analyse the data. Shimadzu Scientific column, LC, Shim-pack Bio Diol-120, 3um, 4.6×300 was used for the separation of ubiquitin dimers. Since peptide bonds absorb light at wavelengths between 180-230 nm,[336] absorbance at 215 nm was chosen as an indicator of protein presence. Peaks appearing at 280 nm, 205 nm,[337] and 260 nm were also monitored.[338]

7.3.2. Mobile phase

Mobile phase used for dimer purification contained: 0.25 M NaCl, 0.1 M Na_2HPO_4, pH 7 in dH_2O. The mobile phase was prepared fresh every week and degassed before use. An isocratic flow of 0.4 mL/min, 30 min run was used in the final method.

7.4. Labelling experiments

7.4.1. Labelling of DUBs by 23, 68 and 71

1 µg of constructs **23**, **68** or **71** was added to 0.2 mL Eppendorf tube, alongside OTUB1 (1 µg), OTUB1$_{C91S}$ (1 µg), Rpn8/11 (2 µg), or HEK293T cell lysate (50 ug). Samples were made up to 30 µL with homogenate buffer. Controls, including the construct being tested, HEK293T cell lysate and OTUB1 alone, were included in separate Eppendorf tubes. Samples were incubated at 37 °C for between 90 min (probe **23**) and 2 h (constructs **68** and **71**) while shaking at 120 rpm. Following incubation, the samples were prepared for SDS-PAGE.

7.4.2. Labelling of DUBs by 31 under UV light, initiated by 36 and 37.

1-2 µg of probe **31** was added to a fresh 0.2 mL Eppendorf tube, alongside OTUB1 (1 µg), or HEK293T cell lysate (50 ug). Samples were made up to 30 µL with homogenate buffer. Controls were included in separate Eppendorf tubes, including probe **31**, lysate and OTUB1 on their own, and a mixture of probe **31** and OTUB1 or HEK293T without **36**/**37** and without UV irradiation. Samples were incubated at 37°C for 90 minutes while gently shaking. In the meantime, 3 µg of initiator **36** and 15 µg co-initiator **37**

were added to a fresh 1.5 mL Eppendorf tube and solubilised in 500 µL of pure DMSO. 250 µL of deionised water was added to the **36**/**37** solution, which was vortexed vigorously, resulting in 250 µM concentration for each. **36**/**37** solution was then degassed under a stream of nitrogen gas for 15 seconds. Protein samples after incubation were treated with 1 µL **36**/**37** solution (or 1 µL H_2O/DMSO, 500/250 µL solution for controls). Samples were degassed under a stream of nitrogen gas. Samples were transferred to clean PTFE-coated LC-MS vials, and these vials were irradiated for 2-3 minutes under direct UV light. Samples were transferred back into their original Eppendorf tubes and kept at 4 °C for further testing.

7.4.3. Di-ubiquitin formation between probe 23 and Ubiquitin K48C, and conjugation of 23 to BSA under UV light, initiated by 36 and 37

2 µg of probe **23** probe was added to between 1 µg and 180 µg of Ubiquitin K48C, and samples were made up to 30 µL in homogenate buffer. Alternatively, 2 µg of probe **23** was added to between 1 ng and 200 µg of BSA (Sigma), and samples were also made up to 30 µL in homogenate buffer. Samples were incubated at 37 °C for 90 minutes while gently shaking. In the meantime, 3 µg of initiator **36** and 15 µg co-initiator **37** were added to a fresh 1.5 mL Eppendorf tube and solubilised in 500 µL of pure DMSO. 250 µL of deionised water was added to the **36**/**37** solution, which was vortexed vigorously, resulting in 250 µM concentration for each. **36**/**37** solution was then degassed with nitrogen gas. Protein samples after incubation were treated with 1 µL **36**/**37** solution (or H_2O:DMSO, 500:250 µL solution as a control). Samples were transferred to clean PTFE-coated LC-MS vials, degassed under a stream of nitrogen gas (each for 15 seconds), and these vials were irradiated for between 2 minutes and 2 hours under direct UV light. Samples including Ubiquitin K48C were transferred back into their original Eppendorf tubes, and dimer formation was checked *via* SDS-PAGE, followed by Western blot and silver staining. Samples including BSA were checked for thiol-yne labelling in the same manner.

7.4.4. Di-ubiquitin construct 44 preparation for HPLC purification

500 µg of thiol-containing Ubiquitin K48C was added to 50 µg of alkyne-containing **23**, and the thiol-yne reaction was performed, as described in subsection 7.4.3. page 134. The sample was concentrated using a 10 kDa MWCO filter (Vivaspin500). The concentrate was then filtered through a 30 kDa MWCO filter (Vivaspin500), and the crude **44** was visualised *via* Western blot and silver stain. Crude di-ubiquitin construct **44** was aliquoted at 10 µL and frozen at -80°C.

7.4.5. Construct 44 templating by OTUB1 C91S

Probe **23** and Ubiquitin K48C were mixed with OTUB1 C91S at various ratios. Samples were made up to 30 µL in the homogenate buffer and incubated at 37 °C for 90 min, 120 rpm. Following incubation, the samples were treated with 1 µL **36**/**37** solution or with water as a control. The samples were transferred to clean PTFE-coated LC-MS vials, degassed under a stream of nitrogen gas (each for 15 sec), and the vials were irradiated for 20 min under direct UV light. Samples were transferred to their original Eppendorf tubes and prepared for SDS-PAGE.

7.4.6. Di-ubiquitin formation between 23 and Ubiquitin K48C, initiated by 33 with 34 or 35 as photosensitisers

33-saturated DMSO solution was prepared by dissolving 50 mg of **33** in 1 mL od DMSO, vortexing for 30 seconds and centrifugation at 13200 rpm for 5 minutes. Riboflavin **33**. Samples containing probe **31** and protein targets were prepared, and made up to 30 µL using **33**, and homogenate buffer. Either UV light or white light irradiation was used as an energy source for the thiol-ene reaction, for between 1 minute and 3 hours of exposure. Compounds **34** or **35** were tested alongside photosensitizer **33**.

7.4.7. Labelling of DUBs by 32 under UV light, initiated by 32

Lithium phenyl-2,4,6-trimethylbenzoyl phosphine (LAP) **32** was solubilised in homogenate buffer. Probe **31** was incubated with OTUB1 and HEK293T cell lysate. Samples were made up to 30 µL of homogenate buffer. LAP **32** was added as a radical initiator of probe **31**, and the samples containing **32** were exposed to either 1 h of white light or 2.5 min of UV light irradiation.

7.4.8. Di-ubiquitin formation between 23 and Ubiquitin K48C, initiated by 1

Irgacure2959 **1** was purchased from Sigma-Aldrich. **1** was solubilised in homogenate buffer to an appropriate concentration. Probe **23** was mixed with Ubiquitin K48C, and samples were made up to 30 µL homogenate buffer. A solution containing **1** was added, and samples were exposed to 2.5 min of UV light irradiation.

7.4.9. Azido-substitution of lysines in BSA by 59

Imidazole-1-sulfonyl azide **59** was solubilised in aqueous K_2CO_3 (350 µL; 10 mg/mL), followed by the addition of aqueous $CuSO_4 \bullet 5H_2O$ (150 µL; 1 mg/mL). BSA was added, samples were mixed, and then incubated at room temperature, 120 rpm for 20 min. The proteins were purified *via* NAP-5 columns, followed by their concentration to 30 µL using 5 kDa Vivaspin500 concentrators.

7.4.10. Azido-substitution of lysines in 31 by 59

Imidazole-1-sulfonyl azide was added to aqueous K_2CO_3 (350 µL; 10 mg/mL), followed by the addition of aqueous $CuSO_4 \bullet 5H_2O$ (150 µL; 1 mg/mL). The solution was mixed with 64.5 µg of probe **31** and incubated at room temperature, 120 rpm for 20 min. The sample was then desalted *via* NAP-5 column, followed by concentration to 30 µL using 5 kDa Vivaspin500 concentrators. The resulting construct **57** was used immediately for LC-MS/MS sample preparation, or CuAAC reaction with probe **23**.

7.4.11. CuAAC reaction between 23 and 57

CuAAC cocktail was prepared fresh by adding $CuSO_4 \bullet 5H_2O$ (4 µL; 250 mM) to homogenate buffer (16 µL; 50 mM Tris-HCl pH 7.4, 5 mM $MgCl_2$, 250 mM sucrose, 1 mM dithiothreitol), followed Tris(benzyltriazolylmethyl)amine (THPTA – 10 µL; 100 mM), and finally, sodium ascorbate (15 µL; 100 mM). The solution was mixed by pipetting after each ingredient was added. CuAAC cocktail (22.5 µL) was added to construct **57** (30 µL, 50 mM), alongside 2 µg of probe **23**. Control samples included azido-substituted and alkyne-containing ubiquitin constructs, and deionised water alone. Samples were incubated at 37 °C for 3 h, at 120 rpm. After incubation, the construct was desalted using a NAP-5 column and concentrated to 30 µL using 5 kDa Vivaspin500 concentrators.

7.4.12. CuAAC reaction between 23, 31 or 44 and 47, followed by labelling of OTUB1.

CuAAC cocktail was prepared fresh by adding CuSO4•5H2O (4 µL; 250 mM) to homogenate buffer (16 µL; 50 mM Tris-HCl pH 7.4, 5 mM MgCl2, 250 mM sucrose, 1 mM dithiothreitol), followed Tris(benzyltriazolylmethyl)amine (THPTA – 10 µL; 100 mM), and finally, sodium ascorbate (15 µL; 100 mM). The solution was mixed by pipetting after each ingredient was added. CuAAC cocktail (22.5 µL) was added to azido-substituted **47** (30 µL, 50 mM), alongside 2 µg of probe **23**. **47** was also mixed with probe **31**, and separately, **47** was mixed with dimer **44**. Samples were incubated at 37 °C for 3 h, at 120 rpm. After incubation, the construct was desalted using a NAP-5 column and concentrated to 30 µL using 5 kDa Vivaspin500 concentrators.

7.4.13. Tri- and multi-ubiquitin formation between Ubiquitin K48C and 58, 23 and 61, or 23 and 63.

Formation of tri-ubiquitin constructs was attempted on three occasions. First time, probe **31** was azido-exchanged, as described in section 7.4.10, resulting in construct **57**. Sample was then purified using NAP-5 column, and concentrated *via* 5 kDa MWCO

filters. Azido-substituted **57** was conjugated *via* CuAAC reaction, as described in section 7.4.11, resulting in dimeric construct **58**, which was once again purified via NAP-5 column and concentrated. This was followed by degassing under nitrogen stream, and thiol-ene reaction with 500 µg of Ubiquitin K48C, with 250 µM of both **36** and **37** as radical initiators, under UV light for 3 min. Samples were then purified *via* a NAP-5 column and concentrated. Results can be seen in **Figure 63**. Second time, di-ubiquitin construct **44** was prepared, as described in section 7.4.3, which was then treated with 10 mg/mL imidazole-1-sulfonyl azide, purified using a NAP-5 column and concentrated, resulting in construct **61**. That construct was treated with probe 23, and CuAAC reaction was performed as described in section 7.4.12, resulting in construct **62**. Results can be seen in **Figure 64**. Third time, construct **63** was formed by reacting probe 23 with imidazole-1-sulfonyl azide, using the same conditions as in section 7.4.10. Following purification with a NAP-5 column and concentration, construct **63** was reacted with additional 2 µg of probe **23** *via* CuAAC reaction, using conditions described in section 7.4.11, resulting in construct **64**. Results can be seen in **Figure 65**.

7.5. Mass Spectrometry analysis

7.5.1. In-solution digestion of proteins

Proteins were extracted using 4x sample volume of ice-cold methanol with 0.1% formic acid. Samples were centrifuged at 13200 rpm for 5 min, and supernatants were disposed of. Urea buffer (50 µL) was added to the extracted protein pellets. Samples were sonicated for 20 sec in an ultrasonic bath, heated for 30 sec at 80 °C, vortexed for 20 sec and sonicated once more for 2 min. Samples were diluted in 250 µL Milli-Q water, vortexed for an additional 20 sec and sonicated for an additional 2 min. To samples which required the removal of disulfide bonds, dithiothreitol (DTT)was added to a final concentration of 10 mM. Samples containing DTT were incubated in the dark at room temperature for 15 min, followed by the addition of iodoacetamide to a final concentration of 50 mM, incubation at room temperature for an additional 15 min, 5 sec of vigorous mixing using a vortex, and centrifugation at 11800 rpm for 15 min. Elastase or Trypsin were added to the samples, once the samples reached room temperature, in a ratio of 1:15 or 1:20 (enzyme to sample protein content), respectively. Digestion was carried out 18 h at 37 °C while shaking at 80 rpm.

7.5.2. Ziptip sample desalting prior to LC-MS/MS analysis

Ziptips were obtained from Merck. They have a capacity for capturing around 5-10 µg of peptide content. 10 µL pipette was fitted with a zip-tip, and the pipette was fully

depressed - 10 µL of Buffer B (80% acetonitrile, 20% ddH_2O, 0.1%TFA) was slowly aspirated to wet the ziptips, without allowing them to dry out or introducing air bubbles. Fluid was discarded. Using the back pipetting technique, fresh 10 µL of Buffer B was aspirated through the filter. 2 x 10 µL of Buffer A (2% acetonitrile, 98% ddH_2O, 0.1% TFA) was then aspirated to equilibrate the ziptip resin. Digested protein content was slowly transferred through the ziptip, 10 µL at a time, and discarded. Ziptip resin was slowly washed with 5 x 10 µL Buffer A to remove salts, discarding the liquid after each wash. Purified peptides were eluted with 2 x 10 µL Buffer B, allowing sufficient time for Buffer B to be in contact with the C18 resin to recover peptides. Samples were dried on a Vacuum Concentrator until fully dry, reconstituted in Buffer A to around 1 mg/mL initial protein content, and centrifuged at 13200 rpm for 5 minutes to remove any particulates. The samples were transferred to PTFE-covered inserts and then into LC-MS vials, stored on ice and submitted for analysis.

7.5.3. Mass spectrometry data acquisition and analysis

Mass spectrometric data acquisition for proteomic samples was performed by Dr. Gary Hessman (TCD, School of Chemistry). Captive spray ionisation was performed using a Thermo Scientific UltiMate 3000RSLCnano LC (Waltham, MA USA) equipped with an Acclaim PepMap C18 (2 µm, 0.075 mm × 150 mm) column. For each injection, 5 µL of a (1 µg/µL) digested peptide was loaded onto a Nano Trap Column (100 µm I.D. × 2 cm, packed with Acclaim PepMap100 C18) at 10 µL/min with 95% water/ 5% acetonitrile/ 0.1% formic acid for 3 min. Trapped peptides were eluted onto the analytical column using a multi-step gradient with a flow rate of 0.3 µL/min. The gradient utilised two mobile phase solutions: A, water/0.1% formic acid and B, acetonitrile: 0 min, A (98%), B (2%); 3 min, A (98%), B (2%); 63 min A (65%), B (35%); 69.5 min A (5%), B (95%); 74 min A (5%), B (95%); 78 min A (98%), B (2%), curve 5 for each step. Peptide digest were analysed on a Bruker compact Qq-TOF mass spectrometer *via* CaptiveSpray nanoBooster (Bremen Germany). Precursor ions were scanned from 150 m/z to 2200 m/z at 2 Hz with a cycle time of 3.0 seconds, with fixed windows excluded (20-350, 1221-1225, 2200-40000). Smart Exclusion was used to ensure only chromatographic peaks were selected as precursors. Active Exclusion enabled the analysis of less-abundant ions to be analysed and not excluded from precursor selection. Data acquired on the Bruker compact was converted to mzXML format for analysis. Data was analysed using the free SearchGUI-4.1.7 software. The modified human protein database (UniProt) was used as a library against which experimental spectra were compared. PeptideShaker-2.2.5 was used for data visualisation.

ESI mass spectra were acquired using a Bruker micrOTOF-QIII spectrometer interfaced to a Dionex UltiMate 3000 LC in positive and negative modes as required. The instrument was calibrated using a tune mix solution, (Agilent Technologies ESI-l Low concentration tuning mix) this was also used as an internal lock mass. Masses were recorded over the range 100-2000 m/z. Operating conditions were as follows: end-plate offset 500V capillary 4500V, nebulizer 2.0Bar, dry gas 8.0 L/min, and dry temperature 180 °C. MicroTof control 3.2 and HyStar 3.2 software were used to carry out the analysis.

APCI experiments were carried out on a Bruker micrOTOF-Q III spectrometer interfaced to a Dionex UltiMate 3000 LC or direct insertion probe. The instrument was operated in positive or negative mode as required. Agilent tuning mix APCI-TOF was used to calibrate the system. Masses were recorded over a range of 100-2000 m/z. Operating conditions were as follows: Capillary voltage 4000V, corona 4000nA, nebulizer gas 2.0 Bar, dry gas 3.0 L/min, dry gas temperature 100-200 °C, vap. temperature 100-400 °C. MicroTof control and HyStar software were used to carry out the analysis.

7.6. General chemical methods

Chemicals were purchased from Acros Organics, Alfa Aesar, Thermo Fisher Scientific, Fluorochem, Sigma-Aldrich, Merck, and TCI Chemicals and were used without further purification. Anhydrous DCM was purchased from Thermo Fisher Scientific. TEA, **34**, and **35** were purchased from Merck and Thermo Fisher Scientific. Nitrogen gas was obtained from BOC gases. Room temperature (rt) refers to 19-21 °C. Flash column chromatography was performed on silica gel, particle size 0.04-0.063 mm, purchased from Sigma Aldrich or VWR. TLC analysis was performed on TLC Silica gel 60 F_{254} plates purchased from Merck and was visualised by UV irradiation (254 nm), as well as ninhydrin stain (1.5 g ninhydrin, 5 mL AcOH, 500 mL 95% EtOH), or potassium permanganate stain (3 g $KMnO_4$, 20 g K_2CO_3, 300 mL H_2O).

In NMR experiments, chemical shifts are reported in parts per million (ppm), while coupling constants are reported in Hertz (Hz) and are accurate to 0.2 Hz. $_{13}$C NMR spectra are proton-decoupled. ^{1}H and ^{13}C NMR spectra were recorded by Dr. John O'Brien on Bruker DPX 400 MHz (400.13 MHz for ^{1}H NMR and 100.61 MHz for ^{13}C NMR), Bruker AV 400 MHz (400.13 MHz for ^{1}H NMR and 100.61 MHz for ^{13}C NMR), Bruker AV 600 MHz (600.13 MHz for ^{1}H NMR and 150.90 MHz for ^{13}C NMR), or Agilent MR400 (400.13 MHz for ^{1}H NMR and 100.61 MHz for ^{13}C NMR) spectrometers. ^{15}N NMR spectra were recorded by Dr. Manuel Ruether using Solid State NMR, using Bruker 400

MHz Avance III HD equipped with a 3.2mm H/X CP-MAS probe. Nitrogen frequency was 40.54 MHz. The carbon low field signal was set to 38.48 ppm. Nitrogen spectra were recorded with a standard CP pulse sequence, with a spin rate of 20 kHz, 80 kHz proton decoupling. A cross-polarisation pulse of 4 ms was used for nitrogen spectra. The sample temperature was set to 20 °C. NMR spectra for each compound were assigned using HSQC and HMBC experiments. For NMR analysis, dry samples were reconstituted in and referenced to their residual deuterated solvent, DMSO-d_6 (δ_H = 2.50 ppm, δ_C = 39.52 ppm) for compounds **65**, **67**, **51**, and **52**.

Infrared (IR) spectra were obtained on Perkin Elmer spectrophotometer. ESI mass spectra of small molecules were acquired by Dr. Gary Hessman, using a Bruker microToF-Q IIIspectrometer interfaced to Dionex UltiMate 3000 LC in positive and negative modes as required. The instrument was calibrated using a standard (Agilent Technologies ESI-I Low concentration tuning mix), which was also used as an internal lock mass. Operating conditions were as follows: end-plate offset 500 V, capillary 4500 V, nebuliser 2.0 Bar, dry gas 8.0 L/min, and dry temperature 180 °C. MicroToF control 3.2 and HiStar 3.2 software were used for data analysis. APCI-ToF experiments were carried out on the same system, with Agilent tuning mix APCI-ToF as calibrant. APCI conditions were as follows: capillary voltage 4000 V, corona 4000 nA, nebuliser gas 2.0 Bar, dry gas 3.0 L/min, dry gas temperature 100-200 °C, vapour temperature 100-400 °C. Data analysis was performed using MicroToF control 3.2 and HiStar 3.2 software.

7.6.1. Synthesis of 3-ethoxy-4-hydrazineylcyclobut-3-ene-1,2-dione (65)

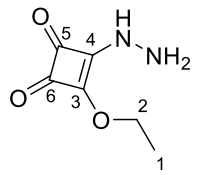

65

Diethyl squarate **67** (187 mg, 1.1 mmol) was dissolved in MeOH (10 mL), while stirring, followed by the addition of hydrazine hydrate (63 µL, 1 mmol), dropwise at room temperature. The reaction mixture turned greyish-blue on hydrazine addition. Hydrazine was reacted with diethyl squarate to completion, over 22 h, as visualised by TLC (water-isopropanol-EtOAc, 2:2:1). Consumption of hydrazine (R_f = 0.23) and diethyl squarate (R_f = 0.8) resulted in the formation of a new product (R_f = 0.9), which was bright orange, when stained with ninhydrin. Reaction was concentrated under reduced

pressure (97.1% yield). The flaky grayish-white solid was stored at -20 °C, and used for ubiquitin probe construction without further purification.

IR (ATR, neat) ν_{max}/cm^{-1}: 3350 (N-H), 2981 (C-H), 2625 (CH, CHO), 1808 (C=O), 1729 (C=O), 1674 (C=O), 1572 (C=O), 1509, 1473, 1380 (C-H), 1334, 1274, 1170, 1124, 1083, 915, 792, 700

^{1}H NMR (600 MHz, DMSO-*d*$_6$): δ = 5.22 (s, 1H, N-H), 4.65 (q, *J* = 7.2 Hz, 2H, H-2), 1.38 (t, *J* = 7.1 Hz, 3H, H-1)

^{13}C NMR (100 MHz, DMSO-*d*$_6$): δ = 196.16 (C-5, C-6), 189.58 (C-3), 184.11 (C-4), 70.66 (C-2), 15.77 (C-1)

^{15}N NMR (40 MHz, DMSO-*d*$_6$): δ = 56.78 (N-H), 52.89 (N-H$_2$)

HRMS (APCI): *m/z* calc. for $C_6H_8N_2O_3$, 157.055 $[M+H]^+$, found = 157.063

7.6.2. Synthesis of 3-((2-aminoethyl)amino)-4-ethoxycyclobut-3-ene-1,2-dione (66)

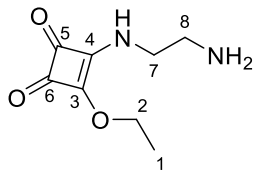

66

Diethyl squarate (187 mg, 1.1 mmol) was dissolved in DCM (10 mL), while stirring, followed by the addition of ethylenediamine (75 µL, 1 mmol), dropwise, at room temperature, for 20 h. TLC analysis (water-isopropanol-EtOAc, 2:2:1) confirmed the consumption of ethylenediamine (R_f = 0.62) and diethyl squarate (R_f = 0.8), resulting in the formation of a new product (R_f = 0.46), which had a faint orange colour when stained with ninhydrin. Upon completion, the reaction was dried under vacuum, without further purification (95.3% yield). Flaky grayish-white solid was stored at -20 °C, and used for ubiquitin probe construction without further purification.

IR (ATR, neat) ν_{max}/cm^{-1}: 3114 (N-H), 2989 (C-H), 2804, 2357, 2161, 1980, 1811 (C=O), 1728 (C=O), 1594 (N-H), 1481, 1382 (C-H), 1336, 1072, 1026, 848, 797, 668

^{1}H NMR (600 MHz, DMSO-*d*$_6$): δ = 10.80 (s, 1H, N-H), 8.23 (s, 2H, N-H$_2$), 4.66 (q, *J* = 7.1 Hz, 2H, H-2), 2.56 (t, *J* = 5.5 Hz, 4H, H-7, H-8), 1.37 (t, *J* = 7.1 Hz, 3H, H-1)

^{13}C NMR (100 MHz, DMSO-d_6): δ = 192.55 (C-6), 190.24 (C-5), 189.58 (C-3), 184.11 (C-4), 70.65 (C-2), 34.86 (C-7), 34.06 (C-8), 15.77 (C-1)

HRMS (APCI): *m/z* calc. for $C_8H_{12}N_2O_3$, 184.08 $[M+H]^+$, found = 184.08

7.6.3. Synthesis of (E)-1-(4-bromobut-2-en-1-yl)-1,3,5,7-tetraazaadamantan-1-ium (56)

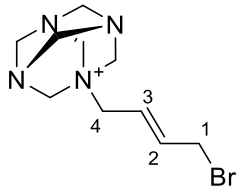

56

The intermediate was synthesised using an established protocol.[308] 1.08 g (7.19 mmol) of (*E*)-1,4-dibromobut-2-ene (**51**) was dissolved in chloroform (9.48 mL) while stirring, and kept under an argon stream to maintain inert conditions. The flask was cooled to 4 °C. At that point, the argon stream was switched off, and 505 mg (3.6 mmol) 1,3,5,7-tetraazaadamantane (HMTA) was added. The nitrogen stream was replaced, and the reaction was warmed up to room temperature. The reaction proceeded under inert conditions, at room temperature, for 16 h. The following day, the product was washed twice with chloroform to remove unreacted starting materials, and the filtered white precipitate was dried *in vacuo*. The white precipitate was solubilised in DMSO for TLC analysis. TLC analysis (water-isopropanol-EtOAc, 2:2:1) confirmed partial disappearance of the starting material ((*T*)-1,4-dibromobut-2-ene, R_f = 0.95), and HMTA (R_f = 0.7), and formation of the product (**56**) (R_f = 0.73), which had a faint orange colour when stained with ninhydrin. Dry powder was stored at -20 °C for up to a week (73.8% yield). Only IR spectrum and mass spectrometric analysis were performed on this intermediate, and the intermediate was used in preparation of compound **51**.

IR (ATR, neat) ν_{max}/cm^{-1}: 3744, 2978 (H-C=C), 2159, 1468 (C=C), 1398, 1370, 1273, 1237, 1214, 1113, 999, 971, 931, 867, 829, 810, 783 (C-Br), 705, 654

HRMS (ESI$^+$): *m/z* calc. for $C_{10}H_{18}BrN_4$, 273.07 M-H^+, found = 273.07

7.6.4. Synthesis of (E)-2-(4-bromobut-2-en-1-yl)isoindoline-1,3-dione (52)

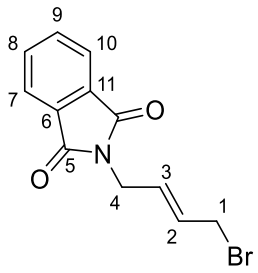

52

920 mg (4.58 mmol) of (*T*)-1,4-dibromobut-2-ene (**51**) was reacted at room temperature with 850 mg (4.58 mmol) of potassium phthalimide (**52**) in 15 mL DMF, while stirring, for 21 h. 20 mL of dH_2O was added to the reaction, followed by 20 mL of diethyl ether, mixed, and the organic phase was collected. Extraction of the aqueous phase with diethyl ether was repeated twice more, and the resulting 60 mL of organic extracts were combined. 20 mL of brine was added to the organic phase, mixed, and the phases were separated. The organic phase was then dried over $MgSO_4$, filtered and dried *in vacuo*. TLC analysis (hexane:EtOAc, 8:2) showed starting material ((*T*)-1,4-dibromobut-2-ene, R_f = 0.7) was almost completely consumed, with a new spot (R_f = 0.2) that turned brownish-red when exposed to potassium permanganate stain. Product (**52**) was purified by flash column chromatography (hexane:EtOAC, 8:2) and obtained as a light-brown solid (86.9% yield). Dry powder was stored at -20 °C for up to a week.

IR (ATR, neat) ν_{max}/cm^{-1}: 3787, 3100 (H-C=C), 2933 (H-C=C), 2531, 2159, 2029, 1976, 1464 (C=C), 1398, 1370, 1326, 1274, 1236, 1214, 1113, 1030, 1000, 970, 930, 810, 783 (C-Br), 704

^{1}H NMR (600 MHz, DMSO-*d*$_6$): δ = 7.88 (dd, *J* = 3.03 Hz, *J* = 5.5, 4H, H-7, H-8, H-9, H-10), 7.75 (dd, *J* = 5.5, 3.0 Hz, 13H), 5.78-6.03 (m, 2H, H-2, H-3), 4.25-4.36 (m, 2H, H-4), 3.93 (dd, *J* = 7.2, 1.0 Hz, 2H, H-1)

^{13}C NMR (100 MHz, DMSO-*d*$_6$): δ = 167.81 (C-5, C-12), 134.11 (C-6, C-11), 132.04 (C-8, C-9), 129.99 (C-3), 128.36 (C-2), 123.42 (C-7, C-10), 38.62 (C-4), 31.26 (C-1)

HRMS (ESI$^+$): *m/z* calc. for $C_{12}H_{10}NO_2Br$ = 278.88

The spectroscopic data are in agreement with those reported in the literature.[339] Melting point: 97-99 °C (literature)[339], 97 °C (experimental).

7.6.5. Synthesis of (E)-4-bromobut-2-en-1-amine (51)

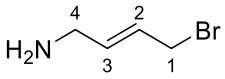

51

The compound was synthesised using an established protocol.[308] Quaternary amine salt **56** (1 g, 3.64 mmol) was hydrolysed in 2M HCl (1.96 mL dH_2O, 9.8 mL EtOH) in reflux conditions, for 2 h. Release of the protecting group was confirmed by the formation of a new spot on TLC that turned orange when treated with ninhydrin stain. Several other spots were seen. Crude reddish oil **51** was not further purified, nor dried, as ion exchange chromatography was required for purification, and the product degraded on basification. NMR and Mass Spectrometric analysis confirmed the presence of the target molecule in the crude. No melting point was established due to issues with product purification.

^{1}H NMR (600 MHz, DMSO-d_6): δ = 8.33 (s, 1H, N-H), 5.84-6.12 (m, 2H, H-2, H-3), 4.24 (d, *J* = 6.4 Hz, 2H, H-1), 3.46 (q, *J* = 5.8 Hz, 2H, H-4)

^{13}C NMR (100 MHz, DMSO-d_6): δ = 131.56 (C-3), 127.33 (C-2), 44.68 (C-1), 39.69 (C-4)

HRMS (APCI): *m/z* calc. for C_4H_8BrN, 150.05 $[M+H]^+$, found = 149.99

References

1. Collins, F.; Green, E.; Guttmacher, A., Guyer, M. S., A vision for the future of genomics research. *Nature* **2003**, *422*(6934):835-47.

2. Zhong, Q.; Xiao, X.; Qiu, Y.; Xu, Z.; Chen, C.; Chong, B.; Zhao, X.; Hai, S.; Li, S.; An, Z.; Dai, L., Protein posttranslational modifications in health and diseases: Functions, regulatory mechanisms, and therapeutic implications. *MedComm*. **2023**, *4*(3):e261.

3. Humphery-Smith, I., The 20th anniversary of proteomics and some of its origins. *Proteomics* **2015**, *15*(11):1773-6.

4. Parker, C. G.; Pratt, M. R., Click Chemistry in Proteomic Investigations. *Cell* **2020**, *180*(4):605-632.

5. Huang, Y.; Zhang, P.; Wang, H.; Chen, Y.; Liu, T.; Luo, X., Genetic Code Expansion: Recent Developments and Emerging Applications. *Chem. Rev.* **2025**, *125*(2):523-98.

6. Yang A, Cho K, Park HS. Chemical biology approaches for studying post-translational modifications. RNA Biol. **2018**, *15*(4-5):427-440.

7. Harel, O.; Jbara, M., Posttranslational Chemical Mutagenesis Methods to Insert Posttranslational Modifications into Recombinant Proteins. *Molecules* **2022**, *27*(14):4389.

8. Naowarojna, N.; Cheng, R.; Lopez, J.; Wong, C.; Qiao, L.; Liu, P., Chemical modifications of proteins and their applications in metalloenzyme studies. *Synth. Syst. Biotechnol*. **2021**, *6*(1):32-49.

9. Li, C.; Li, T.; Tian, X.; An, W.; Wang, Z.; Han, B.; Tao, H.; Wang, J.; Wang, X., Research progress on the PEGylation of therapeutic proteins and peptides (TPPs). *Front. Pharmacol.* **2024**, *15*:1353626.

10. Zuma, L. K.; Gasa, N. L.; Makhoba, X. H.; Pooe, O. J., Protein PEGylation: Navigating Recombinant Protein Stability, Aggregation, and Bioactivity. *Biomed. Res. Int.* **2022**, *2024*:8929715.

11. Zhao, X.; Li, G.; Liang, S., Several affinity tags commonly used in chromatographic purification. *J. Anal. Methods Chem*. **2013**, *2023*:581093.

12. Young, C. L., Britton, Z. T., Robinson, A. S., Recombinant protein expression and purification: a comprehensive review of affinity tags and microbial applications. *Biotechnol. J.* **2012**, *7*(5):620-34.

13. Toseland, C. P., Fluorescent labeling and modification of proteins. *J. Chem. Biol.* **2013**, *6*(3):85-95.

14. Sun, T.; Zhao, H.; Hu, L.; Shao, X.; Lu, Z.; Wang, Y.; Ling, P.; Li, Y.; Zeng, K.; Chen, Q., Enhanced optical imaging and fluorescent labeling for visualizing drug molecules within living organisms. *Acta. Pharm. Sin. B*. **2024**, *14*(6):2428-46.

15. Jayachandran, B.; Parvin, T. N.; Alam, M. M.; Chadna, K.; Balamurali, M. M., Insights on Chemical Crosslinking Strategies for Proteins. *Molecules* **2022**, *27*(23):8124.

16. Giri, P.; Pagar, A. D.; Patil, M. D.; Yun, H., Chemical modification of enzymes to improve biocatalytic performance. *Biotechnol. Adv*. **2021,** *53*:107868.

17. Leonard A. C.; Whitehead, T. A., Design and engineering of genetically encoded protein biosensors for small molecules. *Curr. Opin. Biotechnol.* **2022**, *78*:102787.

18. Desai, M. S.; Lee, S. W., Protein-based functional nanomaterial design for bioengineering applications. *Wiley Interdiscip. Rev. Nanomed. Nanobiotechnol.* **2015**, *7*(1):69-97.

19. Conibear, A. C., Deciphering protein post-translational modifications using chemical biology tools. *Nat. Rev. Chem.* **2020**, *4*:674–95.

20. Tsuchikama, K.; Anami, Y.; Ha, S. Y. Y.; Yamazaki, C. M., Exploring the next generation of antibody-drug conjugates. *Nat. Rev. Clin. Oncol*. **2024**, *21*:203–23.

21. Jin, G., Later but better peptide modulations. *Nat. Rev. Chem.* **2025**, *9*:139.

22. Tann, C. M.; Qi, D.; Distefano, M. D., Enzyme design by chemical modification of protein scaffolds. *Curr. Opin. Chem. Biol.* **2001**, *5*(6):696-704.

23. Brotzel, F.; Mayr, H., Nucleophilicities of amino acids and peptides. *Org. Biomol. Chem*. **2007**, *5*:3814.

24. Miseta, A.; Csutora, P., Relationship between the occurrence of cysteine in proteins and the complexity of organisms. *Mol. Biol. Evol.* **2000**, *17*(8):1232-9.

25. Chalker, J. M.; Bernardes, G. J.; Lin, Y. A.; Davis, B. G., Chemical modification of proteins at cysteine: opportunities in chemistry and biology. *Chem. Asian J.* **2009**, *4*(5):630-40.

26. Crankshaw, M. W.; Grant, G. A., Modification of Cysteine. *Curr. Protoc. Protein Sci.* **1996**, *3*:15.1.1-15.1.18.

27. Li, F.; Allahverdi, A.; Yang, R.; Lua, G. B. J.; Zhang, X.; Cao, Y.; Korolev, N.; Nordenskiöld, L.; Liu, C.-F., A Direct Method for Site-Specific Protein Acetylation. *Angew. Chem. Int. Ed.* **2011**, *50*:9611-4

28. Hoch, D. G.; Abegg, D; Adibekian, A., Cysteine-reactive probes and their use in chemical proteomics. *Chem. Commun.* **2018**, *54*:4501-12.

29. Yang, F.; Chen, N.; Wang, F.; Guogeng, J.; Wang, C., Comparative reactivity profiling of cysteine-specific probes by chemoproteomics. *Curr. Res. Chem. Biol.* **2022**, *2*:100024.

30. Bandyopadhyay, A.; Gao, J., Targeting biomolecules with reversible covalent chemistry. *Curr. Opin. Chem Biol.*, **2016**, *34*:110-6.

31. Wu, G.; Ott, T. L.; Knabe, D. A.; Bazer, F. W., Amino acid composition of the fetal pig. *J. Nutr.* **1999**, *129*(5):1031-8.

32. Zhou, M.; Li, S.; Tan, Y.; Huang, W.; Li, Y.; Yuan, X.; Li, Z., Global Profiling Lysine Reactivity and Ligandability with Oxidant-Triggered Bioconjugation Chemistry. *Angew. Chem. Int. Ed. Engl.* **2025**, *64*(6):e202418473.

33. Kalkhof, S.; Sinz, A., Chances and pitfalls of chemical cross-linking with amine-reactive N-hydroxysuccinimide esters. *Anal. Bioanal. Chem.* **2008**, *392*:305–12.

34. Mancheño, O. G.; Bolm, C., Iron-catalyzed imination of sulfoxides and sulfides. *Org. Lett.* **2006**, *11*(8):2349–52.

35. Nakamura, T.; Kawai, Y.; Kitamoto, N.; Osawa, T.; Kato, Y., Covalent Modification of Lysine Residues by Allyl Isothiocyanate in Physiological Conditions: Plausible Transformation of Isothiocyanate from Thiol to Amine. *Chem. Res. Toxicol.* **2009**, *22*(3):536-42.

36. Cal, P. M. S. D.; Vicente, J. B.; Pires, E.; Coelho, A. V.; Veiros, L. F.; Coideiro, C.; Gois, P. M. P., Iminoboronates: a new strategy for reversible protein modification. *J. Am. Chem. Soc.* **2012**, *134*(24):10299-305.

37. Haque, M.; Forte, N.; Baker, J. R., Site-selective lysine conjugation methods and applications towards antibody–drug conjugates. *Chem. Commun*. **2021**, *57*:10689-702.

38. Hacker, S. M.; Backus, K. M.; Lazear, M. R.; Forli, S.; Correia, B. E.; Cravatt, B. F., Global profiling of lysine reactivity and ligandability in the human proteome. *Nat. Chem.* **2017**, *9*:1181–90.

39. Dal Corso, A.; Catalano, M.; Schmid, A.; Scheuermann, J.; Neri, D., Affinity Enhancement of Protein Ligands by Reversible Covalent Modification of Neighboring Lysine Residues. *Angew. Chem. Int. Ed. Engl.* **2018**, *57*(52):17178-82.

40. Moellering, R. E.; Cravatt, B. F., Functional lysine modification by an intrinsically reactive primary glycolytic metabolite. *Science* **2013**, *341*(6145):549-53.

41. Hofmann, R.; Akimoto, G.; Wucherpfennig, T. G., Zeymer, C., Lysine acylation using conjugating enzymes for site-specific modification and ubiquitination of recombinant proteins. *Nat. Chem.* **2020**, *12*:1008–1015.

42. Leung, D.; Wurst, J. M.; Liu, T.; Martinez, R. M.; Datta-Mannan, A.; Feng, Y., Antibody Conjugates-Recent Advances and Future Innovations. *Antibodies* **2020**, *9*(1):2.

43. Tong, J. T. W.; Harris, P. W. R.; Brimble, M. A.; Kavianinia, I., An Insight into FDA Approved Antibody-Drug Conjugates for Cancer Therapy. *Molecules* **2021**, *26*(19):5847.

44. Ponziani, S.; Di Vittorio, G.; Pitari, G.; Cimini, A. M.; Ardini, M.; Gentile, R.; Iacobelli, S.; Sala, G.; Capone, E.; Flavell, D. J.; Ippoliti, R.; Giansanti, F., Antibody-Drug Conjugates: The New Frontier of Chemotherapy. *Int. J. Mol. Sci.* **2020**, *21*(15):5510.

45. Sadiki, A.; Liu, S.; Vaidya, S. R.; Kercher, E. M.; Lang, R. T.; McIsaac, J.; Spring, B. Q.; Auclair, J. R.; Zhou, Z. S., Site-Specific Conjugation of Native Antibody: Transglutaminase-Mediated Modification of a Conserved Glutamine While Maintaining the Primary Sequence and Core Fc Glycan *via* Trimming with an Endoglycosidase. *Bioconjugate Chem.* **2024,** *35*(4):465-471.

46. Popp M. W.; Antos J. M.; Ploegh H. L., Site-specific protein labeling *via* sortase-mediated transpeptidation. *Curr. Protoc. Protein Sci.* **2009,** *Chapter 15*:15.3.1-15.3.9.

47. Agarwal, P.; van der Weijden, J.; Sletten, E. M.; Rabuka, D.; Bertozzi, C. R., A Pictet-Spengler ligation for protein chemical modification. *Proc. Natl. Acad. Sci. U. S. A.* **2013**, *110*(1):46-51.

48. Hsu, Y.-P.; Nourzaie, O.; Tocher, A. E.; Nerella, K.; Ermakov, G.; Jung, J.; Fowler, A.; Wu, P.; Ayesa, U.; Willingham, A.; Beaumont, M.; Ingale, S., Site-Specific Antibody Conjugation Using Modified Bisected N-Glycans: Method Development and Potential toward Tunable Effector Function. *Bioconjugate Chem.* **2023**, *34*:1633−44.

49. Tornøe, C. W.; Christensen, C.; Meldal, M., Peptidotriazoles on solid phase: 1,2,3-triazoles by regiospecific copper(i)-catalyzed 1,3-dipolar cycloadditions of terminal alkynes to azides. *J. Org. Chem.* **2002**, *67*(9):3057-64.

50. Rostovtsev, V. V.; Green, L. G.; Fokin, V. V.; Sharpless, K. B., A stepwise huisgen cycloaddition process: copper(I)-catalyzed regioselective "ligation" of azides and terminal alkynes. *Angew. Chem. Int. Ed*. **2002**, *41*:2596-9.

51. Hein, J. E.; Fokin, V. V., Copper-catalyzed azide–alkynecycloaddition (CuAAC) and beyond: new reactivity of copper(i) acetylides. *Chem. Soc. Rev*. **2010**, *39*(4):1302-15.

52. Kaur, J.; Saxena, M.; Rishi, N., An Overview of Recent Advances in Biomedical Applications of Click Chemistry. *Bioconjugate Chem.* **2021**, *32*(8):1455-71.

53. Li, L.; Zhang, Z., Development and Applications of the Copper-Catalyzed Azide-Alkyne Cycloaddition (CuAAC) as a Bioorthogonal Reaction. *Molecules* **2016**, *21*:1393.

54. McKenna, S. M.; Florea, B. I.; Zisterer, D. M.; van Kasteren, S. I.; McGouran, J. F., Probing the metalloproteome: an 8-mercaptoquinoline motif enriches minichromosome maintenance complex components as significant metalloprotein targets in live cells. *RSC Chem. Biol.* **2024**, *5*:776-86.

55. Hameed, D. S.; Sapmaz, A.; Burggraaff, L.; Ovaa, H., Development of Ubiquitin-Based Probe for Metalloprotease Deubiquitinases. *Angew. Chem. Int. Ed. Engl.* **2019**, *58*(41):14477-82.

56. Agard, N. J.; Prescher, J. A.; Bertozzi, C. R., A Strain-Promoted 3 + 2 Azide−Alkyne Cycloaddition for Covalent Modification of Biomolecules in Living Systems. *J. Am. Chem. Soc*. **2004**, *126*(46):15046-7.

57. Mbua, N. E.; Guo, J.; Wolfert, M. A.; Steet, R.; Boons, G. J., Strain-Promoted Alkyne-Azide Cycloadditions (SPAAC) Reveal New Features of Glycoconjugate Biosynthesis. *ChemBioChem*. **2011**, *12*(12):1912-21.

58. Oliveira, B. L.; Guo, Z.; Bernardes, G. J. L., Inverse electron demand Diels–Alder reactions in chemical biology. *Chem. Soc. Rev*. **2017**, *46*:4895-950.

59. Wu, H.; Devaraj, N. K., Inverse Electron-Demand Diels-Alder Bioorthogonal Reactions. *Top. Curr. Chem. (Cham)* **2016**, *374*(1):3.

60. Lo Conte, M.; Staderini, S.; Marra, A.; Navarro, M. S.; Dvis, B. G.; Dondon, A., Multi-molecule reaction of serum albumin can occur through thiol-yne coupling. *Chem. Comm.* **2011**, *47*:11086-8.

61. Jasperse, C. P.; Curran, D. P.; Fevig, T. L., Radical reactions in natural product synthesis. *Chem. Rev.* **1991**, *91*(6):1237-86.

62. Lu, Z.; Ju, M.; Wang, Y.; Meinhardt, J. M.; Martinez Alvarado, J. I.; Villemure, E.; Terrett, J. A.; Lin, S., Regioselective aliphatic C-H functionalization using frustrated radical pairs. *Nature* **2023**, *619*(7970):514-20.

63. Gupta, A.; Laha, J. K., Growing Utilization of Radical Chemistry in the Synthesis of Pharmaceuticals. *Chem. Rec.* **2023**, *23*:e202300207.

64. Kehm, R.; Baldensperger, T.; Raupbach, J.; Höhn, A., Protein oxidation - Formation mechanisms, detection and relevance as biomarkers in human diseases. *Redox Biol.* **2021**, *42*:101901.

65. Pérez-Torres, I.; Soto, M. E.; Castrejón-Tellez, V.; Rubio-Ruiz, M. E.; Manzano Pech, L.; Guarner-Lans, V., Oxidative, Reductive, and Nitrosative Stress Effects on Epigenetics and on Posttranslational Modification of Enzymes in Cardiometabolic Diseases. *Oxid. Med. Cell Longev.* **2020**, 2020:8819719.

66. Fancy, D. A.; Melcher, K.; Johnston, S. A.; Kodadek, T., New chemistry for the study of multiprotein complexes: the six-histidine tag as a receptor for a protein crosslinking reagent. *Chem. Biol.* **1996**, 3:551-9.

67. Szijj, P. A.; Kostadinova, K. A.; Spears, R. J.; Chudasama, V., Tyrosine bioconjugation – an emergent alternative. *Org. Biomol. Chem*. **2020**, *18*:9018-28.

68. Meunier, S.; Strable, E.; Finn, M. G., Crosslinking of and coupling to viral capsid proteins by tyrosine oxidation. *Chem. Biol.* **2004**, *11*:319-26.

69. Matheis, G.; Whitaker, J. R., Peroxidase-catalyzed cross linking of proteins. *J. Protein. Chem.* **1984**, *3*:35-48.

70. Minamihata, K.; Goto, M.; Kamiya, N., Site-Specific Protein Cross-Linking by Peroxidase-Catalyzed Activation of a Tyrosine-Containing Peptide Tag. *Bioconjugate Chem.* **2011**, *22*:74–81.

71. Wu, H. C.; Shi, X. W.; Tsao, C. Y.; Lewandowski, A. T.; Fernandes, R.; Hung, C. W.; DeShong, P.; Kobatake, E.; Valdes, J. J.; Payne, G. F.; Bentley, W. E., Biofabrication of antibodies and antigens *via* IgG-binding domain engineered with activatable pentatyrosine pro-tag. *Biotechnol. Bioeng*. **2009**, *103*(2):231-40.

72. Mattinen, M. L.; Kruus, K.; Buchert, J.; Nielsen, J. H.; Andersen, H. J.; Steffensen, C. L., Laccase-catalyzed polymerization of tyrosine-containing peptides. *FEBS J*. **2005**, *272*:3640-50.

73. Hope, T. O.; Reyes-Robles, T.; Ryu, K. A.; Mauries, S.; Removski, N.; Maisonneuve, J.; Oslund, R. C.; Fadeyi, O. O.; Frenette, M., Targeted proximity-labelling of protein tyrosines *via* flavin-dependent photoredox catalysis with mechanistic evidence for a radical–radical recombination pathway. *Chem. Sci.* **2023**, *14*:7327-33.

74. Bosch, J. A.; Chen, C. L.; Perrimon, N., Proximity-dependent labeling methods for proteomic profiling in living cells: An update. *Wiley Interdiscip. Rev. Dev. Biol.* **2021**, *10*(1):e392.

75. Rhee, H. W.; Zou, P.; Udeshi, N. D.; Martell, J. D.; Mootha, V. K.; Carr, S. A.; Ting, A. Y., Proteomic mapping of mitochondria in living cells *via* spatially restricted enzymatic tagging. *Science* **2013**, *339*:1328-31.

76. Deepthi, A.; Sathi, V.; Nair, V., Recent topics of radical-based carbon-carbon bond formations. *Tetrahedron Lett.* **2018**, *59*(29):2767-77.

77. Bottecchia, C.; Rubens, M.; Gunnoo, S. B.; Hessel, V.; Madder, A.; Noël, T., Visible-Light-Mediated Selective Arylation of Cysteine in Batch and Flow. *Angew. Chem. Int. Ed. Engl.* **2017**, *56*(41):12702-7.

78. Mato, M.; Fernández-González, X.; D'Avino, C.; Tomás-Gamasa, M.; Mascareñas, J. L., Bioorthogonal Synthetic Chemistry Enabled by Visible-Light Photocatalysis. *Angew. Chem. Int. Ed. Engl.* **2024**, *63*(47):e202413506.

79. Xiang, H.; He, J.; Qian, W.; Qiu, M.; Xu, H.; Duan, W.; Ouyang, Y.; Wang, Y.; Zhu, C., Electroreductively Induced Radicals for Organic Synthesis. *Molecules* **2023**, *28*:857.

80. Wang, Y.; Dana, S.; Long, H.; Xu, Y.; Li, Y.; Kaplaneris, N.; Ackermann, L., Electrochemical Late-Stage Functionalization. *Chem. Rev.* **2023**, *123*(19):11269-335.

81. Xu, X.; Zhang, Y.; Zhang, X., Recent Advances in C–C Bond Formation *via* Visible Light-Mediated Desulfonylation and Its Application in the Modification of Biologically Active Compounds. *Molecules* **2024**, *29*:5553.

82. Taylor, N. C.; Hessman, G.; Kramer, H. B.; McGouran, J. F., Probing enzymatic activity – a radical approach, *Chem Sci.,* **2020**, *11*:2967-72.

83. Taylor, N. C., McGouran, J. F., Investigating eosin Y as a photocatalyst for the radical-dependent activity-based probing of deubiquitinating enzymes. *Org. Biomol. Chem.* **2021**, *19*(10):2177-81.

84. Campaniço, A., Baran, M.; Bowie, A. G.; Longley, D. B.; Harrison, T.; McGouran, J. F., Chemical- and photo-activation of protein-protein thiol-ene coupling for protein profiling. *Commun. Chem.* **2025**, *8*:25.

85. Griffiths, R. C.; Smith, F. R.; Li, D.; Wyatt, J.; Rogers, D. M.; Long, J. E.; Cusin, L. M. L.; Tighe, P. J.; Layfield, R.; Hirst, J. D.; Müller, M. M.; Mitchell, N. J., Cysteine-Selective Modification of Peptides and Proteins *via* Desulfurative C-C Bond Formation. *Chemistry* **2023**, *29*:e202202503.

86. Smith, F. R.; Meehan, D.; Griffiths, R. C.; Knowles, H. J.; Zhang, P.; Williams, H. E. L.; Wilson, A. J.; Mitchell, N. J., Peptide macrocyclisation *via* intramolecular interception of visible-light-mediated desulfurisation. *Chem. Sci.* **2024**, *15*:9612-9.

87. Ahmadinejad, F.; Geir Møller, S.; Hashemzadeh-Chaleshtori, M.; Bidghori, G.; Jami, M.-S., Molecular Mechanisms behind Free Radical Scavengers Function against Oxidative Stress. *Antioxidants* **2017**, *6*:51.

88. Schauenburg, D.; Weil, T., Chemical Reactions in Living Systems. *Adv. Sci. (Weinh)* **2024**, *11*(8):e2303396.

89. McLean, J. T.; Benny, A.; Nolan, M. D.; Swinand, G.; Scanlan, E. M., Cysteinyl radicals in chemical synthesis and in nature. *Chem. Soc. Rev.* **2021**, *50*: 10857-94.

90. Geng, J.; Li, W.; Zhang, Y.; Thottappillil, N.; Clavadetscher, J.; Lilienkampf, A.; Bradley, M., Radical polymerization inside living cells. *Nat. Chem.* **2019**, *11*:578-86.

91. Williams, C. G.; Malik, A. N.; Kim, T. K.; Manson, P. N.; Elisseeff, J. H., Variable cytocompatibility of six cell lines with photoinitiators used for polymerizing hydrogels and cell encapsulation. *Biomaterials* **2005**, *26*:1211-8.

92. Bryant, S. J.; Nuttelman, C. R.; Anseth, K. S., Cytocompatibility of UV and visible light photoinitiating systems on cultured NIH/3T3 fibroblasts in vitro. *J. Biomater. Sci. Polym. Ed.* **2000**, *11*:439-57.

93. Fedorovich, N. E.; Oudshoorn, M. H.; van Geemen, D.; Hennink, W. E.; Alblas, J.; Dhert, W. J., The effect of photopolymerization on stem cells embedded in hydrogels. *Biomaterials* **2009**, *30*:344-53.

94. Otaka, A.; Hirota, T.; Iwasaki Y., Direct Fabrication of Glycoengineered Cells *via* Photoresponsive Thiol–ene Reaction. *ACS Biomater. Sci. Eng.* **2024**, *10*(4):2068-73.

95. Cadenas, E., Mitochondrial free radical production and cell signaling. *Mol. Aspects Med.* **2004**, *25*(1-2):17-26.

96. Knight, J. A., Review: Free radicals, antioxidants, and the immune system. *Ann. Clin. Lab. Sci.* **2000**, *30*(2):145-58.

97. Flanagan, S. W.; Moseley, P. L.; Buettner, G. R., Increased flux of free radicals in cells subjected to hyperthermia: Detection by electron paramagnetic resonance spin trapping. *FEBS Lett*. **1998**, *431*:285-6.

98. Adjemian, S.; Oltean, T.; Martens, S.; Wiernicki, B.; Goossens, V.; Vanden Berghe, T.; Cappe, B.; Ladik, M.; Riquet, F. B.; Heyndrickx, L.; Bridelance, J.; Vuylsteke, M.; Vandecasteele, K.; Vandenabeele, P., Ionizing radiation results in a mixture of cellular outcomes including mitotic catastrophe, senescence, methuosis, and iron-dependent cell death. *Cell Death Dis*. **2020**, *11*:1003.

99. Racek, J.; Holecek, V.; Sedlácek, D.; Panzner, P., Free Radicals in Immunology and Infectious Diseases. *Epidemiol. Mikrobiol. Imunol*. **2001**, *50*(2):87-91.

100. Pham-Huy, L. A.; He, H.; Pham-Huy, C., Free radicals, antioxidants in disease and health. *Int. J. Biomed. Sci*. **2008**, *4*(2):89-96.

101. Akaike, T., Role of free radicals in viral pathogenesis and mutation. *Rev. Med. Virol*. **2001**, *11*:87-101.

102. Zheng, M.; Liu, Y.; Zhang, G; Yang, Z.; Xu, W.; Chen, Q., The Applications and Mechanisms of Superoxide Dismutase in Medicine, Food, and Cosmetics. *Antioxidants (Basel)* **2023**, *12*(9):1675.

103. Flohé, L.; Toppo, S.; Orian, L., The glutathione peroxidase family: Discoveries and mechanism. *Free Radic. Biol. Med.* **2022**, *187*:113-22.

104. Anwar, S.; Alrumaihi, F.; Sarwar, T. A.; Babiker, Y.; Khan, A. A.; Prabhu, S. V.; Rahmani, A. H., Exploring Therapeutic Potential of Catalase: Strategies in Disease Prevention and Management. *Biomolecules* **2024**, *14*:697.

105. Grant, C. M., Role of the glutathione/glutaredoxin and thioredoxin systems in yeast growth and response to stress conditions. *Mol. Microbiol*. **2001**, *39*(3):533-41.

106. Gozzelino, R.; Jeney, V.; Soares, M. P., Mechanisms of Cell Protection by Heme Oxygenase-1. *Annu. Rev. Pharmacol. Toxicol.* **2010**, *50*:323-54.

107. Nicolussi, A.; D'inzeo, S.; Capalbo, C.; Giannini, G.; Coppa, A., The role of peroxiredoxins in cancer. *Mol. Clin. Oncol*. **2017**, *6*:139-53.

108. Das, K. C.; Das, C. K., Thioredoxin, a singlet oxygen quencher and hydroxyl radical scavenger: redox independent functions. *Biochem. Biophys. Res. Commun*. **2000**, *277*(2):443-7.

109. Furlong, C. E.; Marsillach, J.; Jarvik, G. P.; Costa, L. G., Paraoxonases-1, -2 and -3: What are their Functions?. *Chem. Biol. Interact.* **2016**, *259*(Pt B):51-62.

110. Mirończuk-Chodakowska, I.; Witkowska, A. M.; Zujko, M. E., Endogenous non-enzymatic antioxidants in the human body. *Adv. Med. Sci.* **2018**, *63*(1):68-78.

111. Miller, A. L., Antioxidant flavonoids: Structure, function and clinical usage. *Alt. Med. Rev.* **1996**, *1*:103-11.

112. Bouayed, J.; Bohn, T., Exogenous antioxidants—Double-edged swords in cellular redox state. *Oxid. Med. Cell. Longev.* **2010**, *3*(4):228-37.

113. Schöneich, C., Sulfur Radical-Induced Redox Modifications in Proteins: Analysis and Mechanistic Aspects. *Antioxid. Redox Signal*. **2017**, *26*(8):388-405.

114. Hoshi, T.; Heinemann, S., Regulation of cell function by methionine oxidation and reduction. *J. Physiol.* **2001**, *531*(Pt 1):1-11.

115. Ehrenshaft, M.; Deterding, L. J.; Mason, R. P., Tripping up Trp: Modification of protein tryptophan residues by reactive oxygen species, modes of detection, and biological consequences. *Free Radic. Biol. Med*. **2015**, *89*:220-8.

116. Tanase, M.; Urbanska, A. M.; Zolla, V.; Clement, C. C.; Huang, L.; Morozova, K.; Follo, C.; Goldberg, M.; Roda, B.; Reschiglian, P.; Santambrogio, L., Role of Carbonyl Modifications on Aging-Associated Protein Aggregation. *Sci. Rep.* **2016**, *6*:19311.

117. Corpas, F. J.; Del Río, L. A.; Barroso, J. B., Post-translational modifications mediated by reactive nitrogen species. *Plant Signal Behav.* **2008**, *3*(5):301-3.

118. Yamakura, F.; Ikeda, K., Modification of tryptophan and tryptophan residues in proteins by reactive nitrogen species. *Nitric Oxide* **2006**, *14*(2):152-61.

119. Moosmann, B.; Hajieva, P., Probing the Role of Cysteine Thiyl Radicals in Biology: Eminently Dangerous, Difficult to Scavenge. *Antioxidants* **2022**, *11*:885.

120. Ayala, A.; Muñoz, M. F.; Argüelles, S., Lipid peroxidation: production, metabolism, and signaling mechanisms of malondialdehyde and 4-hydroxy-2-nonenal. *Oxid. Med. Cell Longev.* **2014**, 2014:360438.

121. Mosalmanzadeh, N.; Pence, B. D., Oxidized Low-Density Lipoprotein and Its Role in Immunometabolism. *Int. J. Mol. Sci.* **2024**, *25*:11386.

122. Zhong, S.; Li, L.; Shen, X.; Li, Q.; Xu, W.; Wang, X.; Tao, Y.; Yin, H., An update on lipid oxidation and inflammation in cardiovascular diseases. *Free Radic. Biol. Med.* **2019**, *144*:266-78.

123. Dong, Y.; Yong, V. W., Oxidized phospholipids as novel mediators of neurodegeneration. *Trends Neurosci*. **2022,** *45*(6):419-29.

124. Miller, Y. I.; Shyy, J. Y., Context-Dependent Role of Oxidized Lipids and Lipoproteins in Inflammation. *Trends Endocrinol. Metab.* **2017**, *28*(2):143-52.

125. Dizdaroglu, M.; Jaruga, P., Mechanisms of free radical-induced damage to DNA. *Free Radic. Res*. **2012,** *46*(4):382-419.

126. Kryston, T. B.; Georgiev, A. B.; Pissis, P.; Georgakilas, A. G., Role of oxidative stress and DNA damage in human carcinogenesis. *Mutat. Res.* **2011,** *711*(1-2):193-201.

127. Nakano, T.; Xu, X.; Salem, A. M. H.; Shoulkamy, M. I.; Ide, H., Radiation-induced DNA-protein cross-links: Mechanisms and biological significance. *Free Radic. Biol. Med.* **2017,** *107*:136-45.

128. Kojima, Y.; Machida, Y. J., DNA-protein crosslinks from environmental exposure: Mechanisms of formation and repair. *Environ. Mol. Mutagen.* **2020**, *61*(7):716-29.

129. Saghatelian, A.; Jessani, N.; Joseph, A.; Humphrey, M.; Cravatt, B. F., Activity-based probes for the proteomic profiling of metalloproteases. *Proc. Natl. Acad. Sci. U. S. A*. **2004**, *101*:10000-5.

130. Sadaghiani, A. M.; Verhelst, S. H. L.; Bogyo, M., Tagging and detection strategies for activity-based proteomics. *Curr. Opin. Chem. Biol*. **2007**, *11*, 20-28.

131. Fonović, M.; Bogyo, M., Activity-based probes as a tool for functional proteomic analysis of proteases. *Expert Rev. Proteomics* **2008**, *5*:721-30.

132. Deng, H.; Lei, Q.; Wu, Y.; He, Y.; Li, W., Activity-based protein profiling: Recent advances in medicinal chemistry. *Eur. J. Med. Chem.* **2020**, *191*:112151.

133. Hughes, J. P.; Rees, S.; Kalindjian, S. B.; Philpott, K. L., Principles of early drug discovery. *Br. J. Pharmacol*. **2011**, *162*:1239-49.

134. Gabrielsson, J.; Dolgos, H.; Gillberg, P. G., Bredberg, U.; Benthem, B.; Duker, G., Early integration of pharmacokinetic and dynamic reasoning is essential for optimal development of lead compounds: strategic considerations. *Drug Discov. Today* **2009**, *14*:358-72.

135. Ha, J.; Park, H.; Park, J.; Park, S. B., Recent advances in identifying protein targets in drug discovery. *Cell Chem. Biol*. **2021**, *28*:394-423.

136. Roberts, A. M.; Ward, C. C.; Nomura, D. K., Activity-based protein profiling for mapping and pharmacologically interrogating proteome-wide ligandable hotspots. *Curr. Opin. Biotechnol*. **2017**, *43*:25-33.

137. Fang, H.; Peng, B.; Ong, S. Y.; Wu, Q.; Li, L.; Yao, S. Q., Recent advances in activity-based probes (ABPs) and affinity-based probes (AfBPs) for profiling of enzymes. *Chem. Sci.* **2021**, *12*:8288-310.

138. Nomura, D. K.; Dix, M. M.; Cravatt, B. F., Activity-based protein profiling for biochemical pathway discovery in cancer. *Nat. Rev. Cancer* **2010**, *10*:630-38.

139. Li, Y. M.; Xu, M.; Lai, M. T.; Huang, Q.; Castro, J. L.; DiMuzio-Mower, J.; Harrison, T.; Lellis, C.; Nadin, A.; Neduvelil, J. G.; Register, R. B.; Sardana, M. K.; Shearman, M. S.; Smith, A. L.; Shi, X. P.; Yin, K. C.; Shafer, J. A.; Gardell, S. J., Photoactivated gamma-secretase inhibitors directed to the active site covalently label presenilin 1. *Nature* **2000**, *405*:689-94.

140. Siriwibool, S.; Kaekratoke, N.; Chansaenpak, K.; Siwawannapong, K.; Panajapo, P.; Sagarik, K.; Noisa. P.; Lai, R. Y.; Kamkaew, A., Near-Infrared Fluorescent pH Responsive Probe for Targeted Photodynamic Cancer Therapy. *Sci. Rep*. **2020**, *10*:1283.

141. Zuin, A.; Isasa, M.; Crosas, B., Ubiquitin signaling: extreme conservation as a source of diversity. *Cells* **2014**, *3*(3):690-701.

142. Hochstrasser M., Origin and function of ubiquitin-like proteins. *Nature* **2009**, *458*(7237):422-9.

143. Burroughs, A. M.; Iyer, L. M., Aravind, L., The natural history of ubiquitin and ubiquitin-related domains. *Front. Biosci. (Landmark Ed).* **2012**, *17*(4):1433-60.

144. Jentsch, S., The ubiquitin-conjugation system. *Annu. Rev. Genet.* **1992**, *26*:179-207.

145. Hu H.; Sun, S.-C., Ubiquitin signaling in immune responses. *Cell Research* **2016**, *26*:457-83.

146. Schwarz L. A.; Patrick, G. N., Ubiquitin-dependent endocytosis, trafficking and turnover of neuronal membrane proteins. *Mol. Cell Neurosci.* **2012**, *49*:387-93.

147. Yu, J.; Qin, B.; Lou, Z., Ubiquitin and ubiquitin-like molecules in DNA double strand break repair. *Cell & Bioscience* **2020**, *10*:13.

148. Lecker, S. H.; Goldberg A. L.; Mitch, W. E., Protein degradation by the ubiquitin-proteasome pathway in normal and disease states, *J. Am. Soc. Nephrol.* **2006**, *17*:1807-19.

149. Li W.; Ye, Y., Polyubiquitin chains: functions, structures, and mechanisms. *Cell Mol. Life Sci.* **2008**, *65*:2397-406.

150. French, M. E.; Koehler C. F.; Hunter, T., Emerging functions of branched ubiquitin chains. *Cell Discovery* **2021**, *7*:6.

151. Callis, J., The ubiquitination machinery of the ubiquitin system. *Arabidopsis Book* **2014**, *12*:e0174.

152. Kim, J. H.; Park, K. C.; Chung, S. S.; Bang O.; Chung, C. H., Deubiquitinating enzymes as cellular regulators, *J Biochem.* **2003**, *134*:9-18.

153. van Tilburg, G. B.; Elhebieshy, A. F.; Ovaa, H., Synthetic and semi-synthetic strategies to study ubiquitin signaling. *Curr. Opin. Struct. Biol.* **2016**, *38*:92-101.

154. Beck, D. B.; Werner, A.; Kastner D. L.; Aksentijevich, I., Disorders of ubiquitylation: unchained inflammation. *Nat. Rev. Rheumatol.* **2022**, *18*:435-47.

155. Lopez-Castejon, G., Control of the inflammasome by the ubiquitin system. *FEBS J* **2020**, *287*:11-26.

156. Sun, T.; Liu Z.; Yang, Q., The role of ubiquitination and deubiquitination in cancer metabolism. *Mol. Cancer* **2020**, *19*:146.

157. Schmidt, M. F.; Gan, Z. Y.; Komander, D.; Dewson, G., Ubiquitin signalling in neurodegeneration: mechanisms and therapeutic opportunities. *Cell Death Differ*. **2021**, *28*:570-90.

158. Kitahara, R.; Akasaka, K., Close identity of a pressure-stabilized intermediate with a kinetic intermediate in protein folding. *Proc. Natl. Acad. Sci. U. S. A.* **2003**, *100*:3167-72.

159. Surana, P.; Das, R., Observing a late folding intermediate of Ubiquitin at atomic resolution by NMR. *Protein Sci.* **2016**, *25*:1438-50.

160. Ibarra-Molero, B.; Loladze, V. V.; Makhatadze G. I.; Sanchez-Ruiz, J. M., Thermal versus guanidine-induced unfolding of ubiquitin. An analysis in terms of the contributions from charge-charge interactions to protein stability. *Biochem*. **1999**, *38*:8138-49.

161. Radici, L.; Bianchi, M.; Crinelli, R.; Magnani, M., Ubiquitin C gene: Structure, function, and transcriptional regulation. *Adv. Biosci. Biotechnol*. **2013**, *4*:1057-62.

162. Saitoh, H.; Hinchey, J., Functional heterogeneity of small ubiquitin-related protein modifiers SUMO-1 versus SUMO-2/3. *J. Biol. Chem*. **2000**, *275*:6252-8.

163. Xirodimas, D. P., Novel substrates and functions for the ubiquitin-like molecule NEDD8. *Biochem. Soc. Trans*. **2008**, *36*:802-6.

164. Garvin, A. J.; Walker, A. K.; Densham, R. M.; Chauhan, A. S.; Stone, H. R.; Mackay, H. L.; Jamshad, M.; Starowicz, K.; Daza-Martin, M.; Ronson, G. E.; Lanz,

A. J.; Beesley, J. F.; Morris, J. R., The deSUMOylase SENP2 coordinates homologous recombination and nonhomologous end joining by independent mechanisms. *Genes Dev*. **2019**, *33*:333-47.

165. Gan-Erdene, T.; Nagamalleswari, K.; Yin, L.; Wu, K.; Pan, Z.-Q.; Wilkinson, K. D., Identification and Characterization of DEN1, a Deneddylase of the ULP Family. *J. Biol. Chem*. **2003**, *278*:28892-900.

166. Wong, K.; Gehring, K., Deciphering the catalytic mechanism of bacterial ubiquitination. *Nature* **2018**, *557*:644-5.

167. Hatano, T.; Palani, S.; Papatziamou, D.; Salzer, R.; Souza, D. P.; Tamarit, D.; Makwana, M.; Potter, A.; Haig, A.; Xu, W.; Townsend, D.; Rochester, D.; Bellini, D.; Hussain, H. M. A.; Ettema, T. J. G.; Löwe, J.; Baum, B.; Robinson, N. P.; Balasubramanian, M., Asgard archaea shed light on the evolutionary origins of the eukaryotic ubiquitin-ESCRT machinery. *Nat. Commun*. **2022**, *13*:3398.

168. Rana, A. S. J. B.; Ge, Y.; Strieter, E. R., Ubiquitin Chain Enrichment Middle-Down Mass Spectrometry (UbiChEM-MS) Reveals Cell-Cycle Dependent Formation of Lys11/Lys48 Branched Ubiquitin Chains. *J. Proteome Res*. **2017**, *16*:3363-9.

169. Pickart, C. M.; Fushman, D., Polyubiquitin chains: polymeric protein signals. *Curr. Opin. Chem. Biol*. **2004**, *8*:610-6.

170. Keusekotten, K.; Elliott, P. R.; Glockner, L.; Fiil, B. K.; Damgaard, R. B.; Kulathu, Y.; Wauer, T.; Hospenthal, M. K.; Gyrd-Hansen, M.; Krappmann, D.; Hofmann, K.; Komander, D., OTULIN antagonizes LUBAC signaling by specifically hydrolyzing Met1-linked polyubiquitin. *Cell* **2013**, *153*:1312-26.

171. Matsumoto, M. L.; Dong, K. C.; Yu, C.; Phu, L.; Gao, X.; Hannoush, R. N.; Hymowitz, S. G.; Kirkpatrick, D. S.; Dixit, V. M.; Kelley, R. F., Engineering and structural characterization of a linear polyubiquitin-specific antibody. *J. Mol. Biol*. **2012**, *418*(3-4):134-44.

172. Yu, Y.; Zheng, Q.; Erramilli, S. K.; Pan, M.; Park, S.; Xie, Y.; Li, J.; Fei, J.; Kossiakoff, A. A.; Liu, L.; Zhao, M., K29-linked ubiquitin signaling regulates proteotoxic stress response and cell cycle. *Nat. Chem. Biol*. **2021**, *17*:896-905.

173. Karim, M.; Biquand, E.; Declercq, M.; Jacob, Y.; van der Werf, S.; Demeret, C., Nonproteolytic K29-Linked Ubiquitination of the PB2 Replication Protein of

Influenza A Viruses by Proviral Cullin 4-Based E3 Ligases. *mBio*. **2020**, *11*(2):e00305-20.

174. Liu, C.; Liu, W.; Ye, Y.; Li, W., Ufd2p synthesizes branched ubiquitin chains to promote the degradation of substrates modified with atypical chains. *Nat. Commun.* **2017**, *8*:14274.

175. Ohtake, F.; Saeki, Y.; Ishido, S.; Kanno, J.; Tanaka, K., The K48-K63 Branched Ubiquitin Chain Regulates NF-κB Signaling. *Mol. Cell* **2016**, *64*:251-66.

176. Rana, A.; Ge Y.; Strieter, E. R., Ubiquitin Chain Enrichment Middle-Down Mass Spectrometry (UbiChEM-MS) Reveals Cell-Cycle Dependent Formation of Lys11/Lys48 Branched Ubiquitin Chains. *J. Proteome Res*. **2017**, *16*:3363-9.

177. Meyer H. J.; Rape, M., Enhanced protein degradation by branched ubiquitin chains. *Cell* **2014**, *157*:910-21.

178. Blount, J. R.; Johnson, S. L.; Todi, S. V., Unanchored Ubiquitin Chains, Revisited. *Front. Cell Dev. Biol.* **2020**, *8*:582361.

179. Rajsbaum, R.; Versteeg, G. A.; Schmid, S.; Maestre, A. M.; Belicha-Villanueva, A.; Martínez-Romero, C.; Patel, J. R.; Morrison, J.; Pisanelli, G.; Miorin, L.; Laurent-Rolle, M.; Moulton, H. M.; Stein, D. A.; Fernandez-Sesma, A.; tenOever, B. R.; García-Sastre, A., Unanchored K48-linked polyubiquitin synthesized by the E3-ubiquitin ligase TRIM6 stimulates the interferon-IKKε kinase-mediated antiviral response. *Immunity* **2014**, *40*:880-95.

180. Gui, W.; Paudel, P.; Zhuang, Z., Activity-Based Ubiquitin Probes for Investigation of Deubiquitinases. *Comp. Nat. Prod. III.* **2020**, *2020*:589-602.

181. McCullough, J.; Clague, M. J.; Urbé, S., AMSH is an endosome-associated ubiquitin isopeptidase. *Journ. Cell Bio.* **2004**, *166*:487-92.

182. Qin, B.; Chen, X.; Wang, F.; Wang, Y., DUBs in Alzheimer's disease: mechanisms and therapeutic implications. *Cell Death Discov.* **2024**, *10*(1):475.

183. Sun, S. C., Deubiquitylation and regulation of the immune response. *Nat. Rev. Immunol.* **2008**, *8*:501–11.

184. Lai, K. P.; Chen, J.; Tse, W. K. F., Role of Deubiquitinases in Human Cancers: Potential Targeted Therapy. *Int. J. Mol. Sci.* **2020**, *21*(7):2548.

185. Hanahan, D.; Weinberg, R. A., The Hallmarks of Cancer. *Cell* **2000**, *100*:57-70.

186. Hanahan, D.; Weinberg, R. A., Hallmarks of Cancer: Next Generation. *Cell* **2011**, *144*:646-74.

187. Hanahan, D., Hallmarks of Cancer: New Dimensions. *Cancer Discov.* **2022**, *12*:31-46.

188. Li, M.; Fang, X.; Wei, Z.; York, J. P.; Zhang,P., Loss of spindle assembly checkpoint-mediated inhibition of Cdc20 promotes tumorigenesis in mice. *J. Cell Biol.* **2009**, *185*:983-94.

189. Wang, Z.; Liu, P.; Inuzuka, H.; Wei, W., Roles of F-box proteins in cancer. *Nat. Rev. Cancer* **2014**, *14*:233-47.

190. Gstaiger, M.; Jordan, R.; Lim, M.; Catzavelos, C.; Mestan, J.; Slingerland, J.; Krek, W., Skp2 is oncogenic and overexpressed in human cancers. *Proc. Natl. Acad. Sci. U. S. A.* **2001**, *98*:5043-8.

191. Zhan, T.; Rindtorff, N.; Boutros, M., Wnt signalling in cancer. *Oncogene* **2017**, *36*:1461-73.

192. Sun, K.; He, S.-B.; Yao, Y.-Z.; Qu, J.-G.; Xie, R.; Ma, Y.-Q.; Zong, M.-H.; Chen, J.-X., Tre2 (USP6NL) promotes colorectal cancer cell proliferation *via* Wnt/β-catenin pathway. *Cancer Cell Int.* **2019**, *19*:102.

193. Yang, B.; Zhang, S.; Wang, Z.; Yang, C.; Ouyang, W.; Zhou, F.; Zhou, Y.; Xie, C., Deubiquitinase USP9X deubiquitinates β-catenin and promotes high grade glioma cell growth. *Oncotarget* **2016**, *7*:79515-25.

194. Zou, Q.; Jin, J.; Hu, H.; Li, H. S.; Romano, S.; Xiao, Y.; Nakaya, M.; Zhou, M.; Cheng, X.; Yang, P.; Lozano, G.; Zhu, C.; Watowich, S. S.; Ullrich, S. E., Sun, S. C., USP15 stabilizes MDM2 to mediate cancer-cell survival and inhibit antitumor T cell responses. *Nat. Immunol.* **2014**, *15*:562-70.

195. Liu, H.; Li, X.; Ning, G.; Zhu, S.; Ma, X.; Liu, X.; Liu, C.; Huang, M.; Schmitt, I.; Wüllner, U.; Niu, Y.; Guo, C.; Wang, Q.; Tang, T. S., The Machado–Joseph Disease Deubiquitinase Ataxin-3 Regulates the Stability and Apoptotic Function of p53. *PLoS Biol.* **2016**, *14*:e2000733.

196. Fernández-Majada, V.; Welz, P. S.; Ermolaeva, M. A.; Schell, M.; Adam, A.; Dietlein, F.; Komander, D.; Büttner, R.; Thomas, R. K.; Schumacher, B.; Pasparakis, M., The tumour suppressor CYLD regulates the p53 DNA damage response. *Nat. Commun.* **2016**, *7*:12508.

197. Saldana, M.; VanderVorst, K.; Berg, A. L.; Lee, H.; Carraway, K. L., Otubain 1: a non-canonical deubiquitinase with an emerging role in cancer. *Endocr. Relat. Cancer* **2019**, *26*(1):R1-R14.

198. Lai, K. P.; Chen, J.; Tse, W. K. F., Role of Deubiquitinases in Human Cancers: Potential Targeted Therapy. *Int. J. Mol. Sci.*, **2020**, *21*(7):2548.

199. Lee, M.-S.; Jeong, M.-H.; Lee, H.-W.; Han, H.-J.; Ko, A.; Hewitt, S. M.; Kim, J.-H.; Chun, K.-H.; Chung, J.-Y.; Lee, C.; Cho, H.; Song, J., PI3K/AKT activation induces PTEN ubiquitination and destabilization accelerating tumourigenesis. *Nat. Comm.* **2015**, *6*:7769.

200. de Las Pozas, A.; Reiner, T.; De Cesare, V.; Trost, M.; Perez-Stable, C., Inhibiting Multiple Deubiquitinases to Reduce Androgen Receptor Expression in Prostate Cancer Cells. *Sci. Rep.* **2018**, *8*:13146.

201. Liu, S.; de Boeck, M.; van Dam H.; Ten Dijke, P., Transforming growth factor beta signal transduction. *Int. J. Biochem. Cell Biol.* **2016**, *76*:135-45.

202. Wu, X.; Luo, Q.; Zhao, P.; Chang, W.; Wang, Y.; Shu, T.; Ding, F.; Li, B.; Liu, Z., JOSD1 inhibits mitochondrial apoptotic signalling to drive acquired chemoresistance in gynaecological cancer by stabilizing MCL1. *Cell Death Differ.* **2020**, *27*:55-70.

203. Wang, S.; Juan, J.; Zhang, Z.; Du, Y.; Xu, Y.; Tong, J.; Cao, B.; Moran, M. F.; Zeng, Y.; Mao, X., Inhibition of the deubiquitinase USP5 leads to c-Maf protein degradation and myeloma cell apoptosis. *Cell Death Dis.* **2017**, *8*:e3058.

204. Burrows, J. F.; McGrattan, M. J.; Rascle, A.; Humbert, M.; Baek, K. H.; Johnston, J. A.; DUB-3, a Cytokine inducible Deubiquitinating Enzyme That Blocks Profileration. *J. Biol. Chem.* **2004**, *279*:13993-4000.

205. Xu, M.; Takanashi, M.; Oikawa, K.; Tanaka, M.; Nishi, H.; Isaka, K.; Kudo, M.; Kuroda, M., USP15 plays an essential role for caspase-3 activation during Paclitaxel-induced apoptosis. *Biochem. Biophys. Res. Commun.* **2009**, *388*:366-71.

206. Álvarez, V.; Viñas, L.; Gallego-Sánchez, A.; Andrés, S.; Sacristán, M. P.; Bueno, A., Orderly progression through S-phase requires dynamic ubiquitylation and deubiquitylation of PCNA. *Sci. Rep.* **2016**, *6*:25513.

207. Nijman, S. M.; Huang, T. T.; Dirac, A. M.; Brummelkamp, T. R.; Kerkhoven, R. M.; D'Andrea, A. D.; Bernards, R., The deubiquitinating enzyme USP1 regulates the Fanconi anemia pathway. *Mol. Cell.* **2005**, *17*:331-9.

208. Nishi, R.; Wijnhoven, P.; le Sage, C.; Tjeertes, J.; Galanty, Y.; Forment, J. V.; Clague, M. J.; Urbé, S.; Jackson, S. P., Systematic characterization of deubiquitylating enzymes for roles in maintaining genome integrity. *Nat. Cell Biol.* **2014**, *16*(10):1016-26.

209. Wu, X.; Liu, S.; Sagum, C.; Chen, J.; Singh, R.; Chaturvedi, A.; Horton, J. R.; Kashyap, T. R.; Fushman, D.; Cheng, X.; Bedford, M. T.; Wang, B., Crosstalk between Lys63- and Lys11-polyubiquitin signaling at DNA damage sites is driven by Cezanne. *Genes Dev.* **2019**, *33*:1702-17.

210. Meyer, T.; Jahn, N.; Lindner, S.; Röhner, L.; Dolnik, A.; Weber, D.; Scheffold, A.; Köpff, S.; Paschka, P.; Gaidzik, V. I.; Heckl, D.; Wiese, S.; Ebert, B. L.; Döhner, H.; Bullinger, L.; Döhner, K.; Krönke, J., Functional characterization of BRCC3 mutations in acute myeloid leukemia with t(8;21)(q22;q22.1). *Leukemia* **2020**, *34*:404-15.

211. Cano, A.; Pérez-Moreno, M. A.; Rodrigo, I.; Locascio, A.; Blanco, M. J.; del Barrio, M. G.; Portillo, F.; Nieto, M. A., The transcription factor snail controls epithelial-mesenchymal transitions by repressing E-cadherin expression. *Nat. Cell. Biol.* **2000**, *2*:76-83.

212. Zhou, H.; Liu, Y.; Zhu, R.; Ding, F.; Cao, X.; Lin, D.; Liu, Z., OTUB1 promotes esophageal squamous cell carcinoma metastasis through modulating snail stability. *Oncogene* **2018**, *37*:3356-68.

213. Song, Y.; Li, S.; Ray, A.; Das, D. S.; Qi, J.; Samur, M. K.; Tai, Y. T.; Munshi, N.; Carrasco, R. D.; Chauhan, D.; Anderson, K. C., Blockade of deubiquitylating enzyme Rpn11 triggers apoptosis in multiple myeloma cells and overcomes bortezomib resistance. *Oncogene* **2017**, *36*:5631-8.

214. Song. Y.; Yang, Z.; Ke, Z.; Yao, Y.; Hu, X.; Sun, Y.; Li, H.; Yin, J.; Zeng C., Expression of 14-3-3γ in patients with breast cancer: correlation with clinicopathological features and prognosis. Cancer Epidemiol. **2012**, 36(6):533-6.

215. Kim, J.; Kim, S.; Lim, K.; Kim, J.; Ajjappala, B.; Lee, H.; Choi, J.; Baek, K., Deubiquitinating enzyme USP37 regulating oncogenic function of 14-3-3γ. *Oncotarget* **2015**, *6*(34):36551-76.

216. Jacomin, A. C.; Taillebourg, E.; Fauvarque, M. O., Deubiquitinating Enzymes Related to Autophagy: New Therapeutic Opportunities?. *Cells* **2018**, *7*(8):112.

217. Kim, J. H.; Seo, D.; Kim, S. J.; Choi, D. W.; Park, J. S.; Ha, J.; Choi, J.; Lee, J. H.; Jung, S. M.; Seo, K. W.; Lee, E. W.; Lee, Y. S.; Cheong, H.; Choi, C. Y.; Park, S. H., The deubiquitinating enzyme USP20 stabilizes ULK1 and promotes autophagy initiation. *EMBO Rep.* **2018**, *19*(4):e44378.

218. Bingol, B.; Tea, J. S.; Phu, L.; Reichelt, M.; Bakalarski, C. E.; Song, Q.; Foreman, O.; Kirkpatrick, D. S.; Sheng, M., The mitochondrial deubiquitinase USP30 opposes parkin-mediated mitophagy. *Nature* **2014**, *510*:370-5.

219. Cornelissen, T.; Haddad, D.; Wauters, F.; Van Humbeeck, C.; Mandemakers, W.; Koentjoro, B.; Sue, C.; Gevaert, K.; De Strooper, B.; Verstreken, P.; Vandenberghe, W., The deubiquitinase USP15 antagonizes Parkin-mediated mitochondrial ubiquitination and mitophagy. *Hum. Mol. Genet.* **2014**, *23*:5227-42.

220. Phu, L.; Rose, C. M.; Tea, J. S.; Wall, C. E.; Verschueren, E.; Cheung, T. K.; Kirkpatrick, D. S.; Bingol, B., Dynamic Regulation of Mitochondrial Import by the Ubiquitin System. *Mol. Cell.* **2020**, *77*:1107-23.e1110.

221. Kuzuhara, S.; Mori, H.; Izumiyama, N.; Yoshimura, M.; Ihara, Y., Lewy bodies are ubiquitinated. A light and electron microscopic immunocytochemical study. *Acta Neuropathol.* **1988**, *75*:345-53.

222. Perry, G.; Friedman, R.; Shaw, G.; Chau, V., Ubiquitin is detected in neurofibrillary tangles and senile plaque neurites of Alzheimer disease brains. *Proc. Natl. Acad. Sci. U. S. A.* **1987**, *84*:3033-6.

223. Lowe, J.; Blanchard, A.; Morrell, K.; Lennox, G.; Reynolds, L.; Billett, M.; Landon, M.; Mayer, R. J., Ubiquitin is a common factor in intermediate filament inclusion bodies of diverse type in man, including those of Parkinson's disease, Pick's disease, and Alzheimer's disease, as well as Rosenthal fibres in cerebellar astrocytomas, cytoplasmic bodies in muscle, and mallory bodies in alcoholic liver disease. *J. Pathol.* **1988**, *155*:9-15.

224. Lowe, J.; Morrell, K.; Lennox, G.; Landon, M.; Mayer, R. J., Rosenthal fibres are based on the ubiquitination of glial filaments. *Neuropathol. Appl. Neurobiol.* **1989**, *15*:45-53.

225. Kato, T.; Katagiri, T.; Hirano, A.; Kawanami, T.; Sasaki, H., Lewy body-like hyaline inclusions in sporadic motor neuron disease are ubiquitinated. *Acta Neuropathol.* **1989**, *77*:391-6.

226. Ortega, Z.; Lucas, J. J., Ubiquitin-proteasome system involvement in Huntington's disease. *Front. Mol. Neurosci.* **2014**, *7*:77.

227. Alexopoulou, Z.; Lang, J.; Perrett, R. M.; Elschami, M.; Hurry, M. E.; Kim, H. T.; Mazaraki, D.; Szabo, A.; Kessler, B. M.; Goldberg, A. L.; Ansorge, O.; Fulga, T. A.; Tofaris, G. K., Deubiquitinase Usp8 regulates α-synuclein clearance and modifies its toxicity in Lewy body disease. *Proc. Natl. Acad. Sci. U. S. A.* **2016**, *113*:e4688-97.

228. Liu, X.; Hebron, M. L.; Mulki, S.; Wang, C.; Lekah, E.; Ferrante, D.; Shi, W.; Kurd-Misto, B.; Moussa, C., Ubiquitin Specific Protease 13 Regulates Tau Accumulation and Clearance in Models of Alzheimer's Disease. *J. Alzheimers Dis.* **2019**, *72*:425-41.

229. Banerjee, C.; Roy, M.; Mondal, R.; Chakraborty, J., USP14 as a Therapeutic Target Against Neurodegeneration: A Rat Brain Perspective. *Front. Cell Dev. Biol*. **2023**, *11*:1244890.

230. Melo-Cardenas, J.; Zhang, Y.; Zhang, D. D.; Fang, D., Ubiquitin-specific peptidase 22 functions and its involvement in disease. *Oncotarget* **2016**, *7*:44848-56.

231. Zheng, Q.; Li, G.; Wang, S.; Zhou, Y.; Liu, K.; Gao, Y.; Zhou, Y.; Zheng, L.; Zhu, L.; Deng, Q.; Wu, M.; Di, A.; Zhang, L.; Zhao, Y.; Zhang, H.; Sun, H.; Dong, C.; Xu, H.; Wang, X., Trisomy 21-induced dysregulation of microglial homeostasis in Alzheimer's brains is mediated by USP25. *Sci. Adv.* **2021**, *7*(1):eabe1340.

232. Huo, Y.; Khatri, N.; Hou, Q.; Gilbert, J.; Wang, G.; Man, H. Y., The deubiquitinating enzyme USP46 regulates AMPA receptor ubiquitination and trafficking. *J. Neurochem.* **2015**, *134*:1067-80.

233. Lowe, J.; McDermott, H.; Landon, M.; Mayer, R. J.; Wilkinson, K. D., Ubiquitin carboxyl-terminal hydrolase (PGP 9.5) is selectively present in ubiquitinated inclusion bodies characteristic of human neurodegenerative diseases. *J. Pathol.* **1990**, *161*:153-60.

234. Kawaguchi, Y.; Okamoto, T.; Taniwaki, M.; Aizawa, M.; Inoue, M.; Katayama, S.; Kawakami, H.; Nakamura, S.; Nishimura, M.; Akiguchi, I.; Kimura,

J.; Narumiya, S.; Kakizuka, A., CAG expansions in a novel gene for Machado-Joseph disease at chromosome 14q32.1. *Nat. Genet.* **1994**, *8*:221-8.

235. Liu, Y. C.; Penninger, J.; Karin, M., Immunity by ubiquitylation: a reversible process of modification. *Nat. Rev. Immunol.* **2005**, *5*:941-52.

236. Kovalenko, A.; Chable-Bessia, C.; Cantarella, G.; Israël, A.; Wallach, D.; Courtois, G., The tumour suppressor CYLD negatively regulates NF-kappaB signalling by deubiquitination. *Nature* **2003**, *424*:801-5.

237. Massoumi, R.; Chmielarska, K.; Hennecke, K.; Pfeifer, A.; Fässler, R., Cyld inhibits tumor cell proliferation by blocking Bcl-3-dependent NF-kappaB signaling. *Cell* **2006**, *125*:665-77.

238. Lim, J. H.; Stirling, B.; Derry, J.; Koga, T.; Jono, H.; Woo, C. H.; Xu, H.; Bourne, P.; Ha, U. H.; Ishinaga, H.; Xu, H.; Andalibi, A.; Feng, X. H.; Zhu, H.; Huang, Y.; Zhang, W.; Weng, X.; Yan, C.; Yin, Z.; Briles, D. E.; Davis, R. J.; Flavell, R. A.; Li, J. D., Tumor Suppressor CYLD Regulates Acute Lung Injury in Lethal Streptococcus pneumoniae Infections. *Immunity* **2007**, *27*:349-60.

239. Lim, J. H.; Jono, H.; Koga, T.; C.-H. Woo, H. Ishinaga, P. Bourne, H. Xu, U.-H. Ha, H. Xu and J.-D. Li, Tumor Suppressor CYLD Acts as a Negative Regulator for Non-Typeable Haemophilus influenza-Induced Inflammation in the Middle Ear and Lung of Mice. *PLoS ONE* **2007**, *2*(10):e1032.

240. Hiscott, J., Convergence of the NF-kappaB and IRF pathways in the regulation of the innate antiviral response. *Cytokine Growth Factor Rev.* **2007**, *18*:483-90.

241. Kayagaki, N.; Phung, Q.; Chan, S.; Chaudhari, R.; Quan, C.; O'Rourke, K. M.; Eby, M.; Pietras, E.; Cheng, G.; Bazan, J. F.; Zhang, Z.; Arnott, D.; Dixit, V. M., DUBA: a deubiquitinase that regulates type I interferon production. *Science* **2007**, *318*:1628-32.

242. Li, S.; Zheng, H.; Mao, A. P.; Zhong, B.; Li, Y.; Liu, Y.; Gao, Y.; Ran, Y.; Tien, P.; Shu, H. B., Regulation of Virus-triggered Signaling by OTUB1- and OTUB2-mediated Deubiquitination of TRAF3 and TRAF6. *J. Biol. Chem.* **2010**, *285*:4291-7.

243. Reiley, W. W.; Zhang, M.; Jin, W.; Losiewicz, M.; Donohue, K. B.; Norbury, C. C.; Sun, S.-C., Regulation of T cell development by the deubiquitinating enzyme CYLD. *Nat. Immunol.* **2006**, *7*:411-7.

244. Lineberry, N.; Fathman, C. G., T cell anergy: where it's LAT. *Immuniy* **2006**, *24(5):501-3. Erratum in: Immunity* **2006**, *25(1):175*.

245. Lin, A. E.; Mak, T. W., The role of E3 ligases in autoimmunity and the regulation of autoreactive T cells. *Curr. Opin. Immunol.* **2007**,*19*(6):665-73.

246. Mouchantaf, R.; Azakir, B. A.; McPherson, P. S.; Millard, S. M.; Wood, S. A.; Angers, A., The Ubiquitin Ligase Itch Is Auto-ubiquitylated *in Vivo* and *in Vitro* but Is Protected from Degradation by Interacting with the Deubiquitylating Enzyme FAM/USP9X. *J. Biol. Chem.* **2006**, *281*(50):38738-47.

247. Soares, L.; Seroogy, C.; Skrenta, H.; Anandasabapathy, N.; Lovelace, P.; Chung, C. D.; Engleman, E.; Fathman, C. G., Two isoforms of otubain 1 regulate T cell anergy *via* GRAIL. *Nat. Immunol*. **2004**, *5*(1):45-54.

248. Reiley, W. W.; Jin, W.; Lee, A. J.; Wright, A.; Wu, X.; Tewalt, E. F.; Leonard, T. O.; Norbury, C. C.; Fitzpatrick, L.; Zhang, M.; Sun, S. C., Deubiquitinating enzyme CYLD negatively regulates the ubiquitin-dependent kinase Tak1 and prevents abnormal T cell responses. *J. Exp. Med.* **2007**, *204*(6):1475-85.

249. Jin, W.; Reiley, W. R.; Lee, A. J.; Wright, A.; Wu, X.; Zhang, M.; Sun, S. C., Deubiquitinating enzyme CYLD regulates the peripheral development and naive phenotype maintenance of B cells. *J. Biol. Chem.* **2007**, *282*(21):15884-93.

250. Angot, A.; Vergunst, A.; Genin, S.; Peeters, N., Exploitation of Eukaryotic Ubiquitin Signaling Pathways by Effectors Translocated by Bacterial Type III and Type IV Secretion Systems. *PLoS Pathog.* **2007**, *3*(1):e3.

251. Hermanns, T.; Hofmann, K., Bacterial DUBs: deubiquitination beyond the seven classes. *Biochem. Soc. Transact.* **2019**, *47*(6):1857-1866.

252. Mondal, M.; Cao, F.; Conole, D.; Auner, H. W.; Tate, E. W., Discovery of potent and selective activity-based probes (ABPs) for the deubiquitinating enzyme USP30. *RSC Chem. Biol.* **2024**, *5*(5):439-446.

253. Sui, X.; Wang, Y.; Du, Y.-X.; Liang, L.-J.; Zheng, Q.; Li, Y.-M.; Liu, L., Development and application of ubiquitin-based chemical probes. *Chem. Sci.* **2020**, *11*(47):12633-12646.

254. Kooij, R.; Liu, S.; Sapmaz, A.; Xin, B. T.; Janssen, G. M. C.; van Veelen, P. A.; Ovaa, P. A.; Dijke, P. T.; Geurink, P. P., Small-Molecule Activity-Based Probe for Monitoring Ubiquitin C-Terminal Hydrolase L1 (UCHL1) Activity in Live Cells and Zebrafish Embryos. *J. Am. Chem. Soc*. **2020**, *142*(39):16825-16841.

255. Xian, Y.; Ye, J.; Tang, Y.; Zhang, N.; Peng, C.; Huang, W.; He, G., Deubiquitinases as novel therapeutic targets for diseases. *MedComm. (2020)* **2024**, *5*(12):e70036.

256. Conole, D.; Cao, F.; Am Ende, C. W.; Xue, L.; Kantesaria, S.; Kang, D.; Jin, J.; Owen, D.; Lohr, L.; Schenone, M.; Majmudar, J. D.; Tate, E. W., Discovery of a Potent Deubiquitinase (DUB) Small-Molecule Activity-Based Probe Enables Broad Spectrum DUB Activity Profiling in Living Cells. *Angew. Chem. Int. Ed. Engl.* **2023**;*62*(47):e202311190.

257. Ward, J. A.; McLellan, L.; Stockley, M.; Gibson, K. R.; Whitlock, G. A.; Knights, C.; Harrigan, J. A.; Jacq, X.; Tate, E. W. Quantitative Chemical Proteomic Profiling of Ubiquitin Specific Proteases in Intact Cancer Cells. *ACS Chem. Biol.* **2016**, *11*(12):3268-72.

258. Hershko, A.; Rose, I. A., Ubiquitin-aldehyde: a general inhibitor of ubiquitin-recycling processes. *Proc. Natl. Acad. Sci. U. S. A.* **1987**, *84*(7):1829-33.

259. Lam, Y. A.; Xu, W.; DeMartino, G. N.; Cohen, R. E., Editing of ubiquitin conjugates by an isopeptidase in the 26S proteasome. *Nature* **1997**, *385*(6618):737-40.

260. Ghosh, I.; Considine, N.; Maunus, E.; Sun, L.; Zhang, A.; Buswell, J.; Evans, T. C. Jr.; Xu, M. Q., Site-specific protein labeling by intein-mediated protein ligation. *Methods Mol. Biol.* **2011**, *705:*87-107.

261. Borodovsky, A.; Kessler, B. M.; Casagrande, R.; Overkleeft, H. S.; Wilkinson, K. D.; Ploegh, H. L., A novel active site-directed probe specific for deubiquitylating enzymes reveals proteasome association of USP14. *Embo. J.* **2001**, *20*(18):5187-96.

262. Samara, N. L.; Datta, A. B.; Berndsen, C. E.; Zhang, X.; Yao, T.; Cohen, R. E.; Wolberger, C., Structural insights into the assembly and function of the SAGA deubiquitinating module. *Science* **2010**, *328*(5981):1025-9.

263. Wiener, R.; Zhang, X.; Wang, T.; Wolberger, C., The mechanism of OTUB1-mediated inhibition of ubiquitination. *Nature* **2012**, *483*(7391):618-22.

264. Hemelaar, J.; Borodovsky, A.; Kessler, B. M.; Reverter, D.; Cook, J.; Kolli, N.; Gan-Erdene, T.; Wilkinson, K. D.; Gill, G.; Lima, C. D.; Ploegh, H. L.; Ovaa, H., Specific and covalent targeting of conjugating and deconjugating enzymes of ubiquitin-like proteins. *Mol. Cell Biol.* **2004**, *24*(1):84-95.

265. Ekkebus, R.; van Kasteren, S. I.; Kulathu, Y.; Scholten, A.; Berlin, I.; Geurink, P. P.; de Jong, A.; Goerdayal, S.; Neefjes, J.; Heck, A. J.; Komander, D.; Ovaa, H., On terminal alkynes that can react with active-site cysteine nucleophiles in proteases. *J. Am. Chem. Soc.* **2013**, *135*(8):2867-70.

266. Arkona, C.; Rademann, J., Propargyl Amides as Irreversible Inhibitors of Cysteine Proteases-A Lesson on the Biological Reactivity of Alkynes. *Angew. Chem. Int. Ed. Engl.* **2013**, *52*(32):8210-2.

267. Love, K. R.; Pandya, R. K.; Spooner, E.; Ploegh, H. L., Ubiquitin C-terminal electrophiles are activity-based probes for identification and mechanistic study of ubiquitin conjugating machinery. *ACS Chem. Biol.* **2009**, *4*(4):275-87.

268. Borodovsky, A.; Ovaa, H.; Kolli, N.; Gan-Erdene, T.; Wilkinson, K. D.; Ploegh, H. L.; Kessler, B. M., Chemistry-based functional proteomics reveals novel members of the deubiquitinating enzyme family. *Chem. Biol.* **2002**, *9*(10):1149-59.

269. Swatek, K. N.; Komander, D., Ubiquitin modifications. *Cell Res.* **2016**, *26*(4):399-422.

270. McGouran, J. F.; Gaertner, S. R.; Altun, M.; Kramer, H. B.; Kessler, B. M., Deubiquitinating enzyme specificity for ubiquitin chain topology profiled by di-ubiquitin activity probes. *Chem. Biol.* **2013**, *20*(12):1447-55.

271. Kulathu Y.; Komander D., Atypical ubiquitylation - the unexplored world of polyubiquitin beyond Lys48 and Lys63 linkages. *Nat. Rev. Mol. Cell Biol.* **2012**, *13*(8):508-23.

272. Juang, Y. C.; Landry, M. C.; Sanches, M.; Vittal, V.; Leung, C. C.; Ceccarelli, D. F.; Mateo, A. R.; Pruneda, J. N.; Mao, D. Y.; Szilard, R. K.;, Orlicky, S.; Munro, M.; Brzovic, P. S.; Klevit, R. E.; Sicheri, F.; Durocher, D., OTUB1 co-opts Lys48-linked ubiquitin recognition to suppress E2 enzyme function. *Mol. Cell* **2012**, *45*(3):384-97.

273. Bremm, A.; Freund, S. M.; Komander, D., Lys11-linked ubiquitin chains adopt compact conformations and are preferentially hydrolyzed by the deubiquitinase Cezanne. *Nat. Struct. Mol. Biol*. **2010**, *17*(8):939-47.

274. Li, G.; Liang, Q.; Gong, P.; Tencer, A. H.; Zhuang, Z., Activity-based diubiquitin probes for elucidating the linkage specificity of deubiquitinating enzymes. *Chem. Commun.* **2014**, *50*(2):216-8.

275. Weber, A.; Elliott, P. R.; Pinto-Fernandez, A.; Bonham, S.; Kessler, B. M.; Komander, D.; El Oualid, F.; Krappmann, D., A Linear Diubiquitin-Based Probe for Efficient and Selective Detection of the Deubiquitinating Enzyme OTULIN. *Cell Chem. Biol.* **2017**, *24*(10):1299-1313.e7.

276. Liu, J.; Li, Y.; Deol, K. K.; Strieter, E. R., Synthesis of branched triubiquitin active-site directed probes. *Org. Lett.* **2019**, *21*(17):6790-6794.

277. Rösner, D.; Schneider, T.; Schneider, D.; Scheffner, M.; Marx, A., Click chemistry for targeted protein ubiquitylation and ubiquitin chain formation. *Nat. Protocol.* **2015**, *10*(10):1594-611.

278. Schöneich, C., Photo-Degradation of Therapeutic Proteins: Mechanistic Aspects. *Pharm. Res.* **2020**, *37*(3):45.

279. Calvert, S. H., Pawlak, T., Hessman, G., McGouran, J. F., Rapid diazotransfer for selective lysine labelling. *Org. Biomol. Chem.* **2024**, *22*(39):7976-81.

280. Gillardon, F.; Moll, I.; Meyer, M.; Michaelidis, T. M., Alterations in cell death and cell cycle progression in the UV-irradiated epidermis of bcl-2-deficient mice. *Cell Death Differ.* **1999**, *6*(1):55-60.

281. McMillan, T. J.; Leatherman, E.; Ridley, A.; Shorrocks, J.; Tobi, S. E.; Whiteside, J. R., Cellular effects of long wavelength UV light (UVA) in mammalian cells. *J. Pharm. Pharmacol.* **2008**, *60*(8):969-76.

282. Besaratinia, A.; Kim, S.; Bates, S. E.; Pfeifer, G. P., Riboflavin activated by ultraviolet A1 irradiation induces oxidative DNA damage-mediated mutations inhibited by vitamin C. *Proc. Natl. Acad. Sci. U.S.A.* **2007**, *104*(14):5953-8.

283. Wollensak, G.; Spörl, E.; Reber, F.; Pillunat, L.; Funk, R., Corneal endothelial cytotoxicity of riboflavin/UVA treatment in vitro. *Ophthalmic Res.* **2003**, *35*(6):324-8.

284. Sturm, S.; Niegisch, G.; Windolf, J.; Suschek, C. V., Exposure of Bladder Cancer Cells to Blue Light (λ = 453 nm) in the Presence of Riboflavin Synergistically Enhances the Cytotoxic Efficiency of Gemcitabine. *Int. J. Mol. Sci.* **2024**, *25*(9):4868.

285. Dorsey, T. B.; Grath, A.; Wang, A.; Xu, C.; Hong, Y.; Dai, G., Evaluation of Photochemistry Reaction Kinetics to Pattern Bioactive Proteins on Hydrogels for Biological Applications. *Bioact. Mater.* **2018**, *3*(1):64-73.

286. Nimse, S. B.; Palb, D., Free radicals, natural antioxidants, and their reaction mechanisms. *RSC Adv.* **2015**, *5*(1):27986-8006

287. Lee, Y. B.; Lim, S.; Lee, Y.; Park, C. H.; Lee, H. J., Green Chemistry for Crosslinking Biopolymers: Recent Advances in Riboflavin-Mediated Photochemistry. *Materials* **2023**, *16*(3):1218.

288. BioActs, TAMRA-thiol Product specifications, accessed 26th August 2025, https://www.bioacts.com/item/item_view.php?gcode=14236

289. Mons, E.; Kim, R. Q.; van Doodewaerd, B. R.; van Veelen, P. A.; Mulder, M. P. C.; Ovaa, H., *J. Am .Chem. Soc.* **2021**, *143*(17):6423-33.

290. Jahanban-Esfahlan, A.; Ostadrahimi, A.; Jahanban-Esfahlan, R.; Roufegarinejad, L.; Tabibiazar, M.; Amarowicz, R., Recent developments in the detection of bovine serum albumin. *Int. J. Biol. Macromol.* **2019**, *138*:602-617.

291. Addgene, Feb 8 (2018), Recovering Plasmid DNA from Bacterial Culture, accessed 27th January 2023, https://www.addgene.org/protocols/purify-plasmid-dna/

292. Thermo Fisher Scientific, May 2 (2019), BL21(DE3) Competent Cells, accessed 27th January 2023, https://www.thermofisher.com/document-connect/document-connect.html?url=https://assets.thermofisher.com/TFS-Assets%2FLSG%2Fmanuals%2FMAN0018595_BL21_DE3competent_cells_UG.pdf

293. Faggiano, S.; Alfano, C.; Pastore, A., The missing links to link ubiquitin: Methods for the enzymatic production of polyubiquitin chains. *Anal. Biochem.* **2016**, *492*:82-90

294. Huang, T.; Li, J.; Byrd, R. A., Solution structure of lysine-free (K0) ubiquitin. *Protein Sci*. **2014**, *23*(5):662-7.

295. Fairbanks, B. D.; Scott, T. F.; Kloxin, C. J.; Anseth, K. S.; Bowman, C. N., Thiol-Yne Photopolymerizations: Novel Mechanism, Kinetics, and Step-Growth Formation of Highly Cross-Linked Networks. *Macromolecules* **2009**, *42*(1):211-7.

296. Fantoni, N. Z.; El-Sagheer, A. H.; Brown, T., A Hitchhiker's Guide to Click-Chemistry with Nucleic Acids. *Chem. Rev.* **2021**, *121*(12):7122-54.

297. Gibson, M. S.; Bradshaw, R. W., The Gabriel Synthesis of Primary Amines. Angew. *Chem. Int. Ed. Engl.* **1968**, *7*(12):919-30.

298. Li, J. J., (**2014**) Delépine amine synthesis. In: Name Reactions. Springer, Cham. 10.1007/978-3-319-03979-4_83.

299. Umar, Q.; Luo, M. A., Brief Review: Advancement in the Synthesis of Amine through the Leuckart Reaction. *Reactions* **2023**, *4*(1):117-47.

300. Cope, A.; Trumbull, E., (**2011**) Olefins from Amines: The Hofmann Elimination Reaction and Amine Oxide Pyrolysis. 10.1002/0471264180.or011.05

301. Ghosh, A. K.; Sarkar, A.; Brindisi, M., The Curtius rearrangement: mechanistic insight and recent applications in natural product syntheses. *Org. Biomol. Chem.* **2018**, *16*(12):2006-27.

302. Alfano, A. I.; Pelliccia, S.; Rossino, G.; Chianese, O.; Summa, V.; Collina, S.; Brindisi, M., Continuous-Flow Technology for Chemical Rearrangements: A Powerful Tool to Generate Pharmaceutically Relevant Compounds. *ACS Med. Chem. Lett.* **2023**, *14*(3):326-37.

303. Chatterjee, A. K.; Choi, T.-L.; Sanders, D. P.; Grubbs, R. H.; A General Model for Selectivity in Olefin Cross Metathesis. *J. Am. Chem. Soc.* **2003**, *125*(37):11360-70.

304. Astruc, D., The metathesis reactions: from a historical perspective to recent developments. *New J. Chem.* **2005**, *29*(1):42-56.

305. Gibson, M. S.; Bradshaw, R. W., The Gabriel Synthesis of Primary Amines. *Angew. Chem.* **1968**, *7*(1):919-30.

306. Current Patent Assignee: SHANGHAI INSTITUTE OF MATERIA MEDICA CAS - CN112940004, 2021, A, Location in patent: Paragraph 0135-0137.

307. Osby, J. O.; Martin, M. G.; Ganem. B., An exceptionally mild deprotection of phthalimides. *Tetrahedron Lett.* **1984**, *25*(20):2093-6.

308. Wang, Y.; Zhao, R.; Wan, C.; Guo, X.; Yang, F.; Hou, Z.; Wang, R.; Li, S.; Feng, T.; Yin, F.; Li, Z., A Peptide-Based Ligand-Directed Chemistry Enables Protein Functionalization. *Org. Lett.* **2022**, *24*(39):7205-9.

309. Flierman, D.; van der Heden van Noort, G. J.; Ekkebus, R.; Geurink, P. P.; Mevissen, T. E. T.; Hospenthal, M. K.; Komander, D.; Ovaa, H., Non-hydrolyzable Diubiquitin Probes Reveal Linkage-Specific Reactivity of Deubiquitylating Enzymes Mediated by S2 Pockets Author links open overlay panel. *Cell Chem. Biol.* **2016**; *23*(4):472-82.

310. Lohse, J.; Swier, L. J. Y. M.; Oudshoorn, R. C.; Médard, G.; Kuster, B.; Slotboom, D.-J.; Witte, M. D., Targeted Diazotransfer Reagents Enable Selective Modification of Proteins with Azides. *Bioconjugate Chem.* **2017**, *28*(4):913-917.

311. Baeza, J.; Smallegan, M. J.; Denu, J. M., Site-Specific Reactivity of Non-enzymatic Lysine Acetylation. *ACS Chem. Biol.* **2015**, *10*(1):122-8.

312. Cayot, P.; Tainturier, G., The quantification of protein amino groups by the trinitrobenzenesulfonic acid method: a reexamination. *Anal. Biochem.* **1997**, *249*(2):184-200.

313. Presolski, S. I.; Hong, V. P.; Finn, M. G., Copper-Catalyzed Azide-Alkyne Click Chemistry for Bioconjugation. *Curr. Protoc. Chem. Biol*. **2011**, *3*(4):153-62.

314. Worch, J. C.; Stubbs, C. J.; Price, M. J.; Dove, A. P., Click Nucleophilic Conjugate Additions to Activated Alkynes: Exploring Thiol-yne, Amino-yne, and Hydroxyl-yne Reactions from (Bio)Organic to Polymer Chemistry. *Chem. Rev.* **2021**, *121*(12):6744-76.

315. Marine, J. E.; Liang, X.; Song, S.; Rudick, J. G., Azide-rich peptides *via* an on-resin diazotransfer reaction. *Biopolymers* **2015**, *104*(4):419-26.

316. Baeza, J.; Smallegan, M. J.; Denu, J. M., Site-Specific Reactivity of Non-enzymatic Lysine Acetylation. *ACS Chem. Biol.* **2015**, *10*(1):122-8.

317. Cayot, P.; Tainturier, G., The quantification of protein amino groups by the trinitrobenzenesulfonic acid method: a reexamination. *Anal. Biochem.* **1997**, *249*(2):184-200.

318. Xu, P.; Trinh, M. N.; Kováč, P., Conjugation of carbohydrates to proteins using di(triethylene glycol monomethyl ether) squaric acid ester revisited. *Carbohydr. Res*. **2018**, *456*:24-9.

319. Ardana, A.; Ghosh, S.; Huda, P.; Fletcher, N. L.; Thurecht, K. J.; Williams, C. C., RAFT Polymer–Antibody Conjugation: Squaramide Ester Chemistry Leads to Conjugates with a Therapeutic Anti-EGFR Antibody with Full Retention of Activity and Increased Tumor Uptake In Vivo. *Mol. Pharmaceutics* **2023**, *20*(6):3073-87.

320. Ivancová, I.; Pohl, R.; Hubálek, M.; Hocek, M., Squaramate-Modified Nucleotides and DNA for Specific Cross-Linking with Lysine-Containing Peptides and Proteins. *Angew. Chem. Int. Ed. Engl.* **2019**, *58*(38):13345-8.

321. Wiener, R.; Zhang, X.; Wang, T.; Wolberger, C., The mechanism of OTUB1-mediated inhibition of ubiquitination. *Nature* **2012**, *483*(7391):618-22.

322. Mevissen, T. E. T., Komander, D., Mechanisms of Deubiquitinase Specificity and Regulation. *Annu. Rev. Biochem.* **2017**, *86*:159-92.

323. Hameed, D. S., Sapmaz, A.; Burggraaff, L.; Amore, A.; Slingerland, C. J.; van Westen, G. J. P.; Ovaa H., Development of Ubiquitin-Based Probe for Metalloprotease Deubiquitinases. *Angew. Chem. Int. Ed. Engl.* **2019**, *58*(41):14477-82.

324. Burke, H.; McSweeney, L.; Scanlan, E., Exploring chemoselective *S*-to-*N* acyl transfer reactions in synthesis and chemical biology. *Nat. Commun.* **2017**, *8*:15655.

325. Narayanana, A.; Jones, L. H., Sulfonyl fluorides as privileged warheads in chemical biology. *Chem. Sci.* **2015**, *6*(5):2650-9.

326. Ardana, A.; Ghosh, S.; Huda, P.; Fletcher, N. L.; Thurecht, K. J.; Williams, C. C., RAFT Polymer–Antibody Conjugation: Squaramide Ester Chemistry Leads to Conjugates with a Therapeutic Anti-EGFR Antibody with Full Retention of Activity and Increased Tumor Uptake In Vivo. *Mol. Pharmaceutics* **2023**, *20*(6):3073-87.

327. Marchetti, L. A.; Kumawat, L. K.; Mao, N.; Stephens, J. C.; Elmes, R. B. P., The Versatility of Squaramides: From Supramolecular Chemistry to Chemical Biology, *Chem.* **2019**, *5*(6):1398-485.

328. Tong, H.; Mohammed, F. A.; Elmes, R. B. P., Amino acid – Squaramide conjugates as anion binding receptors. *Results in Chemistry* **2024**, *11*(15):101777

329. Wurm, F.; Steinbach, T.; Klok, H. A., One-pot squaric acid diester mediated aqueous protein conjugation. *Chem. Commun. (Camb)*. **2013**, *49*(71):7815-7.

330. Gregory, J. D., The Stability of N-Ethylmaleimide and its Reaction with Sulfhydryl Groups. *J. Am. Chem. Soc.* **1955**, *77*(14):3922-3.

331. Sekar, V.; Hageman, J. H., Specificity of the serine protease inhibitor, phenylmethylsulfonyl fluoride. *Biochem. Biophys. Res. Commun.* **1979**, *89*(2):474-8.

332. Devés, R.; Angelo, S.; Chávez, P., N-ethylmaleimide discriminates between two lysine transport systems in human erythrocytes. *J. Physiol.* **1993**, *468*:753-66.

333. Paulech, J.; Solis, N.; Cordwell, S. J., Characterization of reaction conditions providing rapid and specific cysteine alkylation for peptide-based mass spectrometry. *Biochim. Biophys. Acta.* **2013**, *1834*(1):372-9.

334. James, G. T., Inactivation of the protease inhibitor phenylmethylsulfonyl fluoride in buffers. *Anal. Biochem.* **1978**, *86*(2):574-9.

335. Chog, S.; Mersha, F. B.; Comb, D. G.; Scott, M. E.; Landry, D.; Vence, L. M.; Perler, F. B.; Benner, J.; Kucera, R. B.; Hirvonen, C. A.; Pelletier, J. J.; Paulus, H.; Xu, M. Q., Single-column purification of free recombinant proteins using a self-cleavable affinity tag derived from a protein splicing element. *Gene* **1997**, *192*(2):271-81.

336. Zhu, J.; Rashidbaigi, A.; Pestka S., Direct nanogram quantitation of nucleic acid and protein with a continuous-flow microcell. *Anal. Biochem.* **1988**, *169*(1):138-41.

337. Middendorf, T.; Aldrich, R.; Baylor, D., Modification of Cyclic Nucleotide–Gated Ion Channels by Ultraviolet Light. *J. Gen. Physiol.* **2000**, *116*(2):227-52.

338. Huss, V. A. R.; Festl, H.; Schleifer, K. H., Studies on the spectrophotometric determination of DNA hybridization from renaturation rates. *Syst. Appl. Microbiol.* **1998**, *4*(2):184-92.

339. Norman, M. H.; Minick, D. J.; Rigdon, G. C., Effect of Linking Bridge Modifications on the Antipsychotic Profile of Some Phthalimide and Isoindolinone Derivatives. *J. Med. Chem.* **1996**, *39*(1):149-57.

Appendices

Appendix A - Trypsin digest of probe **23** (searched against the modified HPD)

Elastase digest of probe **23** (searched against the modified HPD)

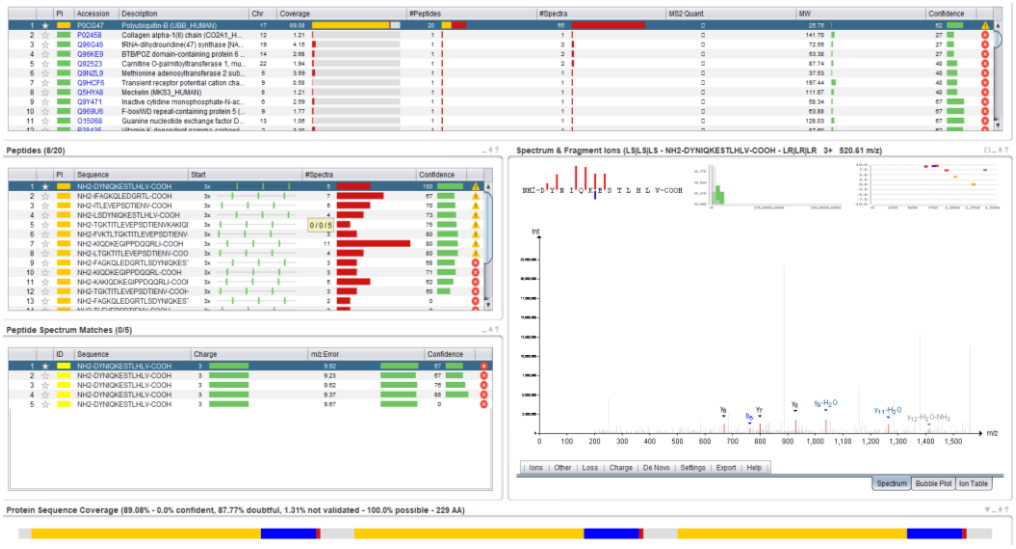

Appendix B - Trypsin digest of probe **31** (searched against the modified HPD)

Elastase digest of probe **31** (searched against the modified HPD)

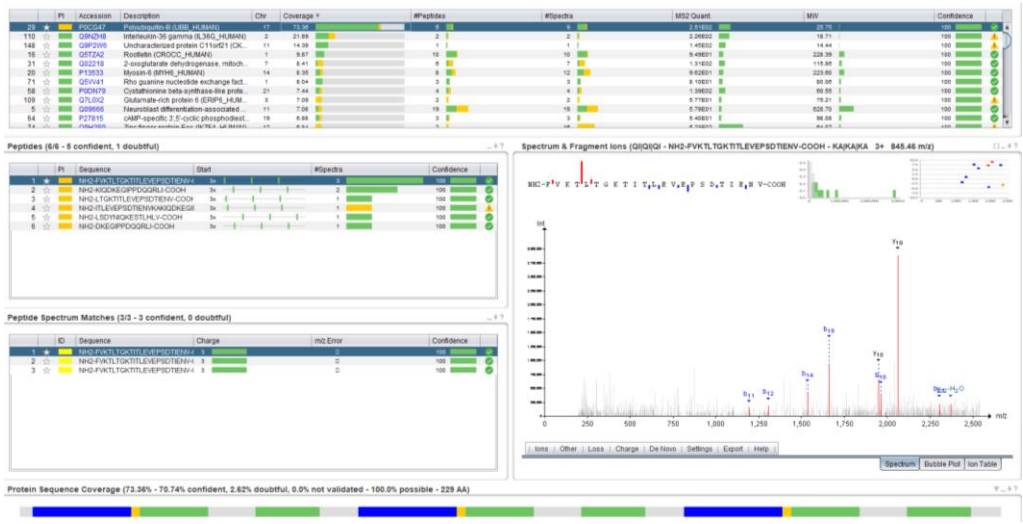

Appendix C - Trypsin digest of BSA (searched against the HPD) – positive control showing up as a 'contaminant'

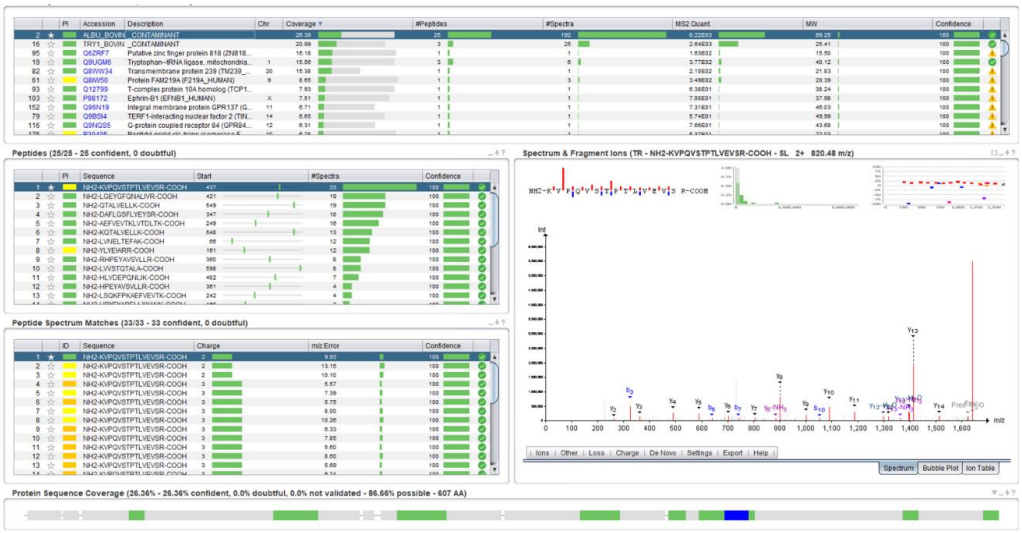

Elastase digest of BSA (searched against the HPD) – positive control showing up as a 'contaminant'

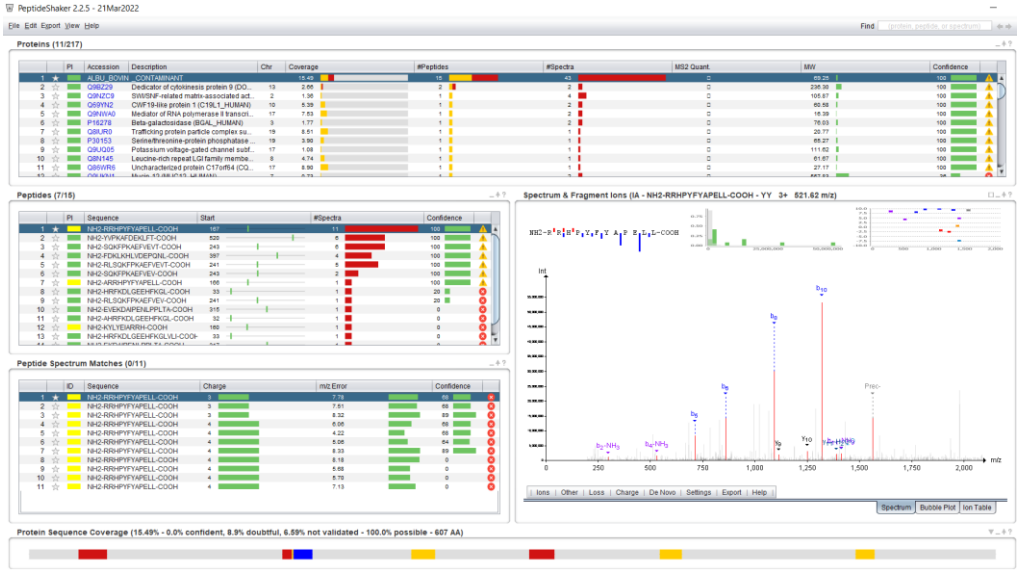

Appendix D -Trypsin digest of a blank water sample (searched against the HPD) – negative control showing up as a 'trypsin contaminant'

Elastase digest of a blank water sample (searched against the HPD) – negative control showing up as a 'chymotrypsin-like elastase contaminant'

Appendix E -Trypsin digest of purified, concentrated UbiquitinK48C – peptide containing K48C mutation was not found, likely due to signal loss

Appendix F - Extracted ion chromatograms of modified and native BSA lysine residues, as well as modified and native K48 Ubiquitin can be found on pages 14-37 in supplementary information of: Calvert, S. H., Pawlak, T., Hessman, G., McGouran, J. F., Rapid diazotransfer for selective lysine labelling. *Org. Biomol. Chem.* **2024**, *22*(39):7976-7981, seen in the link below:

https://www.rsc.org/suppdata/d4/ob/d4ob01094a/d4ob01094a1.pdf